Université de Paris

École doctorale ED562 Bio SPC- Bio Sorbonne Paris Cité

Laboratoire des Maladies Rénales Héréditaires,
Institut Imagine-INSERM UMR1163

"Identification and characterization of new molecular and cellular mechanisms involved in hereditary podocytopathies"

Par Francesco MISCIA

Thèse de doctorat de Biologie Cellulaire et Moléculaire

Dirigée par Géraldine MOLLET

Présentée et soutenue publiquement le 08/07/2021

Devant un jury composé de :

Dr. Olivier NAMY	Université Paris-Saclay	Rapporteur
Dr. Vasiliki KALATZIS	Université de Montpellier	Rapporteuse
Dr. Vincent CANTAGREL	Université de Paris	Examinateur
Dr. Khalil EL KAROUI	Université Paris-Est Créteil	Examinateur
Prof. Nadia BAHI-BUISSON	Université de Paris	Examinatrice

Except where otherwise noted, this is work licensed under
https://creativecommons.org/licenses/by-nc-nd/3.0/fr/

Acknowledgments

Foremost, I would like to express my sincere gratitude to my PhD supervisor Dr. Géraldine MOLLET for guiding and helping me in my research and the writing of this thesis.

Besides my supervisor, I would like to thank Prof. Corinne ANTIGNAC for accepting me as a PhD candidate in her laboratory.

My sincere thanks go to all the members of my jury committee, Dr. Olivier NAMY, Dr. Vasiliki KALATZIS, Dr. Vincent CANTAGREL, Dr. Khalil EL KAROUI and Prof. Nadia BAHI-BUISSON. I am extremely honored that you agreed to evaluate my PhD thesis and I would like to thank you in advance for your time and effort.

I thank my fellow labmates Olivier GRIBOUVAL, Christelle ARRONDEL, Bruno ESTEBE, Aurelien JUVEN who helped me in accomplishing my PhD thesis.

I would like also to thank all the others past or present members of the hereditary kidney diseases laboratory.

Ringrazio enormemente i miei genitori, Tiziana e Nicola, per essere stati sempre al mio fianco, per avermi sostenuto e supportato (sopportato) durante questi anni di dottorato, nonostante la distanza. Ringrazio Nonna Lina, perchè nonostante il tempo passi, sarò sempre il suo piccolo nipote.

E infine ringrazio te Alessandra, l'averti incontrato mi ha cambiato la vita e mi ha reso una persona migliore. Sei stata il mio faro in una notte di tempesta, la mia luce nel buio, la mia guida in un sentiero tortuoso, la mia forza nei momenti difficili e duri. Grazie, non finirò mai di ripeterlo!

ABSTRACT

Hereditary podocytopathies (HP) are rare renal disorders characterized by urinary protein loss and - in case of massive loss - nephrotic syndrome (NS), including steroid-resistant nephrotic syndromes (SRNS). These disorders are due to intrinsic defects of the podocyte, a highly specialized post-mitotic epithelial cell. The identification of more than 50 monogenic causes of SRNS has highlighted the crucial role of podocyte in the glomerular filtration barrier maintenance. The renal disease can be isolated or associated with extra-renal manifestations, the most frequent being neurological such as in Galloway-Mowat syndrome (GAMOS), associating SRNS with microcephaly and neurological impairment. To date mutations identified in 11 different genes encoding proteins mainly involved in RNA metabolism, in particular tRNA and UsnRNA, and in transcriptional regulation. The identification of mutations in these genes that affect both the kidney and the nervous system raises the fascinating question of molecular pathways that could be common to both kidney and brain development and function, in line with growing evidence that podocytes and neurons share a large number of features.

The global aim of this PhD thesis was to identify and characterize new candidate genes for SRNS and GAMOS. Thus, this study first reports the identification by exome sequencing of two novel mutations in the *TSEN54* gene (tRNA splicing endonuclease subunit 54) in patients with either isolated SRNS or GAMOS. The first mutation creates a cryptic splicing site in intron 5 (c.468+48A>G) and the second mutation is a nonsense mutation in exon 8 (c.1015C>T, p.Gln339*). Intriguingly, this intronic mutation is present in the homozygous state in patients with SRNS, whereas it is associated in trans with the Q339* mutation in a patient with GAMOS. TSEN54 is one of the four subunits of the TSEN complex, known to be involved in the splicing of intron-containing tRNAs, together with CLP1 (cleavage and polyadenylation factor 1), another key player in this pathway. Interestingly, mutations have been identified in genes encoding all TSEN complex subunits and *CLP1*, in individuals with pontocerebellar hypoplasia (PCH), a group of rare autosomal recessive neurodevelopmental disorders. Strikingly, no renal involvement has been reported to date in PCH cases, particularly in those linked to *TSEN54* mutations. Thus, this study sought to understand why this particular *TSEN54* mutation, and only this one, causes the isolated renal phenotype by modelling *TSEN54*-linked SRNS and –GAMOS using various cellular models, including immortalized podocytes and induced pluripotent stem cells (iPSC)-derived neural stem cells (NSCs) and kidney organoids, to identify the molecular and cellular mechanisms altered in

each condition.

To confirm the pathogenicity of these variants, we first investigated their impact on mRNA and protein levels in lymphoblastoid cell lines (LCLs) obtained from a SRNS patient and the parents of a GAMOS patient who had died prematurely. We demonstrated that, in the SRNS patient harboring the homozygous intronic mutation, two transcripts are present, one corresponding to the wild-type (WT) and the other to the mutant transcript containing a 47 intronic base-pair retention (named hereafter Ins47), confirming that both the canonical and the cryptic splicing sites are used. In agreement with this result, a small amount of TSEN54-WT protein was detected by western blot in LCLs of the SRNS patient, whereas the mutant proteins (Ins47 and Q339*) were not. Co-immunoprecipitation and mass spectrometry experiments in HEK293T cells showed that transiently overexpressed TSEN54-Ins47 mutant impairs TSEN complex integrity contrary to the Q339* mutant. In addition, we demonstrated that TSEN54-WT interacts with CLP1 and the importin alpha-5 subunit, the latter functioning as an adapter in the nuclear import of proteins and that could be involved in the nuclear localization of the TSEN complex.

As the main function of the TSEN complex is to remove introns in a restricted subset of intron-containing tRNAs, and since it has already been shown that *CLP1* mutations lead to accumulation of intron-containing tRNAs, we performed tRNA-sequencing on LCLs from a healthy individual and the SRNS patient harbouring the intronic Ins47 mutation. Preliminary data showed an increased numbers of reads corresponding to intronic regions suggesting an increase in unspliced tRNAs in the SRNS patient. In addition, to better understand the cellular mechanisms underlying the renal defect, we knocked-down (KD) *TSEN54* using shRNA in immortalized human podocytes to mimic the residual amount of TSEN54-WT protein resulting from the Ins47 mutation. We demonstrated that KD podocytes exhibit reduced proliferation and protein synthesis. Unexpectedly, we did not show evidence of increased apoptosis upon *TSEN54* KD that could explain this decrease in cell proliferation.

Finally, to obtain the disease relevant cell types, we further derived iPSC lines from the SRNS patient and the father of the GAMOS patient bearing the Ins47 mutation in the heterozygous state, this latter iPSC line having then been gene-edited by CRISPR/Cas9 to mimic the genotype of the deceased GAMOS patient. Subsequently, these iPSC lines were differentiated towards neural stem cells (NSCs), late cortical neurons and kidney organoids.

To date, several experiments are in progress, including analyzes of the transcriptomic

profiles of NSCs and podocytes isolated from renal organoids, analysis of intron splicing defects (tRNA-seq) and study of various cellular processes in NSCs. Altogether, these results will help deciphering the pathological cellular and molecular mechanisms linked to mutations in *TSEN54* and underlying SRNS and GAMOS.

RÉSUMÉ

L'étude des formes héréditaires de néphropathies glomérulaires a permis de mettre à jour un nouveau type de pathologies baptisées « podocytopathies héréditaires » sont des maladies rénales rares caractérisées par une perte de protéines dans les urines et - en cas de perte massive - un syndrome néphrotique (SN). Ces maladies sont dues à des altérations intrinsèques de la barrière de filtration glomérulaire (BFG) rénale dont les podocytes sont des composants majeurs. Les podocytes sont des cellules épithéliales post-mitotiques hautement spécialisées qui émettent des prolongements cytoplasmiques appelées pieds primaires qui se ramifient en extensions plus fines appelées pédicelles. Ces pédicelles s'entrecroisent et sont reliés entre eux sur la membrane basale glomérulaire par une jonction modifiée hautement spécialisée appelée le diaphragme de fente (DF).

Les études génétiques de formes familiales de podocytopathies, aussi bien des SNCR de transmission autosomique récessive (AR), que des hyalinoses segmentaires et focales de transmission autosomique dominante (AD), ont permis d'identifier plus de 50 gènes codant pour des protéines podocytaires, de révéler le rôle crucial des podocytes dans le maintien de la BFG et d'en préciser sa structure et son fonctionnement. Ainsi, les deux premiers gènes identifiés comme étant responsables de SNCR AR codent pour des protéines structurales du podocyte localisées au niveau du DF : la néphrine, codée par le gène *NPHS1* et la podocine, codée par le gène *NPHS2* identifié dans le laboratoire. Dans une grande majorité des formes génétiques de SNCR, l'atteinte rénale est isolée, cependant, il existe également de rares formes syndromiques, où l'atteinte rénale s'associe à divers symptômes extra-rénaux, dues à des mutations dans des gènes codant des facteurs de transcription, des protéines mitochondriales voire lysosomales. Dans les formes syndromiques, les manifestations extra-rénales sont le plus souvent d'origine neurologique, comme dans le syndrome de Galloway-Mowat ou GAMOS.

Le syndrome de Galloway-Mowat est une maladie rare autosomique récessive ou liée à l'X, décrite pour la première fois en 1968 par Galloway et Mowat associant un SNCR à une microcéphalie et des anomalies neurologiques. Depuis, une centaine de cas ont été rapportés dans la littérature. Le large spectre des manifestations cliniques rapportées chez les patients atteints de GAMOS a révélé que cette maladie est très hétérogène. La prévalence estimée du GAMOS est de 1<1 000 000, et le pronostic du GAMOS est mauvais avec un décès survenant le plus souvent dans les premières années de vie. La caractéristique constante du GAMOS est la microcéphalie qui consiste en une diminution du périmètre crânien. Lorsqu'elle est présente à la naissance, elle est

appelée microcéphalie primaire, mais elle peut également survenir durant les premiers mois, voire années, de vie et est alors appelée microcéphalie secondaire ou postnatale. La microcéphalie primaire est considérée comme étant due à des anomalies du développement neurologique, consistant principalement en des défauts de prolifération des cellules progénitrices neurales qui déterminent le nombre final de neurones dans le cerveau. D'autre part, la microcéphalie secondaire est considérée comme étant due à des anomalies neurodégénératives ou à des défauts de maturation neuronale. La microcéphalie s'accompagne fréquemment d'anomalies majeures du système nerveux central telles que des malformations du cerveau: atrophie cérébrale ou cérébelleuse, hypoplasie du corps calleux, défauts de myélinisation ou de gyration (lissencéphalie, polymicrogyrie), ces derniers étant dus à des défauts de migration neuronale. On retrouve également une diminution du tonus musculaire, des crises d'épilepsie, une déficience visuelle, une déficience intellectuelle profonde, un retard de croissance, une dysmorphie faciale, une hernie hiatale et des anomalies du squelette. L'atteinte rénale dans GAMOS va de la protéinurie isolée au SNCR, ce dernier pouvant évoluant rapidement vers l'insuffisance rénale terminale. Le SN est le plus souvent d'apparition précoce, mais plusieurs cas d'apparition plus tardive ont été rapportés dans la littérature, voire parfois des cas avec une fonction rénale normale au moment de leur publication.

Plusieurs gènes ont été identifiés comme responsables du GAMOS, mettant en évidence son hétérogénéité génétique et reflétant son hétérogénéité clinique. Jusqu'à présent, des mutations pathogènes ont été identifiées dans onze gènes, dont *WDR73*, *NUP133*, *NUP107*, *WDR4* (composant de l'holoenzyme METTL1/WDR4) et ceux codant pour le complexe KEOPS (*LAGE3*, *OSGEP*, *TP53RK*, *TPRKB*, *YRDC*). Tout récemment, une mutation de *PRDM15* a été identifiée comme une nouvelle cause de GAMOS. Ces gènes codent pour des protéines aux fonctions diverses, principalement impliquées dans le métabolisme des ARN, en particulier les ARN de transfert (ARNt) et les petits ARN nucléaires et nucléolaires (ARNsn et ARNsno, impliqués dans l'épissage des ARN), et dans la régulation transcriptionnelle. L'identification de mutations dans ces gènes soulève la question fascinante des voies moléculaires qui pourraient être communes au développement et à la fonction rénale et cérébrale, les podocytes et les neurones partageant un grand nombre de caractéristiques.

L’objectif global de ce travail de thèse était d’identifier et de caractériser de nouveaux gènes candidats de SNCR et de GAMOS. Ainsi, cette étude rapporte l'identification par séquençage d’exomes de deux nouvelles mutations du gène *TSEN54* (tRNA splicing endonuclease subunit 54) chez des patients avec SNCR isolé ou avec un GAMOS. La première mutation crée un site cryptique d'épissage dans l'intron 5 (c.468+48A>G) et la seconde est une mutation non-sens dans l'exon 8 (c.1015C>T, p.Gln339*). Curieusement, la mutation intronique est présente à l'état homozygote chez les patients avec SNCR, alors qu'elle est à l’état hétérozygote associée en trans à la mutation Q339* chez le patient avec GAMOS. TSEN54 est l'une des quatre sous-unités du complexe TSEN, connu pour être impliqué avec CLP1 dans l'épissage des ARNt contenant des introns. Fait intéressant, des mutations ont été identifiées dans les gènes codant toutes les sous-unités du complexe TSEN et *CLP1*, chez des individus avec hypoplasie pontocérébelleuse (PCH), un groupe de maladies neurodéveloppementales autosomiques récessives rares principalement d'apparition prénatale.

La plupart des patients atteints de PCH présentent une hypoplasie/atrophie prénatale sévère du cervelet et des ponts ventraux, avec une atteinte cérébrale variable et un retard psychomoteur sévère. Les PCH ont été classés en 14 types selon les différentes caractéristiques cliniques, les résultats de neuroimagerie et les causes génétiques. Les familles porteuses de mutations bialléliques dans *TSEN54* ne présentent que des anomalies neurologiques. La PCH de type 2, et en particulier la PCH2A, est le type le plus répandu et également le plus connu de tous les sous-types de PCH, concernant 50 % des patients atteints de PCH. Les patients atteints de PCH2A portent une mutation fondatrice homozygote p.A307S dans le gène *TSEN54* (faux-sens c.919G>T) et représentent la majorité des patients atteints de PCH2. Une évolution clinique plus sévère peut dépendre du type de mutations qui se produit dans *TSEN54*. En effet, une mutation hétérozygote composite (c.919G>T) associée à un site d'épissage, ou une mutation non-sens dans *TSEN54* sont toutes deux associées au type PCH le plus sévère, nommé respectivement PCH4 et PCH5. Étonnamment, aucune atteinte rénale n'a été rapportée à ce jour dans les cas de PCH, en particulier dans ceux liés à des mutations de *TSEN54*. Cependant, il pourrait être possible qu'aucune anomalie rénale ne soit détectée chez les personnes atteintes de PCH en raison du phénotype sévère observé parfois dès la naissance et du décès précoce, survenant principalement avant l'âge d'un an. A noter, il a été montré chez la souris qu'une mutation faux-sens (p.Ala341Ser) ou un knock-out du gène *Ampd2*, connu pour être responsable du PCH de type 9 lorsqu'il est muté chez l'homme, conduit à

un phénotype rénal caractérisé par une protéinurie légère ou un syndrome néphrotique, respectivement, avec effacement du des pédicelles, suggérant que les gènes impliqués dans la PCH pourraient également être responsables de manifestations rénales.

Ainsi, l'objectif de ces travaux a été de chercher à comprendre pourquoi cette mutation particulière du gène *TSEN54*, et seulement celle-ci, provoque le phénotype rénal isolé en modélisant les SNCR et -GAMOS liés à des mutations du gène *TSEN54* à l'aide de divers modèles cellulaires, y compris des podocytes immortalisés, des cellules souches neurales (NSC) et des organoïdes rénaux dérivés de cellules souches pluripotentes induites (iPSCs), pour identifier les mécanismes moléculaires et cellulaires altérés dans chaque condition pathologique.

Pour confirmer la pathogénicité de ces mutations, nous avons d'abord étudié leur impact sur les taux d'ARNm et de protéines dans des lignées lymphoblastoïdes (LCLs) obtenues à partir d'un patient avec SNCR et des parents d'un patient avec GAMOS décédé prématurément. Nous avons démontré que, chez le patient avec SNCR porteur de la mutation intronique homozygote, deux transcrits sont présents, l'un correspondant au transcrit sauvage (WT) et l'autre au transcrit mutant contenant une rétention de 47 paires de bases introniques (nommé ci-après Ins47), confirmant que les deux sites d'épissage canonique et cryptique sont utilisés. En accord avec ce résultat, une petite quantité de protéine TSEN54 WT a été détectée dans les LCLs du patient avec SNCR, alors qu'aucune des protéines mutantes (Ins47 et Q339*) ne l'a été. Des expériences de co-immunoprécipitation et de spectrométrie de masse dans des cellules HEK293T ont montré que le mutant TSEN54-Ins47 surexprimé transitoirement altère l'intégrité du complexe TSEN contrairement au mutant Q339*. De plus, nous avons démontré que TSEN54-WT interagit avec CLP1 et avec la sous-unité importine alpha-5 qui fonctionne comme un adaptateur dans l'import nucléaire de protéines et qui pourrait ainsi être impliquée dans la localisation nucléaire du complexe TSEN.

Comme la fonction principale du complexe TSEN est d'épisser les introns de certains ARNt, et comme il a déjà été démontré que les mutations de *CLP1* entraînent une accumulation d'ARNt contenant des introns, nous avons effectué un séquençage des ARNt (tRNA-seq) sur des LCLs d'un l'individu sain et du patient avec SNCR portant la mutation intronique Ins47. Les données préliminaires montrent un nombre accru de « reads » correspondant aux régions introniques suggérant une augmentation de la quantité d'ARNt non épissés chez le patient avec SNCR. De plus, pour mieux comprendre les mécanismes cellulaires responsables de l'atteinte

rénale, nous avons diminué l'expression de *TSEN54* dans des podocytes humains immortalisés pour mimer l'effet de la mutation Ins47. Nous avons démontré une diminution de la prolifération et de la synthèse protéique dans les podocytes exprimant peu de TSEN54. De manière inattendue, nous n'avons pas mis en évidence une apoptose accrue qui aurait pu expliquer cette diminution de la prolifération cellulaire.

Enfin, pour tenter de comprendre pourquoi les mutations *TSEN54* entraînent un phénotype rénal et/ou neurologique, nous avons généré des lignées iPSC à partir du patient avec SNCR et du père du patient GAMOS porteur de la mutation Ins47 à l'état hétérozygote, cette dernière lignée iPSC ayant ensuite été génétiquement modifiée par CRISPR/Cas9 pour mimer le génotype du patient GAMOS. Par la suite, pour obtenir les types cellulaires pertinents pour la maladie, ces lignées iPSC ont été différenciées en cellules souches neurales (NSCs), en neurones corticaux et organoïdes rénaux.

À ce jour, plusieurs expériences sont en cours, notamment des analyses des profils transcriptomiques des NSCs et des podocytes isolés à partir d'organoïdes rénaux, des analyses des défauts d'épissage des introns (tRNA-seq) et l'étude de divers processus cellulaires dans les NSC. Au total, ces résultats aideront à mieux appréhender les mécanismes cellulaires et moléculaires pathologiques liés aux mutations du gène *TSEN54* et responsables du SNCR et du GAMOS.

TABLE OF CONTENTS

List of Figures 1

Abbreviations 3

INTRODUCTION 7

CHAPTER ONE: KIDNEY 8

1. Structure and function 8

2. Nephron and glomerular filtration barrier 9

    2.1 Nephron, the functional unit of the kidney 9

    2.2 Glomerular filtration barrier (GFB) 10

3. Podocytes and slit diaphragm 12

    3.1 Podocyte structure 12

    3.2 Slit diaphragm 14

4. Nephrogenesis and glomerulogenesis 17

CHAPTER TWO: NEPHROTIC SYNDROME 20

1. Clinical and pathological aspects of NS 20

    1.1 Clinical aspects 20

    1.2 Histopathological aspects 22

2. Genetic causes and molecular basis of SRNS 23

CHAPTER THREE: GALLOWAY-MOWAT SYNDROME 30

1. Clinical and pathological aspects 30

2. Genetic causes and molecular basis 31

    2.1 snRNA processing 32

    2.2 tRNA modifications 33

        2.2.1 t^6A biosynthesis pathway 33

        2.2.2 m^7G modification 34

    2.3 Nucleoporins 34

    2.4 Transcriptional regulator 35

CHAPTER FOUR: tRNA IN HUMAN PHYSIOLOGY AND PATHOPHYSIOLOGY 36

1. tRNA life cycle 36

    1.1 Biogenesis, structure and function 36

1.2 Processing and maturation of tRNAs: overview 38
1.2.1 Early enzymatic processing 39
1.2.2 Intron excision process and ligation in yeast 41
1.2.3 Intron excision process and ligation in mammalians 42
1.2.4 Late enzymatic processing 44
1.3 Post-transcriptional modifications 44
1.4 tRNA subcellular localization 46
1.4.1 Export of tRNAs 47
1.4.2 Retrograde tRNA nuclear import 49
1.4.3 tRNA re-export 49
1.5 tRNA degradation 50
2. tRNA Splicing Endonuclease (TSEN) complex 52
3. tRNA metabolism alterations and Pontocerebellar hypoplasia (PCH) 54
3.1 Clinical and pathological aspects of PCH 54
3.2 Genetic causes and molecular basis of PCH 56
CHAPTER FIVE: DISEASE MODELLING USING iPSCs 59
1. Induced pluripotent stem cells (iPSCs) 59
1.1 General characteristics 59
1.2 iPSC reprogramming 59
2. Combination of CRISPR-Cas 9 and iPSC technologies 60
2.1 CRISPR-Cas 9 principle 60
2.2 Applications in iPSC-based disease modelling 62
3. iPSC differentiation 63
3.1 iPSC-derived kidney organoid 64
3.2 iPSC-derived neural stem cells (NSCs) 66
CONCLUSIONS 70
RESULTS 72
1. Article: Mutations in *TSEN54* are a novel cause of steroid-resistant nephrotic syndrome and Galloway-Mowat syndrome 73
2. Complementary data 112
MATERIAL AND METHODS 138

DISCUSSION AND CONCLUSIONS 155
REFERENCES 171

List of Figures

Figure 1: Schematic representation of the kidney anatomy.

Figure 2: Nephron structure, the functional unit of the kidney.

Figure 3: Glomerulus and the glomerular filtration barrier.

Figure 4: Ultrastructure of the podocyte.

Figure 5: Schematic representation of podocyte architecture.

Figure 6: The slit diaphragm zipper-like structure.

Figure 7: Schematic representation and main molecular components of the slit diaphragm.

Figure 8: Schematic representation of linear segregation of the ureteric bud (UB) and the metanephric mesenchyme (MM).

Figure 9: Schematic representation of nephrogenesis.

Figure 10: Podocytes maturation during nephrogenesis.

Figure 11: Podocyte structure in physiological conditions and upon injury.

Figure 12: Range of glomerular lesions caused by INS

Figure 13: Podocyte genes associated with steroid-resistant nephrotic syndrome.

Figure 14: Microcephaly.

Figure 15: Overview of the cell's cycle of tRNAs in mammalian.

Figure 16: General tRNA cloverleaf structure.

Figure 17: Schematic representation of subtypes of tRNAs containing intron.

Figure 18: Overview of tRNA splicing in yeast.

Figure 19: Overview of tRNA maturation pathways in different organisms, which utilize different enzymes to generate mature tRNA.

Figure 20: Most frequent tRNAs modifications (1).

Figure 21: Most frequent tRNAs modifications (2).

Figure 22: tRNA nuclear-cytoplasmic dynamics in eukaryotic cells.

Figure 23: Overview of tRNA splicing in vertebrates.

Figure 24: Typical structural brain abnormalities in PCH type 2 or type 4&5.

Figure 25: Pie-chart showing the proportion of patients affected by PCH per PCH-related pathological pathway

Figure 26: Overview of the CRISPR-Cas9 system.

Figure 27: Overview of the CRISPR-Cas9-mediated DSB mechanism

Figure 28: Overview of protocols for the generation of kidney organoids from human iPSCs.
Figure 29: Schematic representation of neurogenesis in vivo and in vitro
Figure 30: Schematic representation of all results and hypothesis

Abbreviations

AD: Autosomal dominant

AMP: Adenosine monophosphate

ANG: Angiogenin

aPKC: Atypical protein kinase C

AR: Autosomal recessive

ATP: Adenosine triphosphate

Cas9: CRISPR-associated protein 9

cDNA: Complementary DNA

CD2AP: CD2-Associated Protein

CHIR: Wnt agonist CHIR99021

CLP1: Cleavage factor polyribonucleotide kinase subunit 1

CM: SIX2+ cap mesenchyme

CNS: Central nervous system

CRISPR: Clustered regularly interspaced short palindromic repeat

crRNA: CRISPR RNA

DMS: Diffuse mesangial sclerosis

DNA: Deoxyribonucleic acid

DSB: Double-strand break

dsDNA: Double-strand DNA

EM: Electron microscopy

ER: Endoplasmic reticulum

ESCs: Embryonic stem cells

ESRD: End-stage renal disease

FACS: Fluorescence-activated cell sorting

FGF: Fibroblast growth factor

FP: Foot processes

FSGS: Focal segmental glomerulosclerosis

GAMOS: Galloway-Mowat syndrome

GBM: Glomerular basement membrane

GFB: Glomerular filtration barrier

GFP: Green fluorescent protein

GDP: Guanosine-5'-diphosphate

GTP: Guanosine-5'-triphosphate

gRNA: Guide RNA

HA: Human influenza hemagglutinin

HDR: Homology-directed repair

HEK293: Human embryonic kidney 293 cells

ICM: Inner cell mass

IF: Immunofluorescence

INS: Idiopathic Nephrotic Syndrome

IP: Immunoprecipitation

iPSCs: Induced pluripotent stem cells

LCLs: Lymphoblastoid cell lines

kDA: Kilo Dalton

KD: Knock down

KEOPS: Kinase, endopeptidase and other proteins of small size (complex)

KI: Knock-in

KO: Knock-out

MCD: Minimal change disease

MET: Mesenchymal-to-epithelial transition

MM: Metanephric mesenchyme

MRI: Magnetic resonance imaging

mRNA: Messenger RNA

NSCs: Neural stem cells

Neph1: Immunoglobulin superfamily nephrin like protein-1

NHEJ: Non-homologous end joining

NMD: Nonsense-mediated RNA decay

NPCs: Nephron progenitor cells

NPCs: Neural progenitor cells

NS: Nephrotic syndrome

N-WASP: Neuronal Wiskott-Aldrich syndrome

OCT4: Octamer-binding transcription factor 4

PA: Pretubular aggregates

PAK: p21 activated kinase

PAM: Protospacer-adjacent motif

Par3: Par-3 Family cell polarity Regulator

Par6: Par-6 Family cell polarity Regulator Alpha

PBMC: Peripheral blood mononuclear cell

PBS: Phosphate-buffered saline

PCH: Pontocerebellar hypoplasia

PCR: Polymerase chain reaction

PI3K : Phosphoinositide 3-kinase

PSC: Pluripotent stem cell

qPCR: Quantitative PCR

RNA: Ribonucleic acid

RT: Reverse transcription

RV: Renal vesicle

SD: Slit diaphragm

SEM: Scanning electron microscopy

SNP: Single nucleotide polymorphism

SRNS: Steroid resistant nephrotic syndrome

SSNS: Steroid sensitive nephrotic syndrome

ssODNs: Single-stranded donor oligonucleotides

TEM: Transmission electron microscopy

tiRNAs: tRNA-derived stress-induced RNAs

tracrRNA: Trans-activating crRNA

tRFs: tRNA-derived fragments

tRNA: Transfer ribonucleic acid

TRPC6: Transient receptor potential channel, subfamily C, member 6

TSEN: tRNA Splicing Endonuclease complex

UB: Ureteric bud

VZ: Ventricular zone

WB: Western blotting

WT: Wild type

ZO-1: Zonula occludens-1

INTRODUCTION

CHAPTER 1: KIDNEY

1. Structure and function

The kidneys are the main functional organs of the urinary system lying in the retroperitoneal space of the abdominal cavity. The kidneys receive the blood supply from paired renal arteries that originate from the abdominal aorta and enter the kidney via the hilum. On the other hand, blood exits the kidneys via the paired renal veins to join the inferior vena cava. The kidneys are attached to the ureters, which come out of the hilum and carry the urine to the bladder, where it is stored. Finally, the urine is excreted through the urethra. Each kidney is surrounded by tough fibrous connective tissue, called the renal capsule. The renal parenchyma is divided into two main structures: the innermost one is called the renal medulla and the outer one is called the renal cortex. The medullary portion is composed of numerous roughly triangular-shaped structures, called renal pyramids. They carry urine into structures called renal calyxes. In turn, these structures converge towards the renal pelvis. Then, the urine is channeled from the pelvis into the ureter. The renal cortex, includes microscopic filtering structures called nephrons. These small functional units filter 180 liters of plasma every day, giving rise to the formation of the primitive and then the definitive urine. There are around one million nephrons in each kidney (**Figure 1**).

The primary function of the kidneys is excretion. This is achieved by filtering all blood components as selectively as possible. The modification of the filtered fluid guarantees the homeostasis, the acid-base balance, the water-electrolyte balance and the regulation of arterial blood pressure. Water, glucose and amino acids are reabsorbed, whereas the catabolites eliminated in the urine include uric acid, urea, ammonia, creatinine and as well as metabolic waste products or toxic compounds. Finally, but not less important, the kidneys secrete different hormones including calcitriol, erythropoietin and renin.

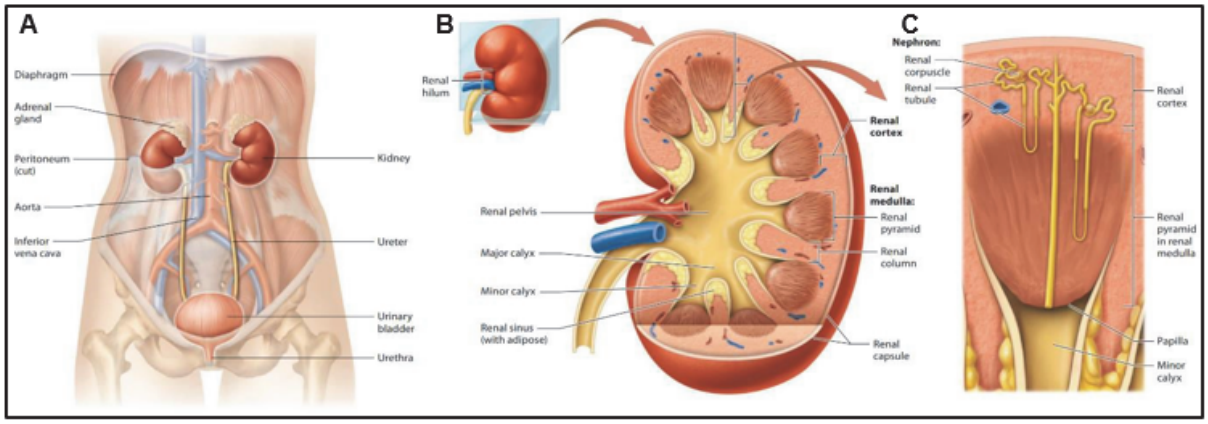

Figure 1: **Schematic representation of the kidney anatomy.** (**A**) Location of the kidneys, (**B**) kidney internal anatomy, frontal section (**C**) Renal parenchyma anatomy. (From Human Anatomy & Physiology, by Erin C. Amerman 2019)

2. Nephron and glomerular filtration barrier

2.1 Nephron, the functional unit of the kidney

Each nephron consists of a glomerulus and tubules. The glomerulus enables the ultrafiltration of the plasma. More precisely, blood enters the glomerulus through the afferent arteriole, which branches into a network of capillaries intertwined called the capillary tuft. The blood is then filtered through a glomerular filtration barrier to produce the plasma filtrate, or primary urine, and the filtered blood exits the glomerulus through the efferent arteriole. The glomerulus is surrounded by the Bowman's capsule or the urinary chamber that allows the fine adjustment of the hydrostatic pressure inside the capillaries. Furthermore, this chamber will collect the primary urine that will be thereafter poured into the renal tubules. The renal tubule is divided into several portions along the nephron. The first segment is called the proximal tubule, and the final segment is called the distal tubule. Between the proximal and distal tubule, there is another duct, the so called loop of Henle, in which it is possible to distinguish a descending and an ascending limbs (**Figure 2**). These structures will then modify the primary filtrate through the secretion and reabsorption of small molecules, electrolytes and water, to finally produce the final urine.

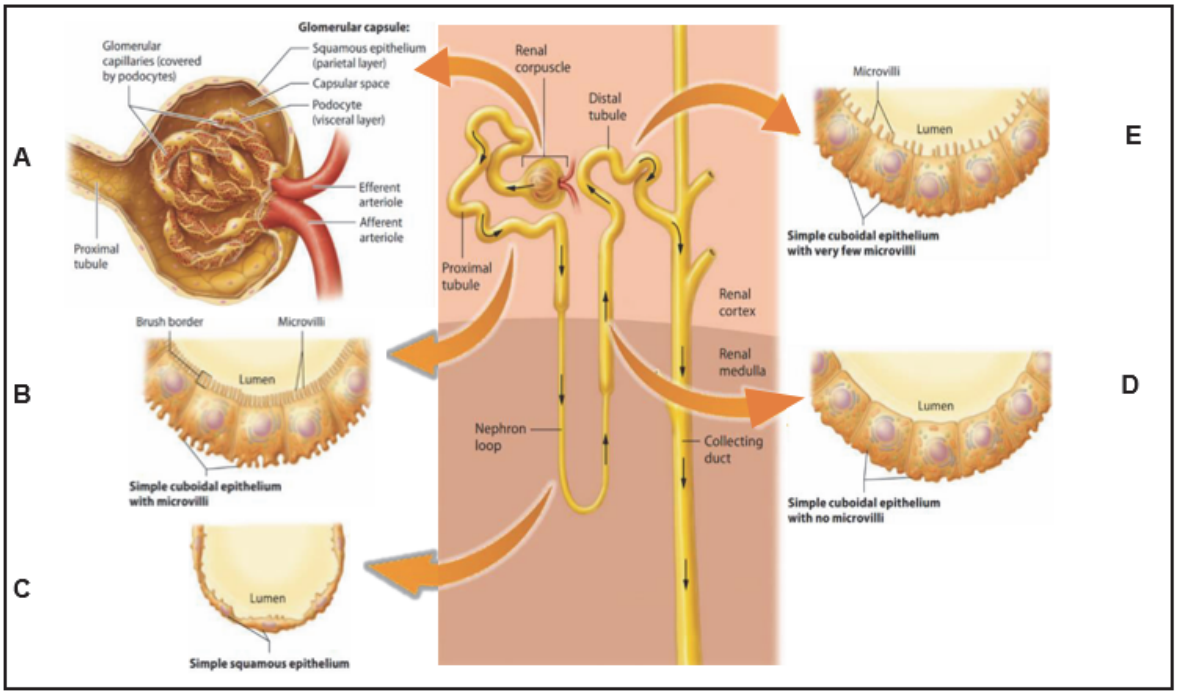

Figure 2: Nephron structure, the functional unit of the kidney (**A**) Glomerulus. The whole is enclosed in the glomerular capsule, (**B**) Proximal tubule. (**C**) Hense's loop thin descending limb. (**D**) Hense's loop thick ascending limb. (**E**) Distal tubule. (From Human Anatomy & Physiology, by Erin C. Amerman 2019)

2.2 Glomerular Filtration Barrier (GFB)

The interface between the circulating blood and the urinary chamber in the glomerulus, is called the glomerular filtration barrier (GFB). Schematically, the GFB is composed of three different layers (**Figure 3**):

- the fenestrated endothelium of glomerular capillaries (Satchell and Braet 2009) which, prevents the passage of cellular elements of the blood, including erythrocytes, leucocytes and platelets, thanks to the presence of large fenestrations with an average diameter of 150 nm. Furthermore, the negative charge of the endothelial glycocalyx prevents the filtration of negatively charged molecules/proteins. Therefore, it represents the principal regulator of vascular permeability;

- the meshwork-like glomerular basement membrane (GBM) (Kretzler 2002; Farquhar 2006) which constitutes an obstacle to the passage of high molecular weight proteins. The GBM is a sheet of extracellular matrix, with a thickness of 300 nm, containing pores with a diameter of 10 nm. It is mainly composed of four major macromolecules: laminins (α5β2γ1), type IV collagen

(α3α4α5), in particular COL4A5, which is expressed only in the GBM and in the skin, agrin, and nidogen (Suh and Miner 2013; Lennon *et al.* 2014);

- the highly specialized epithelial cells called podocytes (Sahali *et al.* 2012), which constitute the final layer. They play a key role in GFB permeability, thanks to their architecture that surrounds the outer surface of glomerular capillaries and because podocytes are covered by a glycocalyx composed of sialyated glycoconjugates, such as podocalyxin, and sulfated molecules.

The maintenance of perm-selectivity, guaranteeing a great size-based selection and a negatively charge selectivity of the filtered elements, constitutes the main role of the glomerular filtration barrier. This means that in homeostatic physiological conditions, GFB facilitates the flow of plasma water, ions, products of cellular metabolism and small proteins with a molecular weight lower than 60-70 kDa. On the other hand, it restricts the flow of blood cells or high molecular weight proteins (Kalluri 2006). Defect in either one or all of the layers of the GFB could be detected with the presence of high amounts of albumin in the urine.

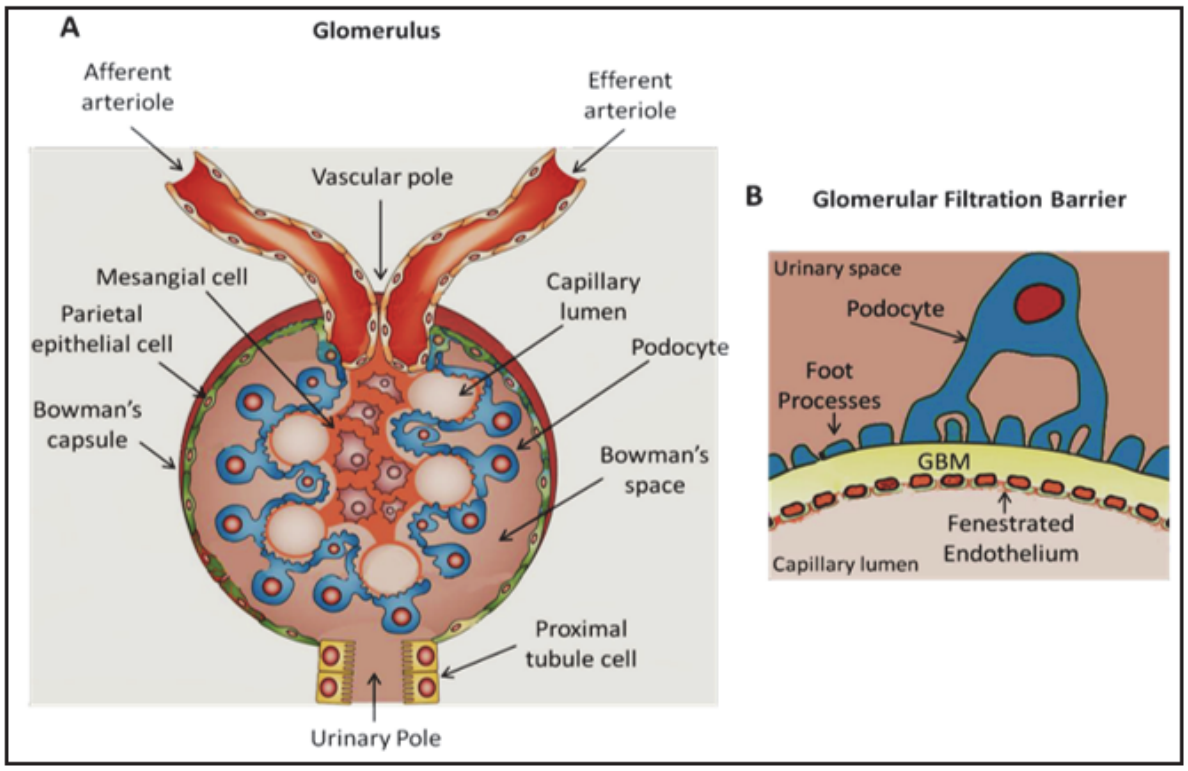

Figure 3: Glomerulus and the glomerular filtration barrier. (**A**) Structure of the glomerulus. (**B**) The glomerular filtration barrier and the three layers: the fenestrated endothelial cells, the glomerular basement membrane (GBM) and the podocytes. (From Patrakka *et al*. 2010, and Shankland *et al*. 2014)

3. Podocytes and slit diaphragm

3.1 Podocyte structure

Mature podocytes are post-mitotic differentiated epithelial cells with a particular octopus-shaped architecture. They have extended processes that interdigitate each other and organize into a network. Podocyte's processes cover the outer surface of the capillary loops at the GBM (**Figure 4**). Podocytes are continuously exposed to mechanical forces and toxins, arising from the filtrate flow. Therefore, they have high plasticity and dynamics and express mechanosensors such as, MEC-1 or MEC-12 (Huber *et al.* 2007).

Podocytes have a large cell body which floats in the urinary space, maintained by thick elongated cell extensions, called primary processes which emanate from the cell body. These primary processes have a cytoskeleton enriched in intermediate filaments, such as vimentin and nestin, and microtubules (Chen *et al.* 2006). They branch further into narrow, interdigitated secondary processes called foot processes (FP) or pedicels that are enriched in actin filaments (Andrews 1981; Kriz *et al.* 1994; Ichimura *et al.* 2003). These pedicels cover the glomerular capillaries (Pavenstädt *et al.* 2003) (**Figure 5**).

Three domains can be distinguished in the podocyte:

- the apical domain, which is covered by an anionic, negatively charged glycocalyx, mainly composed of glycosaminoglycans and sialoproteins, such as the podocalyxin. The glycocalyx maintains the structure of the podocyte, exerting a repulsive force between them, and is also involved in the size selectivity of the GFB (Kerjaschki *et al.* 1984; Pavenstädt 1998; Lawrence *et al.* 2017);

- the junctional domain, which is composed of a particular type of intercellular junction called the slit diaphragm (SD), bridges the foot processes of adjacent podocytes. This structure regulates the selective permeability in the glomerulus;

- the basal domain, which includes the pedicels, the only constituent of podocytes that interacts with the GBM through integrins, in particular α3β1, α1β1 and α2β2 which bind to laminin and type IV collagen, respectively (Mathew *et al.* 2012). Podocytes also attach to GBM via dystroglycan α and β, which also links podocyte actin with GBM laminin and syndecans (Perico 2016).

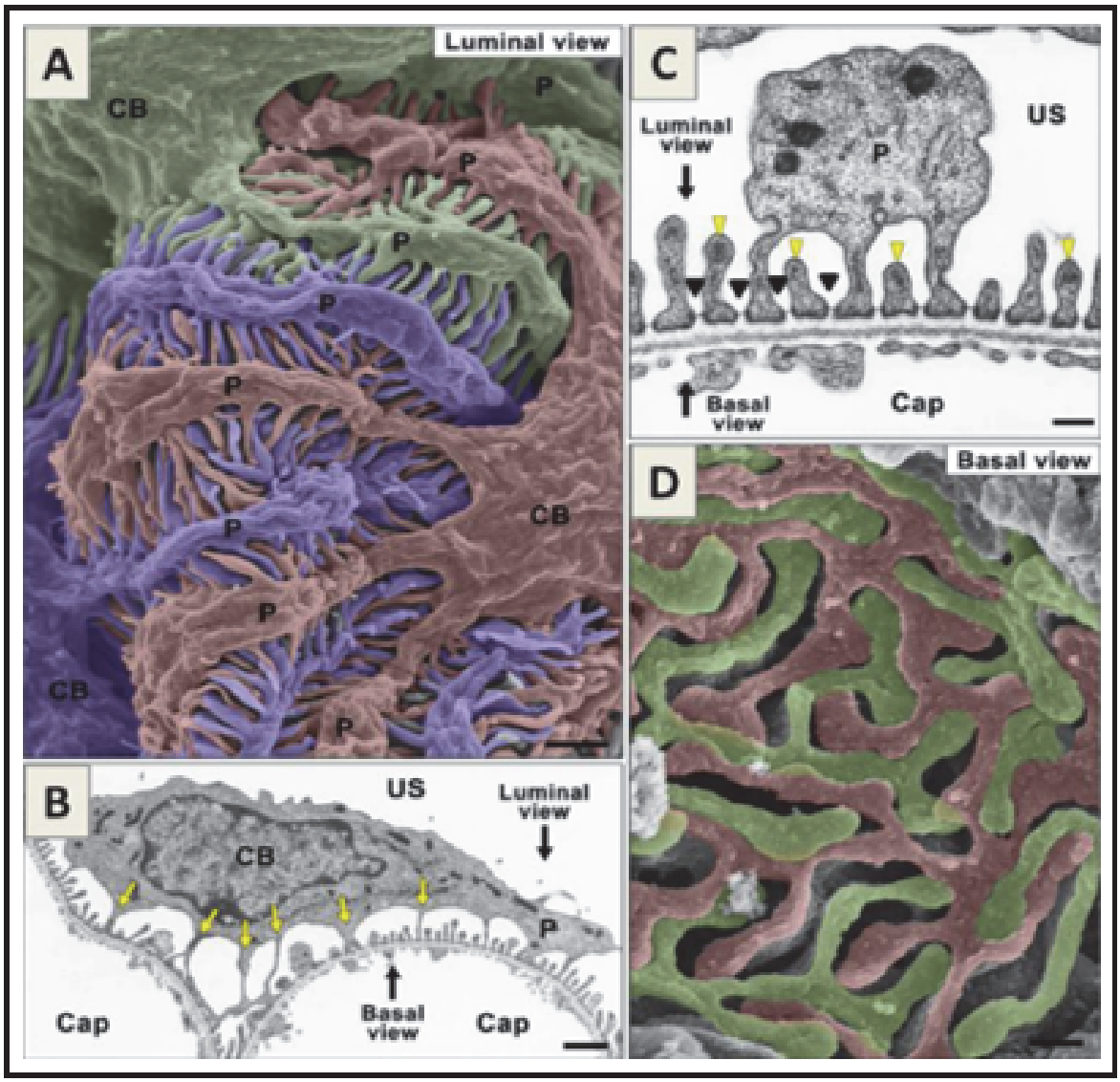

Figure 4: Ultrastructure of the podocyte. (**A**) Scanning electron microscopy images showing the cell body, primary and secondary processes, and foot processes. Individually colored in purple, green and red, foot processes interdigitate among them, (**B**) Transmission electron microscopy images. Foot processes encircle the capillary loops. Yellow arrows point to foot processes protruding from its cell body, (**C**) Transmission electron microscopy images. The thin grey line between neighboring foot processes, correspond to the slit diaphragm (black arrows). Yellow arrows represent electron dense actin-bundle in the apical cytoplasm of foot processes, (**D**) S Electron Microscopy images of the basal surface of podocytes. Bar scales, 1μm in (**A**), (**B**); 200 nm in (**C**), (**D**). (From Ichimura *et al*. 2015.)

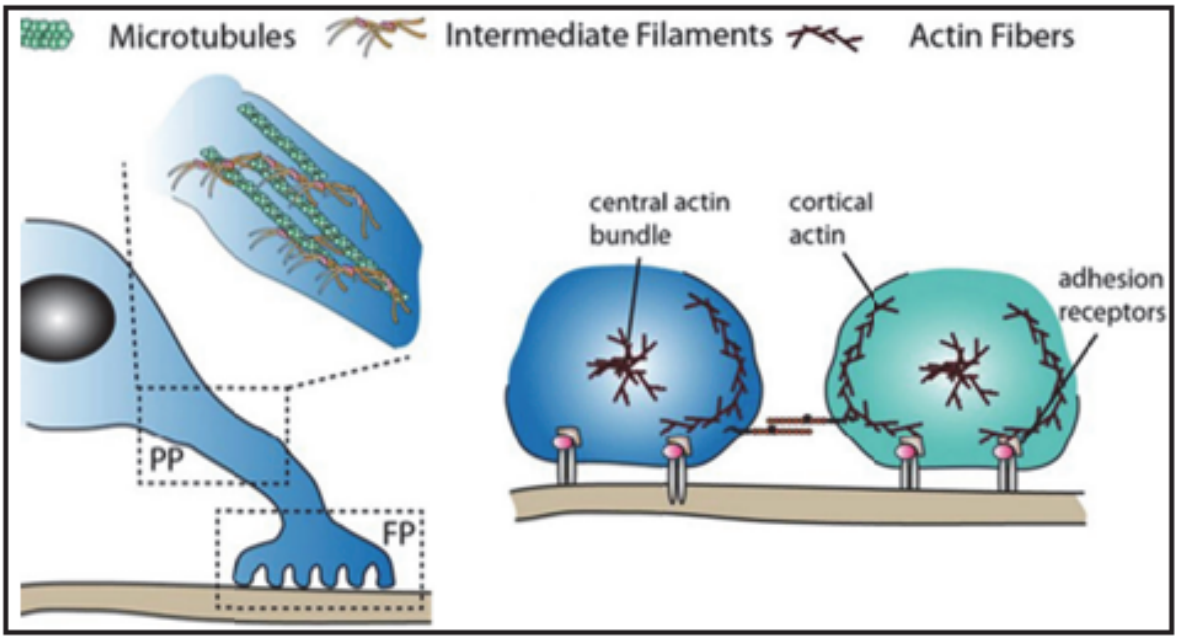

Figure 5: Schematic representation of podocyte architecture. On the left, primary processes (PP) are composed by microtubules and intermediate filaments. On the right, PP further divide into secondary processes, called foot processes (FP), and mainly composed by actin-rich foot processes projection. (From Schell *et al.* 2017.)

3.2 Slit diaphragm

As already mentioned, podocyte foot processes completely surround the capillary loops and are connected to each other through intercellular junctions called slit diaphragms (SD) (Tryggvason et al. 2006). The SD allows the flow of water and small solutes but limit the flow of large molecular weight proteins (Gagliardini *et al.* 2010). SD is a modified intercellular junction with histological features of both tight and adherent junctions. It expresses tight junction proteins such as ZO-1, cingulin and occluding (Schnabel *et al.* 1990; Fukasawa *et al.* 2009), and adherent junction proteins such as, α,β,γ, catenin proteins and P-cadherin (Reiser *et al.* 2000; Lehtonen *et al.* 2004).

The classic view of the slit diaphragm was a static ultrathin electron-dense zipper-like structure functioning as a sieve with pores of 4x14 nm width (Rodewald and Karnovsky 1974; Karnovsky and Ryan 1975). Adjacent transmembrane proteins of podocytes cross the extracellular space and arranged in a thick midline (**Figure 6**). However, this three-dimensional protein network, with an extremely ordered and periodic structure, has been recently described as extremely dynamic, constituting a direct physical barrier to the passage of macromolecules (Grahammer *et al.* 2016).

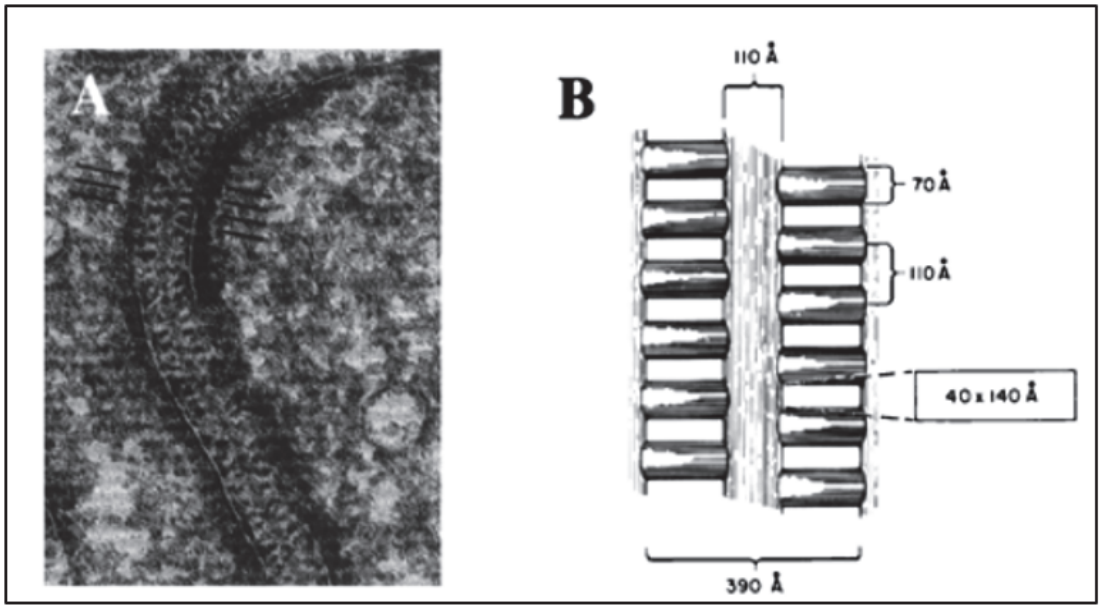

Figure 6: The slit diaphragm zipper-like structure. (**A**) SD of a glomerulus in rat, (**B**) schematic representation of a slit diaphragm. (From Rodewald *et al.* 1974).

The advent of genetics have made a huge contribution to precisely define the molecular structure of the SD. The discovery of nephrin first (encoded by *NPHS1*) followed by the podocin later (encoded by *NPHS2*), constituted the first steps in the molecular characterization of the SD (Kestila and Lenkkeri 1998; Ruotsalainen *et al.* 1999; Boute *et al.* 2000; Wartiovaara *et al.* 2004; Bouchireb *et al.* 2014). Nephrin, which belongs to the immunoglobulin (Ig) superfamily, is a type I transmembrane glycoprotein composed of a large extracellular domain, which contains eight C2-type Ig-like domains and a fibronectin type III domain, and an intracellular cytoplasmic domain. Whereas, podocin is a hairpin-like membrane protein anchored to the inner leaflet of the plasma membrane, shown to interact with nephrin. These discoveries have been followed by those of other essential components including the immunoglobulin superfamily nephrin like protein-1 (Neph1), the transient receptor potential cation channel subfamily C member 6 (TRPC6) and the adapter protein CD2 Associated Protein (CD2AP).

The extracellular overlapping layers of the SD are mainly composed of nephrin and neph1 transmembrane proteins which cover the interpodocyte space. It was initially shown that adjacent podocytes were able to interact forming either homodimer nephrin/nephrin or neph1/neph1 or heterodimer nephrin/neph1 complexes and these dimers constitute the central dense zone observed in the zipper-like structure of the SD. However, recently high resolution ultrastructural studies

(Grahammer *et al.* 2016) have shown that within adjacent podocytes, we find more often interactions in trans of nephrin/nephrin and neph1/neph1 homodimer, with the particularity that the homodimers neph1/neph1 span the SD closer to the GBM (with a width of 23 nm), whereas nephrin/nephrin homodimers span the SD closer to the apical domain (with a width of 45 nm) (**Figure 7**) (Burghardt *et al.* 2015; Grahammer *et al.* 2016).

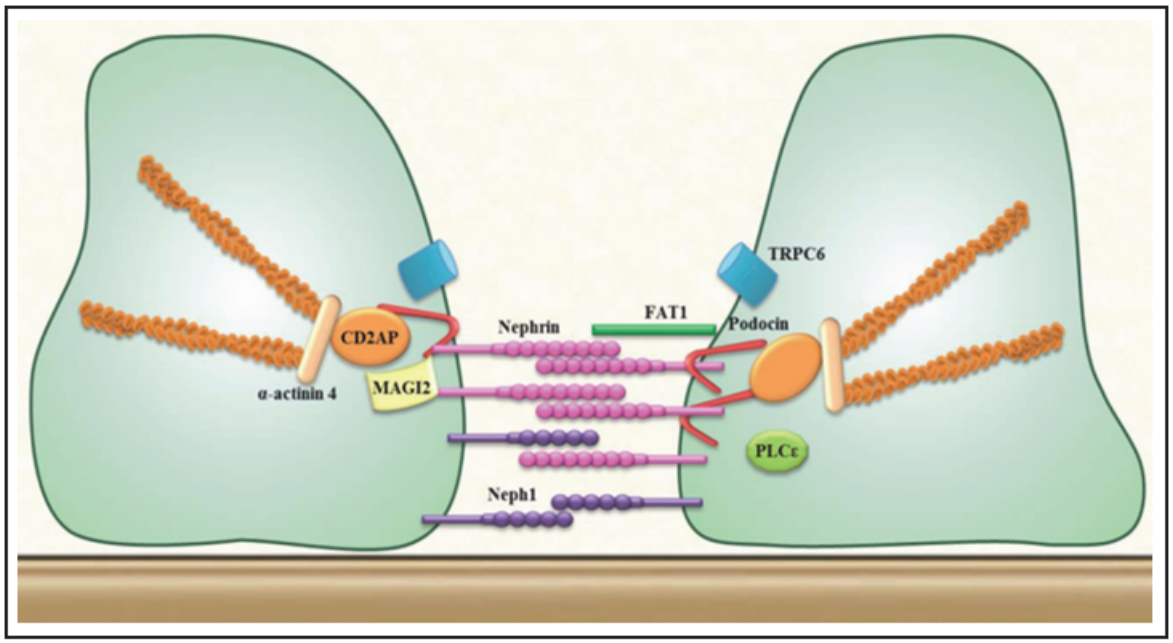

Figure 7: Schematic representation and main molecular components of the slit diaphragm. (Adapted from Grahammer *et al.* 2013).

SD proteins do not only serve as a linker to the actin cytoskeleton of podocytes, but also play a key role as signaling platform binding cytosolic proteins affecting the polarity, the survival, the membrane trafficking and the organization of actin within podocytes (Grahammer *et al.* 2013). For example, the intracellular domain of the nephrin contains several highly conserved tyrosine motifs that can be phosphorylated by different tyrosine kinases such as Fyn, Lyn and Src (Verma *et al.* 2003; Lahdenperä *et al.* 2003; Li 2004). The phosphorylation of these residues induce different intercellular signals that will give rise to various cellular events. If nephrin, once phosphorylated at the tyrosine motifs, binds p85 (the catalytic subunit of PI3K (phosphoinositide 3-kinase), this interaction leads to the activation of Akt and Rac1 pathways, which control cell growth, survival as well as the remodeling of the actin network (Huber *et al.* 2003; Canaud *et al.* 2013; Espiritu *et al.* 2019). Otherwise, if it binds Nck, the latter activates regulatory proteins of the

actin cytoskeleton such as p21 activated kinase (PAK) or the Neuronal Wiskott-Aldrich syndrome protein (N-WASP) (Jones *et al.* 2006; Verma 2006; Zhu *et al.* 2010).

4. Nephrogenesis and glomerulogenesis

In vertebrates, the intermediate mesoderm will give rise to the urogenital system, which is composed of kidneys, gonads and their respective duct systems. More specifically, kidneys derive from the anterior mesoderm-derived ureteric bud (UB) and posterior mesoderm-derived metanephric mesenchyme (MM) precursor tissues (**Figure 8**).

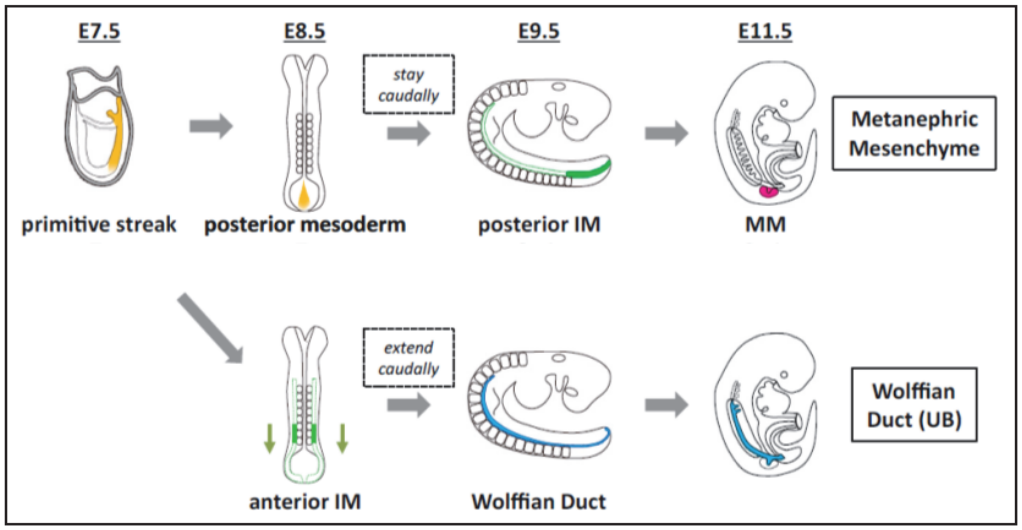

Figure 8: Schematic representation of linear segregation of the ureteric bud (UB) and the metanephric mesenchyme (MM). (From Taguchi *et al.* 2014).

Nephrogenesis begins at approximately five to six weeks of gestation and is characterized by three different anatomical states called: 1) pronephros, a rudimentary vestigial organ, 2) mesonephros, in charge of blood filtration during the fetal life, and 3) metanephros or mature kidney. Under the influence of different signals from the surrounding MM, mesonephros begins to take form with the budding outgrowth from the nephric duct, also called the Wolffian duct (**Figure 9**). Afterwards, the budding will generate the UB, which will start to sprout into the MM. The SIX2+ cap mesenchyme (CM) is formed once the surrounding MM condenses around the sprouting UB tips. The dichotomous sprouting of the UB, which will form the collecting ducts and ureters, is further ensured by a positive feedback loop between CM and UB which release GDNF and Wnt11, respectively. Meanwhile, the UB secretes also Wnt9b. This secretion causes CM cells to

differentiate into pretubular aggregates (PA). Furthermore, fibroblast growth factor (FGF) 8 and Wnt4 signals, in the PA, induce LIM homeobox 1, which in turn initiates mesenchymal-to-epithelial transition (MET). This results in the formation of a lumen, called the renal vesicle stage (RV) (Vainio and Lin 2002).

The glomerulogenesis, includes four different phases also known as: 1) the aforementioned vesicle phase or renal vesicle, 2) comma shaped-body phase, 3) S-shaped body phase with the development of capillary loops, and finally 4) the maturation phase (Takano *et al.* 2007) (**Figure 9**).

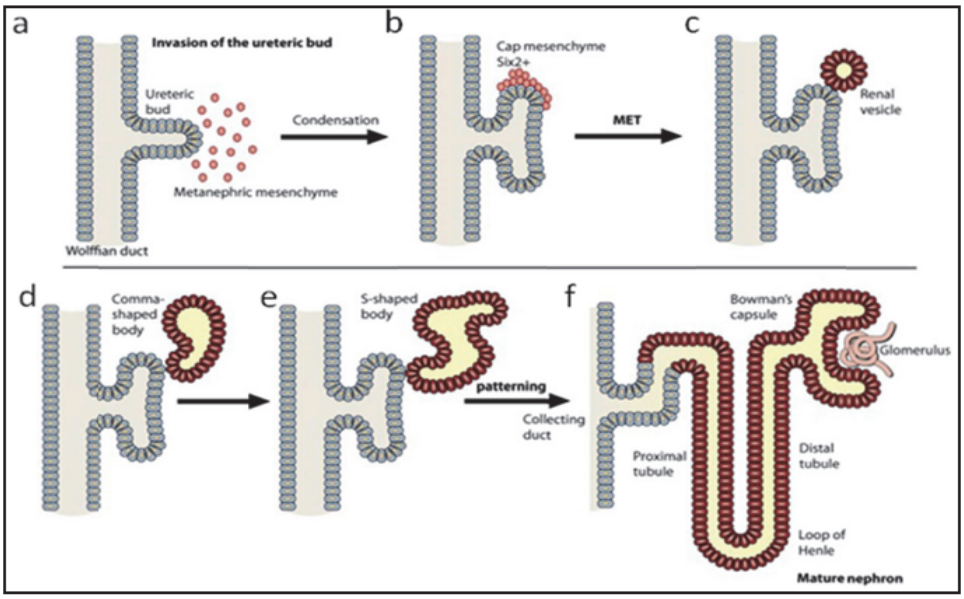

Figure 9: Schematic representation of nephrogenesis. Nephrogenesis begins with the budding outgrowth from the nephrotic duct or Wolffian duct (**a**) followed by the condensation of metanephric mesenchymal cells (**b**), which give rise to the renal vesicle (**c**). During the progressive formation of the comma-body shape (**d**), followed by the S-shape body (**e**), progenitor renal cells are already present. During maturation, progenitor cells move on the nephron and epithelial cells invade the inferior cleft of the S shape body to give rise to glomerular capillaries (**f**). (From Hohenstein Genes Dev 2015)

The RV starts to bend, elongates, and patterns to generate the comma-shaped body and subsequently the S-shaped body. Finally, the S-shaped body continues to differentiate and to transform into the mature nephron, which is connected to the UB-derived collecting duct system. It is important to underline the fact that the cells that will give rise to the glomerulus differentiate from the inferior cleft of S-shaped body. Epithelial cells bordering S-shaped body are cuboidal progenitors, which will give rise to podocytes and to tubular cells (**Figure 10**). These cells are sealed by an apical belt of specific junctions expressing ZO-1 protein. The apical surface expansion

is related to the displacement of cell-cell contacts along the lateral cell side of primitive podocytes, which occupy the vascular cleft in the S-shaped body stage. In particular, when endothelial cells invade the inferior cleft of the S-shape body, and at the same time capillary loops begin to appear, podocyte precursors modify their lateral contacts which starts to migrate to the cell basal pole due to the migration of protein complex Par3-Par6-aPKC and of ZO-1 (Huber *et al.* 2009). Furthermore, adherens-like junctions appear at the basal part of the immature podocytes in parallel to development of capillary loops. At this stage, pedicels begin to arise and specific proteins such as nephrin, podocin and CD2AP begin to be expressed and are recruited to form the slit diaphragm (Kawachi 2000; Li *et al.* 2000; Boute *et al.* 2000). Finally, podocytes are characterized by the three distinct domains: the apical, the intermediate and the basal poles and, wrap around in-growing capillaries and become flatter. Podocyte cell bodies are isolated one from each other, and mature podocytes interdigitate their FPs.

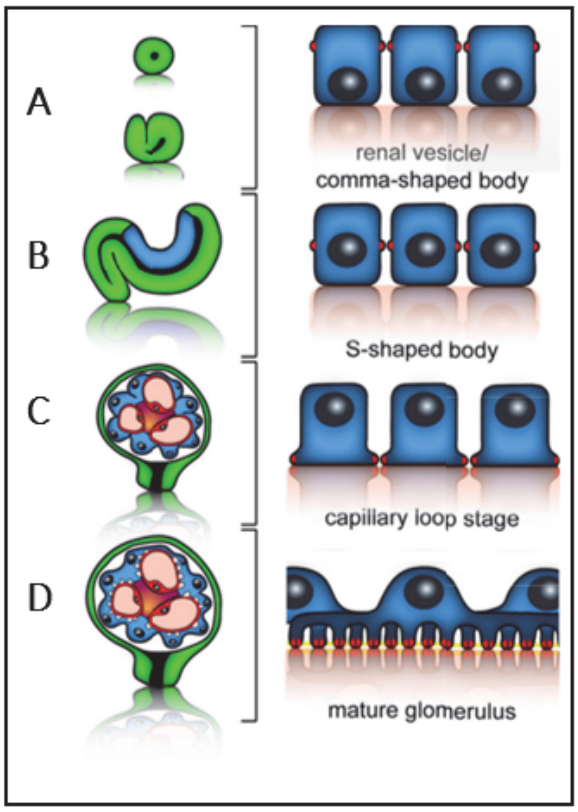

Figure 10: Podocytes maturation during nephrogenesis. (**A**) During the renal vesicle and comma-shaped body phases, podocyte progenitor cells are epithelial cells with junctions situated at the apical pole. (**B**) During the S-shaped body phase, cellular junctions start to migrate towards the basal pole. (**C**) Finally, during the formation of the capillary loops in immature glomeruli, cellular junctions are finally situated in the basal pole and specific proteins of slit diaphragm begin to be expressed in order to give rise to the mature glomerulus (**D**). (From Schell *et al.* 2014)

CHAPTER TWO: NEPHROTIC SYNDROME

1. Clinical and pathological aspects of NS

Podocytopathies defines a group of disorders characterized by podocyte injury and a constant clinical phenotype which is the proteinuria (**Figure 11**). The level of the proteinuria and its consequence on serum albumin level, clinically define the nephrotic syndrome. The earliest morphological hallmark of podocytopathies, which is visible by electron microscopy, is the foot process effacement. Histologically, it is characterized by the simplification or absence of the interdigitating foot processes of neighboring podocytes that lead to the slit diaphragm disappearance (Kriz *et al.* 2013).

1.2 Clinical aspects

Nephrotic syndrome (NS) is characterized by massive proteinuria > 3,5 g/day or 50mg/kg/day in children, and hypoalbuminemia < 3,0 g/dL or < 25g/L. This results in the onset of edema and hypercholesterolemia (Nishi *et al.* 2016). Furthermore, NS can increase the risk of cardiovascular complications, risk of infections and malnutrition. The persistence of the nephrotic syndrome leads to progressive damaging of the glomeruli (glomerulosclerosis), and to fibrosis of the tubular-interstitial compartment. This progresses to end-stage renal disease (ESRD) requiring patients to receive dialysis or kidney transplantation.

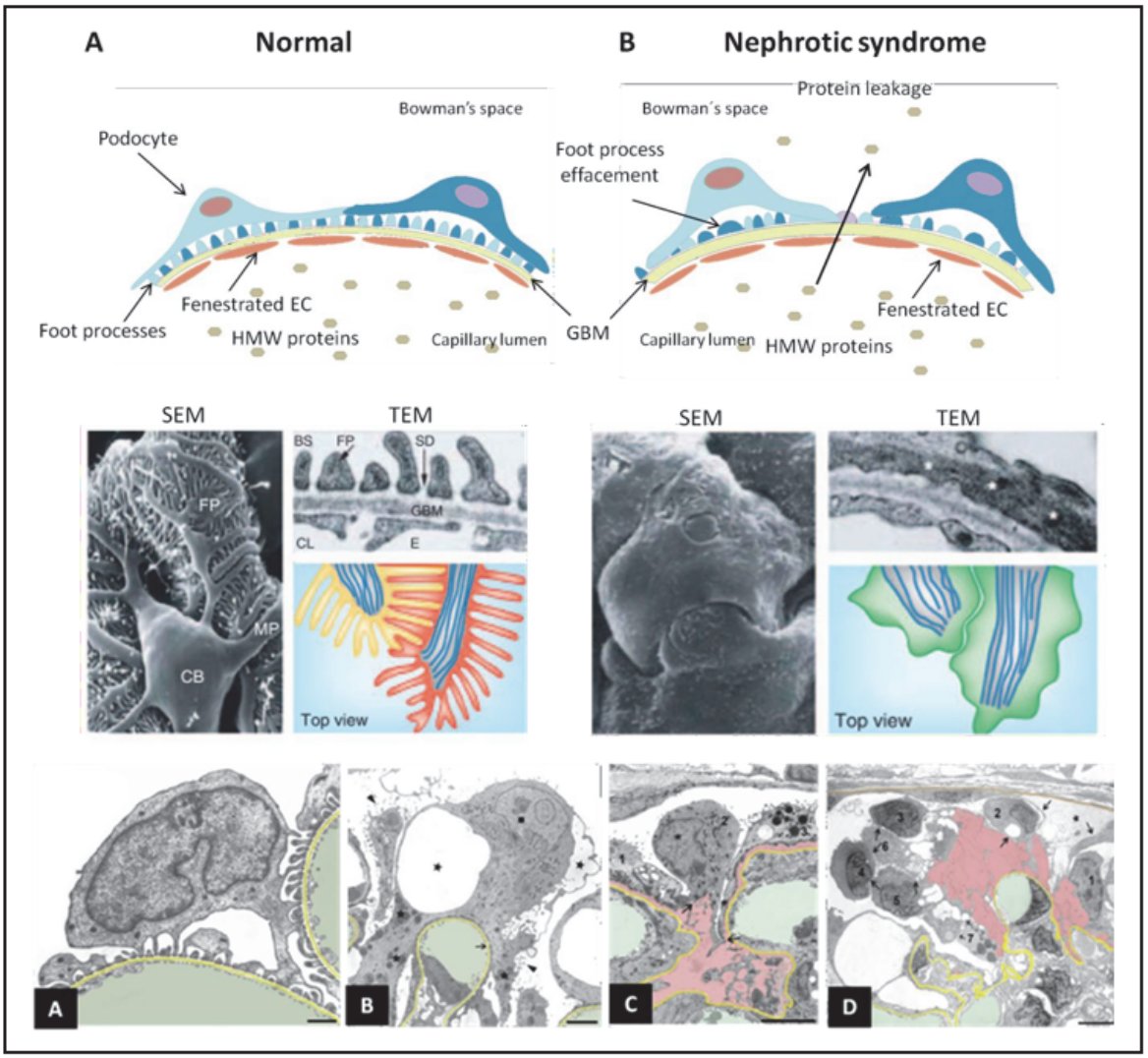

Figure 11: Podocyte structure in physiological conditions and upon injury. (**A**) Upper panel: glomerular filtration barrier in physiological conditions, composed of fenestrated endothelial cells (EC), GBM and podocytes. Middle panel: SEM and TEM images showing healthy podocytes and foot processes (FP), as well as the slit diaphragm (SD) and fenestrated endothelium (E) and a schematic of normal podocyte foot processes. (**B**) Upper panel: in nephrotic syndrome there is podocyte foot process effacement and protein leakage into the urine. Middler panel: SEM and TEM images showing podocyte foot process effacement and loss of SD. The corresponding schema shows a continuous sheet of cytoplasm instead of the well-defined foot process. HMW, high molecular weight; BS, Bowman's space; CL, Capillary lumen. (From Lin *et al.*2016 and Mundel *et al.* 2010.) Lower panel: ultrastructural changes accompanying podocyte injury and detachment. GBM is highlighted in yellow, capillaries in green and spaces between GBM and detaching podocytes in pink. (**A**) Normal podocytes (**B**), Podocyte effacement in response to injury, formation of pseudocysts (stars) and microvillous transformation of the podocyte apical membrane (arrow) (**C** and **D**) Podocyte detachment leaving areas of denuded GBM. Bar scales, 1µm in (**A**) 3 µm in (**B** and **C**); 5 µm in (**D**). (From Kriz *et al.* 2013)

Schematically, NS are divided into primary idiopathic (INS) and secondary glomerular disorders. The latter, includes glomerular damage due to systemic diseases such as metabolic

disorders (diabetes), infections, hematological or immunological disorders and the effects of nephrotoxic drugs. INS patients are usually treated with corticosteroid and the responsiveness to this treatment defines the disease as steroid-resistant (SRNS) or steroid-sensitive (SSNS).

For this reason, INS are defined in two forms:

1) Primary disorders, caused by structural defects of the glomerular filtration barrier and in particular of podocytes (hereditary podocytopathies), which are characterized by the absence of inflammation and immune deposits in biopsy samples. Patients affected with podocytopathies are resistant to immunosuppressants (SRNS), and they generally progress to end-stage renal disease (Kim *et al.* 2005; Wiggins 2007).

2) Immune NS glomerular disorders is caused by an immune defect, believed to be a circulating permeability factor of lymphocyte origin, which leads secondarily to podocytes damage (Antignac 2002). It is more common in children and affected patients respond to corticoids or immune-suppressor treatment. The prognosis is generally favorable in the vast majority of cases (SSNS).

Clinically, hereditary podocythopathies and immune NS glomerular disorders are indistinguishable. Symptoms and clinical presentation are almost the same. However, some differences such as, the presence of other affected organs, and the onset before one year of age, suggesting a genetic defect (Hinkes *et al.* 2007), allow for a distinction to be made. It is important to underlying the fact that, although SRNS do not respond to treatment, they are not likely to relapse after kidney transplantation (Ding *et al.* 2014).

1.2 Histopathological aspects

The most common histological glomerular lesion found in INS is the minimal change disease (MCD). In MCD, the glomeruli are normal or subnormal under light microscopy (**Figure 12**). However, by electron microscopy it is possible to observe the widespread foot process effacement. This feature is common to all histological forms of NS. MCD is more common in children whereas, patients affected by SRNS present major lesions of focal and segmental glomerulosclerosis (FSGS). FSGS is characterized by the sclerosis of a subset of the glomeruli (focal) and a portion of the glomerular tuft (segmental). Histologically, we can observed a segmental obliteration of the glomerular capillaries by extracellular matrix, together with

hyalinosis (**Figure 12**) (D'Agati 2008). The latter, corresponds to the accumulation of entrapped plasma proteins. By electron microscopy, we can observe foot process effacement associated with podocytes detachment. Finally, patients affected by congenital form of NS or Denys-Drash syndrome (caused by mutations in *WT1*) present diffuse mesangial sclerosis (DMS). In DMS, glomeruli are small and condensed, with a progressive sclerosis of the mesangial matrix without mesangial hypercellularity (**Figure 12**). The podocytes are generally hypertrophic over the capillary tuft.

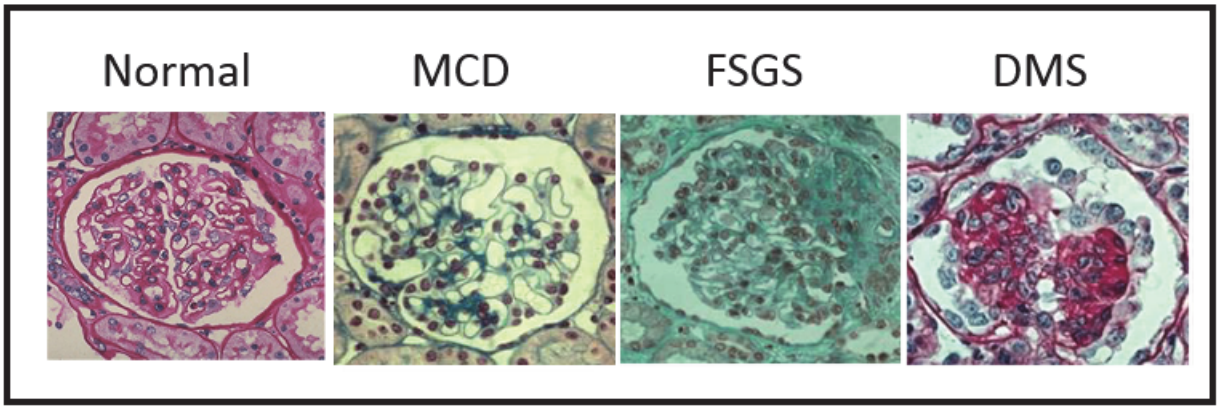

Figure 12: Range of glomerular lesions caused by INS. From left to right: Normal glomerulus, Minimal change disease (MCD), Focal and segmental glomerulosclerosis (FSGS), and Diffuse mesangial sclerosis (DMS) (Adapted from Barisoni *et al*. 2007).

2. Genetic causes and molecular basis of SRNS

Next generation sequencing coupled with DNA sequencing allowed us to better understand the complexity of the syndromic and non-syndromic forms of SRNS, and to highlight phenotypic variability, and revealed mutations in unexpected genes. The identification of more than 50 genes as monogenic causes of SRNS has helped decipher podocyte physiology and pinpoint its crucial role in the pathogenesis of the disease (**Figure 13**). The most frequently mutated genes, with an autosomal recessive pattern, in congenital and infantile NS are *NPHS1* and *NPHS2* (Sadowski *et al.* 2015) that encode nephrin and podocin, respectively, two major components of the SD. It is important to underline the fact that *NPHS1* and *NPHS2* are the first genes of the SD that have been identified. More frequent in young adults, with an incomplete penetrance and variable expressivity, are the mutations in *INF2* and *TRPC6*, which have an autosomal dominant pattern (Brown *et al.* 2014; Sadowski *et al.* 2015).

Monogenic SRNS, resulting in a kidney restricted phenotype and classified as non-syndromic SRNS, are due to mutations in specific genes such as *NPHS1*, *NPHS2*, *PLCE1*, *ACTN4*, *INF2*, *TRPC6*, *MYO1E* or *ADCK4* (Kaplan *et al.* 2000; Winn *et al.* 2005; Sanna-Cherchi *et al.* 2005; Ashraf *et al.* 2013).

However, mutations in one single gene can lead to additional organ involvement defining the syndromic SRNS. In the majority of the cases, the other affected organs are the central nervous system, the genital tract, eyes, muscles, bones or the immune system. Multiple genes are associated with syndromic SRNS, as mentioned in **Table 1**. Among them, it is important to point out mutations in genes encoding proteins for nuclear envelop NXF5 or NUP93, chromatin remodeling proteins such as SMARCAL1, transcription factors as WT1 and LMX1B, GBM components or adhesion molecules, such as Laminin β2 and Integrin α3, some cytoskeleton proteins such as WDR73, INF2 and MYH9, mitochondrial proteins COQ2, COQ10, PDSS2 or mitochondrial leucine tRNA encoded by *MT-TL1*, and lysosomal proteins such as SCARB2 (Pelletier *et al.* 1991; Barbaux *et al.* 1997; Dreyer *et al.* 1998; Ruf *et al.* 2004; Brown *et al.* 2010; Boyer *et al.* 2011, 2013). Therefore, multiple cellular pathways are associated with podocytopathies, underling the complexity of podocyte cells.

For example, *LAMB2*, encoding Laminin B2 subunit, is synthesized by the podocyte and contributes to the constitution of the GBM. However, mutations in this gene lead to a complex syndrome called Pierson syndrome associating renal, ocular, neuromuscular damage and central neurological dysfunctions. Furthermore, mutations in *INF2* can lead to Charcot-Marie-Tooth disease characterized by a peripheral neuropathy and renal defects (Brown *et al.* 2010), and mutations in *WDR73* which are linked with Galloway-Mowat syndrome that I will discuss later in the thesis (Colin *et al.* 2014; Braun, Shril *et al.* 2018; Arrondel *et al.* 2019).

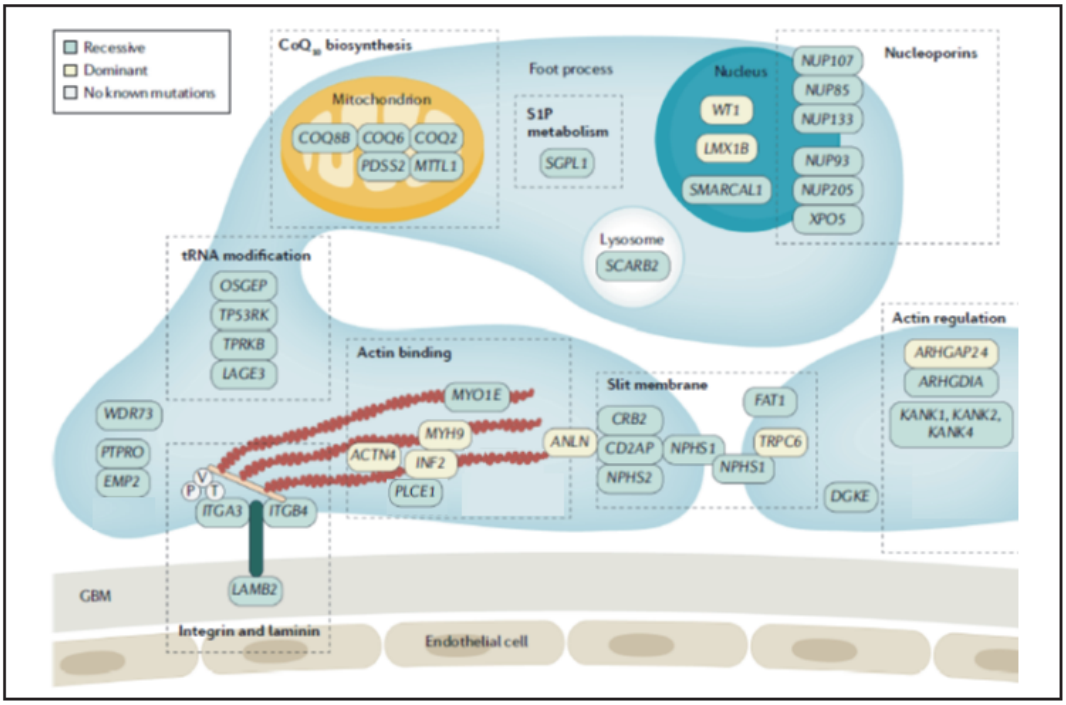

Figure 13: Podocyte genes associated with steroid-resistant nephrotic syndrome. Schematic representation of the genes associated with SRNS (From Kopp, J.B., Anders, HJ., Susztak, K. *et al.* 2020)

Table 1 – List of genes associated with hereditary podocytopathies.

Gene	Protein	Mode of inheritance	Clinical phenotype	Reference
Encoding proteins associated to the SD				
NPHS1	Nephrin	AR	CoNS and infantile SRNS	(Kestila, *et al.* 1998)
NPHS2	Podocin	AR	Infantile and childhood SRNS	(Boute, *et al.* 2000)
CD2AP	CD2-associated protein	AR	Infantile SRNS	(Kim, *et al.* 2003)
TRPC6	Short transient receptor potential channel 6	AD	Juvenile and adult-onset FSGS	(Winn, *et al.* 2005)
FAT1	FAT atypical cadherin 1	AR	Childhood SRNS	(Gee, *et al.* 2016)
MAGI2	Membrane-Associated Guanylate Kinase Inverted 2	AR	CoNS, childhood-onset SRNS	(Bierzynska, *et al.* 2017)
CRB2	Crumbs homolog 2	AR	Early-onset SRNS	(Ebarasi, *et al.* 2015)
KIRREL1	Kin of IRRE-like protein 1	AR	Juvenile SRNS	(Solanki *et al.* 2019)
Encoding proteins related to the cytoskeleton				
ACTN4	α-actinin-4	AD	Juvenile and adult-onset FSGS	(Kaplan, *et al.* 2000)
INF2	Inverted formin-2	AD	Juvenile and adult-onset FSGS	(Brown, *et al.* 2010)
MYO1E	Unconventional myosin IE	AR	FSGS	(Mele, *et al.* 2011)
MYH9	Myosin, heavy chain 9	AD	FSGS Macrothrombocytopenia with sensorineural deafness, Epstein syndrome, Sebastian syndrome, Fechtner syndrome	(Seri, *et al.* 2000)
ARHGAP24	Rho-GTPase-activating protein 24	AD	Infantile and juvenile FSGS	(Akilesh, *et al.* 2011)
ARHGDIA	Rho GDP-dissociation inhibitor 1	AR	CoNS	(Gupta, *et al.* 2013)
ANLN	Anillin	AD	Adult onset FSGS	(Gbadegesin, *et al.* 2014)
KANK1/2/4	Kidney ankyrin repeat-containing protein 1/2/4	AR	Childhood SSNS/SRNS	(Gee, *et al.* 2015)
Encoding GBM proteins and related proteins				
LAMB2	Laminin subunit β2	AR	CoNS (either isolated or as an aspect of Pierson syndrome)	(Zenker, *et al*. 2004)
ITGB4	Integrin β4	AR	Epidermolysis bullosa	(Kambham *et al.* 2000)
ITGA3	Integrin α 3	AR	Epidermolysis bullosa, Interstitial lung disease, SRNS/FSGS	(Has, *et al.* 2012)
CD151	CD151 tetraspanin tetraspanin	AR	Epidermolysis bullosa, Sensorineural deafness, ESRD	(Karamatic, *et al.* 2004)
Encoding nuclear proteins				
WT1	Wilms tumour protein	AD	Denys–Drash syndrome, Frasier syndrome or isolated SRNS	(Pelletier, *et al.* 1991)

LMX1B	LIM homeobox transcription factor 1β	AD	Nail patella syndrome	(Dreyer, *et al.* 1998)
PAX2	Paired box gene 2	AD	Adult-onset FSGS, Renal coloboma syndrome	(Amiel, *et al.* 2000)
MAFB	MAF BZIP Transcription Factor B	AD	Carpo-tarsal osteolysis progressive ESRD	(Zankl, *et al.* 2012)
LMNA	Lamin A/ C	XD	Familial partial lipodystrophy, FSGS	(Javor, *et al.* 2004)
NXF5	Nuclear RNA export factor 5	XR	SRNS/FSGS cardiac conduction disorder	(Esposito, *et al.* 2013)
NUP93	Nucleoporin 93kD	AR	Infantile SRNS	(Braun, *et al.* 2016)
NUP205	Nucleoporin 205kD	AR	Infantile SRNS	(Braun, *et al.* 2016)
XPO5	Exportin 5	AR	Infantile SRNS	(Braun, *et al.* 2016)
NUP107	Nucleoporin 107kD	AR	Galloway-Mowat syndrome	(Rosti, *et al.* 2017)
NUP133	Nucleoporin 133kD	AR	Galloway-Mowat syndrome	(Fujita *et al.* 2018)
NUP85	Nucleoporin 85kD	AR	Childhood SRNS	(Braun *et al.* 2018)
NUP160	Nucleoporin 160kD	AR	Juvenile SRNS	(Braun *et al.* 2018)
SMARCAL1	SWI/SNF-related matrix- associated actin-dependent regulator of chromatin subfamily A-like protein 1	AD	Schimke immuno-osseous dysplasia	(Boerkoel, *et al.* 2002)
Encoding mitochondrial proteins				
COQ2	4-hydroxybenzoate-polyprenyltransferase	AR	Early onset SRNS, coenzyme Q_{10} deficiency	(Quinzii, *et al.* 2006)
COQ6	Ubiquinone biosynthesis monooxygenase COQ6	AR	SRNS with sensorineural deafness	(Heeringa, *et al.* 2011)
COQ8B	Atypical kinase COQ8B, mitochondrial	AR	SRNS, coenzyme Q_{10} deficiency	(Ashraf *et al.* 2013)
PDSS2	Decaprenyl-diphosphatesynthase subunit 2	AR	SRNS, coenzyme Q_{10} deficiency	(Lopez, *et al.* 2006)
ADCK4	AarF domain containing kinase 4	AR	Childhood-onset SRNS, CoQ10 deficiency	(Ashraf, *et al.* 2013)
MT-TL1	Mitochondrial Leu (UUR) tRNA	Maternal mtDNA	MELAS	(Kurogouchi, *et al.* 1998)
OCRL	Inositol polyphosphate 5-phosphatase	XR	Dent disease	(Hoopes *et. al* 2005)
Encoding lysosomal proteins				
SCARB2	Scavenger receptor class B, member 2	AR	Progressive myoclonic epilepsy with or without renal failure	(Berkovic, *et al.* 2008)
Encoding tRNA modifiers proteins				

GON7	GON7 subunit of KEOPS complex	AR	Galloway-Mowat syndrome	(Arrondel *et al.* 2019)
WDR4	WD repeat domain 4	AR	Galloway-Mowat syndrome	(Trimouille *et al.* 2018)
TPRKB	TP53RK binding protein	AR	Galloway-Mowat syndrome	(Braun *et al.* 2017)
TP53RK	TP53 regulating kinase	AR	Galloway-Mowat syndrome	(Braun *et al.* 2017)
OSGEP	O-sialoglycoprotein endopeptidase	AR	Galloway-Mowat syndrome	(Braun *et al.* 2017)
LAGE3	L antigen family member 3	XR	Galloway-Mowat syndrome	(Braun *et al.* 2017)
YRDC	yrdC N6-threonylcarbamoyltransferase domain containing	AR	Galloway-Mowat syndrome	(Arrondel *et al.* 2019)
Encoding endosomes-vesicular trafficking proteins				
TBC1D8B	TBC1 domain family member 8B	XL	Early-onset SRNS	(Dorval *et al.* 2019)
ANKFY1	Rabankyrin-5	AR	Childhood SRNS	(Hemle *et al.* 2018)
GAPVD1	GTPase-activitating protein and VPS9 domain-containing protein 1	AR	Infantile SRNS	(Hemle *et al.* 2018)
Encoding other proteins				
PLCE1	Phospholipase C ε1	AR	Infantile and childhood SS/SRNS	(Hinkes *et al.* 2006)
PTPRO	Receptor-type tyrosine-protein phosphatase O	AR	SRNS	(Ozaltin, *et al.* 2011)
EMP2	Epithelial membrane protein 2	AD	Childhood SRNS/SSNS	(Gee, *et al.* 2014)
DGKE	Diacylglycerol kinase-ε	AR	Atypical hemolytic uremic syndrome, membranoproliferative lesions	(Lemaire, *et al.* 2013)
SGPL1	Sphingosine-1-phosphate lyase 1	AR	SRNS and facultative ichthyosis and adrenal insufficiency	(Lovric *et al.* 2017)
PMM2	Phosphomannomutase 2	AR	Congenital disorder of glycosylation, type Ia	(Matthijs *et al.* 1997)
ALG1	B1,4 mannosyltransferase	AR	Congenital disorder of glycosylation, type Ik	(Swhwarz *et al.* 2014)
CFH	Complement factor H	AD, AR	Complement factor H deficiency: Secondary FSGS	(Vogt *et al.* 1995)
CFI	Complement factor I	AR	Complement factor I deficiency	(Sadallah *et al.* 1999)
APOL1	Apolipoprotein L1	AR	Susceptibility to develop NS with FSGS	(Genovese *et al.* 2010)
APOA1	Apolipoprotein A	-	Variants associated with general disorder of lipid metabolism in NS	(Santucci *et al.* 2011)
PTPRO	Tyrosine phosphatase receptor-type O	AR	Childhood SRNS	(Ozaltin *et al.* 2011)

DGKE	Diacylglycerol kinase-ε	AR	Atypical hemolytic uremic syndrome, membranoproliferative lesions	(Lemaire *et al.* 2013)
TTC21B	Tetratricopeptide repeat domain 21B	AR	Nephronophthisis , FSGS	(Cong, *et al.* 2014)
EDN1	Endothelin-1	-	Polymorphisms association with the clinical NS phenotype	(Yang *et al.* 2014)
WDR73	WD repeat domain 73,	AR	Galloway-Mowat syndrome, SRNS/FSGS	(Colin, *et al.* 2014)
PODXL	Podocalyxin	AR/AD	Congenital SRNS; FSGS	(Kang *et al.* 2017)
ZMPSTE24	Zinc metallo-proteinase	AR	Mandibuloacral dysplasia with type B lipodystrophy	(Agarwal *et al.* 2006)

Abbreviation: CoNS: congenital nephrotic syndrome; MELAS, mitochondrial encephalomyopathy, lactic acidosis and stroke-like episodes

CHAPTER THREE: GALLOWAY-MOWAT SYNDROME

The renal disease can be isolated or associated with extra-renal disorders. The most frequent is neurological as in Galloway-Mowat syndrome (GAMOS), which associates NS to microcephaly and neurological impairment. For that reason, GAMOS raises the fascinating question of deciphering the molecular pathways that could be common to both kidney and brain development and function. This is in agreement with many publications showing that podocytes and neurons share a large number of molecular pathways.

1. Clinical and pathological aspects

Galloway-Mowat syndrome is a rare autosomal, or X-linked, recessive disorder, reported for the first time in 1968 by Galloway and Mowat in two siblings with no consanguinity of the parents. The two siblings suffered from early-onset NS, microcephaly, and hiatal hernia (Galloway and Mowat 1968). Since then, approximately 100 cases have been reported in the literature. The broad spectrum of the clinical manifestations reported in GAMOS patients revealed that this disorder is highly heterogeneous. The estimated prevalence of GAMOS is 1<1,000,000. However, we should take in consideration that many cases remain undiagnosed. Unfortunately, the prognosis of GAMOS is still poor and patients affected by GAMOS die in the first years of life (Sartelet *et al.* 2008; Colin *et al.* 2014; Zeybek *et al.* 2016; Braun *et al.* 2017; Braun, Shril *et al.* 2018).

The most prominent and consistent hallmark of GAMOS is the microcephaly. It consists in the decrease of the head circumference, which is often present at birth (**Figure 14**). When presents at birth it is called primary microcephaly, however microcephaly can also occur lately in the postnatal life and is then referred to secondary or post-natal microcephaly. Primary microcephaly is considered to be due to neurodevelopmental abnormalities, consisting mainly in proliferation defects of neural progenitor cells which determine the final neuron numbers in brain. On the other side, secondary microcephaly is considered to be due to neurodegenerative abnormalities or neuronal maturation defects. Microcephaly is frequently accompanied by major central nervous system (CNS) abnormalities such as cerebral or cerebellar atrophy, corpus callosum hypoplasia, myelination or gyration defects (lissencephaly, polymicrogyria), the latter being due to neuronal migration defects. Moreover, severe psychomotor delay, hypotonia, epilepsy and intellectual

disability have been reported (Meyers *et al.* 1999; Pezzella *et al.* 2010; Ekstrand 2012).

The renal abnormalities in GAMOS can range from isolated proteinuria to SRNS, the latter rapidly progressing to ESRD. Commonly, NS has an early-onset, but it has been also reported in literature, cases of GAMOS with late-onset NS, and even a normal renal function at the time of publication (Colin *et al.* 2014; Rosti *et al.* 2016). Renal biopsies revealed lesions ranging from MCD to FSGS (Meyers *et al.* 1999; Sartelet *et al.* 2008).

Additional clinical manifestations of GAMOS include low birthweight, intrauterine growth retardation, facial dysmorphism (hypertelorism, ear abnormalities, micrognathia), hiatal hernia, optic atrophy, hypothyroidism, arachnodactyly, or endocrine abnormalities (Hou and Wang 1995; Meyers *et al.* 1999; Chen, Lin *et al.* 2011; Jinks *et al.* 2015).

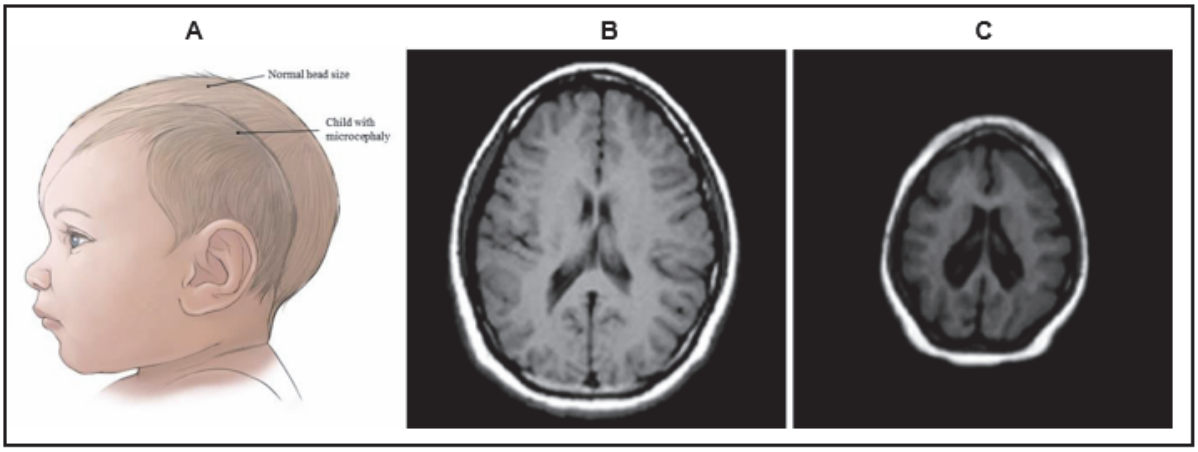

Figure 14: Microcephaly. (**A**) Normal versus microcephalic head size, (**B**) Normal brain MRI, transversal section (**C**) Microcephalic brain MRI, transversal section. (Adapted from Prezi.com and Pang *et al.* 2008)

2. Genetic causes and molecular basis

Several genes have been identified to be responsible for GAMOS, highlighting its genetic heterogeneity and reflecting its clinical heterogeneity. So far, disease-causing mutations have been identified in eleven genes, including *WDR73*, *NUP133*, *NUP107*, *WDR4* (component of the METTL1/WDR4 holoenzyme) and those encoding KEOPS complex (*LAGE3*, *OSGEP*, *TP53RK*, *TPRKB, YRDC*) (Colin *et al.* 2014; Rosti *et al.* 2016, 2017; Braun *et al.* 2017; Fujita *et al.* 2018a; a; Braun, Shril *et al.* 2018; Arrondel *et al.* 2019). Quite recently, a recurrent variant in *PRDM15* has been identified as a novel cause of GAMOS (Mann *et al.* 2021). These genes encode proteins

with various functions, mainly involved in RNA metabolism, in particular tRNA and UsnRNA, and in transcriptional regulation.

2.1 snRNA processing

Mutations in *WDR73* have been linked for the first time to GAMOS in 2014 by Pr Antignac's group (Colin *et al.* 2014). Up to date, mutations in *WDR73* has been reported in 19 families (Colin *et al.* 2014; Ben-Omran *et al.* 2015; Jinks *et al.* 2015; Vodopiutz *et al.* 2015; Rosti *et al.* 2016). Patients present a particular phenotype characterized by postnatal microcephaly, with marked cerebellar atrophy, whereas the renal involvement is rather of late-onset or absent.

WDR73 is expressed in all human tissues, including brain and kidney. It encodes a protein predicted to contain six WD40 repeats. Each WD40 repeat folds into a four-stranded antiparallel beta-sheet blade that assemble into domains containing a seven-blade propeller called WD40 domain. These domains are used as scaffolds for protein complex assembly thus playing a role in many signaling pathways (Stirnimann *et al.* 2010). Initial functional studies have proposed a role for WDR73 in the regulation of microtubule organization and dynamics, cell survival and mTOR signaling (Colin *et al.* 2014; Jinks *et al.* 2015). However, recent studies of our laboratory demonstrated that WDR73 could interact with the subunits INTS9 and INTS11 of the Integrator complex, a multiprotein complex playing a role in RNA metabolism and transcription regulation (Tilley 2021). Indeed, *WDR73*-depleted podocytes and neural progenitor cells derived from *WDR73* mutated patients displayed defects in cellular pathways regulated by Integrator complex, such as the 3' processing of uridylate-rich small nuclear RNA (UsnRNA) and small nucleolar RNA (snoRNA), and the transcriptional response to epidermal growth factor (EGF). Furthermore, *WDR73* and *INTS11* depletion in podocytes led to altered expression of genes encoding cell cycle regulators including an upregulation of *CCND1*, encoding cyclin D1, and a downregulation of *CDKN1A*, encoding p21 (Tilley 2021). Altogether, these results suggest that perturbations of the spliceosome (misprocessing of UsnRNA), EGF responsiveness and cell cycle are particularly critical for neurons and podocytes and likely contribute to GAMOS pathogenesis.

2.2 tRNA modifications

2.2.1 t^6A biosynthesis pathway

Threonylcarbamoylation of adenine at position 37 of ANN codon-specific tRNAs (t^6A) is a universally post-transcriptional modification, which is conserved in all organisms and is essential for the efficiency and accuracy of translation (Yarian *et al.* 2002; El Yacoubi *et al.* 2011; Srinivasan *et al.* 2011; Daugeron *et al.* 2011). This modification occurs in two steps. Firstly, YRDC synthesizes threonylcarbamoyl (TC)-AMP intermediate, which is unstable. Then, TC-AMP group is transferred to the tRNA substrate by the KEOPS complex (kinase, endopeptidase and other proteins of small size complex) (Costessi *et al.* 2012; Lauhon 2012; Thiaville *et al.* 2014; Wan *et al.* 2017). The human KEOPS complex contains 5 subunits: LAGE3, OSGEP, TP53RK, TPRKB and GON7, the latter subunit homologous to yeast Gon7 contributing to the stability of KEOPS complex and to its enzymatic activity (Downey *et al.* 2006; Wan *et al.* 2017; Braun *et al.* 2017; Arrondel *et al.* 2019).

The first KEOPS complex functions, initially described in yeast, were related to genome maintenance, control of telomere length, regulation of gene transcription and in telomere-associated DNA-damage response signaling (Downey *et al.* 2006; Hecker *et al.* 2009; Oberto *et al.* 2009; Peterson *et al.* 2010). The KEOPS complex is conserved in Archaea and Eukarya and the majority of these genes are considered essential genes for cell survival (Yacoubi and Bailly 2012; Blomen *et al.* 2015).

t^6A defect has been identified as a novel pathogenic mechanism contributing to GAMOS pathogenesis by the identification of mutations in all the genes encoding proteins involved in the t^6A biosynthesis pathway. Up to date, mutations in these genes have been reported in 42 families (Edvardson *et al.* 2017; Braun *et al.* 2017; Wang *et al.* 2018; Al-Rakan *et al.* 2018; Hyun *et al.* 2018; Arrondel *et al.* 2019). All individuals bearing mutations in KEOPS complex subunits and *YRDC* present similar clinical features, whereas mutations identified in *GON7* result in a less severe clinical outcome, suggesting that *GON7* is not essential in humans. Functional *in vivo* studies in animal models (zebrafish and mice knock-out models) showed that these models recapitulate features of microcephaly with severe lethality, however without any renal phenotype (Braun *et al.* 2017). Functional studies *in vitro* using primary patient fibroblasts and KEOPS knock-down (KD)

podocyte lines demonstrated alterations in several cellular processes such as proliferation, apoptosis, migration and protein synthesis. Most importantly, t^6A levels were decreased in KEOPS KD podocytes and in patient fibroblasts (Braun *et al.* 2017; Arrondel *et al.* 2019).

2.2.2 m^7G modification

7-methylguanosine (m7G) modification is one of the most conserved modification on tRNAs. It occurs in bacteria and eukaryotes and is found at position 46. This modification plays crucial roles in regulation of mRNA export, splicing and translation. This modification requires a holoenzyme composed of the RNA methyltransferase catalytic subunit METTL1 and its binding partner, the non-catalytic subunit WDR4 (Alexandrov *et al.* 2002). Mutations in the human METTL1/WDR4 complex have been shown to lead to microcephalic primordial dwarfism (microcephaly with intellectual disability and severe growth retardation (Shaheen *et al.* 2015; Trimouille *et al.* 2018). Recently, a homozygous mutation has been identified in a family with GAMOS (Braun, Shril *et al.* 2018).

2.3 Nucleoporins

Mutations in genes encoding structural constituents of the nuclear pore complex, have also been reported in patients affected with GAMOS (Alazami *et al.* 2015; Bierzynska *et al.* 2017; Rosti *et al.* 2017; Fujita *et al.* 2018a). Nuclear pore complexes (NPC) are large structures composed of over 30 nucleoporins that mediate bidirectional nucleocytoplasmic transport and are also involved in a wide variety of cellular processes including regulation of transcription, chromatin organization and cell division (González-Aguilera and Askjaer 2012; Beck and Hurt 2017). Mutations have been identified in patients with isolated SRNS in several nucleoporin genes including *NUP107* and *NUP133*, which encode two nucleoporins that interact together and are part of the Nup 107-160 complex (González-Aguilera and Askjaer 2012; Morchoisne-Bolhy *et al.* 2015; Beck and Hurt 2017), a critical player in NPC assembly (Miyake *et al.* 2015; Braun, Lovric *et al.* 2018). Recently, mutations have been identified in these two NUP genes in individuals presenting with a GAMOS phenotype, characterized by microcephaly, mild to profound intellectual disability and childhood-onset SRNS: one homozygous missense mutation in the *NUP107* gene (c.303G>A, p.Met101Ile)

found in four different families, and one homozygous mutation in the *NUP133* gene found in a consanguineous family (Rosti *et al.* 2017; Fujita *et al.* 2018b).

2.4 Transcriptional regulator

Finally, mutations in *PRDM15* cause clinical manifestations ranging from isolated NS to a GAMOS type syndrome with microcephaly, mixed glomerular and tubular disease, and developmental delay (Mann *et al.* 2021). PRDM15 is a zinc finger transcriptional regulator of the PRDM family whose members are involved in transcription regulation and chromatin structure. It has been shown that the depletion of *PRDM15* in Xenopus laevis leads to abnormal pronephrogenesis with downregulation of multiple pronephros markers such as wt1 and fxyd2 (Mann *et al.* 2021). In addition, depletion of *PRDM15* in podocyte cell lines using CRISPR/Cas9 led to deregulation of genes involved in kidney development, including *WT1*, a zinc finger protein expressed by podocytes and playing a crucial role in nephrogenesis.

CHAPTER FOUR: tRNA IN HUMAN PHYSIOLOGY AND PATHOPHYSIOLOGY

1. tRNA life cycle

1.1 Biogenesis, structure and function

Transfer RNAs (tRNAs) are small non-coding RNAs that play an essential role in protein translation by delivering amino acids to the ribosomes. They are expressed from a large number of genes, ranging from 89 in *Escherichia coli* to 568 in *Caenorhabditis elegans* (http://gtrnadb.ucsc.edu/), with 429 predicted high confidence tRNA genes in humans to decode 64 genetic codons that specify 20 amino acids (Chan and Lowe 2016). The diversity of tRNA genes is due to gene duplication and generates a diversity in tRNA isodecoders and isoacceptors. It is important to underline the fact that isodecoders are tRNAs that recognize the same anticodon but have a different RNA sequence, whereas isoacceptors are tRNAs that decode multiple related codons but still carry the same amino acid.

In prokaryotes, RNAs, including tRNAs are transcribed by a single RNA polymerase. In eukaryotes, tRNA transcription is mediated by RNA polymerase III, which is recruited to tRNA genes by the transcription factors TFIIIB and TFIIIC. The aforementioned transcription factors recognize two internal promotor elements, called box A and box B, respectively (Huet and Sentenac 1992; Flores *et al.* 1999; Schramm 2002; Moqtaderi *et al.* 2010). After transcription, they undergo a series of post-transcriptional processing and modification steps prior to reach their mature and functional state (Jackman and Alfonzo 2013; Swinehart and Jackman 2015; Chatterjee *et al.* 2018; Hirata 2019; Dixit *et al.* 2019; Hopper and Nostramo 2019) (**Figure 15**).

Early on, tRNAs were known only to help decoding mRNA information by the ribosome and delivering amino acids to the extending polypeptide chain during mRNA translation. However, recently discoveries showed that tRNAs serve also as an abundant source of small noncoding RNA (ncRNA) playing fundamental roles in RNA metabolism.

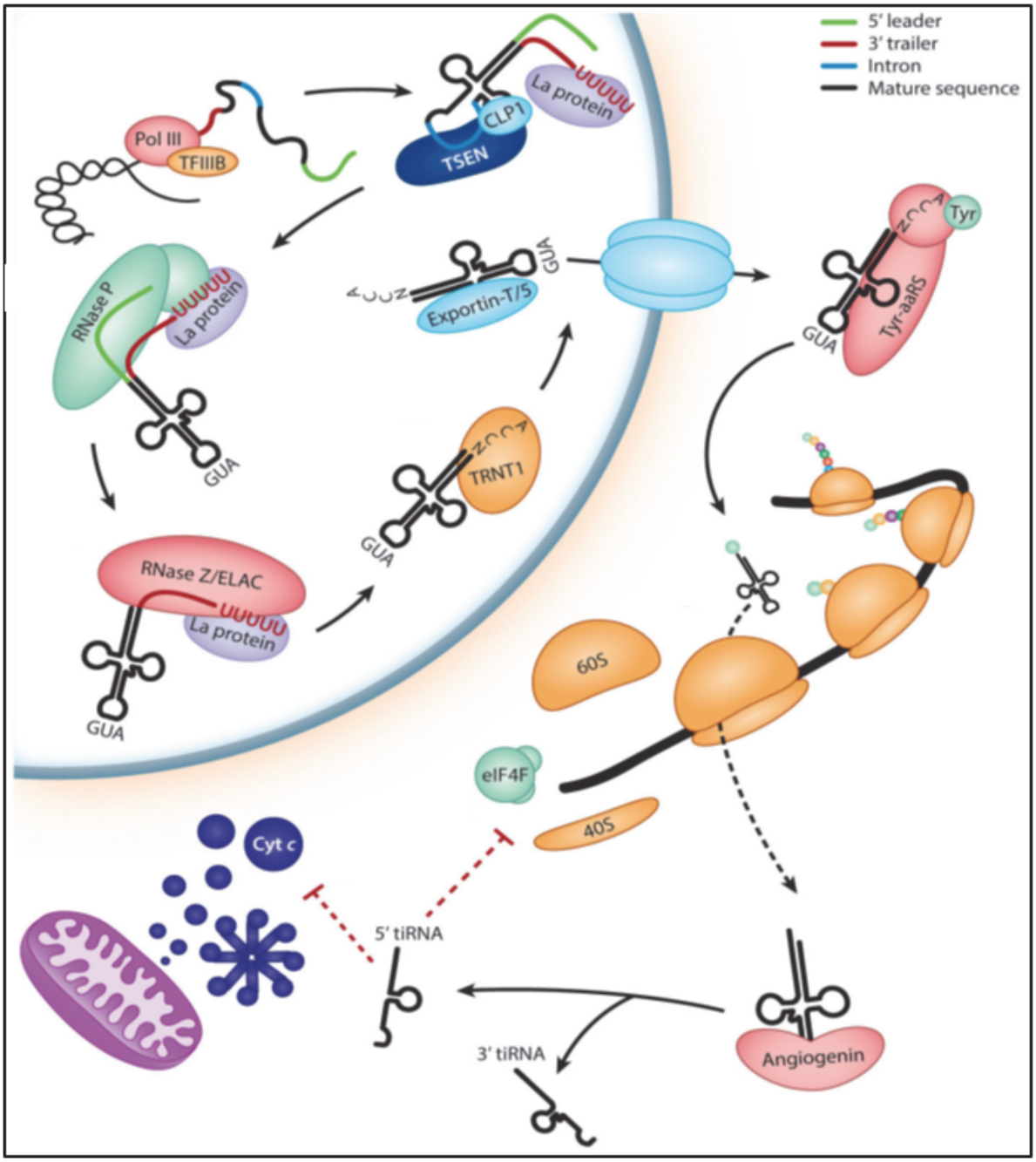

Figure 15: Overview of the cell's cycle of tRNAs in mammalians. tRNAs are transcribed by the RNA polymerase III and after this event different maturation processes occur, including 5' leader and 3' trailer cutting, intron excision and nucleotides modifications, leading to the mature form of tRNAs. Once tRNAs are in the cytosol, they are aminoacylated and they participate in translation through incorporation into the ribosomal A-site, decoding mRNA and delivering amino acids to the growing polypeptide chain. tRNA species may be cleaved by angiogenin into 5' and 3' tRNA halves (tiRNAs). Furthermore, 5' tiRNAs inhibit translation initiation through competitive binding with the EiF4F complex and inhibit the formation of the apoptosome through competitive binding of cytochrome c (From Schaffer *et al.* 2019).

Mature tRNAs range in length from approximately 70 to 90 nucleotides. This feature is largely conserved throughout evolution. tRNAs adopt a clover leaf secondary structure and contain five major structural elements: **1**) the acceptor stem to which the amino acid is attached, **2**) the D-arm, **3**) the anticodon arm, **4**) the variable loop, and **5**) the T-arm, also known as the TΨC arm (**Figure 16**). Each arm has a double-stranded stem and single-stranded loop. To go into details, the acceptor stem and D-arm are involved in aminoacyl-tRNA synthetase recognition, which is required for amino acid charging at the acceptor stem. The anticodon loop interacts with mRNA codons in order to guarantee the delivery of the proper amino acid. Finally, the T-arm is involved in ribosome-tRNA interaction. This helps to have an efficient translation.

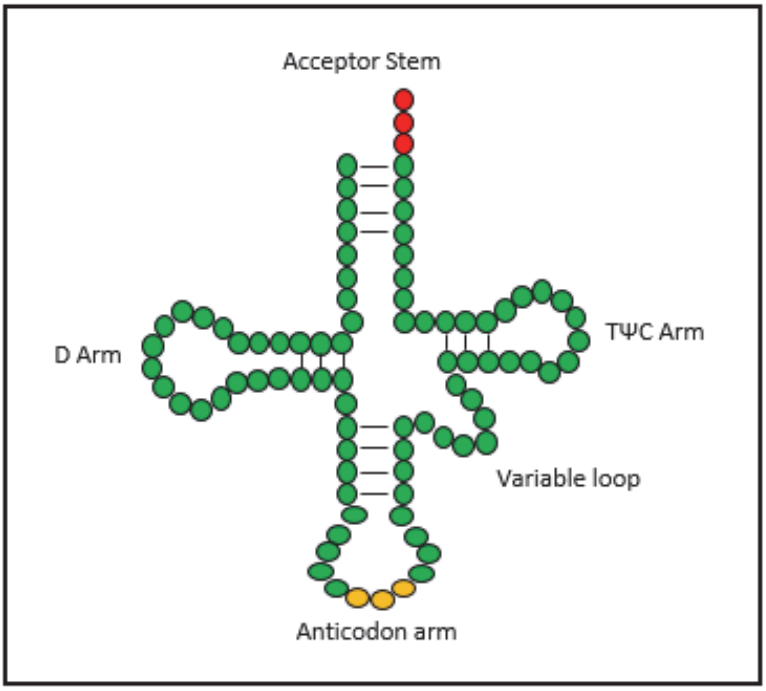

Figure 16: General tRNA cloverleaf structure. tRNA contains the D arm, TΨC arm, acceptor stem, anticodon arm and the variable loop. Red circles represent nucleotides which constitute the acceptor stem. Yellow circles represent nucleotides of the anticodon arm. (Adapted from Kessler *et al.* 2018)

1.2 Processing and maturation of tRNAs: overview

In both, eukaryotes and prokaryotes, tRNAs are transcribed as pre-tRNAs which go through tRNA processing that will give rise to mature tRNAs. Early processing steps include the removal of the 5' leader, 3' trailer and introns of variable length in cistronic tRNA genes. Finally, late

enzymatic processing will consist in the addition of CCA to the 3' terminus and the export of the mature tRNA transcript from the nucleus to the cytoplasm. Pre-tRNA transcripts gain post-transcriptional modifications throughout the maturation process. All these aforementioned maturation steps are highly conserved in eukaryotes.

1.2.1 Early enzymatic processing

Pre-tRNAs contains a 5' leader and 3' trailer that are removed by two distinct endonucleolytic cleavage events. The removal of 5' leader sequences is mediated by the holoenzyme RNaseP. The binding of this enzyme to the substrate is regulated by the phosphorylation of La protein at position S366 (Intine *et al.* 2000). RNase P-mediated cleavage is an endonuclease that removes the 5' leaders from tRNAs, leaving a 5' monophosphate (Robertson *et al.* 1972). Furthermore, it is a ribonuclear protein (RNP) complex, located in the nucleolus and consisting of RPR1, the RNA subunit and nine essential proteins, Pop 1-3-4-5-6-7-8, Rpp1, and Rpr2 (Xiao *et al.* 2002). ELAC2 in eukaryotes or the bacterial homolog RNase Z mediates the enzymatic processing of the 3' trailer. This event is dependent on the level of 3' oligouridylation (Schiffer 2002; Takaku 2003). RNase Z activity results in a 3' hydroxyl and a single 3' overhang acceptor stem. It has been shown that the 3' processing might be divided depending the species of pre-tRNA whose trailer sequences contain an oligouridylation sequences suitable for La protein recruitment. Species that are able to recruit La protein, La-dependent processing, is thought to be the dominant form of 3' trailer removal. On the other hand, pre-tRNA species that are not suitable substrates for La protein, the 3' trailer removal is trimmed by Rxp1p. Rxp1p is a 3' to 5' exonuclease implicated in 3' processing and it is in competition with La protein (Copela *et al.* 2008; Ozanick *et al.* 2009).

The last step included in the early tRNA modification is the intron excision. A conserved subset of intron-containing tRNA genes is found across all three domains of life (Abelson *et al.* 1998; Fujishima and Kanai 2014; Chan and Lowe 2016). 28 out of the 429 genes encoding tRNAs in humans, contain introns (Chan and Lowe 2016). Intron-containing tRNA genes, in humans, are Leucine, Isoleucine, Tyrosine and Arginine and introns must be removed during tRNA maturation process (**Figure 17**). The complete maturation of these tRNAs is fundamental in order to become functional. In bacteria, tRNA introns are self-spliced (Abelson *et al.* 1998), whereas, in archaea

and eukaryotes, the tRNA splicing endonuclease complex, called TSEN, catalyze the excision of tRNA introns (Abelson *et al.* 1998; Calvin and Li 2008; Yoshihisa 2014; Lopes *et al.* 2015; Hirata 2019). The enzyme activity of the heterotetrameric tRNA endonuclease complex, TSEN, results in 5' and 3' exons formation (Trotta *et al.* 1997; Wolin and Matera 1999). It is important to underline the fact that this event occurs in the nucleus in mammalian cells (example: nucleoplasm in Hela cells). On the other hand, in yeast, SEN is located on the cytoplasmic surface of mitochondria in budding and fission yeast (Yoshihisa *et al.* 2003, 2007; Paushkin *et al.* 2004; Wan and Hopper 2018).

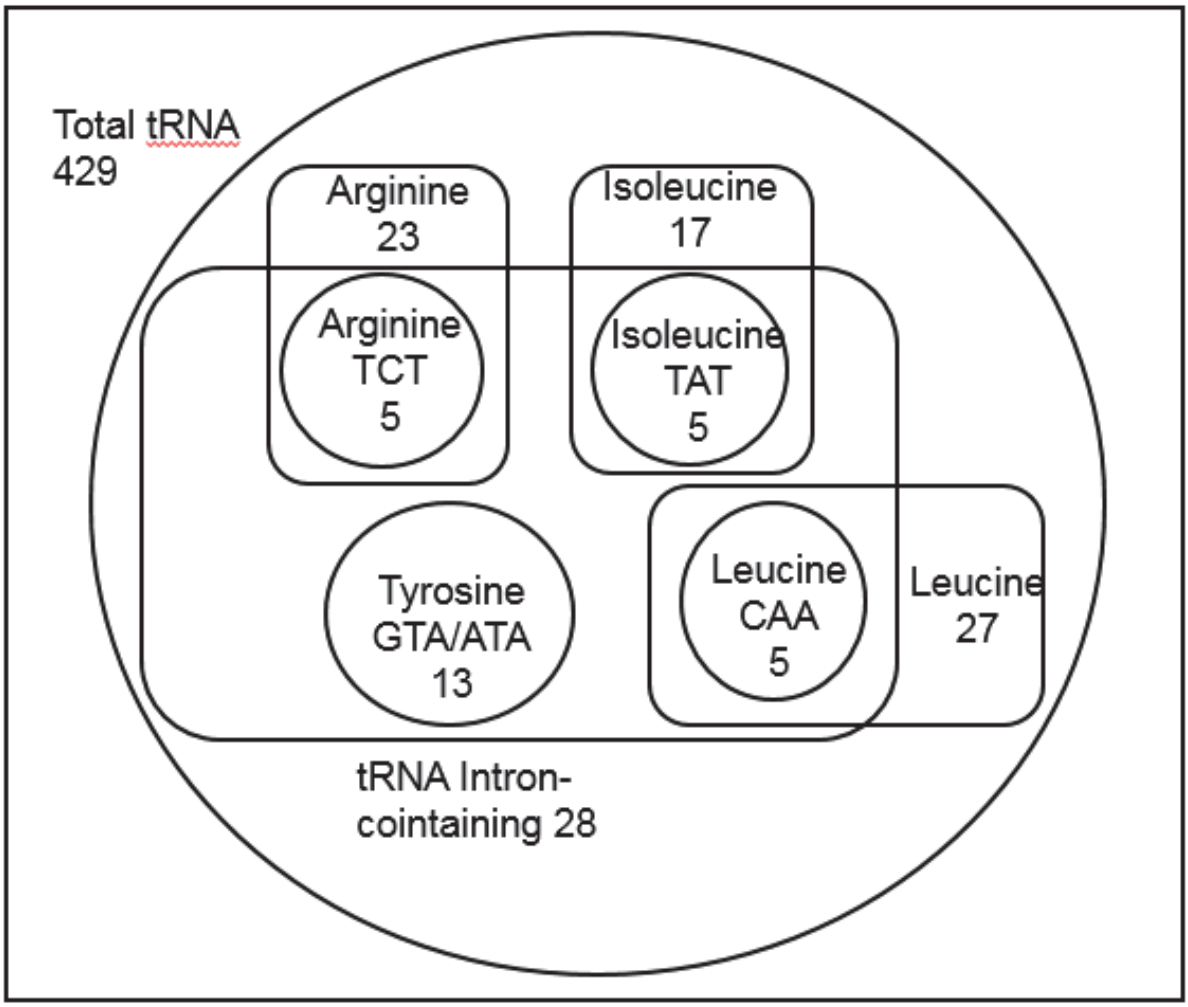

Figure 17: Schematic representation of subtypes of tRNAs containing intron. 28 out of the 429 genes codifying tRNAs in humans, contain introns (From F. Miscia).

tRNA intronic sequences have been identified only between the anticodon and TΨC loops with variable length varying between 14 and 60 nucleotides. In humans, introns are always located

at the same position, namely one nucleotide 3' to the anticodon, between nucleotides 37 and 38 of the mature tRNAs. Eukaryotic pre-tRNA second structure contains a distinctive base pair, known as the proximal base pair that is absolutely critical for cleavage at the 3' splice site (Baldi *et al.* 1992; Schmidt *et al.* 2019).

In the following paragraphs, I will briefly explain the differences and similarities of intron excision process among yeast and mammalians.

1.2.2 Intron excision process and ligation in yeast

In yeast, this process is accomplished by the SEN complex, a tetrameric complex composed by SEN54, SEN2, SEN34 and SEN15. The eukaryotic SEN complex was first discovered in yeast in the 1990s (Rauhut *et al.* 1990; Trotta *et al.* 1997). Recent work in yeast revealed that each individual SEN subunit is required, even when all intron-containing tRNA genes are replaced with intronless variants. This suggest that the complex has a fundamental cellular role beyond tRNA splicing (Cherry *et al.* 2018). SEN endonucleolytically cleaves tRNAs on both sides of the intron (**Figure 18**). SEN complex recognized and cleaved the 5' exonic and intronic sequences, resulting in 5' hydroxyl group on the 3' exonic sequence, as well as a 2', 3'–cyclic phosphodiester on the 3' and of the 5' exonic sequence following cyclization (Peebles *et al.* 1983; Rauhut *et al.* 1990; Trotta *et al.* 1997).

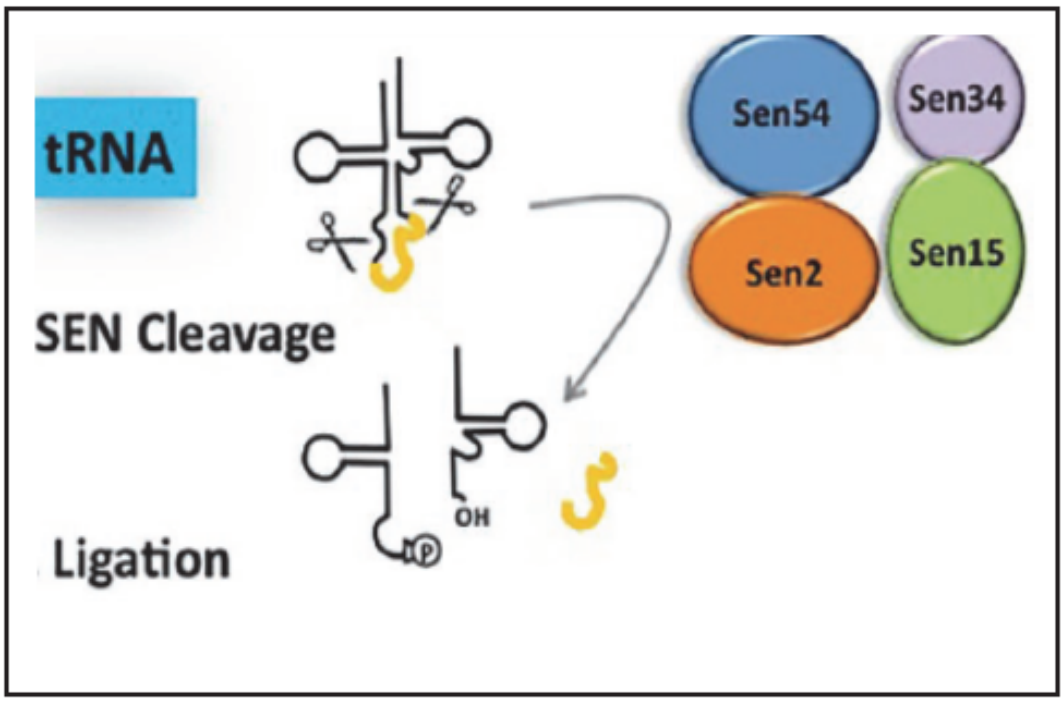

Figure 18: Overview of tRNA splicing in yeast. Heterotetrameric SEN complex, composed of SEN54, SEN34, SEN2 and SEN15, at the outer surface of the mitochondrial membrane, cuts and generates a 2'-3' cyclic phosphate (triangle and P in white circle) at the 3'end of the 5' exon and a hydroxyl group at the 5' end of the 3' exon. (From Hopper and Nostramo 2019.)

In yeast, the ligation process is catalyzed by Rlg1/Trl1 which has 2', 3' cyclic phosphodiesterase, 5' RNA kinase, and RNA ligase activities (Englert 2005). Ligation by Rlg1/Trl1 generates a splice junction with two phosphates: the extra 2' phosphate is removed via a transferase activity catalyzed by Tpt1 (Culver *et al.* 1997). Then, the ligation of the two exons is achieved by the tRNA ligase, Trl1 which converts the 2', 3' cyclic phosphate to a 2' phosphate and 3' hydroxyl, and also phosphorylates the 5' hydroxyl of the 3' exon allowing for the ligation of the two exons. Finally, Tpt1 removes the 2' phosphate (Culver *et al.* 1997) (**Figure 19**).

1.2.3 Intron excision process and ligation in mammalians

In vertebrates, the intron excision is accomplished by the tRNA endonuclease tetrameric complex called TSEN (Paushkin *et al.* 2004). I will better detail the role and function of TSEN complex in the **section 2**. After the intron excision, the ligation can be complete by two distinct processes, which are called the "yeast-like pathway" and the "animal pathway". The "yeast-like

pathway", named healing and sealing pathway (Sawaya *et al.* 2003), consists in the phosphorylation of the downstream exon (phosphorylation of the 3 exonic fragment) by the RNA kinase CLP1 (cleavage and polyadenylation factor 1) (Ramirez *et al.* 2008). CLP1 activity is similar to the Trl1 one (Weitzer and Martinez 2007; Hanada *et al.* 2013; Karaca 2014), but the enzyme that resolve 2', 3' cyclic phosphate, ligate the two halves and remove the resultant 2' phosphate is still unknown. On the other hand, in the "animal pathway", the RNA ligase HSPC117 acts on the 2',3' cyclic phosphate to ligate the second exon (Popow *et al.* 2011; Yoshihisa 2014; Cherry *et al.* 2018). In particular, the enzyme complex consisting of HSPC117, a RtcB-like ligase (Tanaka *et al.* 2011), catalyzes direct joining of the cleaved 5' exon bearing a 3' phosphate (via 2',3' phosphodiesterase activity of the ligase) with the 5' hydroxyl on the 3' exon (Popow *et al.* 2011) (**Figure 19**).

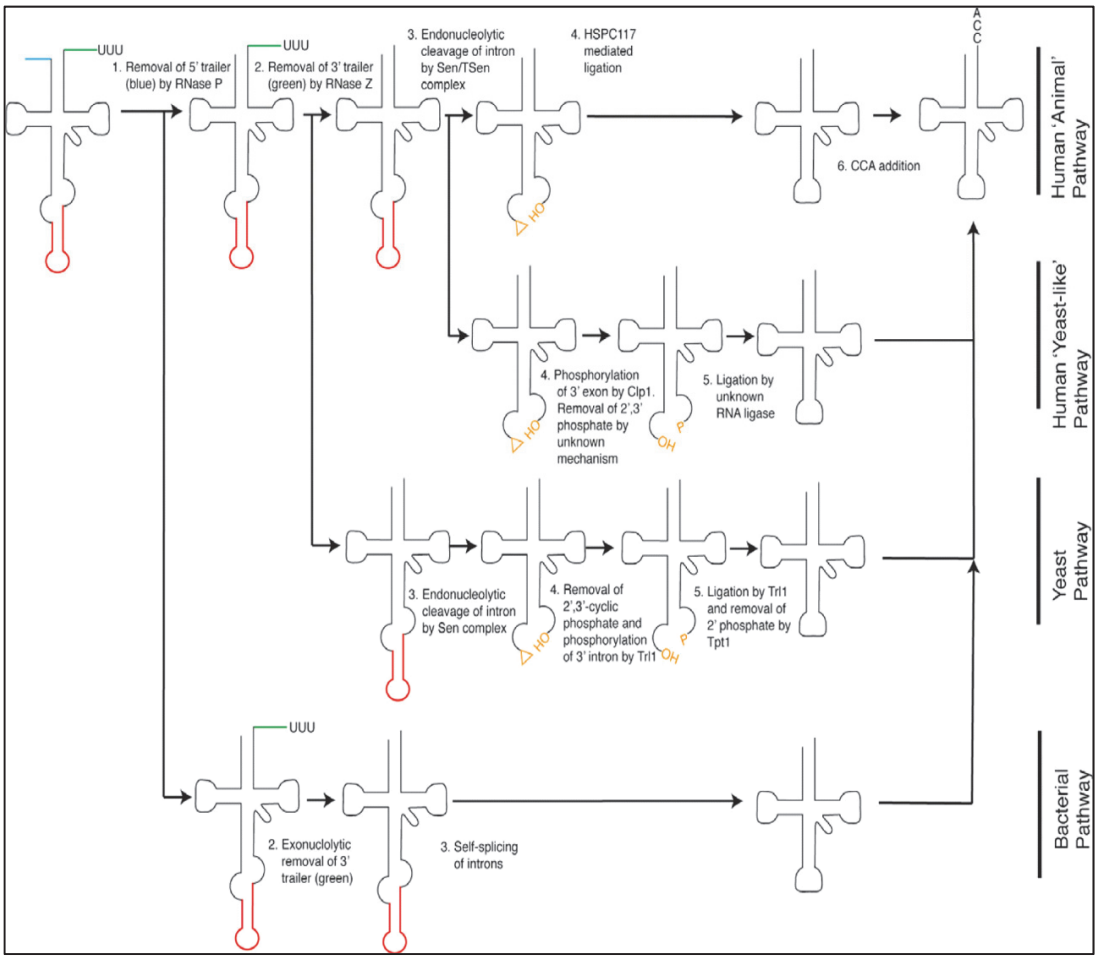

Figure 19: Overview of tRNA maturation pathways in different organisms, which utilize different enzymes to generate mature tRNA. Pre-tRNA contain a 5' leader (blue), a 3' trailer (green), and, in some instances, an intron (red) located within anticodon loop. (From Lyons *et al.* 2018).

1.2.4 Late enzymatic processing

Concerning late modification steps, of relevant importance is the addition of the CCA tail to the 3' terminus. This is achieved by the tRNA nucleotidyltransferase 1 (TRNT1) in humans and CCA1 in yeast (Sprinzl and Cramer 1979; Lipowsky *et al.* 1999; Nagaike *et al.* 2001). This modification is required for nuclear export and serves as a substrate for tRNA aminoacyltransferases. The 5' of the CCA, called also the "discriminator base" and other sequence elements in the anticodon stem-loop, are immediately recognized by the aminoacyl tRNA synthetases and this guides tRNA charging with the proper amino acid (Crothers *et al.* 1972).

1.3 Post-transcriptional modifications

The total number of modifications present in RNA are more than 170, of which 93 are found in tRNA. However, the frequency and distribution can vary among species (Boccaletto *et al.* 2018). The most abundant nucleoside modification on tRNA is the pseudouridine Ψ. This modification is universally found in the loop of the T-arm at position 55 (**Figure 20**). It facilitates the proper formation of the tertiary structure in which the loop of the T-arm interacts with the loop of the D-arm via Ψ55 (Robertus *et al.* 1974; Gray 2000). In addition to Ψ55 modification, methylation at position 9 and 55, m^1A9 and m^1A55 respectively, confer additional structure stability to the tRNA tertiary structure (Helm *et al.* 1998; Voigts-Hoffmann *et al.* 2007). Modifications that facilitate the interactions between the tRNA and mRNA are often found at position 34, the wobble base in the anticodon, or just 3' of the anticodon at position 37. The modification G37 to Y37 is able to stabilize the interaction codon-anticodon within the A site of the ribosome. Thus, providing increased base-stacking and ionic interactions (Grosjean *et al.* 1976; Konevega *et al.* 2004) (**Figure 20**).

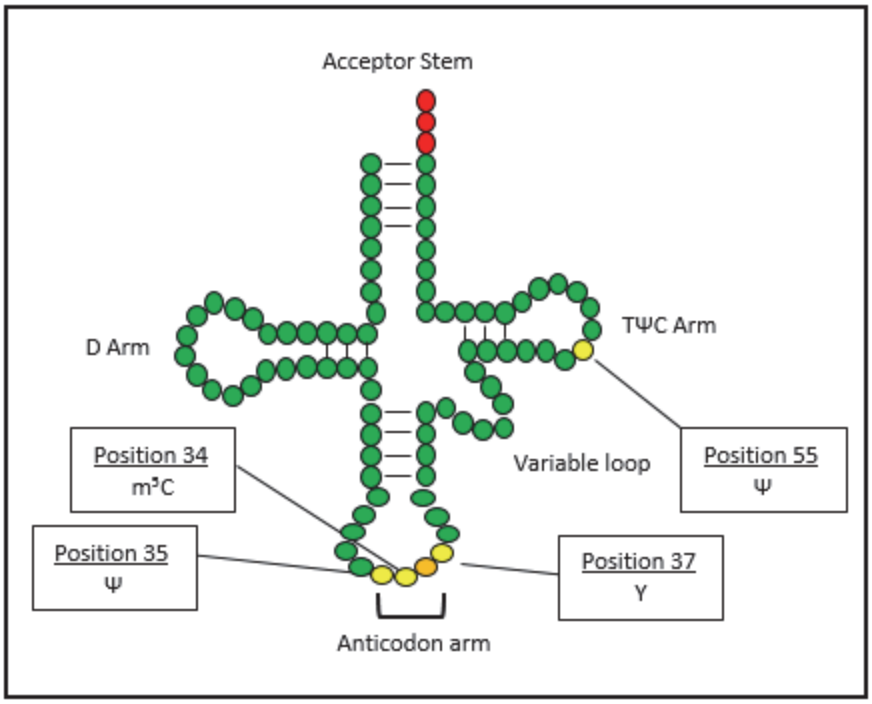

Figure 20: Most frequent tRNA modifications (1). These modifications include Ψ55 and Ψ35 (pseudouridine), m^5C_{34} (3 methyl cytosine), and Y37 (wybutosine). (Adapted from Kessler *et al* 2018.)

The presence of introns in pre-tRNAs might interfere with the nucleotide modifications. As a matter of fact, we can mention several examples in which tRNA processing is required for efficient tRNA modification. The modification U35 to Ψ35, which is essential for an efficient codon recognition, requires the presence of an intron in the $tRNA^{Tyr}$ (van Tol and Beier 1988), whereas, the modification C34 to m^5C34, required the presence of an intron in the $tRNA^{Leu}$ (Strobel and Abelson 1986) (**Figure 21**). To conclude, some tRNA positions are never modified, in particular the CCA tail remains unmodified as several positions in the variable loop (Boccaletto *et al.* 2018).

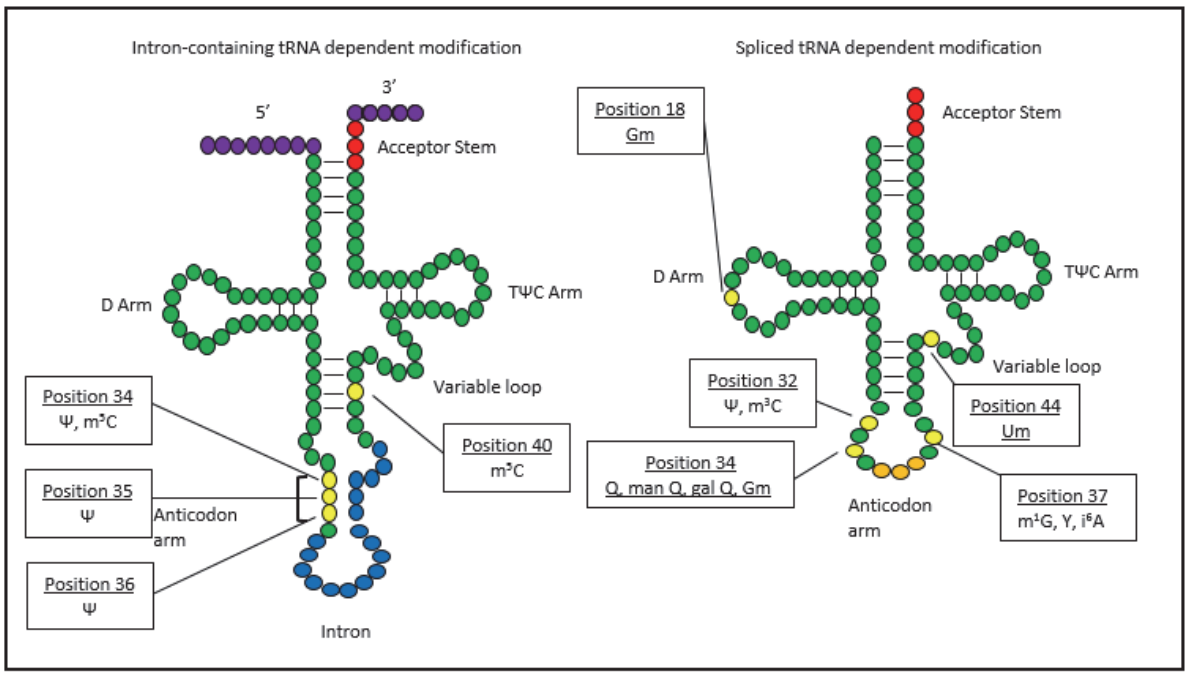

Figure 21: Most frequent tRNA modifications (2). Several modifications depend on the presence of an intron in tRNAs whereas others are only added after splicing. The intron is an essential recognition element for their enzyme. Modifications that are added only to intron-containing tRNAs includes Ψ (pseudouridine) at position 34-36 and m^5C (5 methyl cytosine) at positions 34 and 40. Whereas modifications that are added only to spliced tRNAs includes Ψ32 (pseudouridine), m^3C_{32} (3 methyl cytosine), Um_{44} (methyl uridine) and Gm_{18} (methyl guanine). Red circles represent nucleotides which constitutes the acceptor stem. Yellow circles represents nucleotides of the anticodon arm. Blue circles represents nucleotides of the intron. Purple circles represents nucleotides of the 3' and 5' tail that will be removed during the tRNAs maturation processes. (Adapted from Kessler *et al.* 2018.)

1.4 tRNA subcellular localization

tRNAs travel bi-directionally between the nucleus and cytoplasm. Intron-containing and intronless pre-tRNAs are first exported out of the nucleus (primary tRNA nuclear export). Then, spliced tRNAs are charged by aminoacyl tRNA synthetases and are imported back into the nucleus (retrograde tRNA import process). Finally, tRNAs are exported out of the nucleus for the second time (tRNA re-export process) (**Figure 22**). This bidirectional travel serves as numerous functions i.e. regulation of translation, tRNA modification and tRNA quality control. In particular, tRNAs's export might be considered as the final checkpoint before leaving the nucleus and entering into the cytoplasm.

1.4.1 Export of tRNAs

Export of tRNAs out of the nucleus is an active process, although tRNAs are smaller in size than the 40kD cut-off required for passive diffusion across NPCs (Zasloff 1983). The major tRNAs nuclear exporter for tRNA primary nuclear export is Exportin-T/Los1/PAUSED which belongs to the conserved β-importin family. β-importin family members are known to use the Ran pathway. Ran is a small GTPase that is in a GTP-bound state in the nucleus and in a GDP-bound state in the cytoplasm creating a nuclear-cytoplasmic Ran-GTP-bound gradient that dictates the directionality of movement across the nuclear membrane (Terry *et al.* 2007; Wente and Rout 2010). Exportin-T and its orthologues, Los1 and PAUSED, are critical for primary nuclear export of mature tRNA species and are RanGTP-dependent mechanisms (Hopper *et al.* 1980; Hurt *et al.* 1987; Kutay *et al.* 1998; Arts 1998; Hunter *et al.* 2003; Cherkasova *et al.* 2012). The formation of ternary complex with or without Ran family GTPases is crucial for the tRNA export. Exportin-T mediates nuclear export thanks to the recognition of the acceptor stem, proper processing of the 5' leader, 3' trailer, intron excision, and correct secondary structure, including TΨC and D-loop formation. Exportin-T preferentially binds end-processed tRNAs in vitro, relying on the recognition of a properly folded tRNA backbone, but does not discriminate between the presence or absence of introns (Hellmuth *et al.* 1998; Lund 1998; Arts 1998; Lipowsky *et al.* 1999; Cook 2009; Huang and Hopper 2015). It is important to underline the fact that human Exportin-T binds different tRNA species (Li and Sprinzl 2006). Furthermore, the export of some intron-containing pre-tRNAs is highly dependent on Los1, whereas other tRNAs are Los1 independent (Chatterjee *et al.* 2017).

In yeast, the splicing machinery localizes into the cytoplasm and in particular on the cytosol leaflet of the outer mitochondrial membrane, contrary to mammalian cells where the splicing machinery resides in the nucleus (**Figure 22**). The fact that Exportin-T does not discriminate between intron-containing and intronless tRNAs, allows all tRNAs to be transported into the cytoplasm. In yeast, Exportin-T, Los1, and Msn5, export pre-cistronic tRNA, for further processing by the SEN complex on the cytosol leaflet of the outer mitochondrial membrane (Huang and Hopper 2015). However, deletion/knock-out of the yeast Exportin-T (Los1) is non-essential for viability (Hopper *et al.* 1980; Sarkar and Hopper 1998; Hellmuth *et al.* 1998). This indicates that Exportin-T is the major exportin required for tRNA export (Hellmuth *et al.* 1998; Lund 1998; Arts 1998; Lipowsky *et al.* 1999; Cook 2009; Huang and Hopper 2015), but alternative pathways to

export tRNAs from the nucleus to cytoplasm also exist (Hurt *et al.* 1987; Hunter *et al.* 2003; Li and Chen 2003; Cherkasova *et al.* 2012). As a matter of fact, it has been shown, that tRNAs are also exported by the Exportin-5 in vertebrates or its homolog Msn5 in yeast or HASTY in plants. This provides an alternative pathway for primary tRNA nuclear export (Arts 1998; Calado *et al.* 2002; Bohnsack 2004; Park *et al.* 2005; Shibata *et al.* 2006). To conclude, recent studies in budding yeast revealed two potential additional exporters for primary tRNA nuclear export (Wu *et al.* 2015). The first one is Crm1 (Xpo1 in vertebrates) (Hutten and Kehlenbach 2007), whereas the second potential exporter is Mex67-Mtr2 heterodimer (NFX-NXT in vertebrates) (Chatterjee *et al.* 2017).

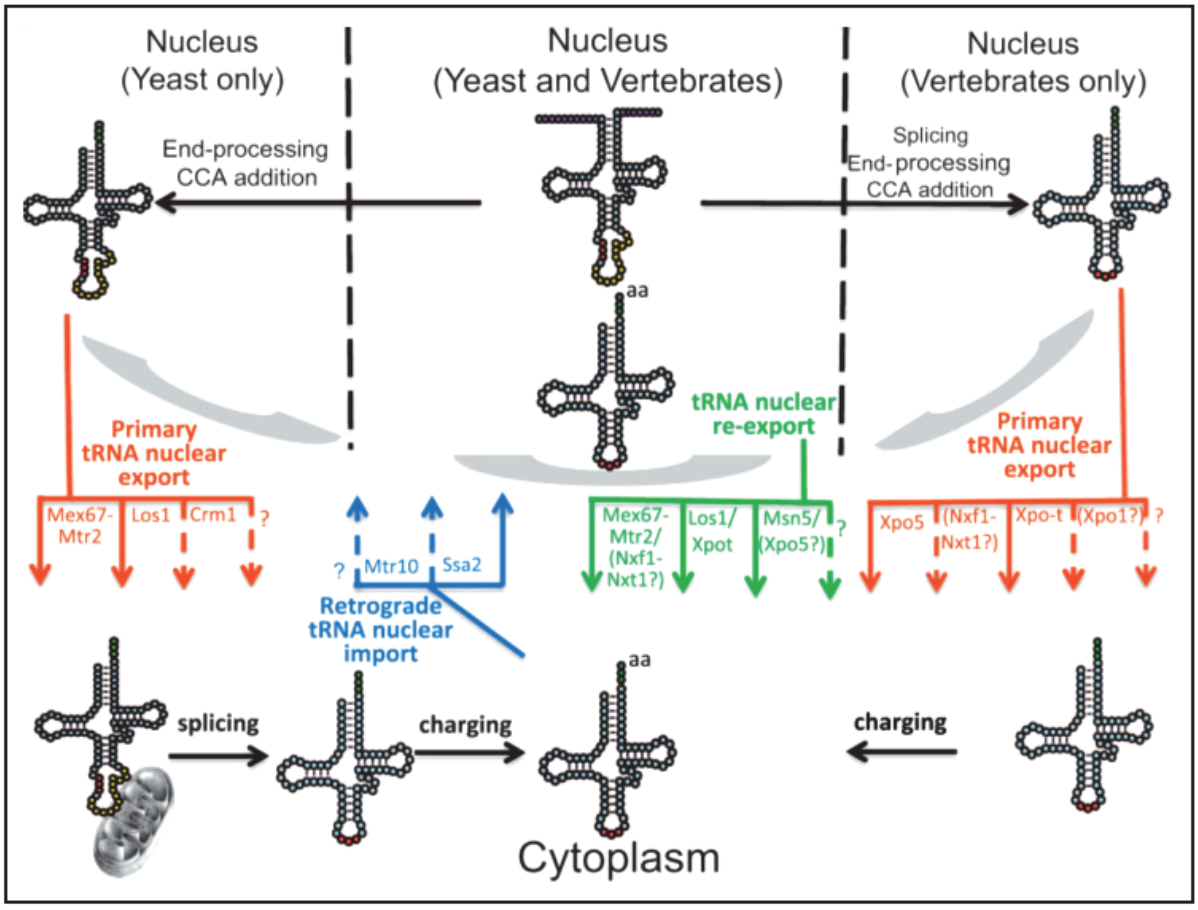

Figure 22: tRNA nuclear-cytoplasmic dynamics in eukaryotic cells. In vertebrates tRNA splicing takes place in the nucleus, whereas in yeast takes place on the outer mitochondrial membrane. Both intron-containing and intronless pre-tRNAs are escorted out of the nucleus by the primary tRNA nuclear export process. After this event the nuclear cytoplasmic pathways converge in yeast and vertebrates. Spliced tRNAs are charged by aminoacyl tRNA synthetases. The tRNAs are then imported back to the nucleus by retrograde tRNA import process. The third and last step of tRNA trafficking includes tRNA nuclear re-export. Imported nuclear tRNAs are exported out of the nucleus by the tRNA re-export process. (From Chatterjee *et al.* 2018.)

1.4.2 Retrograde tRNA nuclear import

The tRNAs re-entry back or re-import into the nucleus is commonly called, the retrograde tRNA nuclear import (Zaitseva *et al.* 2006; Huynh *et al.* 2010; Barhoom *et al.* 2011; Miyagawa *et al.* 2012; Watanabe *et al.* 2013; Chen 2016). One of the key function of retrograde tRNA import into the nucleus is to permit to several tRNAs to achieve a proper modifications and maturation state (Ohira and Suzuki 2011; Kessler *et al.* 2018). Furthermore, tRNA import has also been identified to play a role in tRNA quality control, without having stringent substrate specificity. Different cellular processes as translation regulation, cell cycle control and regulation of retroviral replication are also impacted by retrograde tRNA nuclear import (Zaitseva *et al.* 2006; Chu and Hopper 2013; Chen 2016). The retrograde tRNA nuclear import is energy-dependent utilizing both RanGTPase (Shaheen and Hopper 2005) and Ran independent pathways. Mtr10, which is member of the family of β-importin, has been associated to the retrograde tRNAs nuclear import process either directly or indirectly. Direct interaction with tRNAs has not been detected yet, although, data support a role for Mtr10 in tRNA nuclear import (Takano *et al.* 2015). In contrast, Ssa2, a constitutively expressed protein of the Hsp70 heat-shock family, was previously identified as a tRNA-binding protein. Using a biochemical approach, this experiment reinforce is role as retrograde tRNAs nuclear import (Takano *et al.* 2015).

1.4.3 tRNA re-export

tRNAs are finally re-exported back to the nucleus to take part in the cytoplasmic protein synthesis (Whitney *et al.* 2007). The nuclear re-export represents the third and last shuttling step of tRNAs. Using biochemical studies in yeast, it has been shown that Los1 binds spliced tRNAs, strengthening its role in the nuclear re-export step (Hellmuth *et al.* 1998; Huang and Hopper 2015). This characteristic of Los1 to interact with tRNAs is conserved from yeast to vertebrates. Furthermore, its activity results independent of the amino acylation status of tRNAs (Kutay *et al.* 1998; Arts 1998; Lipowsky *et al.* 1999; Kuersten *et al.* 2002; Huang and Hopper 2015). Since Los1 is unessential in all organisms, multiple Los1 independent pathways for tRNAs re-export have been described so far. β-importin Msn5 or its orthologues, Exportin-5 in vertebrates and HASTY in plants has been reported to serve a minor role in tRNA nuclear export (Calado *et al.* 2002). Using

in vivo co-immunoprecipitation (co-IP), it has been shown that nuclear re-export Msn5/Exportin-5 dependent, preferentially interacts with aminoacylated tRNAs (Huang and Hopper 2015). This is in contrast with the capacity of Los1 to bind either aminoacylated, as well as, uncharged tRNAs.

1.5 tRNA degradation

tRNA modifications are required for tertiary structure stability. Indeed, hypo-modified tRNAs could be targeted for degradation by the nuclear exosome, since they are less stable (Kadaba 2004). They are also less efficiently exported by the Exportin-T (Lipowsky *et al.* 1999). Furthermore, hypo-modified tRNA might also be targeted for degradation via the rapid tRNA decay in the cytoplasm (Alexandrov *et al.* 2006; Chernyakov *et al.* 2008). However, in the last years, many studies proposed that sometimes degradation products of tRNAs are not random products, but they represent functional molecules called transfer RNA-derived small RNA or tsRNAs (Lee *et al.* 2009). tsRNAs regroup tRNA-derived stress-induced RNAs (tiRNAs) and tRNA-derived fragments (tRFs) (Zong *et al.* 2021) (**Table 2**). tsRNAs have a precise sequence structures, specific biological functions, but they are not fully understood.

The biogenesis of tiRNAs, which are 28-36 nucleotides long, occurs when cells are in stress conditions (Li *et al.* 2018). tRNAs are cleaved under stress condition by the angiogenin (ANG), a member of the ribonuclease A superfamily (Fu *et al.* 2009; Emara *et al.* 2010; Ivanov *et al.* 2012; Saikia *et al.* 2012) present into the cytoplasm. tiRNAs can be additionally divided into two subtypes, namely 5-tiRNAs and 3'-tiRNAs, depending on the cleavage site. ANG cleaves only in the anti-codon loop of mature tRNA (Yamasaki *et al.* 2009). Similar to tiRNAs, tRFs are 15-32 nucleotides in length that are produced in stress condition (Kumar *et al.* 2015). tRFs have different cleavage sites at the tRNA terminus. As for the tiRNAs, according to the type of ribonuclease, tRFs can be subdivided into type I tRFs and type II tRFs. The formation of type I tRFs required the activity of Dicer, whereas the formation of type II tRFs required the cleavage by RNase Z (which forms the 5' end) followed by the activity of RNA polymerase III to terminate the transcription at the 3' (Haussecker *et al.* 2010). However, apart from the aforementioned classification based on the type of endonuclease, tRFs are generally divided into three types based on the cleavage sites. There are tRF-5, tRF-3 and tRF-1, which are further divided into different subtypes. Finally we can include also other types of tRFs, such as tRF-2 and i-tRF (Goodarzi *et al.* 2015; Zhu *et al.* 2019).

Table 2: Classification of tsRNAs (From Zong *et al.* 2020)

tsRNAs	Category	Length (nts)	Nucleases	Cleavage sites	References
tiRNAs	5′-tiRNAs	28-36	ANG (mammals)	The anti-codon loop of mature tRNA	(Yamasaki et al. 2009) (Fu et al. 2009)
	3′-tiRNAs				
tRFs	tRF-5a	14-16	Dicer (mice, *Drosophila* and *Schizosaccharomyces. pombe*)	D-loop or the stem region between D-loop and anti-codon loop of mature tRNAs	(Kumar et al. 2014) (Kumar et al. 2015)
	tRF-5b	22-24			
	tRF-5c	28-30			
	tRF-3a	~18	ANG (human)	TΨC loop of mature tRNAs	(Kumar et al. 2014) (Li et al. 2012)
	tRF-3b	~22			(Wang et al. 2013)
	tRF-1	15- 32	RNase Z or ELAC2 (human)	Near the 3′-ends of pre-tRNAs	(Lee et al. 2009) (Wang et al. 2013) (Babiarz et al. 2008) (Liao et al. 2010)
	tRF-2	15- 32	Not Acquired	Not Acquired	(Goodarzi et al. 2015) (Zhu et al. 2019)
	i-tRF	15- 32	Not Acquired	Not Acquired	(Zhu et al. 2019)

As mentioned before, tsRNAs are specific fragments with regulatory functions. Among them, we can mentioned regulation of rRNA synthesis, regulation of RNA reverse transcription, stress granule formation, inhibition of mRNAs translation initiation, canonical and non-canonical miRNA pathway and regulation of oncogenic mRNA stability (Kawaji *et al.* 2008; Fu *et al.* 2009; Emara *et al.* 2010; Ivanov *et al.* 2012; Maute *et al.* 2013; Huang *et al.* 2017). Finally, tsRNAs may also participate in other potential functional mechanisms such as cell proliferation and migration (Mo 2019), signaling among cells and in immune response (Chiou *et al.* 2018).

tsRNAs play a fundamental role in the occurrence and development of various types of disease. Neurological diseases and in particular neurodegenerative diseases are ones of the diseases most correlated with the accumulation of tsRNAs.

The latter are characterized by the loss of specific neurons leading to deterioration and dysfunction of the brain. For example, NSUN2 is a tRNA cytosine34-c5-methyltransferase that catalyzes the methylation of cytosine to 5-methylcytosine, at position 48 or 49 in Leucine tRNAs. It stabilizes the codon-anticodon pairing and helps the mRNA translation. It has been observed in mice deficient for *NSUN2*, an accumulation of 5' tRNA-derived small RNA fragments (tiRNAs) that has been shown to be responsible for protein synthesis defects (Abbasi-Moheb 2012; Blanco

et al. 2014). The phenotype observed in mice includes decreased size and weight of brain, mainly the cortex, the hippocampus and striatum. In humans, *NSUN2* mutations are linked with Dubowitz-like syndrome and with an intellectual disability syndrome (Abbasi-Moheb 2012; Blanco *et al.* 2014).

2. tRNA Splicing Endonuclease (TSEN) complex

tRNA Splicing endonuclease TSEN complex is a tetrameric complex composed of four subunits, namely TSEN54, TSEN34, TSEN2 and TSEN15 (Paushkin *et al.* 2004) (**Figure 23**). The TSEN complex is essential for eukaryotic life (Kasher *et al.* 2011; Cherry *et al.* 2018). It is mostly involved in tRNA processing and in particular in the excision of the intron of certain tRNAs. It is hypothesized that defects in the TSEN complex result in tRNA splicing defects and in the decrease in protein translation (Sekulovski *et al.* 2020). Furthermore, TSEN complex may also be involved in the mRNA 3' end processing (Paushkin *et al.* 2004). However, is role in mRNA processing and maturation is unclear, but it might maintain the stability of the 3' polyadenylation machinery or it might be the catalytic subunit.

TSEN2 and TSEN34 are the catalytic subunits, containing metal ion independent nucleases that cleave the 5' and 3' splice sites, respectively. They generate the 5' exon with a 2'-3'-cyclic phosphate and the 3' exon with a 5'-hydroxyl group (Trotta *et al.* 1997, 2006). On the other side, TSEN15 and TSEN54 are the structural subunits or non-catalytic structural proteins and their precise role in the splicing process is still unknown (Trotta *et al.* 1997, 2006). Intriguingly, upon isolation of the TSEN complex from human cells, an additional TSEN-binding partner was identified: the polyribonucleotide 5'-hydroxyl-kinase, CLP1 (cleavage and polyadenylaton factor 1) (Paushkin *et al.* 2004). CLP1 could be consider as a member of the mRNA 3' polyadenylation machinery (Haddad *et al.* 2012; Weitzer *et al.* 2015) and is conserved-across eukaryotes. The role of CLP1 in tRNA splicing is still unclear, but it might maintain the integrity of the TSEN complex or be involved in the ligation pathway or be responsible for the degradation/turnover of the intron (Weitzer *et al.* 2015). Recently it has been proposed that CLP1 phosphorylates the 5' ends of the 3' tRNA halves after splicing by TSEN complex, in preparation of the ligation of the spliced tRNA halves. The ligase that operates the ligation of the mature tRNA, is so far unknown.

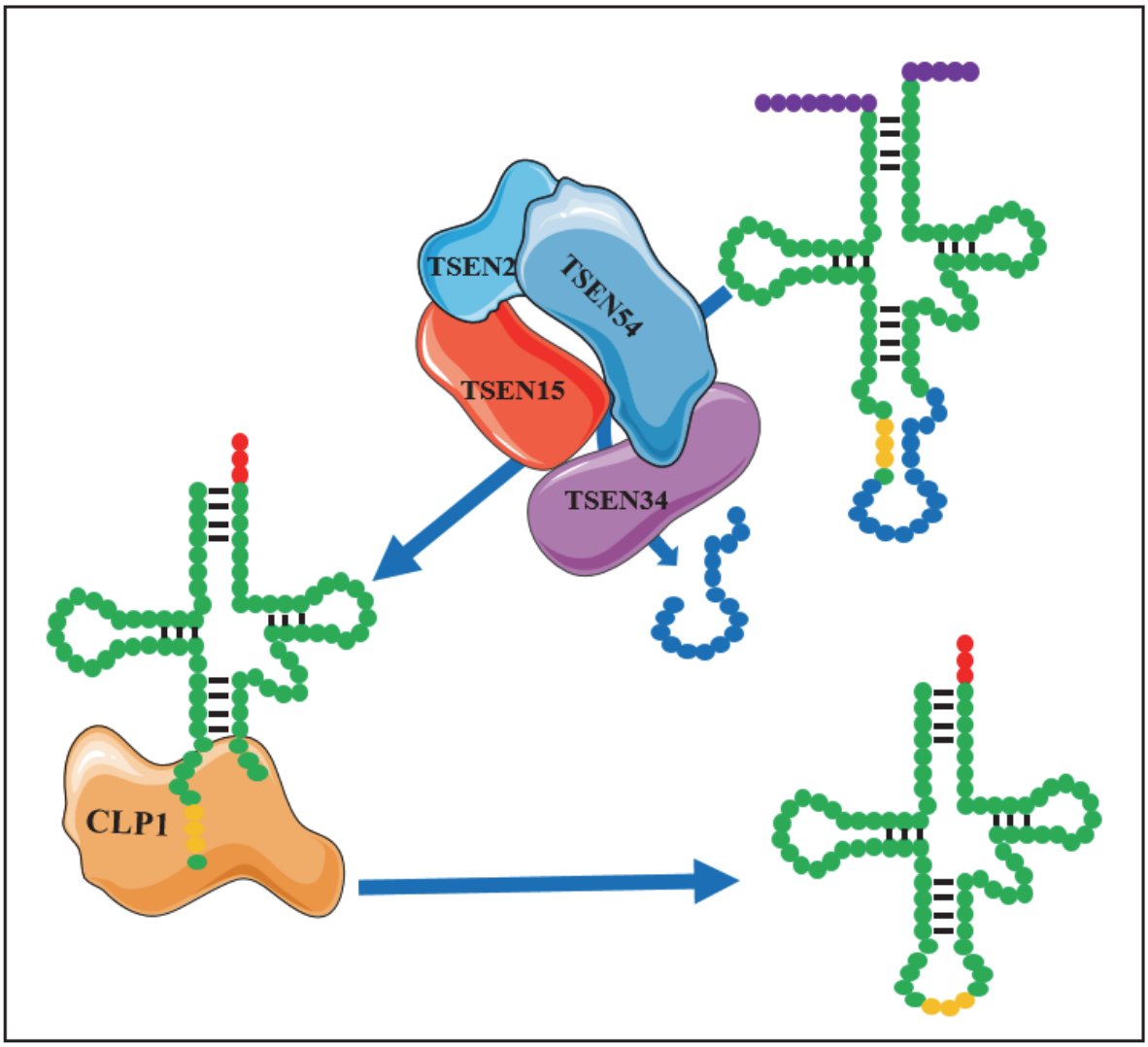

Figure 23: Overview of tRNA splicing in vertebrates. TSEN2 and TSEN34 cleave the 5' and 3' splice sites, respectively, generating the 5' exon with a 2'-3'-cyclic phosphate and the 3' exon with a 5'-hydroxyl group. CLP1 phosphorylates the 5' ends of the 3' tRNA halves after splicing by TSEN complex. The ligase that operates the ligation of the mature tRNA is so far unknown (Adapted from Kessler *et al.* 2018).

Interestingly, mutations have been identified in genes encoding all TSEN complex subunits and CLP1, in individuals with pontocerebellar hypoplasia (PCH), a group of rare autosomal recessive neurodevelopmental disorders. In the next paragraph, I will briefly discussed the involvement of *TSEN54* in PCH.

3. tRNA metabolism alterations and Pontocerebellar hypoplasia (PCH)

Pontocerebellar hypoplasia (PCH) describes a rare heterogeneous group of autosomal recessive neurodegenerative disorders, principally with prenatal onset. Most of the patients affected by PCH present with severe prenatal-onset hypoplasia/atrophy of cerebellum and ventral pons, with variable cerebral involvement and severe psychomotor retardation. Here, I will focus on the clinical aspects and genetic causes of 4 types of PCH linked to tRNA metabolism, namely PCH2A/B/C and D and PCH4/5 and 10, which are due to mutations in the genes encoding all the TSEN complex subunits and CLP1.

3.1 Clinical and pathological aspects of PCH

The main clinical feature of patients affected by PCH is severe psychomotor retardation and in many cases, the condition is fatal early in life (Namavar, Barth, Poll-The *et al.* 2011). The treatment is still symptomatic and no curative treatment is available for any type of PCH. For that reason, the correct diagnosis of PCH is fundamental in order to provide suitable care and counseling regarding prognosis.

PCH type 2A is distinguished by generalized clonus and incoordination of sucking and swallowing in the neonate. Moreover, patients suffer from spasticity, dystonia/chorea and epilepsy. They show a lack of voluntary motor development, grasping and complete absence of cognitive development (Budde *et al.* 2008; Namavar, Barth, Kasher *et al.* 2011; Namavar, Barth, Poll-The *et al.* 2011). Sleeping disorders, feeding problems, apneas, recurrent infections and problem in temperature regulation are reported in the majority of the patients. Microcephaly is progressive and caused by supratentorial atrophy and for that reason the life expectancy is reduced. In one particular case (homozygosity for the p.A307S in *TSEN54*), it has been observed a specific MRI pattern of the cerebellum called “dragonfly” configuration, in which the severely affected cerebellar hemispheres correspond to the “wings” and the sparing of the vermis represents the “body” (Budde *et al.* 2008; Namavar, Barth, Kasher *et al.* 2011; Namavar, Barth, Poll-The *et al.* 2011). All the subtypes *TSEN2*-PCH2B, *TSEN34*-PCH2C, *TSEN15*-PCH2F share with PCH2A common structural defects of the pons and cerebellum, evident on brain imaging (Namavar, Barth, Kasher *et al.* 2011; Bierhals 2013). PCH4 and PCH5 represent the most severe forms of the *TSEN54*-

related PCH spectrum. PCH2, 4 and 5 differ mainly in life expectancy. Patients affected by PCH2 usually succumb before ten years old, whereas those affected by PCH4 or PCH5 succumb as neonates with prenatal onset of symptoms including polyhydramnios, congenital contractures, clonus, hypertonia and hypoventilation (Namavar, Chitayat, Barth *et al.* 2011). The similar common feature among PCH2, PCH4 and PCH5 is the severe microcephaly during development. Hypoplasia affects the hemispheres more severely than the vermis. PCH4 and PCH5 show also delayed maturation and reduced growth of the cerebral cortex, extensive gliosis and a decreased number of neurons in the thalamus (**Figure 24**). Cerebellar hemispheres are severely hypoplastic and devoid of Purkinje cells (Barth *et al.* 2007; Rudaks *et al.* 2011).

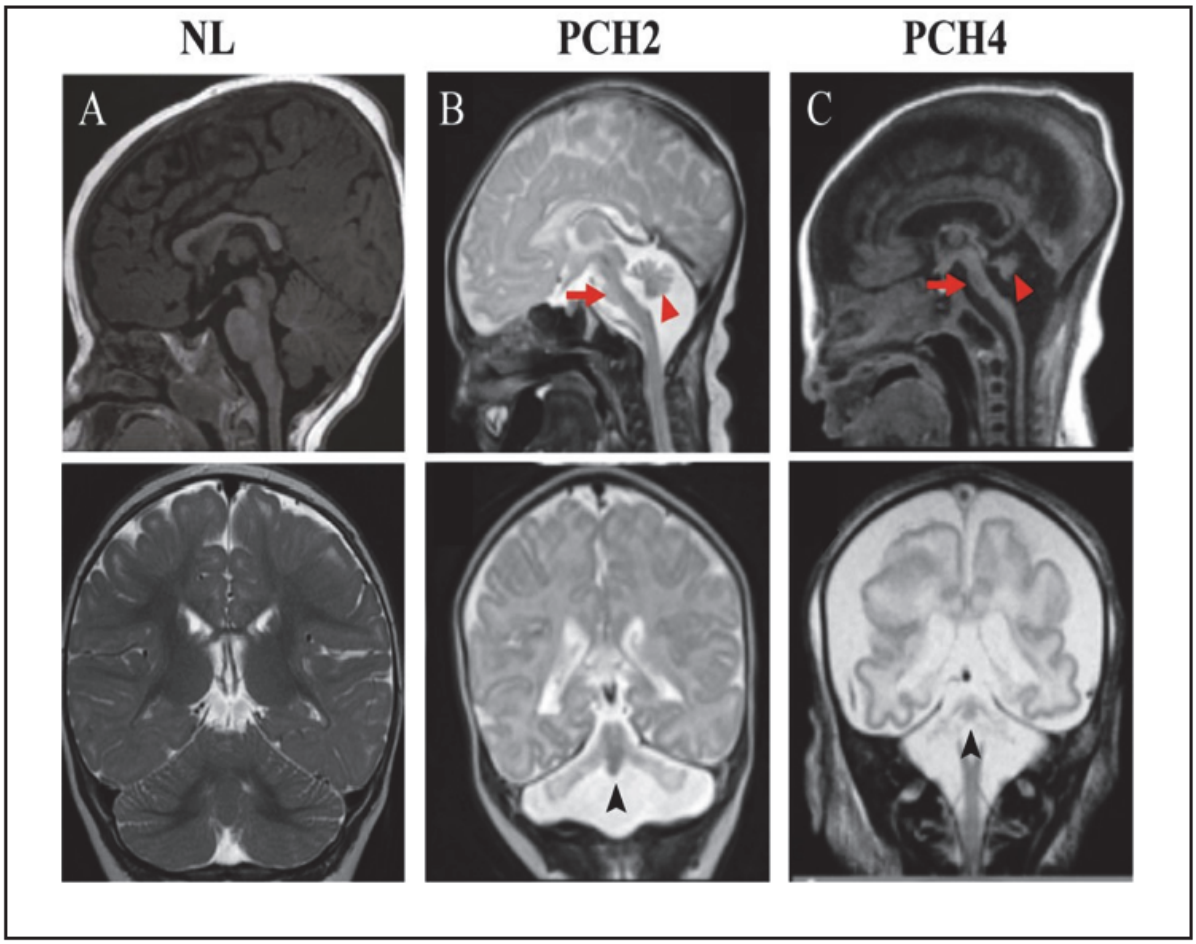

Figure 24: Typical structural brain abnormalities in PCH type 2 or type 4&5. Midline-sagittal (top figures) and coronal (bottom figures) brain MRIs of a healthy individual (**A**) and patients with PCH2 (**B**) and PCH4 (**C**). Sagittal MRIs show variable degree of pontine (red arrow) and cerebellar atrophy/hypoplasia (red arrowhead). Coronal MRIs display the typical "dragon fly pattern" of the cerebellum, with severe flattening of the cerebellar hemispheres and relative sparing of the vermis (black arrowhead). Abbreviation: NL, normal. (From Appelhof *et al.*, 2019; Haldipur and Millen, 2019).

Finally, patients affected by PCH10 present severe developmental delay, seizures, facial dysmorphism, spasticity, microcephaly and signs of axonal neuropathy. In particular, MRI showed hypoplasia of ventral pons, a thin corpus callosum and delay in myelination (Karaca 2014; Schaffer *et al.* 2014).

3.2 Genetic causes and molecular basis of PCH

PCHs have been classified into 13 types according to different clinical features, neuroimaging results and genetic causes (van Dijk *et al.* 2018), with a 14th type recently described (Ucuncu *et al.* 2020) (**Table 3**). Few functional studies have investigated mutations in genes related to PCHs and the majority of them have been subject to limitations due to the lack of patients. However, it has been shown that mutations in genes encoding various RNA-linked processes can be related to distinct PCHs (Budde *et al.* 2008) (**Figure 25**).

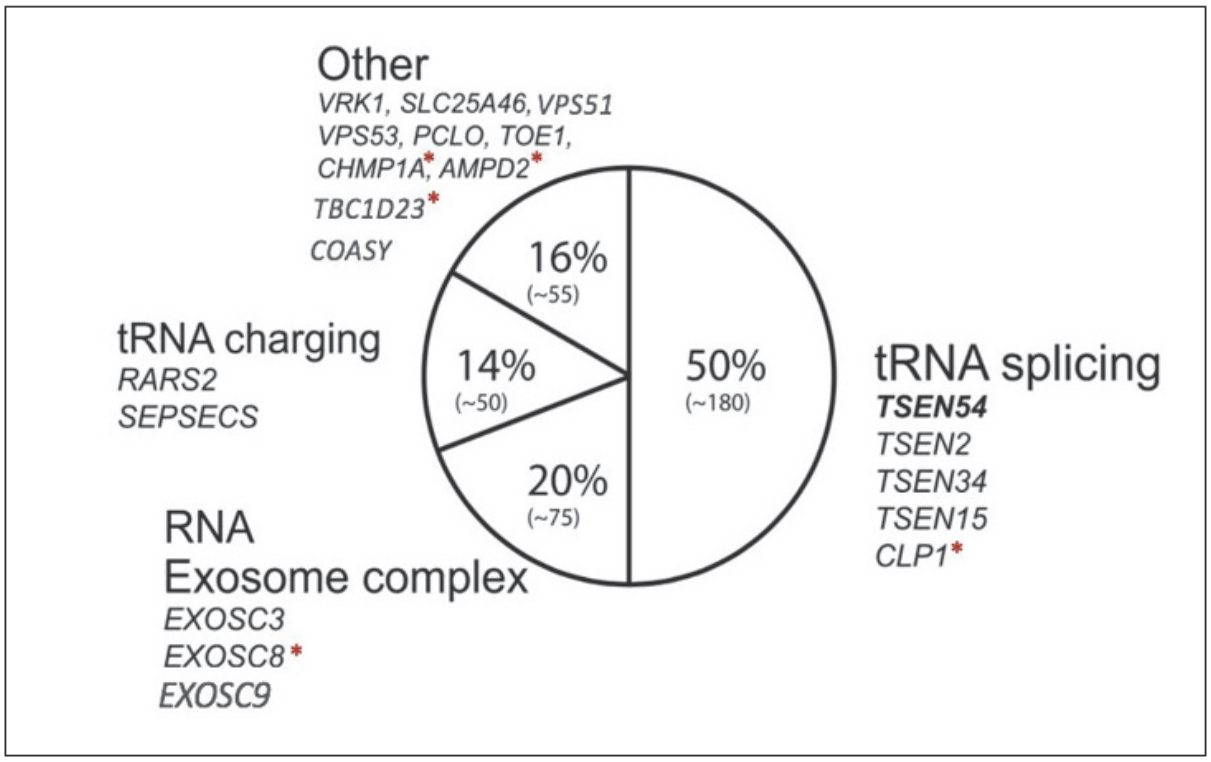

Figure 25: Pie-chart showing the proportion of patients affected by PCH per PCH-related pathological pathway (From van Dijk et al., 2018.).

PCH type 2, and in particular PCH2A, is the most prevalent and also well-known type of all the PCH subtypes concerning 50% of the PCH affected patients. Patients affected by PCH2A harbor the homozygous founder mutation p.A307S in the *TSEN54* gene (missense c.919G>T, substitution of the Alanine 307 with Serine) and represent the majority of patients affected by PCH2 (Budde *et al.* 2008). Its frequency is low than one per 200,000 person (Sánchez-Albisua *et al.* 2014; Maraş-Genç *et al.* 2015). Until now, around 20 different mutations have been identified in the *TSEN54* gene that can cause different subtypes of PCH. A more severe clinical course can depend upon the type of mutations that occurs in *TSEN54*. Indeed, a compound heterozygous mutation (c.919G>T) associated to a splice site, or a nonsense mutations in *TSEN54* are both associated with the more severe PCH type, classified as PCH4 and PCH5, respectively (Patel *et al.* 2006; Namavar, Barth, Poll-The *et al.* 2011; Namavar, Chitayat, Barth *et al.* 2011). More rarely, recessive mutations have been also identified in the three other genes encoding the TSEN complex subunits *TSEN2*, *TSEN34* and *TSEN15*, in individuals with a phenotype similar to PCH2 and classified as PCH subtypes PCH2B, PCH2C and PCH2F, respectively (Budde *et al.* 2008; Breuss *et al.* 2016). Finally, another gene involved in the tRNA splicing process has been linked to PCH. As a matter of fact, mutations in *CLP1*, cleavage and polyadenylation factor 1, have been identified as causal in PCH10 (Karaca 2014; Schaffer *et al.* 2014).

Functional studies in vitro, using stable cell lines expressing wild-type and mutant HisFlag-tagged TSEN15 (Breuss *et al.* 2016), or wild-type and the A307S mutant TSEN54 (Sekulovski *et al.* 2020), showed that some mutations in *TSEN15* or *TSEN54* affect the stability of the proteins, the interactions with other subunits or the function of the TSEN complex. Furthermore, it has been shown that mutations in *TSEN15* and *CLP1* lead to an accumulation of intron-containing tRNAs (Karaca 2014; Schaffer *et al.* 2014; Breuss *et al.* 2016). Finally, mutations in *CLP1* enhanced cell death of neuronal progenitors associated with decrease in cortical neurons number (Karaca 2014) and are responsible of the accumulation of tRNA fragments which induce an oxidative stress (Schaffer *et al.* 2014).

Table 3. PCH subtypes (From van Dijk *et al.* 2018)

Subtype	Subcategory	Gene	Gene Function	Reference
PCH1	PCH1A	*VRK1*	Neuronal migration	(Renbaum et al. 2009)
	PCH1B	*EXOSC3*	mRNA degradation	(Wan et al. 2012)
	PCH1C	*EXOSC8*	mRNA degradation	(Boczonadi et al. 2014)
	PCH1D	*SLC25A46**	Mitochondrial fission and fusion	(Wan et al. 2016)
PCH2	PCH2A	*TSEN54*	tRNA splicing	(Budde et al. 2008)
	PCH2B	*TSEN2*	tRNA splicing	(Budde et al. 2008)
	PCH2C	*TSEN34*	tRNA splicing	(Budde et al. 2008)
	PCH2D	*SEPSECS**	Selenocysteine synthesis	(Agamy et al. 2010)
	PCH2E	*VPS53*	Membrane trafficking	(Feinstein et al. 2014)
	PCH2F	*TSEN15*	tRNA splicing	(Breuss et al. 2016)
PCH3		*PCLO**	Regulation synaptic protein & vesicle formation	(Rajab et al. 2003)
PCH4		*TSEN54*	tRNA splicing	(Budde et al. 2008)
PCH5		*TSEN54*	tRNA splicing	(Patel et al. 2006)
PCH6		*RARS2**	Arginyl tRNA synthetase	(Edvardson et al. 2007)
PCH7		*TOE1*	RNA processing	(Lardelli et al. 2017)
PCH8		*CHMP1A*	Regulation INK4A	(Mochida et al. 2012)
PCH9		*AMPD2*	Regulation GTP synthesis	(Akizu et al. 2013a)
PCH10		*CLP1*	tRNA splicing	(Karaca et al. 2014; Schaffer et al. 2014)
PCH11		*TBC1D23*	Intracellular vesicle transport	(Ivanova et al. 2017)
PCH12		*COASY*	Coenzyme A synthesis	(van Dijk et al. 2018a)
PCH13		*VPS51*	Membrane trafficking	(Uwineza et al. 2019)
PCH14		*MINPP1*	Inositol phosphate metabolism	(Ucuncu et al. 2020)

PCH subtypes with postnatal onset neurodegeneration are marked with *. Abbreviations: DSD, disorders of sex development.

CHAPTER FIVE: DISEASE MODELLING USING iPSCs

Induced pluripotent stem cells (iPSCs) have emerged as a novel cellular model, complementary to animal models and immortalized cell lines, and open up new avenues to unravel new pathophysiological mechanisms and elucidate disease pathogenesis. Since our study takes advantage of using iPSCs, this chapter will introduce iPSC technology, advances in iPSC application in the field of disease modelling, including CRISPR/Cas9 technology applied to iPSCs, and the relevance of using iPSCs to model hereditary podocytopathies.

1. Induced pluripotent stem cells (iPSCs)

1.1 General characteristics

Induced pluripotent stem cells (iPSCs) are "embryonic stem cell-like" cells that derived from the reprogramming of adult somatic cells. They are the equivalent of embryonic stem cells (ESCs) which are derived from the inner cell mass (ICM) of the blastocyst of pre-implantation stage embryo. iPSCs express all ESC-specific markers and show a high rate of proliferation. iPSCs have unlimited self-renewal and they are pluripotent, giving rise to the three germ cell layers, namely, endoderm, mesoderm, and ectoderm, meaning that they have the potential to differentiate into any cell type of the body (Takahashi and Yamanaka 2006; Takahashi *et al.* 2007). In 2006, the discovery of Yamanaka's reprogramming factors revolutionized the potential use of human pluripotent stem cells.

1.2 iPSC reprogramming

Yamanaka and Takahashi, using a reductionist approach, identified candidate reprogramming factors, selecting 24 highly expressed transcription factors in embryonic stem cells. The researchers initially administered the 24 reprogramming factors to mouse fibroblasts, and then they removed one transcription factor at a time. Therefore, they reduced the initial list to a set of 4 reprogramming factors genes: Oct4, Sox2 and the oncogenes Klf4 and c-Myc (Yamanaka's factors or *OSKM* factors). The same principle has been shown to be valid in human cells (Takahashi and

Yamanaka 2006). Later on, Thomson's group reprogrammed human fibroblast using a different set of transcription factors containing Oct4, Sox2, Nanog and Lin28 (Thomson/Yu's factors or *OSNL* factors) (Yu *et al.* 2007).

Two categories of reprogramming methods exist: the integrative systems and the non-integrative techniques. Integrative systems include retro (Takahashi and Yamanaka 2006) or lentiviral vectors (Yu *et al.* 2007), linear DNA transfection (Soldner *et al.* 2009), and piggyback transposon systems (Woltjen *et al.* 2009), whereas the non-integrative technics include replication-defective adenoviral vectors (Stadtfeld *et al.* 2008), non-replicative (Okita *et al.* 2008) or replicative (Yu *et al.* 2009) episomal vectors, F-deficient Sendai viral vectors (Fusaki *et al.* 2009), minicircle vectors (Jia *et al.* 2010), synthetic mRNA (Warren *et al.* 2010), protein delivery (Zhou *et al.* 2009) and small-molecule compounds (Hou *et al.* 2013).

In this study, we used peripheral blood mononuclear cells (PBMCs) as cell source for iPSC derivation because they are easily accessible via an invasive blood sampling. CD34+, a small fraction of hematopoietic progenitor's cells, can be expanded and efficiently reprogrammed to iPSCs (Meng 2012; Zhang 2013).

2. Combination of CRISPR/Cas9 and iPSC technologies

2.1 CRISPR-Cas9 principle

Due to its simplicity, efficiency and versatility, CRISPR-Cas9 represents the best suited system for DNA editing. Up to date, CRISPR-Cas9 technology has the greatest editing efficiency on different cell types (Jinek *et al.* 2012; Byrne *et al.* 2014; Chen *et al.* 2015; Hockemeyer and Jaenisch 2017).

CRISPR/Cas9 stands for clustered regularly interspaced short palindromic repeats (CRISPR)/CRISPR-associated protein (Cas) 9, where Cas9 is a nuclease. This system represents an adaptive immune defense system used by many prokaryotes to protect themselves against entry of foreign nucleic acids from virus and plasmids by using RNA-guided nucleases that will cleave pathogenic/exogenous DNA (Marraffini 2013).

This immune defense system has been adapted to target and modify any genetic locus of interest in either *in vitro* cellular models or *in vivo* animal models. The CRISPR/Cas9 system is based on two components: a guide RNA (gRNA) and a Cas nuclease (**Figure 26**):

- the gRNA is a RNA sequence, which specifically target a DNA region, recruiting the Cas nuclease. Synthesized gRNA are composed of a crispr RNA (crRNA) and a tracrRNA, which are fused into a single chimeric structure (Jinek *et al.* 2012). crRNA is a 20 nucleotide sequence containing a short protospacer-adjacent motif (PAM), whereas the tracrRNA binds the Cas nuclease. The gRNA can be inserted into the cells directly as a simple RNA, or as DNA within a eukaryotic expression vector;

- the CRISPR-associated protein (Cas9) endonuclease, which recognize specific PAM sequences, giving a greater cut precision and specificity. The most commonly used CRISPR-Cas9 is the derived from *Streptococcus pyogenes* (SpCas9) which recognizes a canonical 5'-NGG-3'sequence as PAM sequence (where "N" can be any nucleotide base). Although CRISPR-Cas 9 system results simple and efficient, it presents some limitations. In particular, the most important limit concerns the target site selection and the sgRNA design. This is because DNA sequences might be a potential target sites, inducing mutations in both target and in the off-target regions. Therefore, it is necessary to evaluate the effect of these unwanted mutations.

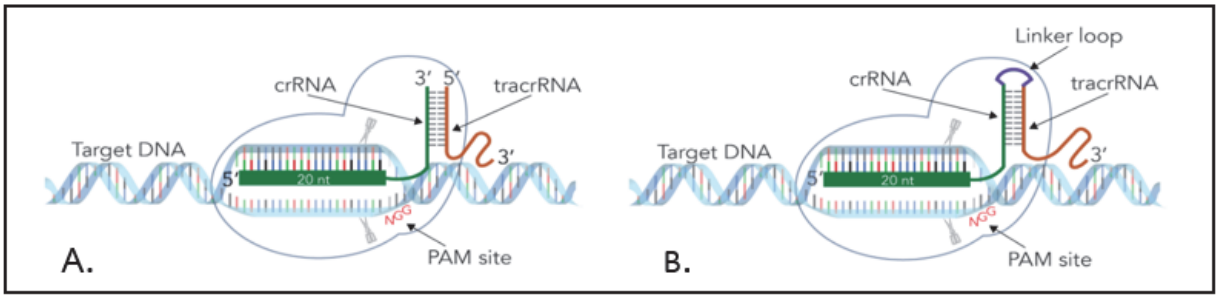

Figure 26: Overview of the CRISPR-Cas9 system. (**A**) Crispr-Cas9 system using crRNA and tracRNA, (**B**) CRISPR-Cas 9 system, using RNA-guide endonuclease (gRNA), in which crRNA and tracrRNA are fused into a single chimeric structure. (From https://sgidtna.com)

The gRNA will pair with the 20 nucleotide targeted sequence and direct the Cas9 towards the site adjacent to the PAM, where the nuclease domain will cut both strands of the target DNA introducing a double strand break (DSB). This DSB triggers cellular repair mechanisms that can give rise to DNA editing through two main pathways (**Figure 27**):

1- the non-homologous end joining repair (NHEJ) pathway, in which the DSB is repaired in a random way (error-prone NHEJ) introducing small indels (insertions or deletions) disrupting the reading frame and generating functional knock-out;

2- the homology-directed repair (HDR) pathway, in which DSB is repaired by homologous recombination where an exogenous donor repair template is provided to be inserted into the target region. The DNA template can be a single-stranded donor oligonucleotides (ssODNs) or a double-strand DNA (dsDNA) or a plasmid (Choulika *et al.* 1995; Perez *et al.* 2008; Chen, Pruett-Miller *et al.* 2011; Ran *et al.* 2013). This system is used to correct genetic defect or to perform knock-in since any desired mutation can be introduced into the exogenous donor template.

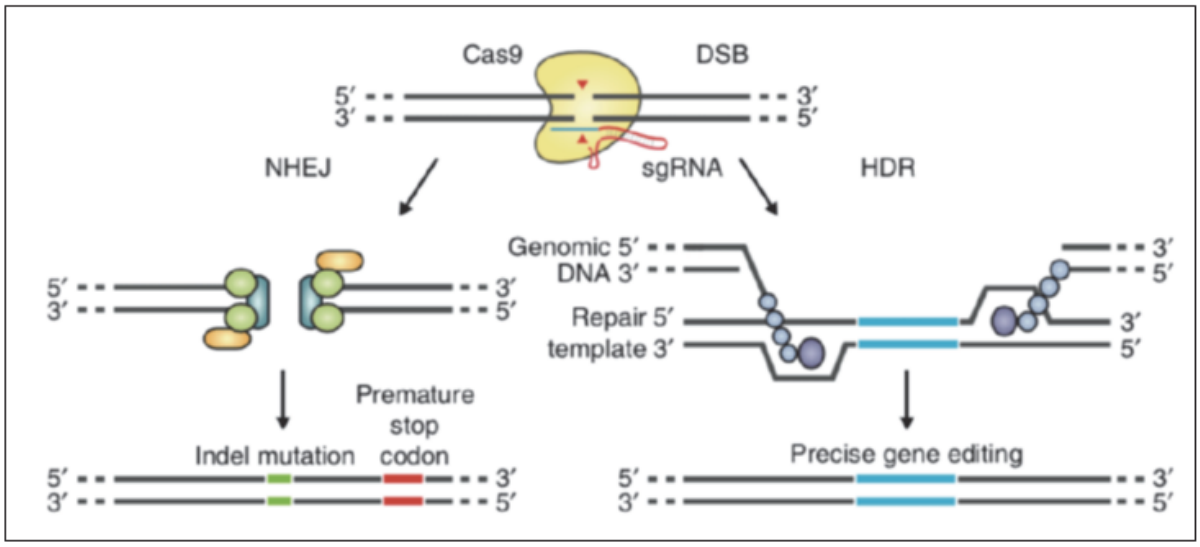

Figure 27: Overview of the CRISPR-Cas9-mediated DSB mechanism. Abbreviation: sgRNA, single guide-RNA. (From Ran et al. 2013)

2.2 Applications in iPSC-based disease modelling

Animal models and immortalized cell lines, commonly used over the last years, have been extremely useful to understand certain aspects of diseases (such as signaling pathway or cellular processes). However, these models have some limitations including the fact that they not fully recapitulate the same phenotypes as those observed in humans. This is mainly due to the difference in animal physiology and genome, but also the absence of the cellular complexity of certain organs (such as the brain or the kidney). The breakthrough discovery of iPSC generation has revolutionized the field of disease modeling. Indeed, iPSCs offer an unlimited resource of material

due to their self-renewal capacity, and offer a variety of different cell types thanks to their ability to differentiate into any cell types. This makes iPSCs a valuable and a great resource for studying disease mechanisms *in vitro*.

More recently, the possibility to generate organoids from iPSCs, permit to mimic the human development *in vitro*. These organoids represent a more physiologically relevant human model, allowing more complex tissue structures and different cell types to be modelled simultaneously. In the future, this tool might be also used to repair tissue damages, paving the way for the regenerative medicine.

iPSCs are a great tool to study monogenic genetic disease thanks to the possibility to derive iPSCs from patients affected with genetic disease. iPSCs with the same genetic background of the patient, can also be used to obtain kidney derived podocytes or neural progenitor cells *in vitro*, with biological and biochemical characteristics comparable to those of the affected podocytes and/or neural progenitor cells. Thus, permitting to study complex genetic diseases, such as in GAMOS syndrome. Furthermore, the use of iPSCs combine with gene-editing using CRISPR/Cas9 permit to insert mutations in specific genes (KI) or to invalidate a gene (KO).

However iPSCs, present some limitations such as, the high variability between different iPSC lines and even between clones of the same iPSC line due to the genetic background of individuals and/or incomplete reprogramming, which will be reflected in the iPSC derivatives too. Therefore, it is necessary the use of isogenic controls, which have the same exact genetic background except for the unique mutation.

3. iPSC differentiation

iPSCs have the potential to give rise to all the derivatives of the three germ layers: endoderm, mesoderm and ectoderm. Specific protocols have progressively emerged allowing direct iPSC differentiation towards a great number of different cell types. In addition to be able to obtain 2D monolayer culture of homogeneous differentiated cell populations, these protocols evolved to further differentiate the iPSCs into 3D structures composed of multiple organ specific cell types called organoids. Here, I will mainly focus on iPSC differentiation towards renal (podocytes and kidney organoids that come from the mesoderm) and neuronal (late cortical

progenitor cells that come from the ectoderm) lineages, the two cellular lineage relevant for modeling podocytopathies and GAMOS.

3.1 iPSC-derived kidney organoid

Three main laboratories headed by Dr R. Nishinakamura (Japan), Pr M. Little (Australia) and Dr J.V. Bonventre (USA) have been the pioneers in the field of iPSC differentiation towards kidney organoids *in vitro* (Taguchi *et al.* 2014; Takasato *et al.* 2015; Morizane *et al.* 2015). Since the first published protocols in 2014/2015, several adapted and improved versions of these protocols as well as new protocols have been established in a quite short time lapse. In general, kidney organoids can be generated on average within 21 to 25 days. The principle of these protocols is to mimic the embryonic renal development and the main stages including **1**) the induction of the primitive streak, giving rise to the emergence of mesodermal progenitors, **2**) the induction of the intermediate mesoderm, **3**) the generation of nephron progenitors (NPCs), and finally arising from these NPCs **4**) the emergence of ordered nephron-like structures containing glomeruli, proximal tubules, loop of Henle and distal tubules (**Figure 28**). The following paragraph summarizes the main factors used for the different induction steps.

In the first step of these protocols aimed at inducing and maintaining the nascent mesoderm, the predominant factor used in all the different protocols is the activation of the canonical Wnt signaling using the Wnt agonist CHIR99021 (CHIR). However, the duration of the CHIR treatment, as well as the CHIR concentration, may vary between protocols, depending on the intrinsic responsiveness of each iPSC clone or cell lines. Then, to establish the mesodermal regions and induce posterior intermediate mesoderm, Activin A is mainly used, sometimes in combination with BMP4. At this stage, the predominant cell population that will selectively arise is the metanephric mesenchyme (MM), at the expense of the ureteric bud (UB) population. Thereafter, the addition of FGF9, mimicking the UB-derived stimulation existing *in vivo*, is sufficient to differentiate posterior intermediate mesoderm towards metanephric mesenchyme (MM) containing the NPCs. Finally, the formation of renal vesicles is induced by a treatment combining CHIR and FGF9 followed by FGF9 alone. Finally no growth factor are added to the media, and kidney organoids with nephron-like structures form through self-organization (**Figure 28**).

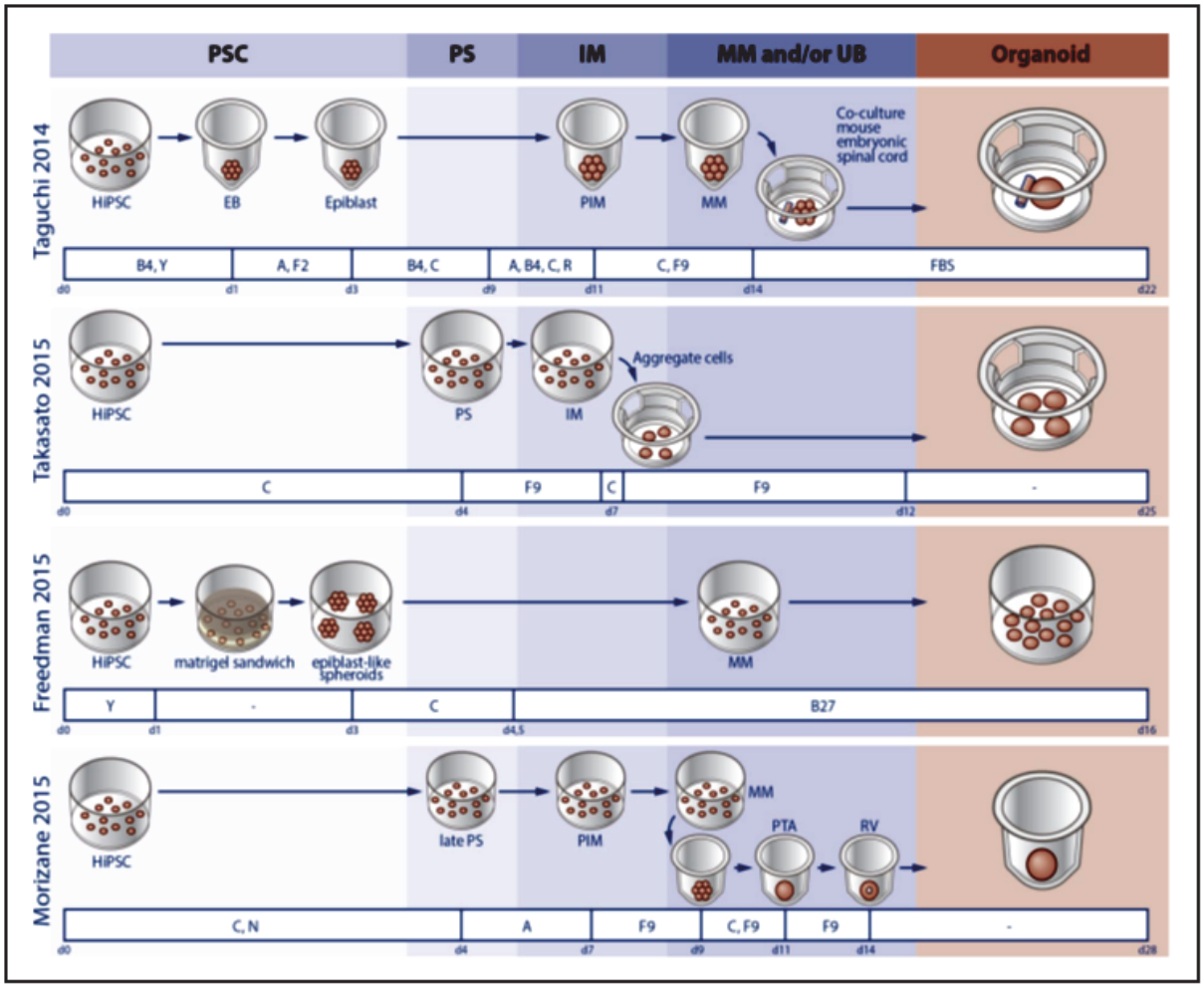

Figure 28: Overview of protocols for the generation of kidney organoids from human iPSCs. Abbreviations: A, activin A ; B, BMS493; B4 , bone morphogenic protein 4; B27, B27 medium; C, CHIR99021; EB, embryoid body; F, fibroblast growth factor; FBS, fetal bovine serum; G, glial cell-derived neurotrophic factor; hiPSCs, human-induced pluripotent stem cells; IM, intermediate mesoderm; KOSR, knockout serum replacement; L, LDN193189; MM, metanephric mesenchyme; N, noggin; PIM, posterior intermediate mesoderm; PS, primitive streak; PSC, pluripotent stem cells; PTA, pretubular aggregate; R, retinoic acid; RV, renal vesicle; S, SB431542; UB, ureteric bud; WD, wolffian duct; Y, Y27632. (From M.Koring *et al.* 2020)

Despite some differences among protocols, all of them result in the formation of kidney organoids containing nephron-like structures.

However, kidney organoids have some limitations including the fact that they do not have structured capillaries, resulting in kidney organoids with avascular glomeruli, and with the lack of the fenestrated endothelium, which is part of the glomerular filtration barrier. Podocytes are chaotically interconnected among them and they do not form the "true SD" (Taguchi *et al.* 2014; Takasato *et al.* 2015; Morizane *et al.* 2015; Freedman *et al.* 2015). Finally, transcriptome profiling

of these kidney organoids is closely similar to the one of human fetal kidney during the 1st and 2nd trimester of gestation, thus resulting immature (Takasato *et al.* 2015; Garreta *et al.* 2019).

Kidney organoids have been initially used to model ADPKD, the most common hereditary kidney disease (Freedman *et al.* 2015), showing that the CRISPR/Cas9-mediated KO of *PKD1* and *PKD2* led to cyst formation in organoids. Then, kidney organoids were used to model nephronophthisis NPHP, a kidney ciliopathy. Indeed, kidney organoids derived from a patient mutated for *IFT140* displayed abnormal shortened and club-shaped primary cilia in tubular cells (Forbes *et al.* 2018). This ciliary phenotype was restored upon CRISPR/Cas9 correction of one of the mutated allele.

Concerning podocytopathies, kidney organoids have been first used to model congenital NS due to either missense or truncating mutations in the nephrin-encoding *NPHS1* gene (Tanigawa *et al.* 2018; Hale *et al.* 2018; Ohmori *et al.* 2021). Patient-derived kidney organoids displayed hypertrophic podocytes by scanning electron microscopy, a decrease, or even an absence, of nephrin expression depending of the mutation, and a decreased podocin expression. Furthermore, nephrin mutants failed to localize at the podocyte surface, therefore preventing the formation of slit diaphragm (Yoshimura *et al.* 2019; Ohmori *et al.* 2021). Finally, it has been shown that KO podocalyxin kidney organoids exhibited a defect in microvilli assembly at the apico-lateral side of developing podocytes, a defect that is phenocopied in capillary-loop stage glomeruli of podocalyxin KO mice (Doyonnas *et al.* 2001), highlighting the crucial role of podocalyxin in the development of podocytes (Kim *et al.* 2017). Altogether, kidney organoids can be useful tool for renal disease modeling in general, but also for hereditary NS modelling. Even if they are not fully mature, they can recapitulate some features of the disease, and help to better understand the pathophysiological mechanisms in complement of animal and other 2D cellular models

3.2 iPSC-derived neural stem cells (NSCs)

Based on the same principle of mimicking the *in vivo* organ development through direct differentiation *in vitro*, the neural aspect of GAMOS can be modeled from iPSCs.

The central nervous system (CNS) formation begins in human development at day 19 and ends up after birth. The germinative ectoderm sheet generates the neural tissue that will give rise to both central and peripheral nervous system. The ectoderm, through a multi-step process called

neurulation or neural induction, generates the neural plate, which subsequently transforms into the neural tube. This neural tube develops into a multi-layered structure in which the neuroepithelium (NE) represents the most inner layer of cells called the ventricular zone (VZ). In this VZ, the cuboidal neuroepithelial cells, called neural stem cells (NSCs) or neural progenitor cells (NPC), and their progeny (the radial glial cells) will give rise to all neural cell types including neurons, astrocytes and oligodendrocytes during neurogenesis (Gilbert 2010).

iPSCs are a suitable model system to study cellular and molecular mechanisms of normal and abnormal neural development (**Figure 29**). *In vitro*, the neuronal differentiation is based on the dual inhibition of the BMP and SMAD pathway (Xu *et al.* 2008). This is responsible of the inhibition of the phosphorylation of Activin and TGFβ receptors, blocking downstream the Smad2/3 signaling (Chambers *et al.* 2009). The BMP signaling has a key role in ectoderm specification. Higher levels favor the epidermal fate, intermediate levels lead to the formation of neural crest cells, whereas low BMP conditions is responsible of a "default state" of the ectoderm, called the neural plate. Neural cells that differentiate from the iPSCs are oriented towards the neuroectodermal fate, exhibiting anterior neuroectoderm markers including PAX6, FOXG1 and OTX2 (Zhang *et al.* 2001; Pankratz *et al.* 2007; Chambers *et al.* 2009). Furthermore, neural cells spontaneously self-organize *in vitro*, into three-dimensional epithelial structures called "neural rosettes", identified by the neuroectoderm markers PAX6 and SOX1. Neural rosettes express numerous features of the neural tube and their formation follows mechanisms and phases similar to those described in the nervous system. Neural rosettes are composed of polarized cells that follow a radial arrangement, organizing themselves around a central lumen. As well, the neural progenitors show similar features as the cells present in the neural tube. The rosettes represent the early stage of neural stem cells present *in vivo*. Furthermore, in the rosettes, we can observed an asymmetrical arrangement of different proteins and cellular junctions that permit to identify an apical region and a basal one. Polarized cells of the rosette along the cell body, showing a radial structure, are marked by nestin, a protein of the intermediate filaments. N-cadherin, an adherent-junction protein has a luminary mark. Finally, we can appreciate the ZO-1 marking, a protein of occluding junctions still in the lumen, but more precisely in the apical position (Zhang *et al.* 2001; Espuny-Camacho *et al.* 2013). After several enzymatic passages, neural rosettes spontaneously dissociate. This will lead to the formation of a homogeneous and stable population of late cortical

progenitor cells, which will principally differentiate into glutamatergic neurons (Boissart *et al.* 2013).

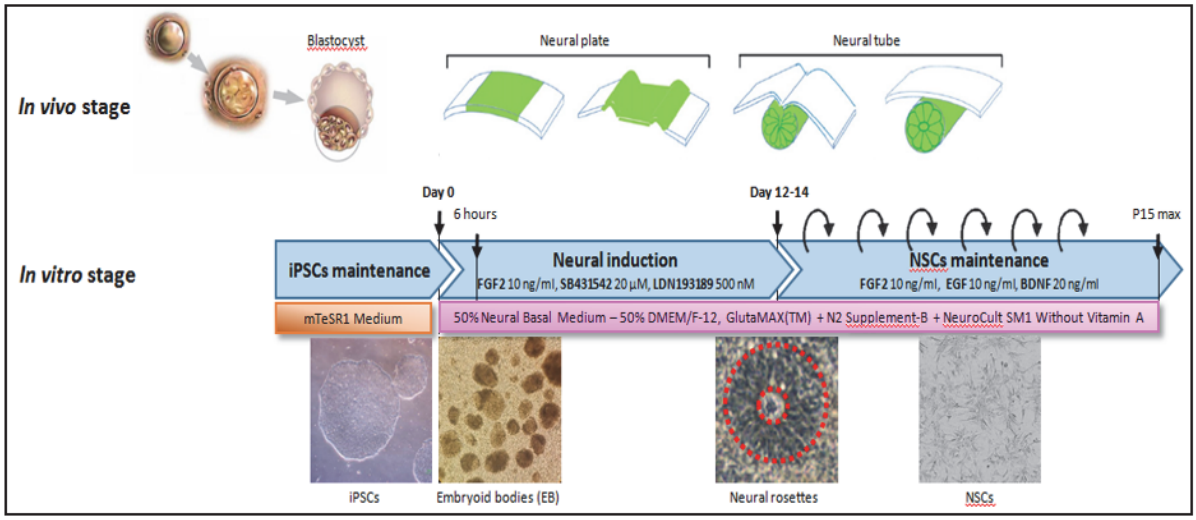

Figure 29: Schematic representation of neurogenesis *in vivo* and *in vitro*. (From M. Boisson and G. Menara)

NSCs can be used for *in vitro* studies to study cellular processes such as proliferation, apoptosis, the ability to differentiate into a homogeneous population of neurons and finally to study neurons degeneration (Ferraris *et al.* 2019)**.**

Furthermore, iPSCs have also been used to model and well characterized primary or secondary microcephaly, which represents the main feature in GAMOS syndrome, through the generation of cerebral organoids from neural progenitor cells (NPCs) (Lancaster *et al.* 2013; Kraemer *et al.* 2015; Gabriel *et al.* 2017). One of the first example using iPSC-derived cerebral organoids concerns iPSCs bearing compound heterozygous truncating mutations in *CDK5RAP2* gene, which encodes for the CDK5 regulatory subunit-associated protein 2, and whose mutations are linked with primary microcephaly, leading to the decrease of the cerebellar cortex and mental retardation (Lancaster *et al.* 2013). *CDK5RAP2* encodes a protein critical for centrosomal functions, and mutations in this gene result in aberrantly functioning centrosomes which lead to human NSC proliferation defects. The use of patient-derived brain organoids, with mutations in *CDK5RAP2* permit to recapitulate real *in vivo* organ development and decipher the cellular mechanisms leading to microcephaly.

Normally, NSCs divide symmetrically, in order to maintain cell proliferative pool, and asymmetrically to differentiate. The decreased of symmetric divisions leads to NSCs pool depletion and premature differentiation. This event impair the brain development and the structural organization of the primitive cortical plate in a developing brain, causing microcephaly (Lancaster *et al.* 2013). The decision to go through a symmetric or asymmetric division is regulated by normal or altered spindle orientation. Normally, radial glial cells division plans are oriented horizontally, as a signature of symmetric expansion that will give rise to a large pool of NPCs and finally generate a structurally normal-sized brain. However, in patients-derived brain organoids, radial glial cells displayed oblique and vertical oriented spindles, leading to asymmetric division that is responsible of premature differentiation. Indeed, patient-derived brain organoids, with mutations in *CDK5RAP2*, displayed smaller neuroepithelial tissues and reduced organoid size, caused by the exhaustion of the neural progenitor's pools, due to premature neuronal differentiation and the consequent reduction of mature neurons, which is not caused by apoptosis (Lancaster *et al.* 2013).

CONCLUSIONS

Next generation sequencing coupled with DNA sequencing allowed us to better understand the complexity of the syndromic and non-syndromic forms of steroid-resistant nephrotic syndrome (SRNS) and to highlight phenotypic variability, revealing mutations in unexpected genes. Indeed, recent data in the literature indicate that the renal disease can be associated with extra-renal manifestations, the most frequent being neurological such as in Galloway-Mowat syndrome (GAMOS), associating SRNS with microcephaly and neurological impairment. To date, mutations have been identified in 11 different genes encoding proteins mainly involved in RNA metabolism, in particular tRNA, such as t^6A (KEOPS) or m^7G (WDR4) modifications or maturation of UsnRNA/snoRNA (WDR73), and in transcriptional regulation, revealing unexpected physiopathological mechanisms involved in GAMOS. The identification of mutations in genes that affect both the kidney and the nervous system raises the fascinating question of molecular pathways that could be common to both kidney and brain development and function, in line with growing evidence that podocytes and neurons share a large number of features. For all that reasons, the global aim of this PhD thesis was to identify and characterize new candidate genes for SRNS and GAMOS.

This study reports the identification by exome sequencing of two novel mutations in the *TSEN54* gene (tRNA splicing endonuclease subunit 54) in patients with either isolated SRNS or GAMOS, with a renal disease-onset ranging from congenital to early adulthood. To confirm the pathogenicity of these variants, we used different approaches using various cellular models, including lymphoblastoid cell lines (LCLs), immortalized podocytes and induced pluripotent stem cells (iPSC)-derived neural stem cells (NSCs) and kidney organoids, in order to identify the molecular and cellular mechanisms altered in each condition. We investigate the impact of *TSEN54* variants on mRNA and protein levels, as well as on tRNA intron splicing by using tRNA-sequencing. In addition, to unravel the SRNS and/or GAMOS molecular and cellular mechanisms, we depleted *TSEN54* using shRNA in immortalized human podocytes to study transcriptome profil changes upon *TSEN54* depletion (RNA-seq) and various cellular processes such as proliferation, apoptosis and protein synthesis. At the time writing this manuscript, several experiments are still in progress, including analyzes of the transcriptomic profiles of NSCs and of podocytes isolated

from kidney organoids, analysis of intron splicing defects (tRNA-seq) and study of various cellular processes in NSCs.

Altogether, these results will help deciphering the pathological cellular and molecular mechanisms linked to mutations in *TSEN54* and underlying SRNS and GAMOS pathogenesis. This study represents the first work that demonstrate the unexpected involvement of *TSEN54* and its role in the tRNA splicing processing as a cause of GAMOS and SRNS, providing novel insights into the genetic, molecular and phenotypic spectrum of these rare diseases.

RESULTS

ARTICLE

Mutations in *TSEN54* are a novel cause of steroid-resistant nephrotic syndrome and Galloway-Mowat syndrome

In this part of my PhD thesis, I will report the work I performed that aim to unravel the pathophysiological molecular and cellular mechanisms involved in *TSEN54*-linked GAMOS and SRNS. The results are presented in the form of an article "in preparation" although some of the analyses are still in progress and unfortunately incomplete at the time of writing the manuscript.

Here I report the identification of mutations in *TSEN54* gene in individuals affected with SRNS or GAMOS and the description of the clinical manifestations in these individuals. Furthermore, I report the impact of *TSEN54* variants on mRNA and protein levels, the functional and molecular studies in *TSEN54* knock-down podocytes and the impact of *TSEN54* variants on tRNA-intron splicing. Finally, I present the generation of *TSEN54* induced pluripotent stem cells (iPSCs) by reprogramming cells of the SRNS affected individual and by using CRISPR/Cas9-mediated gene editing to obtain iPSCs mimicking the genotype of the GAMOS affected child.

Mutations in *TSEN54* are a novel cause of steroid-resistant nephrotic syndrome and Galloway-Mowat syndrome

Francesco Miscia [1], Bruno Estebe [1], Christelle Arrondel [1], Olivier Gribouval [1], Aurélien Juven [1], Fabien Nevo [1], Nathalie Lefort [2], Caroline Chariau [3], Quentin Francheteau [3] Erwin van Dijk [4], Delphine Naquin [4], Ida Chiara Guerrera [5], Nicolas Cagnard [6], Mélanie Parisot [7], Cherif Noureddine [8], Tackwa Khalifeh [9], Jamil Hachicha [10], Fadi Fakhouri [11], Marion Rabant [12], Nathalie Boddaert [13], Corinne Antignac [1, 14], Géraldine Mollet [1].

1 Université de Paris, *Imagine* Institute, Laboratory of Hereditary Kidney Diseases, INSERM UMR 1163, Paris, France

2 iPSC Core Facility, Imagine Institute, INSERM UMR 1163, Université de Paris, Paris, France

3 PFiPSC, SFR-SANTE, INSERM, CNRS, UNIV NANTES, CHU NANTES, Nantes, France

4 High Throughput Sequencing Platform, Institute for Integrative Biology of the Cell (I2BC), CEA, CNRS, University Paris-Sud, University Paris-Saclay, Gif-sur-Yvette, France

5 Proteomics platform Necker, Université de Paris - Structure Fédérative de Recherche Necker, INSERM US24/CNRS UMS3633, Paris, France

6 Genomics Core Facility, Imagine Institute, Structure Fédérative de Recherche Necker, INSERM U1163 and INSERM US24/CNRS UMS3633, Université de Paris, Paris, France

7 Bioinformatic Core Facility, Structure Fédérative de Recherche Necker, INSERM US24/CNRS UMS 3633, Imagine Institute, Université de Paris, Paris, France

8 Medical Center El Farabi, Ariana, Tunis, Tunisia

9 Service Medico-Chirurgical de Pédiatrie, CHU de Poitiers, Poitiers, France

10 Unité de Recherche de Pathologie Rénale, Service de Néphrologie, Faculté de Médecine, CHU Hedi Chaker, Sfax, Tunisie.**11** Department of Nephrology, Centre Hospitalier Universitaire (CHU) de Nantes, Nantes, France.

12 Service d'anatomie pathologique, Hôpital Necker-Enfants-Malades, Paris, France.

13 Department of Pediatric Radiology, and *Imagine* Institute, INSERM UMR 1163 and INSERM U1000, Université de Paris, Hôpital Necker-Enfants Malades, Paris, France

14 Département de Génétique, Assistance Publique - Hôpitaux de Paris, Hôpital Necker-Enfants Malades, Paris, France

ABSTRACT

Several studies have reported *TSEN54* mutations to be causative of pontocerebellar hypoplasia (PCH), a group of rare autosomal recessive neurodevelopmental disorders. Here we reported the unexpected discovery of two novel variants in *TSEN54* in individuals with either isolated steroid-resistant nephrotic syndrome (SRNS) or Galloway-Mowat syndrome (GAMOS). Intriguingly, the child with GAMOS exhibited structural brain anomalies reminiscent of *TSEN54*-linked PCH type 2. One of the mutations is located in an intron and creates a cryptic splicing site that is used with the canonical splicing site, leading to the expression of a low amount of TSEN54 WT protein in the cells of patients harboring this mutation. We also demonstrated that mutant proteins were not detectable by WB, suggesting mRNA decay or protein degradation. In addition, *TSEN54*-depleted podocytes exhibited a decrease in cell proliferation and protein synthesis. Interestingly, tRNA-sequencing performed on lymphoblastoid cells showed an increase in unspliced tRNAs in the SRNS-affected individual. Finally, we successfully generated induced pluripotent stem cells by direct reprogramming or gene-editing to model *TSEN54*-linked SRNS and GAMOS. Taken together, our results demonstrated that mutations in *TSEN54* perturb different cellular pathways and, support the consensus that dysregulation of tRNA maturation process is critical for cell homeostasis, and may contribute to SRNS or GAMOS pathogenesis.

INTRODUCTION

Transfer RNAs (tRNAs) are non-coding RNAs that play an essential role in protein translation by delivering amino acids to the ribosomes. They are expressed from a large number of genes, ranging from 89 in *Escherichia coli* to 568 in *Caenorhabditis elegans* (http://gtrnadb.ucsc.edu/), with 429 predicted high confidence tRNA genes in humans to decode 64 genetic codons that specify 20 amino acids (Chan and Lowe 2016). tRNA life cycle starts in the nucleus where they are transcribed by RNA Polymerase III into a precursor tRNA (pre-tRNA) that undergoes several steps of post-transcriptional modifications to generate a mature tRNA. Early processing steps involve the removal of the 5' leader, 3' trailer and introns of variable length in tRNA genes, and the late processing steps include the addition of CCA to the 3' terminus and export of the mature tRNAs to the cytoplasm (Schaffer *et al.* 2019). In humans, 28 out of the 429 predicted tRNA genes contain an intron and correspond to all the tRNA genes encoding in particular four isodecoder families, namely Arginine-TCT (5 genes), Isoleucine-TAT (5 genes), Leucine-CAA (5 genes) and Tyrosine-GTA (13 genes). Intron removal from pre-tRNA transcripts is not carried out by the spliceosome, but by a specific multi-protein complex, namely the tRNA splicing endonuclease (TSEN) complex, a tetrameric complex containing two structural subunits, TSEN15 and TSEN54, and two catalytic subunits, TSEN34 and TSEN2 (Paushkin *et al.* 2004). In addition to TSEN complex that performs intron excision, an additional TSEN binding partner, the cleavage and polyadenylation factor 1 (CLP1), is required for the 3' exonic end phosphorylation before religation of both tRNA halves by a ligase not yet discovered (Paushkin *et al.* 2004; Weitzer and Martinez 2007; Ramirez *et al.* 2008).

These last years, growing body of evidences have linked defects in tRNA metabolism to human genetic diseases, in particular neurological disorders (Schaffer *et al.* 2019; Suzuki 2021). Indeed, recessive mutations in the genes encoding all the four subunits of TSEN complex and CLP1 have been identified in individual affected with pontocerebellar hypoplasia (PCH), a group of rare autosomal recessive neurodevelopmental disorders characterized by hypoplasia and/or atrophy of the cerebellum and pons, often associated with severe progressive microcephaly, without any renal involvement described so far (Budde *et al.* 2008; Schaffer *et al.* 2014). However, defects in tRNA modifications are not always associated with neurological disorders as we recently highlighted by identifying t^6A tRNA modification defects in a rare disorder, that is Galloway-Mowat syndrome (GAMOS), characterized by the co-occurrence of microcephaly, neurological abnormalities and

renal manifestations. Indeed, mutations have been identified in the genes encoding all the components of the t^6A biosynthesis pathway, namely YRDC and the 5 subunits of the KEOPS complex (Braun *et al.* 2017; Wang *et al.* 2018; Arrondel *et al.* 2019). The renal manifestations in GAMOS mainly consist in congenital or infantile onset of steroid-resistant nephrotic syndrome (SRNS), due to an intrinsic defect of the podocyte, a highly specialized post-mitotic epithelial cell of the kidney filtration barrier. However, GAMOS cases with isolated proteinuria, late-onset SRNS or without renal involvement have also been described (Colin *et al.* 2014; Vodopiutz *et al.* 2015; Braun *et al.* 2017, 2018). The consistent morphological feature of GAMOS is microcephaly, which may be detected at birth or postnatally, and neurological manifestations often include intellectual disability, global development delay, but also hypotonia, seizure and spasticity. A wide range of structural brain abnormalities is present including cerebellar and cortical atrophy, and myelination and/or neural migration defects. GAMOS is genetically heterogeneous with, to date, mutations identified in 11 different genes encoding proteins mainly involved in RNA metabolism, in particular tRNA modifications (KEOPS complex and WDR4) and UsnRNA processing (WDR73), but also in transcriptional regulation and nuclear pore assembly/function (NUP133, NUP107, PRDM15) (Colin *et al.* 2014; Rosti *et al.* 2016, 2017; Braun *et al.* 2017, 2018; Fujita *et al.* 2018; Arrondel *et al.* 2019; Mann *et al.* 2021).

In this study, we describe the unexpected discovery of biallelic new variants in the *TSEN54* gene in one child affected by GAMOS. More surprisingly, one of these variants was also found in the homozygous state in six individuals from two unrelated consanguineous families with isolated SRNS. We demonstrated by tRNA-sequencing an increase in unspliced tRNAs in the SRNS affected individual. Functional studies in *TSEN54*-depleted immortalized human podocytes revealed that loss of TSEN54 led to defects in proliferation and protein synthesis similarly to what have been previously shown in individuals with GAMOS and t^6A defects. In addition, RNA-sequencing analysis on these depleted podocytes showed the involvement of TSEN54 in biological processes involved in regulation of cell size and cell growth, in cell differentiation, synapse organization or cell development. Finally, we successfully generated induced pluripotent stem cells (iPSCs) by reprogramming peripheral blood mononuclear cells from a SRNS affected individual and by CRISPR/Cas9 gene-editing to obtain iPSCs mimicking the GAMOS affected individual genotype. We propose that altered levels of TSEN54 and of its role in tRNA intron splicing are directly linked with GAMOS and SRNS, although further studies should be undertaken to further characterize the molecular and cellular mechanisms involved in these rare diseases.

RESULTS:

Identification of mutations in *TSEN54* gene in individuals with SRNS or GAMOS

To identify novel molecular causes of SRNS and/or GAMOS, we performed whole exome sequencing (WES) in a nonconsanguineous family (Family A) with one affected child exhibiting clinical features consistent with GAMOS (**Figure 1A and Table 1**) and previously screened negative using a customized gene panel for podocytopathies, including all known GAMOS genes. WES was performed using a trio strategy (the proband and his parents) and then analyzed for potentially deleterious rare biallelic variants (MAF<1%). We thus identified two novel variants in the *TSEN54* gene (NM_207346.3), one variant in intron 5 (c.468+48 A>G) and one nonsense mutation in exon 8 (c.1015C>T, p.Gln339*) (**Figure 1B-C**). Intriguingly, we had previously identified the intronic variant in 2 unrelated consanguineous families (Family B and C) with 3 affected individuals in each family presenting with isolated SRNS without any extrarenal symptoms, and no other genetic causes of SRNS (**Figure 1A**, **Table 1**). These two families originated from the same region of Tunisia and shared a common haplotype at the *TSEN54* locus indicating a founder effect. The intronic variant found in both families was the only rare variant with impact on protein or mRNA sequences and was found after identification by homozygosity mapping of a small region of homozygosity on chromosome 17 and complete genomic sequencing of this 2.1 Mb interval (data not shown). Both variants segregated with the disease in all families (**Figure 1A**) and were absent, or present at a very low frequency (MAF: $1{,}6x10^{-5}$) in gnomAD. None of them was referenced in ClinVar and HGMD databases. According to splice site prediction programs (MaxEntScan /GeneSplicer), the intron variant was predicted to create a cryptic donor splice site with a mean score of 8.5 higher than the canonical one which had a mean score of 7.6 (**Figure 1D**). In case this cryptic splice site is used, it would result, at the protein level, in the insertion of 20 amino acids after Gln156 leading to a truncated protein of 176 amino acids, named hereafter Ins47 (**Figure 1C**). On the other side, the nonsense variant would lead to a truncated protein of 339 amino acids named hereafter Q339* (**Figure 1C**).

Clinical manifestations of individuals harboring *TSEN54* variants

The individual A.II-2, diagnosed with GAMOS and harbouring the biallelic mutations in *TSEN54*, presented with a neurological phenotype consisting of developmental delay and microcephaly detected at birth (HC=31, -2.7 SD) (**Table 1**). The child also displayed axial hypotonia and spasticity at 2 years, with no language skills and inability to sit. Brain MRI at 4 months showed structural abnormalities consisting of asymmetric cerebellar hypoplasia, moderately flattened pons and a thin corpus callosum (**Figure S1A**). Early-onset proteinuria was evidenced by urine dipstick at 6 months and rapidly progressed towards nephrotic syndrome (NS) at 2 years, and the child eventually died within 3 months from respiratory complications. Intriguingly, some of the structural brain anomalies involving the pons and the cerebellum were reminiscent of type 2 pontocerebellar hypoplasia (PCH). In all affected individuals carrying the intronic variant in the homozygous state, the disease was discovered at an advanced stage with nephrotic-range proteinuria, chronic renal failure evolving rapidly to end-stage kidney disease in the adolescence (14 to 16 years) in Family C, and in early adulthood (19 to 22 years) in Family B, respectively (**Table 1**). In the youngest brother in Family C (B.II-1), non-nephrotic proteinuria was discovered at 22 years with FSGS lesions on renal biopsy, and leads to ESRD several years later (**Figure S1B**). Neither displayed extra-renal symptoms at the age of 28 to 46 years.

Impact of *TSEN54* variants on mRNA and protein levels

To study the impact of the *TSEN54* variants on mRNA and protein levels, in particular the impact of the intronic variant on *TSEN54* mRNA splicing, we derived lymphoblastoid cell lines (LCLs) from the parents of the GAMOS affected child corresponding to individuals A.I-1 and A.I-2, bearing, in the heterozygous state, the intronic splice variant and the nonsense variant, respectively, and from two individuals affected with isolated SRNS and carrying the intronic splice variant in the homozygous state (B.II-1 and B.II-4) (red stars on **Figure 1A**). We performed RT-PCR on LCLs cDNA using primers covering exon 3 to exon 8, and demonstrated the presence of two transcripts in the individuals bearing the intronic splice variant, one transcript of 446 base pair (bp) corresponding to the wild-type (WT) allele and one transcript of 493 bp corresponding to the mutated allele (**Figure 2A**). This latter corresponds to the insertion of 47 intronic bp (named hereafter "Ins47") confirming that both the canonical and the cryptic splicing sites are used (**Figure**

1D). RT-PCR using several pairs of primers covering the full *TSEN54* cDNA did not show any other aberrant transcripts in none of the individuals carrying either variants (data not shown). We next performed quantitative RT-PCR using 3 couples of primers amplifying either all *TSEN54* transcripts, or only the WT or the Ins47 transcript (**Figure S2**). LCLs of individual A.I-2 carrying the nonsense variant expressed approximatively two times less total and WT transcripts suggesting that the transcript derived from this mutant allele is subject to nonsense-mediated RNA decay (NMD). Concerning individuals bearing the intronic variant, we could observed that, whatever the status of the variant is, the mutated Ins47 allele produced a small amount of WT transcript in addition to the Ins47 transcript. However, these data did not allow us to conclude whether the Ins47 transcript was subjected to NMD and to precisely quantify the amount of Ins47 transcript compared to the WT.

Since no other known mutations in *TSEN54* led to a renal phenotype in PCH, we hypothesized that the expression of the Ins47 mutant protein could be responsible for the renal phenotype observed in patients carrying specifically this intronic variant. We therefore performed western blotting (WB) on LCL protein lysates using antibodies directed against the N-terminal part of the TSEN54 protein to detect WT and mutant proteins. In line with the qRT-PCR data, we detected TSEN54 WT protein at the expected size of 54 kDa in all samples, with, as expected, less WT protein expressed by the affected SRNS individual B.II-4, homozygous for the Ins47 variant, compared to the individual A.I-1, heterozygous for the Ins47 variant (**Figure 2B-C**). However, compared to B.II-4, the individual A.I-2 expressed less TSEN54 WT protein while carrying a WT allele and being healthy. Given the possibly NMD of the transcript with the nonsense variant, the Q339* mutant protein could not be detected at its 39 kDa predicted size. The same was observed for the Ins47 mutant protein that could not be detected at its expected size of 20 kDa, while the Ins47 transcript could be detected by qRT-PCR, suggesting either absence of Ins47 transcript translation or protein degradation (**Figure 2B-C**). Altogether, we demonstrated that the intronic variant creates a cryptic splice site that is used together with the canonical one, leading to the expression of a residual amount of TSEN54 WT protein in the SRNS affected individual. In addition, none of the mutant proteins could be detected by WB in these LCLs dismissing our initial hypothesis that the Ins47 mutant protein could be responsible for the renal phenotype.

Functional and molecular studies in *TSEN54* knock-down podocytes

Transient depletion of the expression of the t^6A biosynthesis pathway components, whose mutations are responsible for GAMOS, has been shown to result in defects in various cellular processes such as proliferation (Braun *et al.* 2017; Arrondel *et al.* 2019). Similarly here, we transiently depleted the expression of *TSEN54* in an immortalized human podocyte cell line using two different shRNA (Sh1 and Sh2), therefore mimicking the effect of the Ins47 variant that leads to the expression of a residual amount of TSEN54 WT protein. We first validated the two shRNA against *TSEN54* by qRT-PCR and WB and demonstrated that, although the Sh1 induces a stronger knock-down (KD) compared to the Sh2 (**Figure 3A**), both shRNAs lead to a similar drastic decrease of TSEN54 protein level (**Figure 3B-C**). Then, using a colorimetric MTT assay over 7 days, we demonstrated that reduced expression of *TSEN54* decreased cell proliferation, as early as day 3 for Sh2 and day 4 for Sh1(**Figure 3D**). Since tRNAs are essential components of the protein synthesis machinery and since TSEN54 is part of a complex that modifies tRNAs, we hypothesized that *TSEN5*4 KD may impact global translation. We thus quantified the newly synthetized protein levels in Sh1 and Sh2 *TSEN54* KD, and demonstrated a significant decreased in both KD cells compared to scrambled-treated podocytes (**Figure 3E**). We next performed RNA-sequencing upon *TSEN54* KD to try to identify molecular pathways deregulated by reduced expression of *TSEN54* in podocytes. Although both shRNAs result in a very low TSEN54 protein expression level, principal component analysis (PCA) of RNA-seq data revealed a tight clustering of all triplicates and the separation of the scrambled shRNA (control) in green from the Sh1-*TSEN54* in orange (SH1) and from the Sh2-*TSEN54* in gray (SH2). However, the PCA also highlighted the great difference between both *TSEN54* KD lines **Figure S3A**). To take into account only the transcriptional changes linked to *TSEN54* depletion, we identified the shared genes that were differentially regulated in both *TSEN54* knockdown podocyte lines (Sh1 and Sh2) compared to control (scrambled shRNA). We found 59 genes that were up regulated and 309 genes that were downregulated upon *TSEN54* depletion (**Figure S3B**). Gene ontology analyses performed on the 59 upregulated and 309 downregulated genes highlighted biological processes related to regulation of cell growth, cell size, cell differentiation, synapse organization or cell development, suggesting that *TSEN54* may play a key role in these processes (**Figure S3C**).

Impact of *TSEN54* variants on tRNA-intron splicing

As the main function of the TSEN complex is to remove introns in a restricted subset of intron-containing tRNAs, and since it has already been shown that *CLP1* mutations lead to accumulation of linear tRNA introns (Schaffer *et al.* 2014)**,** we performed a preliminary tRNA-sequencing analysis on one sample obtained from LCLs of an unrelated healthy individual (Ctrl-2 from Figure 2A) and the SRNS individual B.II-4 homozygous for the intronic Ins47 mutation (**Figure 4**). tRNAs were size-selected and enriched from LCLs total RNAs, and subjected to partial alkaline hydrolysis prior to tRNA-seq library preparation using a protocol adapted from (Gogakos *et al.* 2017). A home-made bioinformatics pipeline allowed us to quantify the number of reads mapping the intron (representative of unspliced tRNAs) and the number of reads spanning the intron/exon junction (spliced tRNAs). This allowed us to calculate a percentage of unspliced tRNA in each individual for each of the four tRNA isodecoder families containing an intron (tRNA-Arg-TCT, tRNA-Ile-TAT, tRNA-Leu-CAA and tRNA-Tyr-GTA). By taking into account a fold change >1.5 for the ratio of unspliced tRNA percentage in the affected individual compared to the control one, we evidenced an increase in unspliced tRNA derived from nine tRNA isoforms (Arg-TCT-2-1, Arg-TCT-3-2, Arg-TCT-5-1, Ile-TAT-2-1, Leu-CAA-1-1, Leu-CAA-1-2, Tyr-GTA-1-1,Tyr-GTA-3-1 and Tyr-GTA-8-1) in the LCLs of the SRNS affected individual (**Figure 4**). Although these preliminary data do not allow us to determine if the increase observed is statistically significant and whether the increase is always observed for these particular set of tRNA isoforms, it seems that the Ins47 variant in *TSEN54* affects the processing of several tRNA resulting in an increase in unspliced tRNAs, as already shown in *in vitro* experiments for *TSEN15* mutations (Breuss *et al.* 2016). To confirm these results, further experiments are needed on additional samples from SRNS and GAMOS affected individuals.

Generation of *TSEN54* induced pluripotent stem cells (iPSCs) by reprogramming of affected individual cells and by CRISPR/Cas9-mediated gene editing

The next step to study more deeply the pathophysiological mechanisms leading to SRNS and GAMOS in *TSEN54* mutated individuals, we decided to take advantage of the use of iPSCs and their ability to be differentiated into any given cell type, including podocytes and neurons, the two relevant cell types in these disorders. We first derived iPSCs from the parents of the GAMOS

affected individual (individuals A.I-1 and A.I-2) and from the SRNS affected individual B.II-4 bearing the Ins47 intronic variant in the homozygous state (**Figure 1A**). All the iPSC lines generated by reprogramming and CRISPR/Cas gene-editing are summarized in **Table 2**. Then, we performed gene-editing using the CRISPR/Cas9 technology to generate an iPSC line mimicking the GAMOS affected individual A.II-2 genotype with *TSEN54* compound heterozygous variants. To do so, we used one clone of the iPSC line derived from the father of the GAMOS individual, who already carries the c.468+48 A>G variant (Ins47) in the heterozygous state (Heterozygous 1, iPSC CT297-03), and decided to create an exonic nonsense mutation to reproduce the effect of the maternal c.1015 C>T (p.Q339*) variant. Since this nonsense mutation has to be in trans of the Ins47 variant, we chose to insert a nonsense mutation in exon 5 to easily further screen and analyze the gene-edited iPSC clones. Before single guide RNA (sgRNA) design, we sequenced the *TSEN54* exon 5/intron 6 in the Heterozygous 1 (CT297-03) iPSCs to avoid any genetic variations such as SNP or indels that could alter the CRISPR/Cas9 on-target specificity. We selected a Crispr RNA guide (crRNA) with the highest specificity score according to the Crispor software (http://crispor.tefor.net) and with the lowest number of predicted off-targets (**Figure 5A**). Briefly, the Cas9 ribonucleoprotein (RNP) complex was formed by mixing the HiFi Cas9 nuclease with the selected crRNA and a fluorochrome-labeled tracrRNA, the latter two forming the sgRNA. The Heterozygous 1 (CT297-03) iPSCs were nucleofected with this RNP complex, seeded and enriched in fluorescent positive cells 24h later using fluorescence-activated cell sorting (FACS) with finally 4500 positive cells plated as single cells. Fourteen days later, 10 emergent clones were picked and expanded for further Sanger sequencing analysis. Two out of the 10 clones, named GAMOS 1 and GAMOS 2 (GAM-3B and GAM-3H), presented the same one base pair deletion (c.410del) in exon 5 in trans of the Ins47 variant recapitulating the compound heterozygous GAMOS-like genotype (**Figure 5B and 5C**). This deletion would lead to a frame shift and a premature stop codon generating a truncated TSEN54 protein with a predicted molecular weight of 16 kDa (p.Ile137Thrfs*9, named hereafter I137Tfs*9) (**Figure 5D**). Two other gene-edited iPSC clones, in which gene-editing failed and thus heterozygous for the Ins47 variant, Heterozygous 2 and Heterozygous 3 (CT297-3D and CT297-3J), were kept as isogenic controls. We next assessed the off-target cleavage sites in the four *TSEN54* iPSC gene-edited clones, by verifying 20 out of the 164 potential off-target sites for the selected gRNA by Sanger sequencing without finding any detectable variants in the potential off-target region and even 100 bp around it (**Table S1**). We confirmed the stemness of all iPSC lines by verifying the expression of the pluripotency markers

OCT4 and SOX2 by immunofluorescence (**Figure S5A**). In addition, all iPSC lines had a normal karyotype (**Figure S5B**) and the reprogrammed and gene-edited iPSC clones were authenticated using STR analysis, showing their matching with the healthy and affected individuals PBMCs from which iPSC lines were derived (data not shown). Altogether, we successfully generated iPSC lines either by direct reprogramming of PBMC from healthy controls, one SRNS affected individual (B.II-4) and the parents of the GAMOS affected child (A.I-1 and A.I-2), or using CRISPR/Cas9 gene-editing to generate two iPSC lines with a genotype mimicking the one of the GAMOS affected child (compound heterozygous for Ins47) and two isogenic iPSC lines.

DISCUSSION

In this study, we reported the identification of two novel variants in the *TSEN54* gene, encoding a subunit of the TSEN complex involved in tRNA intron splicing, in individuals affected either with GAMOS or isolated SRNS. The intronic variant (c.468+48 A>G, Ins47) is present in the homozygous state in the SRNS affected individuals, whereas it is in compound heterozygous state associated with a nonsense variant (c.1015C>T, p.Gln339*) in the GAMOS affected child. We demonstrated that the intronic variant creates a cryptic splice site that is used together with the canonical one, leading to the expression of a residual amount of TSEN54 WT protein in the SRNS affected individual. Depletion of *TSEN54* in an immortalized human podocyte cell line leads to a decrease in podocyte proliferation and protein synthesis. In addition, we showed an increase in unspliced tRNAs in one third of the intron-containing tRNAs in LCLs of the SRNS affected individual. Altogether, our results are in favour of a pathogenic effect of both *TSEN54* variants and a contribution of tRNA intron splicing defect to SRNS and GAMOS pathogenesis.

This study represents the first work that demonstrate the unexpected involvement of *TSEN54* and its role in the tRNA splicing processing as a cause of GAMOS and SRNS, providing novel insights into the genetic, molecular and phenotypic spectrum of these diseases. Strikingly, no renal involvement has been reported to date in PCH cases, particularly in those linked to *TSEN54* mutations. However, it could be possible that no renal abnormalities are detected in PCH affected individuals due to the severe phenotype from birth and the early death, mostly occurring before one year of age. Indeed, the renal disease in the SRNS affected individual is of childhood- and adult-onset.

It is also not clear whether this specific intronic variant, never described in *TSEN54*-linked PCH affected individuals, could be solely responsible for the renal phenotype in the SRNS and GAMOS affected individuals, and whether the nonsense Q339* variant could be responsible for the brain phenotype in the GAMOS affected child. However, both variants lead to the decrease of *TSEN54* transcripts and TSEN54 WT protein expression levels, with none of the mutant proteins expressed in LCLs. We cannot rule out the fact that the cryptic splicing site may be regulated in a spatiotemporal manner such as this cryptic splice site is only used in specific cell-types, here in podocytes and/or neural stem cells, at specific developmental stages (mature podocytes, neural progenitor cells or neurons) (Boisson *et al.* 2018). Consequently, the decrease in TSEN54 WT protein expression would lead to a reduction in the pool of active TSEN complex and therefore to a partial loss of TSEN complex enzymatic activity leading to defect in tRNA intron splicing. The accumulation of unspliced tRNA would lead to protein translation, and thus proteostasis, defects to which neurons and podocytes may be particularly sensitive (Kapur *et al.* 2017; Navarro-Betancourt *et al.* 2020). Indeed, experiments on *TSEN54* KD podocytes are in favor of this hypothesis since the *TSEN54*-depleted podocytes exhibited decreased protein synthesis. This result has also been observed in patients harboring mutations in genes encoding all the subunits of the KEOPS complex, involved in tRNA t^6A modification biosynthesis, which might suggest that alterations in tRNAs misprocessing, and consequently defect in protein synthesis and proteostasis, may represent a common pathological feature in GAMOS (Braun *et al.* 2017; Arrondel *et al.* 2019).

To go deeper into our understanding of the pathophysiological mechanisms leading to SRNS and GAMOS in *TSEN54* mutated individuals, we successfully generated iPSCs that will be further differentiated into any given cell type, including podocytes and neurons, the two relevant cell types in these disorders. The use of iPSC-derived kidney organoids and neural stem cells (NSCs)/neurons will be instrumental to further investigate the molecular and cellular mechanisms with both podocytes and NSCs/neurons that could be used for transcriptomic analyses, and/or for tRNA-sequencing to assess the impact of both variants on the intron splicing activity of the TSEN complex.

MATERIAL AND METHODS

Patients and families

Written informed consent was obtained from participants or their legal guardians. All methods were performed in accordance with relevant guidelines and regulations. Methods of sample collection, storage and experimental protocols for induced human pluripotent stem cells (iPSCs) and their derivatives were declared to the French research ministry (identification DC 2015-2595) and have obtained approval from the ethical Committee "CPP Ile-de-France II" on September 5th, 2016. Genomic DNA samples were isolated from peripheral blood leukocytes using standard procedures.

Whole-exome sequencing and mutation calling

We performed whole-exome sequencing using Agilent SureSelect All Exon 51 Mb V5 capture-kit on a HiSeq2500 (Illumina) sequencer (paired-end reads: 2 × 100 bases). Sequences were aligned to the human Genome Reference Consortium Human Build 37 (GRCh37) genome assembly with the Lifescope suite from Life Technologies. Variant calling was made using the Genome Analysis Toolkit pipeline. Then, variants were annotated using a pipeline designed by the Paris Descartes University Bioinformatics platform. We assumed the causal variant: (i) segregates with the disease status, (ii) is novel or has a minor allele frequency <1/1000 in gnomAD, (iii) was not found in >10/2352 projects of our in-house database. Splice site variant pathogenicity was evaluated using in silico prediction tools (MaxEntScan and Human Splice Finder). Sanger sequencing was used to validate the variant identified by exome sequencing and to perform segregation analysis in the families. Sequences were analyzed with the Sequencher software (Gene Codes, Ann Arbor, MI) and positions of mutations were numbered from the A of the ATG-translation initiation codon.

Antibodies

Primary antibodies used in this work include: mouse anti-actin [Sigma Cat. No. A2228, used at 1:2000 for western blot (WB)], mouse anti-OCT3/4 (C-10) [Santa Cruz Biotechnology Cat. No. sc-5279, used at 1:100 for immunofluorescence (IF)], rabbit anti-TSEN54 [Abcam, Cat. No.

EPR10062 (ab178696), used at 1:1000 for WB], rabbit anti-SOX2 [EMD Millipore Corp Cat. No. AB 5603-25 VG, used at 1:1000 for IF]. Secondary antibodies used in this study include: IRDye 800CW Donkey anti-rabbit, [LI-COR Cat. No. 926-32213, used at 1:15000 for WB], IRDye 680RD Donkey anti-mouse [LI-COR Cat. No. 926-68072, used at 1:15000 for WB], Alexa Fluor 488 Donkey anti-rabbit IgG, [Life Technologies ThermoFischer Cat. No. A21206, used at 1:400 for IF] and Alexa Fluor 555 Donkey anti-mouse IgG [Life Technologies ThermoFischer Cat. No. A31570, used at 1:400 for IF].

Cell culture and establishment of podocyte cell lines

Lymphoblastoid cells were cultured at 37°C with 7% CO_2 and maintained in RPMI 1640 (Gibco®, Life Technologies) supplemented with 10% fetal bovine serum (FBS), glutamine and penicillin/streptomycin. Conditionally immortalized human podocytes (Saleem *et al.* 2002) were routinely cultured at 33°C with 7% CO_2 and maintained in RPMI 1640 (Gibco®, Life Technologies), supplemented with 10% FBS, 1% insulin/transferrin/selenium, glutamine and penicillin/streptomycin (all from Life Technologies). The shRNA sequences described below (**Supplementary Table 2**) were cloned into the lentiviral pLKO.1-TRC Cloning Vector (Plasmid 10878, Addgene) using the AgeI and EcoRI restriction sites. Lentiviral particles were produced by the lentivector production facility "Structure Fédérative de Recherche BioSciences Gerland-Lyon Sud (UMS3444/US8). To establish a line of immortalized podocytes stably expressing Sh1 or Sh2 *TSEN54*, cells were transduced at a multiplicity of infection (MOI) of 2; the minimum MOI at which cells also survived the subsequent puromycin selection (2µg/ml). All constructs were verified by Sanger sequencing.

RNA isolation, RT-PCR and real-time quantitative RT-PCR

Total RNA was extracted using RNeasy® columns and DNAse-treated using RNase-free DNase (Qiagen). For RT-PCR and quantitative PCR, first-strand cDNAs were synthetized from 1µg of RNA, using SuperScript™ II Reverse Transcriptase (Invitrogen), 10ng/µl random primers (Invitrogen), dNTP 1.25mM, dithiothreitol 10mM and RiboLock Rnase inhibitor (2U/µl). To quantitate transcripts, absolute quantitative PCR was performed using Power SYBR Green ROX Mix (ThermoFischer Scientific). For each sample, the expression was normalized to HGPRT.

Experimental results are analyzed with the $2^{-\Delta\Delta Ct}$ method. All primers are listed in **Supplementary Table 2**.

Immunoblotting

Proteins were extracted in lysis buffer containing 150 mM NaCl, 50 mM Tris-HCl pH 7, 0.5% Triton-X100, 1mM EDTA, with Complete™ protease inhibitors (Roche). Cells were incubated on ice for 10 minutes and centrifuged at 12,500 rpm at 4°C for 10 minutes. Protein concentration was determined using BCA assay (Thermo). Equal amounts of proteins, diluted in 4X sample buffer (Bio-Rad) supplemented with β-mercaptoethanol were loaded onto acrylamide gels and transferred onto nitrocellulose membranes (Bio-Rad). The membranes were blocked in Odyssey (LI-COR Bioscience) blocking buffer. Membranes were then incubated with the indicated primary antibodies overnight at 4°C, washed three times with PBS, and then incubated for 1 hour at room temperature (RT) with LI-COR IRDye secondary antibodies and then washed a further 3 times before revelation. Signals were acquired with Odyssey CLx LICOR near-infrared fluorescent imaging system (LI-COR Bioscience). Densitometry quantification was performed using Image studio lite software (version 5.2).

Immunofluorescence

IPSCs were grown on matrigel coverslips (10-20 000 cells/cm2). Cells were fixed in 4% paraformaldehyde (PFA) for 20 minutes at RT. After fixing, samples were washed once in 1X PBS and once in 1X PBS 30 mM glycine. The day after, cells were permeabilized with 0.5% Triton TX-100 (Sigma) in 1X PBS for 5 minutes and incubated in blocking buffer containing 1% bovine serum albumin (BSA, Sigma) for 1 hour at RT. Then, cells were incubated in the appropriate primary and secondary antibodies for 1 hour each at RT. Finally, cells were washed once in 1X PBS, nuclei were stained with DAPI (sc-3598, Santa Cruz Biotechnology) at RT for 5 minutes and mounted on slides using Mowiol 4-88 mounting medium (81381, Sigma-Aldrich).

Cell proliferation and protein synthesis assays

Cell proliferation rates and protein synthesis were assessed in shRNA scrambled- or *TSEN54*-treated podocytes using the CellTiter 96 Aqueous Non-Radioactive Cell Proliferation Assay (MTT) (G5421, Promega), and the Click-iT HPG Alexa Fluor 488 Protein Synthesis Assays (C10428 ThermoFisher Scientific), respectively, according to the manufacturer's instructions (described in Arrondel at al. 2019). Absorbance measurement was performed on day 1, 2, 3, 4, 7 for podocytes on a TriStar multimode reader (LB941, Berthold Technologies) using a 560 measurement filter and subtracting the blank background absorbance. The shRNA *TSEN54*-treated podocytes were seeded at a density of 15 000 cells per well into 96 well-plates and HPG protein synthesis assay were performed 48 hours later, the fluorescence intensities were normalized to nuclear fluorescence intensity as internal control.

Generation and characterization of human induced pluripotent stem cell (iPSC) lines

The iPSC lines from patients and controls were generated from peripheral blood mononuclear cells (PBMCs) either at the iPSC core facility of Nantes University or at Imagine Institute iPSC platform. At the iPSC core facility of Nantes University, PBMCs were reprogrammed by Sendai viruses expressing Oct4, Sox2, Klf4 and c-Myc (CytoTune^{TM}-IPS 2.0 Sendai Reprogramming kit, Life Technologies). The iPSC clones were picked and expanded on mouse embryonic fibroblasts (MEFs) feeder cells in KSR-FGF2 medium (DMEM/F12 supplemented with 0.1% β-mercaptoethanol, 20% knockout serum replacement, 10 ng/mL basic fibroblast growth factor, 2 mmol/L l-glutamine and 1% NEAA). Until P10, colonies were mechanically passaged with a needle. At P10, iPSC clones were adapted to feeder-free culture conditions: stem cell-qualified Matrigel-coated plates (0.1 mg/mL; BD Bioscience) with mTeSR (Stem Cell Technologies). Feeder-free iPSCs were passaged using the Passaging Solution XF (StemMACS^{TM}, Miltenyi Biotec). The control iPSC lines from the Imagine Institute iPSC plateform (IMAGINi005 and IMAGINi013) are described at https://hpscreg.eu/cell-line/IMAGINi013-A and https://hpscreg.eu/cell-line/IMAGINi005-A, and in (Quelennec *et al.* 2020) for IMAGINi005. Mycoplasma detection is realized with the MycoAlert™ kit (LONZA, LT07-318). Quality controls included the expression assessment of pluripotency markers (OCT4 and SOX2) by immunofluorescence, the verification of absence of chromosomal anomalies using a SNP array (Infinium Core-24 v1.2 Kit (Illumina) 300,000 SNPs), and identity match (matching the iPSC genotype with that of parental PBMCs for 8 informative SNPs), and trilineage potential evaluation

was performed using immunofluorescence staining with ectodermal TUJ1, mesodermal α-SMA and endodermal α-FP markers. Human iPSC culture and storage protocols were performed with approval from the French research Ministry (DC2015-2595, 09/05/2016). iPSCs were cultured in mTeSR Plus (05825, StemCell Technologies) medium on Matrigel LDEV-free hESC-qualified matrix (354277, Corning) coated 35 or 60 mm dishes according to the Stemcell technologies protocols. iPSCs colonies morphology was daily monitored under a Lynx Stereo Dynascopic Microscope (Vision Engineering) to manually remove differentiated cells and ensure maintenance of an undifferentiated state. iPSCs were passaged once a week by mechanical procedure or using RelesR reagent according to the provider protocol (05872, Stemcell technologies).

Generation of genome-edited iPSCs

The CRISPR RNA guide was designed online with the tool proposed by http://crispor.tefor.net. Potential off-target sites for the guide RNA (gRNA) were determined using the CFD score (Cutting Frequently Determination). We choose our gRNA (3' AGACCTGCCACTGTCTATCC 5') focusing on the MIT score that is more reliable on sensitivity and specificity. Nucleofection was performed with the "CA-137" program of the 4D Nucleofector (AAF-1002B, AAF-1002X, Lonza) with the "P3 Primary Cell X-unit Kit S" (Lonza, Reference: V4XP-3032). In order to reduce off-target probability, we choose a High Fidelity Cas9 (mutated in p.R691A) "Alt-R® S.p. HiFi Cas9 Nuclease V3" (integrated DNA technologies (IDT), reference: 1081061) with "Alt-R® CRISPR-Cas9 crRNA XT" (IDT, reference: 1081061) and "Alt-R® CRISPR-Cas9 tracrRNA, ATTO550" (IDT, reference: 1075928) to be able to sort transfected cells based on ATTO550 signal. Before nucleofection, iPSCs were seeded at 10 000 cells / cm² on matrigel coated 60 mm dishs from 3 to 4 days and dissociated with TrypLE select (Life Technology Reference: 12563011). We used 800 000 cells for nucleofection, including two non-nucleofected negative controls (with and without ATTO550 RNP complex). When cells reached confluency of at least 20% (24h-48h of culture), nucleofected cells were sorted on SH800 Cell Sorter (130µm nozzle) using the ATTO550 highest signal intensity. The nucleofected cells were seeded at a clonal density of 25 cells/cm² on CellAdhere Laminin-521 (77003, StemCell Technologies) - coated culture dishes in mTeSR Plus medium supplemented with CloneR *(*05888, StemCell Technologies) to increase clonal cell survival. After two weeks of culture, the clones of interests were identified by Sanger sequencing,

amplified and frozen. Selected potential off-target sites of the gRNA determined using the CFD score were Sanger sequenced on the DNA of gene edited IPSC clones (**Supplementary Table 1**).

RNA-sequencing and analysis

RNA was extracted from cells using the RNeasy Micro kit (74004, Qiagen) according to manufacturer's instructions. RNA quantity and quality was assessed by automated electrophoresis using the TapeStation system (Agilent Technologies). RNA-Seq libraries were prepared starting from 1µg of total RNA using the Ovation SoLoRNA-Seq System kit (0500-32, Nugen) according to manufacturer's instructions. Briefly, after DNase treatment and random primer annealing, the first cDNA strand was synthetized from total RNA. Second cDNA strand was produced and then ligated to Illumina compatible adaptors containing both sample index and a Unique Molecular Index (UMI). The cDNA produced was PCR amplified after an initial test to evaluate the suitable number of PCR cycles to apply to each sample. cDNAs corresponding to ribosomal RNA were selectively fragmented using the AnyDeplete technology. Few PCR cycles were performed to finalize the RNAseq library preparation. An equimolar pool of the final indexed RNA-Seq libraries was prepared and sequenced on a HiSeq2500 (paired-end reads of 130 bases + 130 bases; Illumina). A total of ~50 millions of passing filter paired-end reads was produced per library. FASTQ files were mapped to the ENSEMBL GRCh38/hg38 reference human genome using Hisat2 and counted by featureCounts from the Subread R package. Read count normalizations and groups comparisons were performed by three independent and complementary statistical methods: DESeq2, edgeR and LimmaVoom. Flags were computed from counts normalized to the mean coverage. All normalized counts <20 were considered as background (flag 0) and ≥20 as signal (flag=1). Cluster analysis was performed on DESeq2 P50 lists, regrouping the genes showing flag=1 for at least half of the compared samples, by hierarchical clustering using the Spearman's correlation similarity measure and Ward's linkage algorithm. Samples were compared using the DESeq2 statistical method, applying the Bonferroni and Benjamin-Hochberg corrections for multiple hypothesis testing. Statistically significant upregulated and downregulated gene lists (BH-corrected p-value<0.05) were subjected to GO enrichment analysis for biological process on geneontology.org.

tRNA-sequencing and analysis

For tRNA-seq library preparation, a protocol adapted from a method described by Gogakos et al., (Gogakos *et al.* 2017) was followed. The resulting fragmented and end-repaired RNA was used for small RNA library preparation using the NEBNext kit (NEB) following the manufacturer's instructions. FASTQ files were mapped to the ENSEMBL Human (GRCh38/hg38) reference using Hisat2 allowing no soft clip and intron length max at 25. Bams were then filtered at mapping quality >1. To detect the intron/exon junctions, we have filtered the CIGAR strings including «N» and computed the coordinates. To detect the absence of junctions we have selected the reads mapped inside or at least with 5 bases overlapping to the position of intron. We then counted those reads with or without junction for each tRNA. All the counts have been normalized to the mean of total number of reads of the two samples.

Statistical analysis

Statistical analysis were performed using GraphPad PRISM 8.0 software. All values are shown as mean ±s.e.m. of a least 3 independent experiments. data sets comparing more than three conditions (to a control group) were analyzed with ANOVA followed by Dunnett's multiple comparisons test or by using Kruskal–Wallis test followed by a Dunn's multiple comparisons test. A standard confidence interval of 95% was applied in all analyses. Displayed in the figures are the mean values of all technical replicates for each of the independent experiments (displayed as single data points).

Acknowledgements:

We acknowledge the use of the bioresources of the Necker Imagine DNA biobank (BB-033-00065). We also thank Gisèle Froment, Didier Nègre and Caroline Costa from the lentivector production facility / SFR BioSciences Gerland – Lyon Sud (UMS3444/US8). We greatly thank Meriem Garfa-Traoré and Nicolas Goudin from the Cell Imaging Facility for images acquisitions, and Maria-Emilia Puig Lombardi from the *Imagine* Institute Bioinformatic core facility for her help on RNA-seq analysis.

REFERENCES

Arrondel C., Missoury S., Snoek R., Patat J., Menara G., Collinet B., Liger D., Durand D., Gribouval O., Boyer O., Buscara L., Martin G., Machuca E., Nevo F., Lescop E., Braun D. A., Boschat A.-C., Sanquer S., Guerrera I. C., Revy P., Parisot M., Masson C., Boddaert N., Charbit M., Decramer S., Novo R., Macher M.-A., Ranchin B., Bacchetta J., Laurent A., Collardeau-Frachon S., van Eerde A. M., Hildebrandt F., Magen D., Antignac C., van Tilbeurgh H., and Mollet G. (2019). Defects in t6A tRNA modification due to GON7 and YRDC mutations lead to Galloway-Mowat syndrome. *Nat Commun* **10**, 3967. doi:10.1038/s41467-019-11951-x

Boisson B., Honda Y., Ajiro M., Bustamante J., Bendavid M., Gennery A. R., Kawasaki Y., Ichishima J., Osawa M., Nihira H., Shiba T., Tanaka T., Chrabieh M., Bigio B., Hur H., Itan Y., Liang Y., Okada S., Izawa K., Nishikomori R., Ohara O., Heike T., Abel L., Puel A., Saito M. K., Casanova J.-L., Hagiwara M., and Yasumi T. (2018). Rescue of recurrent deep intronic mutation underlying cell type–dependent quantitative NEMO deficiency. *Journal of Clinical Investigation* **129**, 583–597. doi:10.1172/JCI124011

Braun D. A., Rao J., Mollet G., Schapiro D., Daugeron M.-C., Tan W., Gribouval O., Boyer O., Revy P., Jobst-Schwan T., Schmidt J. M., Lawson J. A., Schanze D., Ashraf S., Ullmann J. F. P., Hoogstraten C. A., Boddaert N., Collinet B., Martin G., Liger D., Lovric S., Furlano M., Guerrera I. C., Sanchez-Ferras O., Hu J. F., Boschat A.-C., Sanquer S., Menten B., Vergult S., De Rocker N., Airik M., Hermle T., Shril S., Widmeier E., Gee H. Y., Choi W.-I., Sadowski C. E., Pabst W. L., Warejko J. K., Daga A., Basta T., Matejas V., Scharmann K., Kienast S. D., Behnam B., Beeson B., Begtrup A., Bruce M., Ch'ng G.-S., Lin S.-P., Chang J.-H., Chen C.-H., Cho M. T., Gaffney P. M., Gipson P. E., Hsu C.-H., Kari J. A., Ke Y.-Y., Kiraly-Borri C., Lai W., Lemyre E., Littlejohn R. O., Masri A., Moghtaderi M., Nakamura K., Ozaltin F., Praet M., Prasad C., Prytula A., Roeder E. R., Rump P., Schnur R. E., Shiihara T., Sinha M. D., Soliman N. A., Soulami K., Sweetser D. A., Tsai W.-H., Tsai J.-D., Topaloglu R., Vester U., Viskochil D. H., Vatanavicharn N., Waxler J. L., Wierenga K. J., Wolf M. T. F., Wong S.-N., Leidel S. A., Truglio G., Dedon P. C., Poduri A., Mane S., Lifton R. P., Bouchard M., Kannu P., Chitayat D., Magen D., Callewaert B., van Tilbeurgh H., Zenker M., Antignac C., and Hildebrandt F. (2017). Mutations in KEOPS-complex genes cause nephrotic syndrome with primary microcephaly. *Nat Genet* **49**, 1529–1538. doi:10.1038/ng.3933

Braun D. A., Shril S., Sinha A., Schneider R., Tan W., Ashraf S., Hermle T., Jobst-Schwan T., Widmeier E., Majmundar A. J., Daga A., Warejko J. K., Nakayama M., Schapiro D., Chen J., Airik M., Rao J., Schmidt J. M., Hoogstraten C. A., Hugo H., Meena J., Lek M., Laricchia K. M., Bagga A., and Hildebrandt F. (2018). Mutations in *WDR4* as a new cause of Galloway-Mowat syndrome: Mutations in *WDR4* as a new cause of Galloway-Mowat syndrome. *Am J Med Genet* **176**, 2460–2465. doi:10.1002/ajmg.a.40489

Breuss M. W., Sultan T., James K. N., Rosti R. O., Scott E., Musaev D., Furia B., Reis A., Sticht H., Al-Owain M., Alkuraya F. S., Reuter M. S., Abou Jamra R., Trotta C. R., and Gleeson J. G. (2016). Autosomal-Recessive Mutations in the tRNA Splicing Endonuclease Subunit TSEN15 Cause Pontocerebellar Hypoplasia and Progressive Microcephaly. *The American Journal of Human Genetics* **99**, 785. doi:10.1016/j.ajhg.2016.08.009

Budde B. S., Namavar Y., Barth P. G., Poll-The B. T., Nürnberg G., Becker C., van Ruissen F., Weterman M. A. J., Fluiter K., T te Beek E., Aronica E., van der Knaap M. S., Höhne W., Toliat M. R., Crow Y. J., Steinlin M., Voit T., Roelens F., Brussel W., Brockmann K., Kyllerman M., Boltshauser E., Hammersen G., Willemsen M., Basel-Vanagaite L., Krägeloh-Mann I., de Vries L. S., Sztriha L., Muntoni F., Ferrie C. D., Battini R., Hennekam R. C. M., Grillo E., Beemer F. A., Stoets L. M. E., Wollnik B., Nürnberg P., and Baas F. (2008). tRNA splicing endonuclease mutations cause pontocerebellar hypoplasia. *Nature Genetics* **40**, 1113–1118. doi:10.1038/ng.204

Chan P. P., and Lowe T. M. (2016). GtRNAdb 2.0: an expanded database of transfer RNA genes identified in complete and draft genomes. *Nucleic Acids Res* **44**, D184–D189. doi:10.1093/nar/gkv1309

Colin E., Huynh Cong E., Mollet G., Guichet A., Gribouval O., Arrondel C., Boyer O., Daniel L., Gubler M.-C., Ekinci Z., Tsimaratos M., Chabrol B., Boddaert N., Verloes A., Chevrollier A., Gueguen N., Desquiret-Dumas V., Ferré M., Procaccio V., Richard L., Funalot B., Moncla A., Bonneau D., and Antignac C. (2014). Loss-of-Function Mutations in WDR73 Are Responsible for Microcephaly and Steroid-Resistant Nephrotic Syndrome: Galloway-Mowat Syndrome. *The American Journal of Human Genetics* **95**, 637–648. doi:10.1016/j.ajhg.2014.10.011

Fujita A., Tsukaguchi H., Koshimizu E., Nakazato H., Itoh K., Kuraoka S., Komohara Y., Shiina M., Nakamura S., Kitajima M., Tsurusaki Y., Miyatake S., Ogata K., Iijima K., Matsumoto N., and Miyake N. (2018). Homozygous splicing mutation in *NUP13* 3 causes Galloway-Mowat syndrome: Galloway-Mowat Syndrome. *Ann Neurol.* **84**, 814–828. doi:10.1002/ana.25370

Gogakos T., Brown M., Garzia A., Meyer C., Hafner M., and Tuschl T. (2017). Characterizing Expression and Processing of Precursor and Mature Human tRNAs by Hydro-tRNAseq and PAR-CLIP. *Cell Reports* **20**, 1463–1475. doi:10.1016/j.celrep.2017.07.029

Kapur M., Monaghan C. E., and Ackerman S. L. (2017). Regulation of mRNA Translation in Neurons—A Matter of Life and Death. *Neuron* **96**, 616–637. doi:10.1016/j.neuron.2017.09.057

Mann N., Mzoughi S., Schneider R., Kühl S. J., Schanze D., Klämbt V., Lovric S., Mao Y., Shi S., Tan W., Kühl M., Onuchic-Whitford A. C., Treimer E., Kitzler T. M., Kause F., Schumann S., Nakayama M., Buerger F., and Shril S. (2021). Mutations in PRDM15 Are a Novel Cause of Galloway-Mowat Syndrome. *J Am Soc Nephrol.* **32**, 580–596. doi:10.1681/ASN.2020040490

Navarro-Betancourt J. R., Papillon J., Guillemette J., Iwawaki T., Chung C.-F., and Cybulsky A. V. (2020). Role of IRE1α in podocyte proteostasis and mitochondrial health. *Cell Death Discov.* **6**, 128. doi:10.1038/s41420-020-00361-4

Paushkin S. V., Patel M., Furia B. S., Peltz S. W., and Trotta C. R. (2004). Identification of a Human Endonuclease Complex Reveals a Link between tRNA Splicing and Pre-mRNA 3′ End Formation. *Cell* **117**, 311–321. doi:10.1016/S0092-8674(04)00342-3

Quelennec E., Banal C., Hamlin M., Clémantine D., Michael M., and Lefort N. (2020). Generation of two induced pluripotent stem cell lines IMAGINi004-A and IMAGINi005-A from healthy donors. *Stem Cell Research* **48**, 101959. doi:10.1016/j.scr.2020.101959

Ramirez A., Shuman S., and Schwer B. (2008). Human RNA 5'-kinase (hClp1) can function as a tRNA splicing enzyme in vivo. *RNA* **14**, 1737–1745. doi:10.1261/rna.1142908

Rosti R. O., Dikoglu E., Zaki M. S., Abdel-Salam G., Makhseed N., Sese J. C., Musaev D., Rosti B., Harbert M. J., Jones M. C., Vaux K. K., and Gleeson J. G. (2016). Extending the mutation spectrum for Galloway-Mowat syndrome to include homozygous missense mutations in the WDR73 gene. *Am. J. Med. Genet.* **170**, 992–998. doi:10.1002/ajmg.a.37533

Rosti R. O., Sotak B. N., Bielas S. L., Bhat G., Silhavy J. L., Aslanger A. D., Altunoglu U., Bilge I., Tasdemir M., Yzaguirrem A. D., Musaev D., Infante S., Thuong W., Marin-Valencia I., Nelson S. F., Kayserili H., and Gleeson J. G. (2017). Homozygous mutation in *NUP107* leads to microcephaly with steroid-resistant nephrotic condition similar to Galloway-Mowat syndrome. *J Med Genet* **54**, 399–403. doi:10.1136/jmedgenet-2016-104237

Saleem M. A., O'Hare M. J., Reiser J., Coward R. J., Inward C. D., Farren T., Xing C. Y., Ni L., Mathieson P. W., and Mundel P. (2002). A Conditionally Immortalized Human Podocyte Cell Line Demonstrating Nephrin and Podocin Expression. *JASN* **13**, 630–638. doi:10.1681/ASN.V133630

Schaffer A. E., Eggens V. R. C., Caglayan A. O., Reuter M. S., Scott E., Coufal N. G., Silhavy J. L., Xue Y., Kayserili H., Yasuno K., Rosti R. O., Abdellateef M., Caglar C., Kasher P. R., Cazemier J. L., Weterman M. A., Cantagrel V., Cai N., Zweier C., Altunoglu U., Satkin N. B., Aktar F., Tuysuz B., Yalcinkaya C., Caksen H., Bilguvar K., Fu X.-D., Trotta C. R., Gabriel S., Reis A., Gunel M., Baas F., and Gleeson J. G. (2014). CLP1 Founder Mutation Links tRNA Splicing and Maturation to Cerebellar Development and Neurodegeneration. *Cell* **157**, 651–663. doi:10.1016/j.cell.2014.03.049

Schaffer A. E., Pinkard O., and Coller J. M. (2019). tRNA Metabolism and Neurodevelopmental Disorders. *Annu. Rev. Genom. Hum. Genet.* **20**, 359–387. doi:10.1146/annurev-genom-083118-015334

Suzuki T. (2021). The expanding world of tRNA modifications and their disease relevance. *Nat Rev Mol Cell Biol*. doi:10.1038/s41580-021-00342-0

Vodopiutz J., Seidl R., Prayer D., Khan M. I., Mayr J. A., Streubel B., Steiß J.-O., Hahn A., Csaicsich D., Castro C., Assoum M., Müller T., Wieczorek D., Mancini G. M. S., Sadowski C. E., Lévy N., Mégarbané A., Godbole K., Schanze D., Hildebrandt F., Delague V., Janecke A. R., and Zenker M. (2015). *WDR73* Mutations Cause Infantile Neurodegeneration and Variable Glomerular Kidney Disease. *Human Mutation* **36**, 1021–1028. doi:10.1002/humu.22828

Wang P. Z. T., Prasad C., Rodriguez Cuellar C. I., and Filler G. (2018). Nephrological and urological complications of homozygous c.974G>A (p.Arg325Gln) OSGEP mutations. *Pediatr Nephrol* **33**, 2201–2204. doi:10.1007/s00467-018-4060-x

Weitzer S., and Martinez J. (2007). The human RNA kinase hClp1 is active on 3′ transfer RNA exons and short interfering RNAs. *Nature* **447**, 222–226. doi:10.1038/nature05777

Table 1. Recessive variants in the *TSEN54* gene in two families with SRSN and one family with GAMOS.

Family Individual	Nucleotide change	Type of mutation	Exon (Zygosity, Segregation)	GnomAD	Gender	Ethnic origin	Consan-guinity	Age of proteinuria (Age of ESRD) *Age at Death*	Extrarenal Manifestations	Renal Biopsy (at age)	Comments
Family A											
A.II-2 (N4326)	c.468+48 A>G (het) c.1015 C>T	Splice (create cryptic donor splice site) nonsense p.Gln339*	Exon 5 (het) m(wt), p(het) Exon 8 (het) m(het), p(wt)	G=4 / G=248496, No hom None	M	Caucasian, France	no	6 mon (2 yrs) *2 yrs*	Brain: Primary microcephaly (HC=31, -2.7 SD, at birth) Cranial imaging (4 mon): asymmetric cerebellar hypoplasia ("butterfly" pattern, moderately flattened pons, thin corpus callosum Other (2 yrs): axial hypotonia, spasticity, no language skills		
Family B											
B.II-1 (N1745)	c.468+48 A>G (Hom)	Splice (create cryptic donor splice site)	Exon 5 (Hom) m(het), p(het)	G=4 / G=248496, No hom	M	Caucasian, Tunisia	yes	14 yrs Nephrotic-range Pu (14 yrs)	No		Alive with a functioning graft at 28 yrs
B.II-2 (N1104)	c.468+48 A>G (Hom)	Splice (create cryptic donor splice site)	Exon 5 (Hom) m(het), p(het)	G=4 / G=248496, No hom	M	Caucasian, Tunisia	yes	13 yrs 7 mon Nephrotic-range Pu (13 yrs 7 mon)	No		Alive with a functioning graft at 31 yrs
B.II-4 (N1111)	c.468+48 A>G (Hom)	Splice (create cryptic donor splice site)	Exon 5 (Hom) m(het), p(het)	G=4 / G=248496, No hom	M	Caucasian, Tunisia	yes	13 yrs Nephrotic-range Pu (16 yrs)	No		Alive with a functioning graft at 29 yrs
Family C											
C.II-1 (N1332)	c.468+48 A>G (Hom)	Splice (create cryptic donor splice site)	Exon 5 (Hom) m(het), p(het)	G=4 / G=248496, No hom	M	Caucasian, Tunisia	yes	22 yrs 5 mon non-nephrotic-range Pu (N/A)	No	FSGS	Alive with a functioning graft at 42 yrs
C.II-2 (N1333)	c.468+48 A>G (Hom)	Splice (create cryptic donor splice site)	Exon 5 (Hom) m(het), p(het)	G=4 / G=248496, No hom	M	Caucasian, Tunisia	yes	22 yrs 5 mon (23 yrs 1 mon)	No		Alive with a functioning graft at 46 yrs
C.II-3 (N694)	c.468+48 A>G (Hom)	Splice (create cryptic donor splice site)	Exon 5 (Hom) m(het), p(het)	G=4 / G=248496, No hom	M	Caucasian, Tunisia	yes	19 yrs 7 mon Nephrotic-range Pu (19 yrs 7 mon) *N/D*	No		Deceased after 30 yrs

Notes: ESRD, end stage renal disease, Pu, proteinuria; FSGS, focal segmental glomerulosclerosis, het, heterozygous, Hom, homozygous, M, male, N/A, not applicable, N/D, no data, yrs, years; mon, months; HC, head circumference; SD, standard deviation, MRI, magnetic resonance imaging

Table 2 – iPSC lines used in the study.

Patients	Gender	iPSC lines	Clone number	Abbreviation in figures	Genotype at *TSEN54* locus	Disease
B.II-4	male	SN289	SN289-01 SN289-02	SN289c01 SN289c02	c.468+48A>G (Hom)	SRNS
A.I-2	female	CT296	CT296-1A CT296-1B	CT296c1A CT296c1B	c.1015>T (het)	healthy control
A.I-1	male	CT297	CT297-05 CT297-03	CT297c05 CT297c03	c.468+48 A>G (het)	healthy control
		IMAGINi005-A*#	IMAGINi005c04	CT05c4	WT	healthy control
		IMAGINi013-A*	IMAGINi013c19	CT13c19	WT	healthy control
		IMAGINi009-A	IMAGINi009c09	CT09c9	WT	healthy control
Gene-edited iPSC lines derived from iPSC CT297-03						
			CT297c03D CT297c03J	CT297-3D CT297-3J	c.468+48A>G (het)	control
			CT297c03B CT297c03H	GAM-3B GAM-3H	c.468+48A>G (het) + c.410 del (het)	GAMOS

***** IMAGINi005 and IMAGINi013 are described at https://hpscreg.eu/cell-line/IMAGINi005-A and https://hpscreg.eu/cell-line/IMAGINi013-A, # IMAGINi005-A line is described in Quelennec et al. (2020). Hom, homozygous; het, heterozygous, SRNS, steroid-resistant nephrotic syndrome; GAMOS, Galloway-Mowat syndrome.

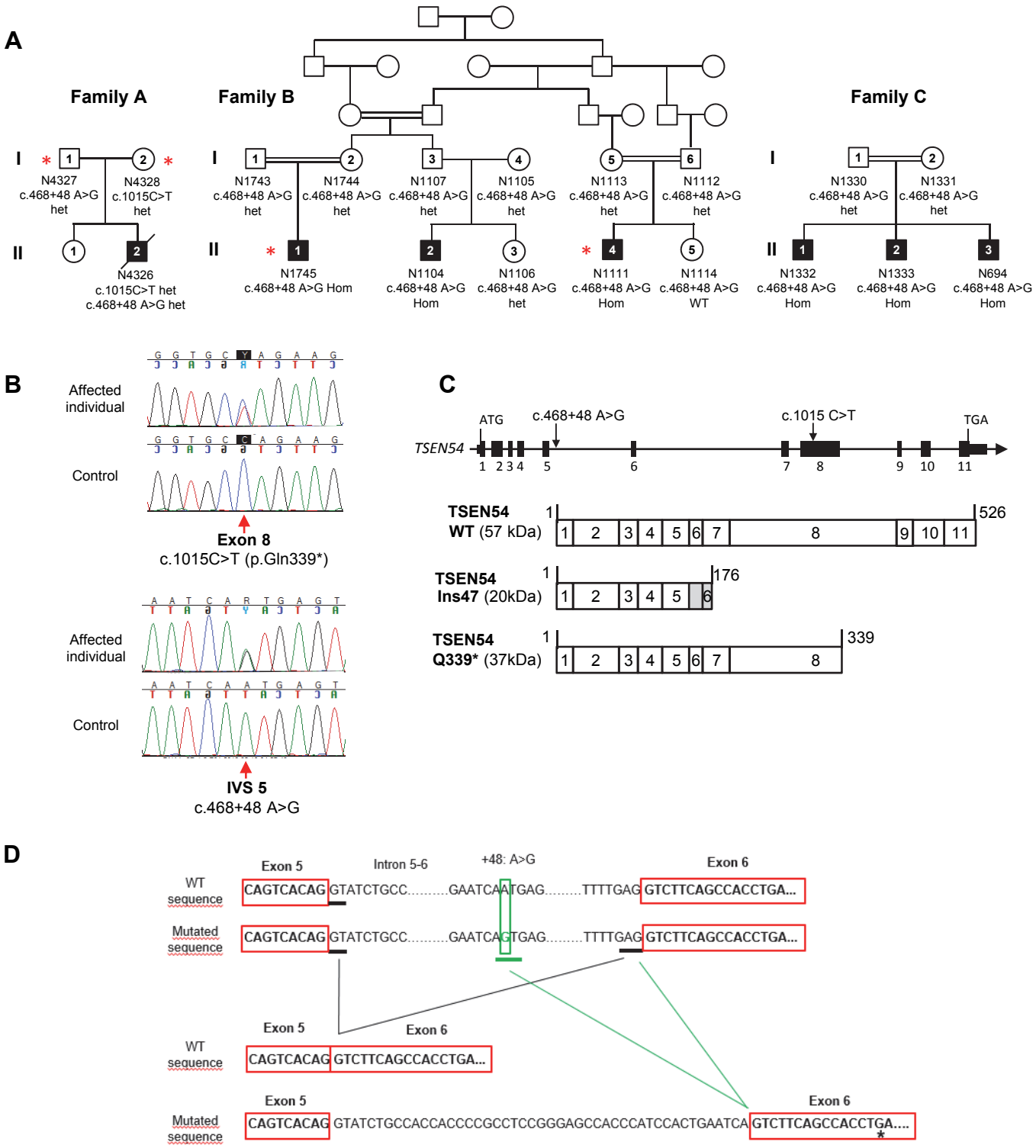

Figure.1 Identification of *TSEN54* variants, gene structure and predicted mutant proteins.
(**A**) Pedigrees of families with mutations in the *TSEN54* gene. Pedigrees of individuals affected with GAMOS (Family A) and affected with SRNS (Family B and C). The affected status is indicated by filled symbols and the allele status is given below each tested individual. Red star indicates individuals from which cell lines were derived and used in this study. Abbreviations are as follow: Hom, homozygous and het, heterozygous. (**B**) Representative chromatograms show the identified variants with the mutated nucleotide indicated with a red arrow, in affected and control individuals. (**C**) Schematic overview of the organization of exons (black boxes) in *TSEN54* gene. Position of start and stop codons are indicated. Arrows indicate the position of the identified mutations. Lower panels show the corresponding predicted proteins, wild-type (WT) and mutants proteins with their expected molecular weight (kDa). (**D**) Schematic representation of the intron splicing in the wild-type (WT) transcript and in the transcript carrying the intronic variant. Acceptor and donor splice sites are underlines and the mutated nucleotide is indicated in green. Red squares indicate the exon. The star indicates the stop codon created in exon 6.

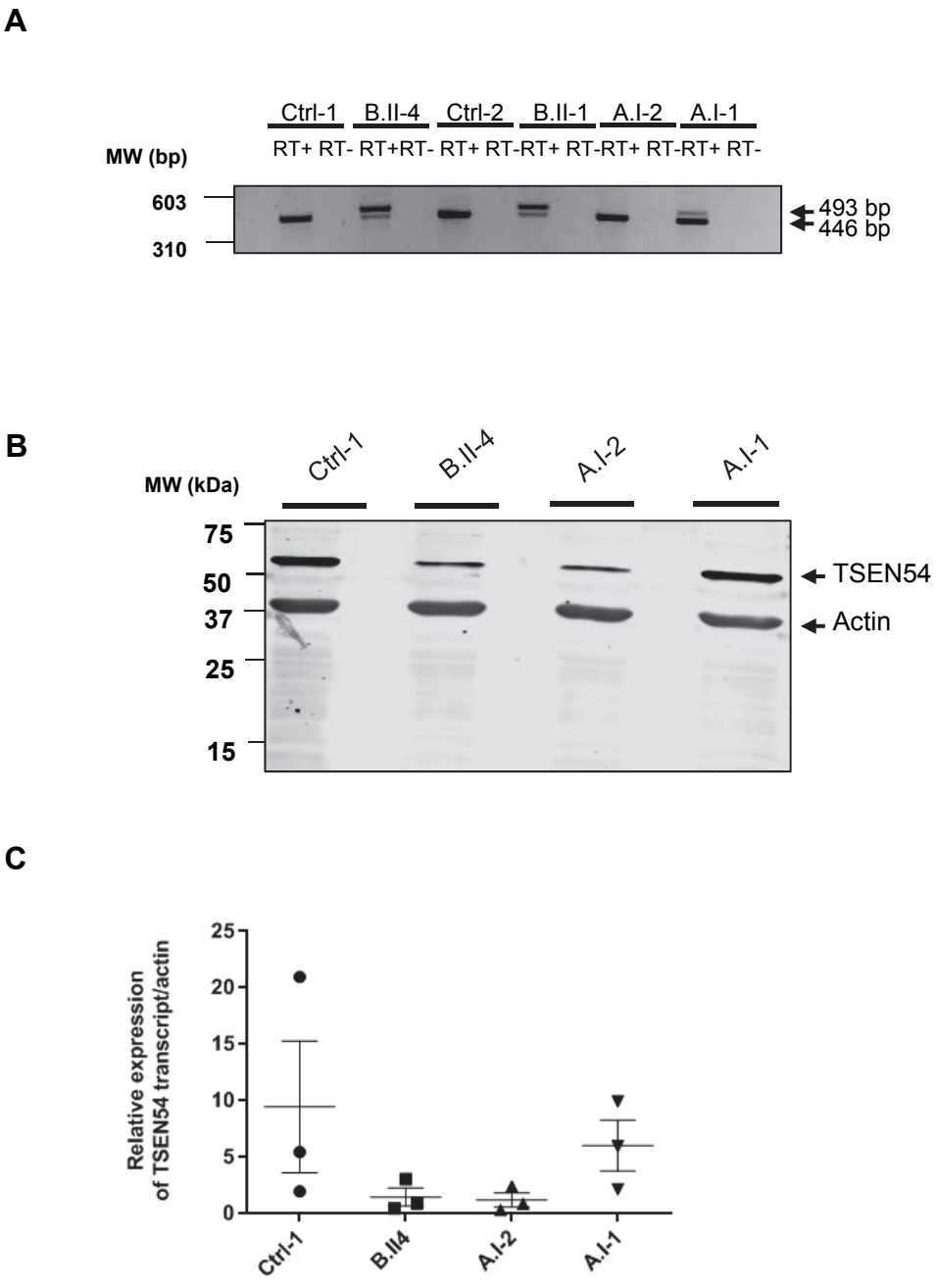

Figure 2 Impact of *TSEN54* variants on mRNA and protein levels.
(**A**) RT-PCR on lymphoblastoid cell line (LCLs) from control individuals (Ctrl-1 and Ctrl-2), SRNS affected individuals, homozygous for Ins47 variant (B.II-1 and B.II-4), and the parents of the affected GAMOS child, the father heterozygous for the Ins47 variant (A.I-1) and the mother heterozygous for the non sense variant Q339* (A.I-2). RT-PCR have been performed with primers covering the region corresponding to *TSEN54* exon 3 to exon 8. RT-PCR shows that, in the SRNS affected individuals B.II-1 and B.II-4, two transcripts are detected corresponding to the wild-type (WT) *TSEN54* transcript (lower band, 446 bp) and the mutant Ins47 transcript (upper band, 493 bp). (**B**) Western blot analysis of TSEN54 protein expression level in LCLs cell lysates from Ctrl-1, SRNS affected individual B.II-4 and the parents of the affected GAMOS child, A.I-1 and A.I-2. One representative western blot is shown (three independent experiment were performed). β-Actin was used as loading control. The SRNS affected individual homozygous for the Ins47 variant shows lower expression of WT TSEN54 (57 kDa) compared to control. None of the mutant TSEN54 proteins are expressed in B.II-4, A.I-1 and A.I-2 individuals. (**C**) Quantification of relative TSEN54 protein expression level in (B). normalized to β-Actin from three independent replicates (mean ±s.e.m of *n*=3 experiments).

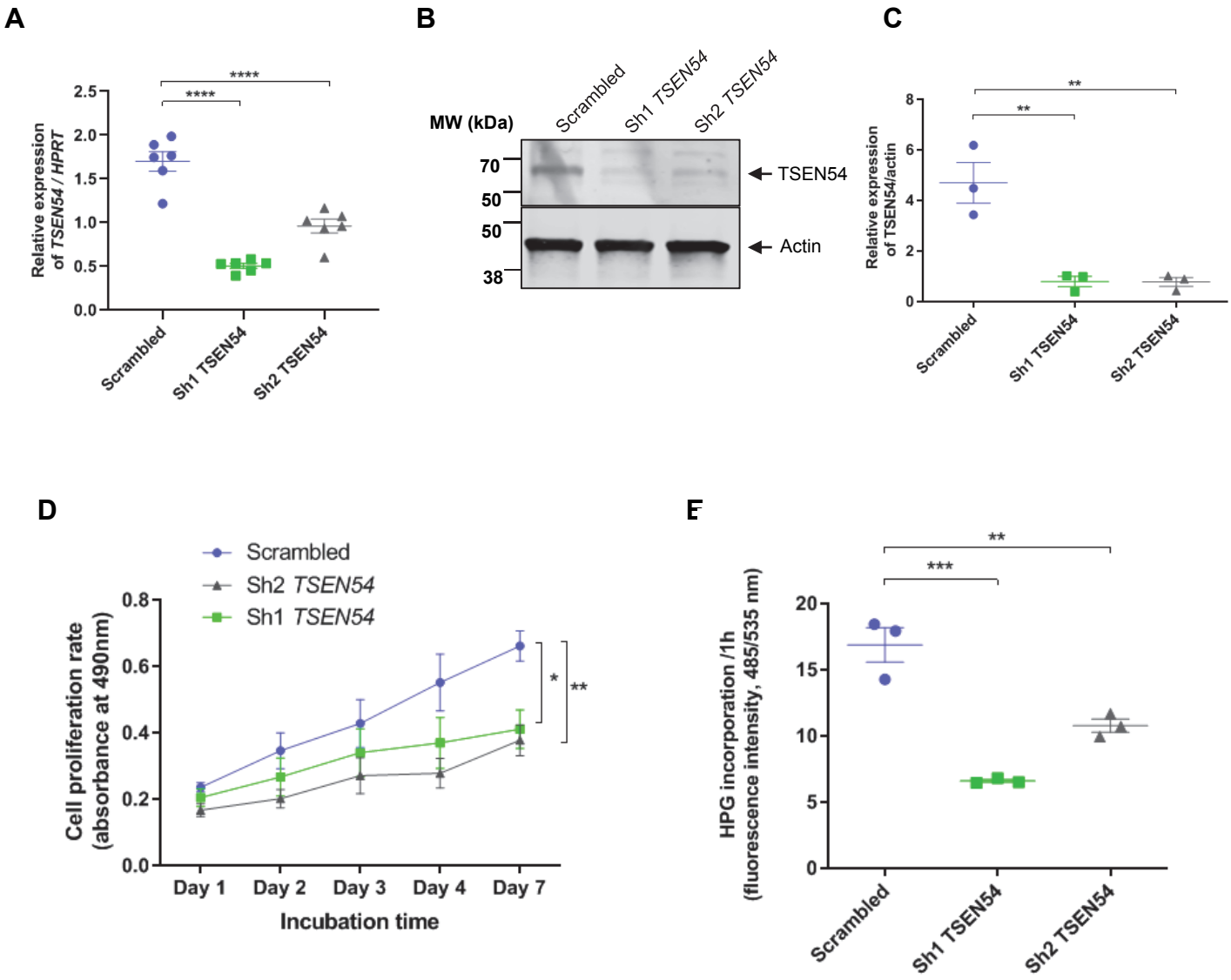

Figure 3. Proliferation and protein synthesis defects upon *TSEN54* KD in podocytes. Transient KD of *TSEN54* was performed by lentiviral transduction of shRNA in an immortalized human podocyte cell line with a scrambled (non-targeting) shRNA as control. (**A**) Relative expression of *TSEN54* transcript normalized to *HPRT* in KD and control scrambled-treated podocytes (mean ±s.e.m of *n*=6 experiments, with each experiment performed in triplicate; one-way ANOVA (F (2,15) =56.51, p < 0.0001), Dunnett's multiple comparisons test, ****p< 0.0001). (**B**) Western blot analysis on total protein extract from *TSEN54* KD podocytes using anti-TSEN54 antibodies directed against the N-terminal part of TSEN54 (Abcam, ab178696). b-Actin was used as loading control. (**C**) Quantification of relative TSEN54 protein expression level in (B). normalized to b-Actin from three independent replicates (mean ±s.e.m of *n*=3 experiments; one-way ANOVA (F (2,6) =21,34, p=0.0019), Dunnett's multiple comparisons test, **p< 0.0024). (**D**) Cell proliferation was assessed using a colorimetric MTT assay over 7 days, measuring absorbance at 490 nm at days 1, 2, 3, 4, and 7 (mean ± s.e.m. of n=4 experiments, with each experiment performed in triplicate; two-way ANOVA (p < 0.0001), Dunnett's multiple comparisons test, n.s. = 0.0588, *p <0.0280, **p < 0.0085). (**E**) Protein biosynthesis rates were assessed on the basis of incorporation of HPG, an alkyne-containing methionine analog. After 2 h, alkyne-containing proteins were quantified on the basis of fluorescence intensity (485/535 nm). Absolute values were normalized to DAPI fluorescence intensity as an internal control and compared to control cells (mean ± s.e.m. of n= 3 experiments, with each experiment performed in triplicate, one-way ANOVA (F (2,6) = 40.50, p= 0.0003), Dunnett's multiple comparisons test, **p =0.0033, ***p <0.0002).

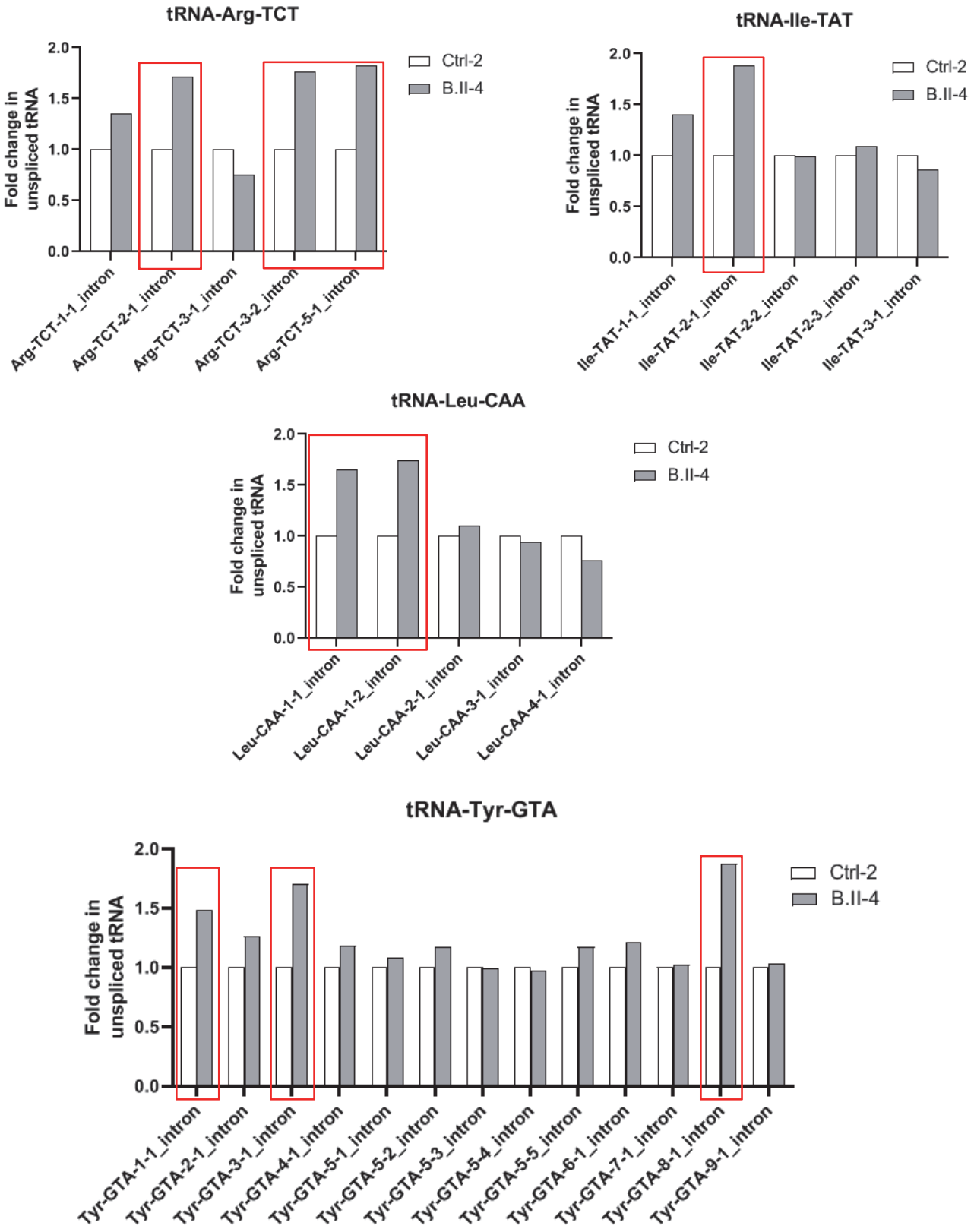

Figure 4. tRNA intron splicing defect in LCLs from a SRNS affected individual. tRNAs were size-selected and enriched from total RNAs from LCLs from the control Ctrl-2 and the SRNS affected individual B.II-4 bearing the homozygous Ins47 variant, and subjected to partial alkaline hydrolysis prior to tRNA-seq library preparation using a protocol adapted from Gogakos et al. The four isodecoder tRNA families which contain an intron are tRNA-Arg-TCT, tRNA-Ile-TAT, tRNA-Leu-CAA and tRNA-Tyr-GTA. The number of reads mapping the intron (I) (representative of unspliced tRNAs) and the number of reads spanning the intron/exon junction (IEJ) (spliced tRNAs) were counted to calculate a percentage [I / (IEJ+ I)*100] of unspliced tRNA (UnS) in each individual. The results are expressed as a fold change relative to the Ctrl-2 (% UnS B.II-3 / % UnS Ctrl-2), with red squares indicating a fold change > 1.5. The GtRNAdb gene symbol for each intron-containing tRNA is indicated in abscisse. Abbreviations used are: Arg, arginine; Ile, isoleucine; Leu, leucine and Tyr, tyrosine.

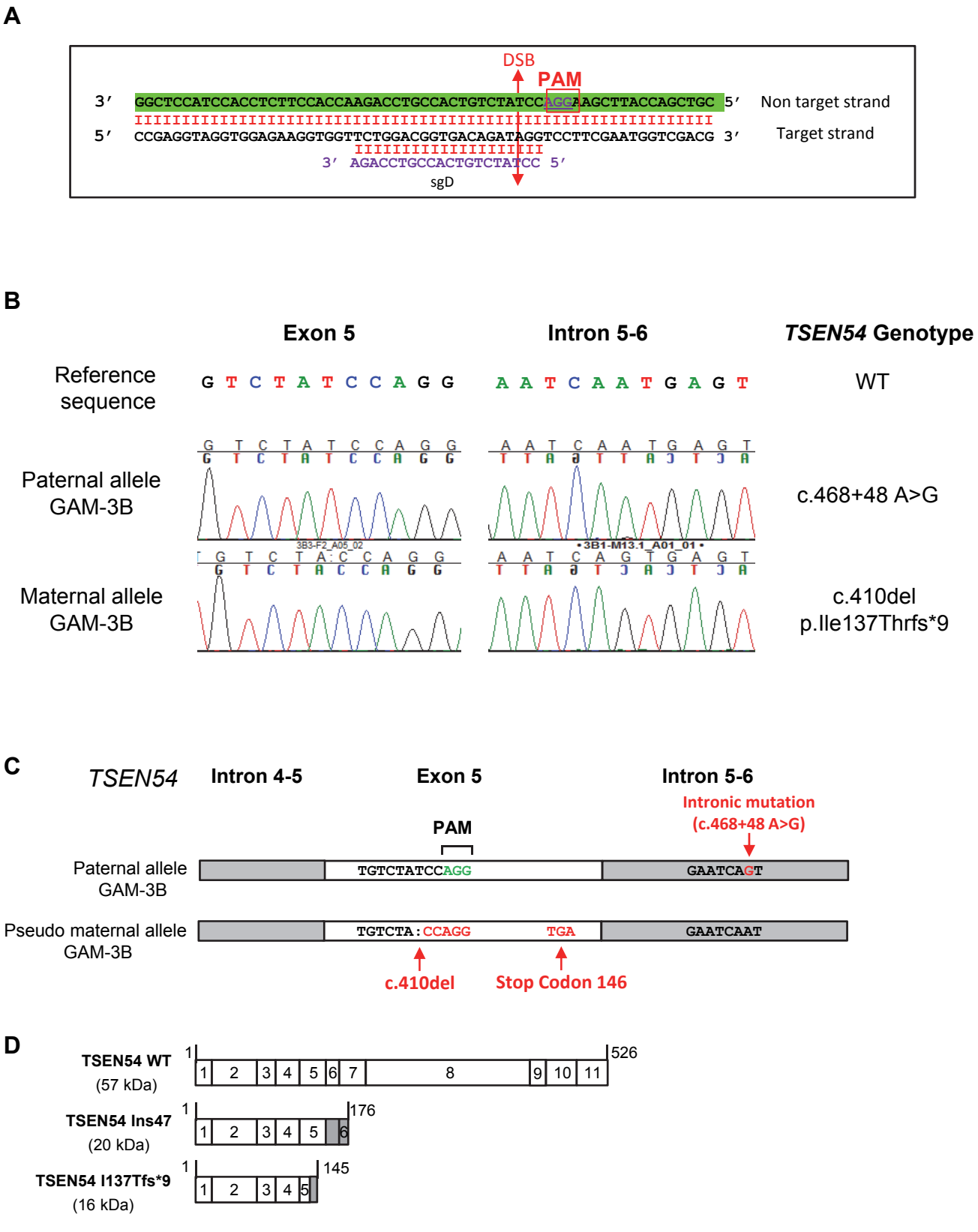

Figure 5. Generation of *TSEN54* gene-edited iPSC lines. (**A**) sgRNA designed with the Crispor software with the PAM (red square) located in the *TSEN54* exon 5 sequence (chr17:73513638-73513736, hg19). The selected guide (sgD) is in violet. Localization of the expected double strand break (DSB) is indicated by the red arrow. (**B**) Sanger sequencing of exon 5 showing the two different variants in one of the CRISPR/Cas9-edited clone, GAM-3B. (**C**) Schematic representation of the clone GAM-3B genotype. (**D**) Schematic overview of the corresponding TSEN54 mutant proteins, with their expected size (kDa).

Supplementary Table 1 - Genomic location of the 20 selected off target sites and primers used for Sanger sequencing

Name	Amplicon Location (hg19)	Forward Primer Sequence	Reverse Primer Sequence
TSEN54 Exon 5-Intron 5-6	chr17:73513523-73514018	TTCTTGATGCGCTGCTGAGA	CAACTCTACCCACCCCCAAC
pGEMT easy M13 primers	-	M13 forward GTTTTCCCAGTCACGACGTT	M13 Reverse GGAAACAGCTATGACCATGA
T01	chr3:124487489-124488372	CCGTTGATGGACATGTGGTT	ACTAGGACAATGTTGGGGCA
T02	chr21:46840558-46841090	TTTCCTGGGCCTGTATCCTG	CTGTCTGTCCGTCTGTCCTT
T03	chr7:29546652-29547108	CTCAGACCCTACCTCCCTCT	TGCCCTCACTTGACAAGACA
T04	chr10:12876606-12877068	TTGTCTCCGGGGAACTTCTC	GCCCCATCTTTCGAAGCAAA
T05	chr6:144980750-144981330	TGGCCTCTTGTCCTGTGTTT	CCGGCAAACTTCCTTCAGAC
T06	chr2:152536279-152536786	TCGCATCAGTTCTCAGGTCA	CCCAGAGGTTCCTACTGCAA
T07	chr22:39771889-39772417	TCCCCTCTCTCTTCCCCTAC	TCTCCAGTGACCATGCTACC
T08	chr17:72355298-72355885	CTAGCCCTGTGGTTCCAAAC	CCCCTCAGAGCTGTTTCCAA
T09	chr8:95734885-95735351	ACCTGTCTGTCTATGTGCCA	ACATCCACAAAAGTAACCTGCT
T10	chr20:30650801-30651387	CATTCTCCCCTTCCCCTTCA	CACTGAAGCCATGCCTTAAAAG
T11	chr7:7494570-7495141	ACTAGGACCTCTGCCAATGG	ATAAATGACACCTGGCCCCT
T12	chr4:97574338-97574999	CCCTGTGCCTGCTTTGATTT	GAGTGACAGACCAGCTCTCA
T13	chr7:39462846-39463397	CCATCTTGACTGTCCTGCCT	CTGTTTGGGCAAGGGAAGTG
T14	chr20:44587802-44588368	GCCTCACTCTGTCATCCTGA	TACAGAAAAGGAGCCAGGGG
T15	chr8:141959646-141960309	CTGAGCCTGAGTCTGTCACA	AGCTCTTTCAGTCCCTGCAT
T16	chr5:12717313-12717989	CAAGTATGTGCACTCAGGGC	GGCAATGTGGTGAGCAAGAA
T17	chrX:42225383-42226071	GGATTTTGGTATCTTTGCAGGGA	CTTAGGCCCCACTCTTGTCA
T18	chr7:157985910-157986587	AGGACAAGGCCAAGAACCAG	CTTGCTGGAATGTGGAGGTG
T19	chr4:171967327-171967873	GAGAGAGGTACCGTGTAGCC	CTAGGAGCTATGGGTGTGGG
T20	chr11:85675186-85675733	TCAGAAAGTGAGGCTAGTGGA	GACATAACAGAGCACGGCAG

Supplementary Table 2 - Primers used for shRNA and primers used in RT-PCR and qRT-PCR experiments

Primer name	**Sequence 5'-3'**
sh1	GTACCCAGACTCTAACCTGTA
sh2	CCAGACTCTAACCTGTAGCTT
TSEN54 cDNA Exon 3 Forward	GCTTGGTGGCTGCCGAGTGGA
TSEN54 cDNA Exon 8 Reverse	CTTGGGTTGCAGGGAGTTGTC
qPCR TSEN54 Exon 3 Forward	AGAGGGCTTCGTGGAGTTGA
qPCR TSEN54 Exon 4 Reverse	TACAAGGCCTCTTCCGGGTGAA
qPCR TSEN54 Exon 5-6 Forward	AGTACCAGGTCTTCAGCCA
qPCR TSEN54 Exon 7 Reverse	TTGCCATCTCCATCCTCCAAGT
qPCR TSEN54 INS47 Forward 2	GCTGCTGCTGACCGACCACACT
qPCR TSEN54 INS47 Reverse 2	GGATGGGTGGCTCCCGGAGG
HPRT Forward	TCTTTGCTGACCTGCTGGATT
HPRT Reverse	GTTGAGAGATCATCTCCACCAATTACT

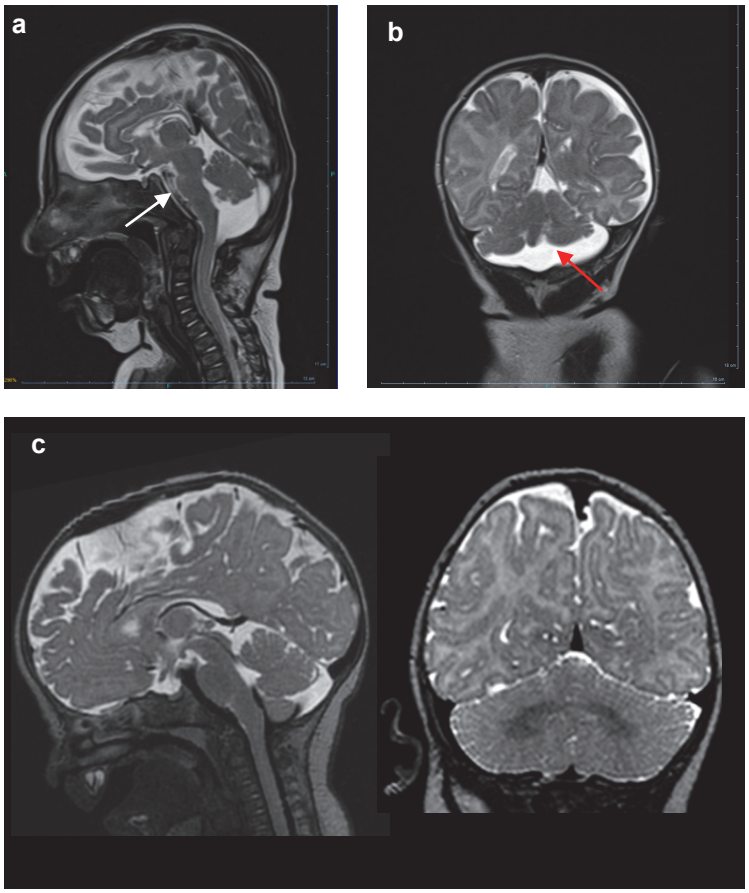

Figure S1. Neurological features of GAMOS affected individual. Brain MRI abnormalities in individual A.II-2 with GAMOS at 4 months. (**a**) Sagittal T2-weighted image shows microcephaly with cerebellum hypoplasia, moderately flattened pons (arrow), thin corpus callosum. (**b**) Coronal T2-weighted image shows moderate cerebellar hypoplasia presenting with a butterfly pattern (red arrow) without cerebellar cortex atrophy. Enlarged pericerebral fluid spaces. (**c**) Sagittal T2- and coronal T2-weighted images of a 4-month old patient control with craniostenosis but no brain abnormalities .

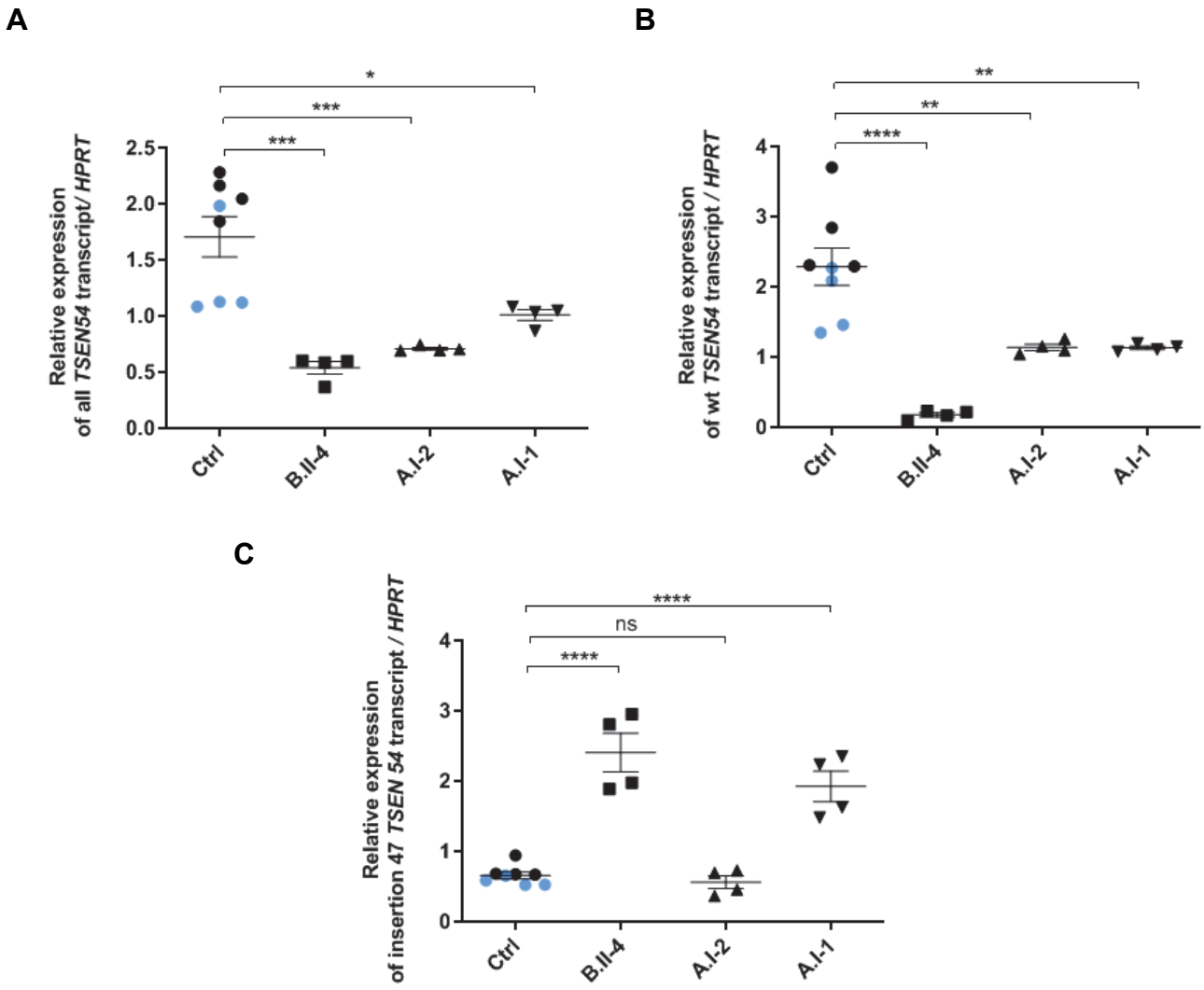

Figure S2. Relative expression of *TSEN54* transcripts in LCLs of healthy and affected individuals. Relative expression of total, wild-type (WT) and Ins47 *TSEN54* transcripts normalized to *HPRT* in LCLs from healthy (Ctrl, A.I-1 and A.I-2) and SRNS affected (B.II-4) individuals. Data for control (Ctrl) individuals correspond to the pool of 2 healthy individuals (Ctrl-1 and Ctrl-2) **A.** Relative expression of total *TSEN54* transcripts (mean ± s.e.m. of *n*=4 experiments, Kruskal-Wallis test followed by Dunn's *post-hoc* test in, ***p =0.0003, *p=0.0173 ns=0.2931). **B.** Relative expression of WT *TSEN54* transcripts (mean ± s.e.m. of *n*=4 experiments, Kruskal-Wallis test followed by Dunn's *post-hoc* test in, ***p =0.0003, ns=0.0817). **C.** Relative expression of Ins47 *TSEN54* transcripts (mean ± s.e.m. of *n*=4 experiments, Kruskal-Wallis test followed by Dunn's *post-hoc* test in, **p =0.0090, *p=0.0472, ns>0.9999).

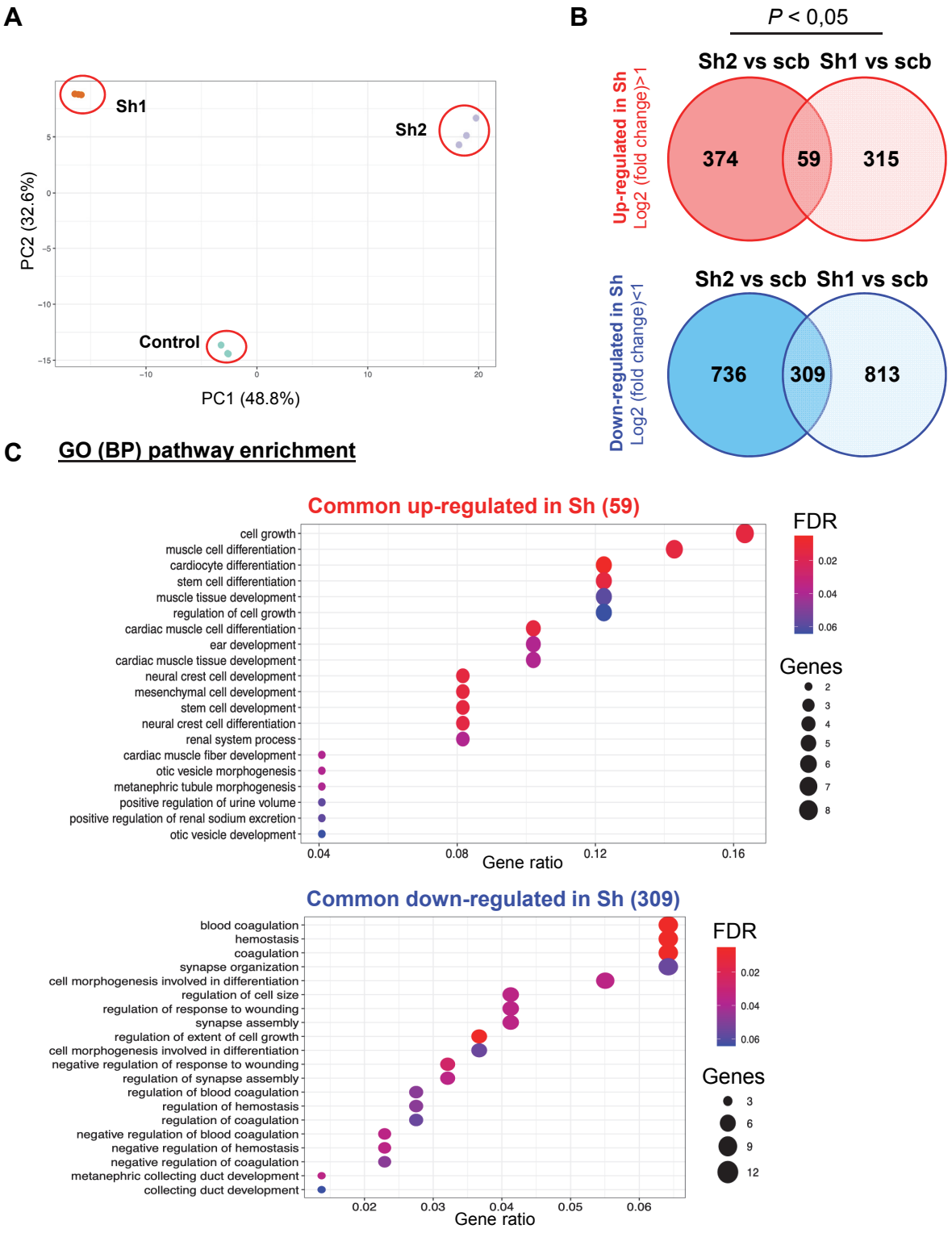

Figure S3. Whole transcriptome profiling (RNA-seq assay) upon *TSEN54* KD in podocyte lines. **(A)** Principal component analysis (PCA) of the RNA-seq data for 9 podocyte samples. Principal components 1 (x-axis) and 2 (y-axis) are shown. Percentages represent variance captured by each principal components 1 and 2. Controls samples (3 samples) are shown in green and *TSEN54*-suppressed (*TSEN54* KD) podocytes Sh1 (3 samples) and Sh2 (3 samples) are colored differently. **(B)** Venn diagrams showing the number of common upregulated (top) or downregulated (bottom) genes found in *TSEN54*-suppressed podocytes Sh1 and Sh2 compared to control. Genes were considered to be differentially expressed to a statistically significant extent if the following criteria were met: $P < 0.05$ and $|\log2(\text{fold change}) > 1|$. Differential expression was tested using the the *DEseq2.0* R framework. **(C)** Gene set enrichment analysis based on functional annotation (Gene Ontology—Biological Process database) of common differentially expressed genes (DE) found in Sh1 and Sh2 vs control. Dot size shows the number of DE genes found within each pathway whilst dot colors indicate FDR values for the gene set enrichment analysis.

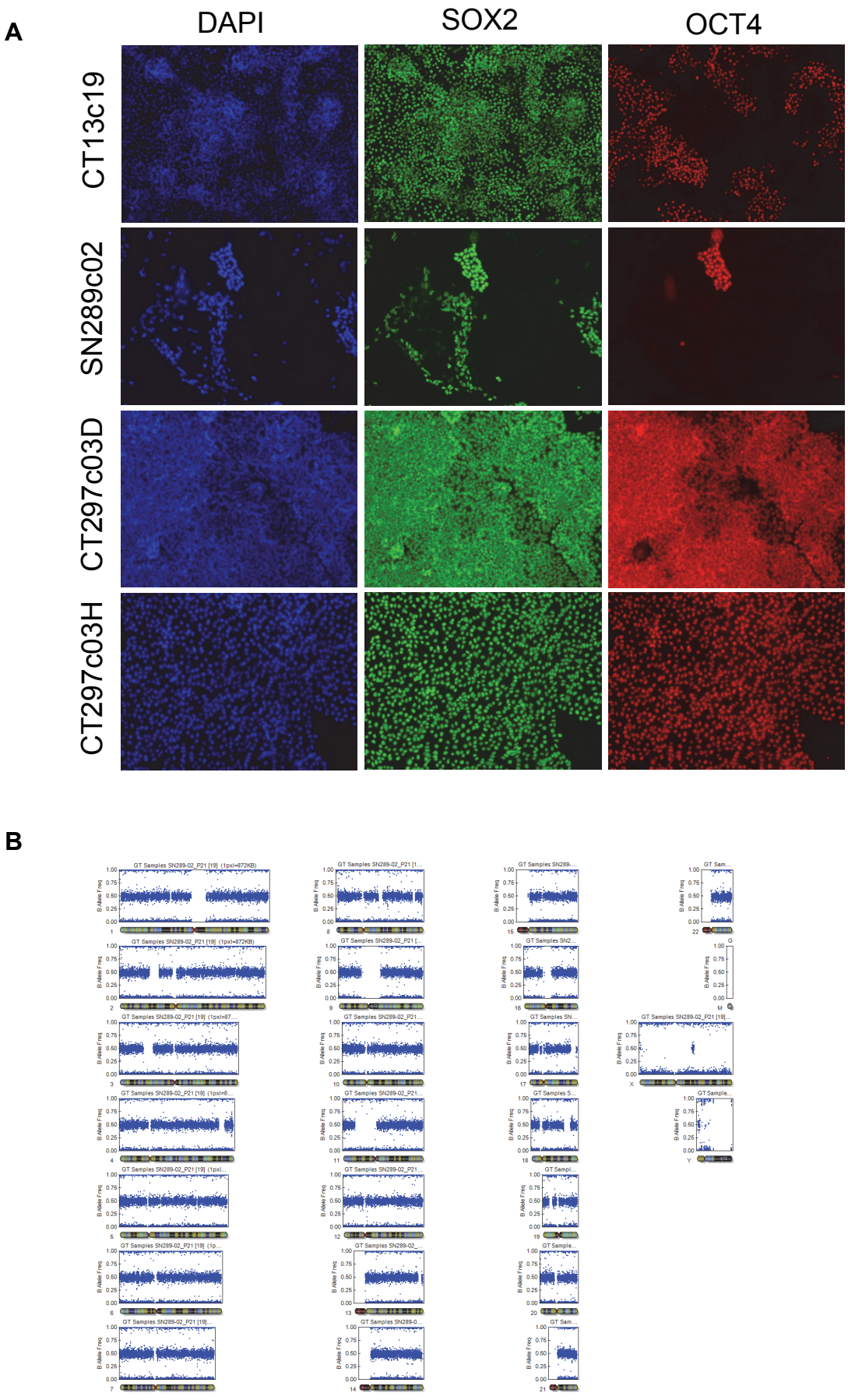

Figure S4. Assessment of stemness and genome integrity in iPSC lines. A : Immunofluorescence of SOX2 (green), OCT4 (red) and DAPI (blue) in the following iPSC clones: control CT13c19, SN289c02 (SRNS affected individual), CT297c03D (isogenic control) and GAM-3H (GAMOS affected individual). **B** : SN289c02 (at passage 21) genomic SNP array analysis showing a normal karyotype. The same result has been observed for all other iPSC clones used in this study.

COMPLEMENTARY DATA

Here, I report additional results, which are complementary to the article and which include some experiments that are still ongoing and unfortunately incomplete at the time writing my thesis manuscript. The results presented here will require further validation and/or analysis but they will be crucial for a better understanding of the pathophysiological mechanisms involved in *TSEN54*-linked GAMOS and SRNS.

Here I report the impact of *TSEN54* variants on TSEN complex stability and identification of potential TSEN54-interacting proteins. The investigation of *TSEN54* variants impact on mRNA and protein levels using patient-derived and CRISPR/Cas9 gene-edited iPSCs and iPSC-derived neural progenitor cells (NSCs). Furthermore, I present the generation of iPSC-derived kidney organoids and isolation of kidney organoid-derived podocytes. Finally, I report the investigation of *TSEN54* variants impact on transcriptomic profiles of iPSC-derived NSCs and kidney organoid-derived podocytes, and on tRNA-intron splicing in NSCs.

A) Impact of *TSEN54* variants on TSEN complex stability and identification of potential TSEN54-interacting proteins

It has been shown that variants in *TSEN15* and *TSEN54* could impact the steady-state levels of the mutant proteins and/or affect the overall stability of the TSEN complex impairing its function in pre-tRNA processing (Breuss *et al.* 2016; Sekulovski *et al.* 2020). Since we detected a transcript corresponding to the Ins47 mutant allele, our first hypothesis was that the renal disease might be caused specifically by the presence of the Ins47 mutant protein that would interact with podocyte-specific proteins and interfere with normal podocyte function, explaining the absence of renal involvement in PCH cases. However, we were not able to detect the mutant proteins (Ins47 and Q339*) in LCLs protein lysates by western blots analysis (see **Figure 2B** of article), dismissing this initial hypothesis. Anyway, we still decided to perform co-immunoprecipitation (co-IP) and proteomic studies with the different TSEN54 mutant proteins fused to GFP as baits in HEK293 cells which are of kidney origin. We thus performed a proteomic analysis of GFP immunoprecipitates isolated from HEK293T cells transiently overexpressing GFP-TSEN54 wild-type (WT) or GFP-TSEN mutant proteins: Ins47, Q339* and A307S, this latter corresponding to the most common variant c.919 G>T reported in *TSEN*-linked PCH cases and responsible for PCH type 2 in the homozygous state (van Dijk and Baas 2009).

The interactome of each GFP-TSEN54 proteins (WT and mutants), compared to that of the control (GFP "empty"), is represented as a volcano plot, where enriched proteins, with a high fold change (FC) and statistically significant, are represented on the right of the volcano center (**Complementary Figure 1A**). Two p-values thresholds were established on the volcano plot (line 1 and 2) to classify interacting protein into two categories "class A" (threshold $p<0.01$ and "class B" (threshold $p< 0.05$), the proteins in class A being those with the highest fold change and significant p-value. We noticed that TSEN54-WT and A307S have a few class A interactors (8 and 7, respectively) compared to the two other mutants, Ins47 and Q339* (115 and 172, respectively).

A

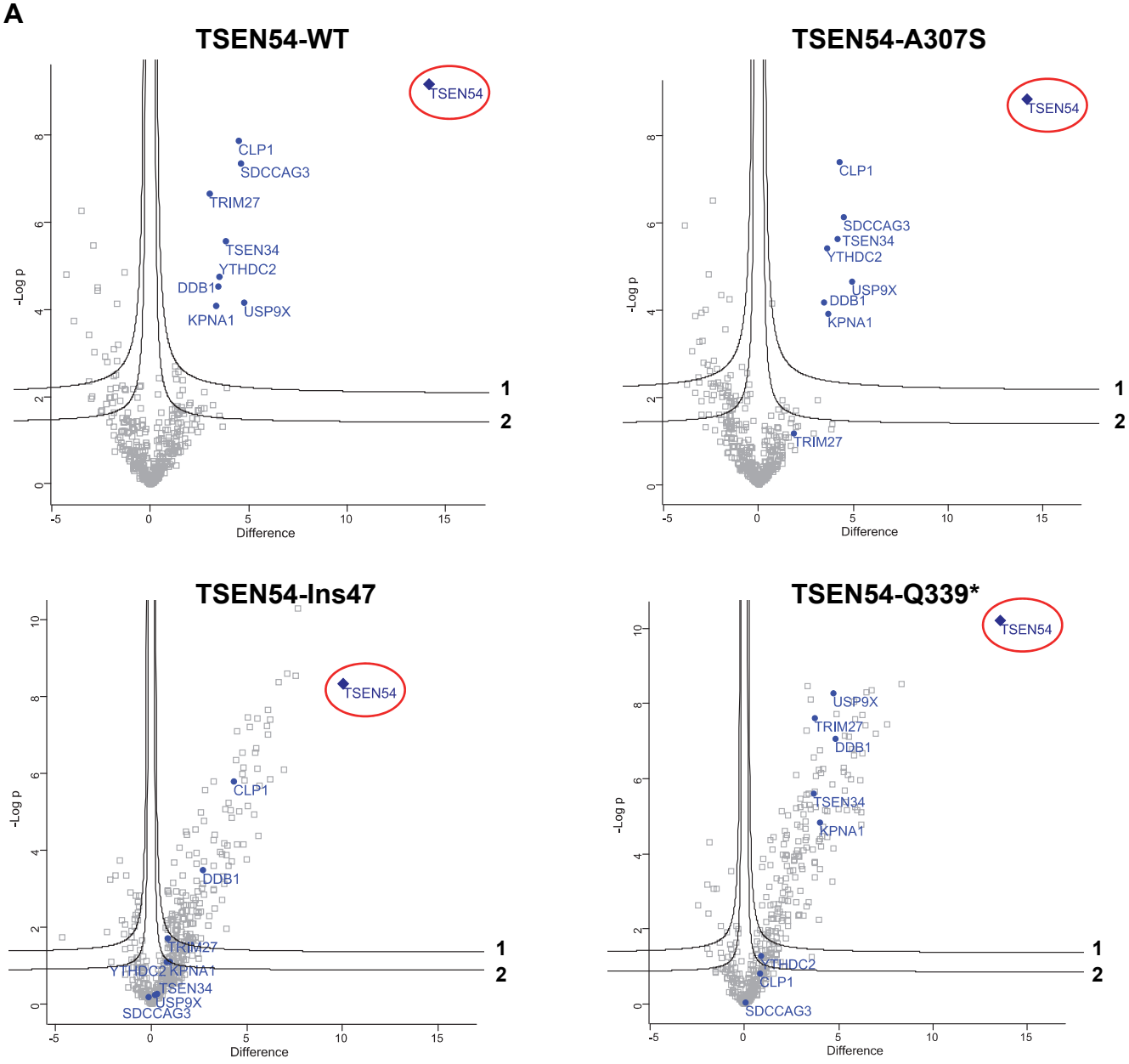

B

	Empty vs WT	Empty vs A307S	Empty vs ins47	Empty vs Q339*
CLP1	+	+	+	-
TSEN34	+	+	-	+
KPNA1	+	+	-	+

Complementary Figure 1: TSEN54 interacts with TSEN34, CLP1 and KPNA1 (A) Volcano plot representations of mass spectrometry analysis of GFP-immunoprecipitates isolated from HEK293T cell line transiently expressing either GFP TSEN54 WT or GFP-TSEN54 mutants, Ins47, Q339* and A307S. Proteins which were significantly enriched in the GFP-IP from GFP-TSEN54 expressing HEK293T cells compared to GFP-only are found in the region right of the central 'volcano'. Numbers (1 and 2) indicate two different p value thresholds applied to the data (Threshold 1: p<0,01 and threshold 2: p<0,05). Blue colour highlights the nine proteins significantly (above threshold 1) interacting with GFP-TSEN54-WT protein. Data is representative of six technical repeats. **(B)** Table showing the status of interaction of the different TSEN54 proteins with TSEN34, CLP1 and KPNA1.

Regarding the TSEN complex, among the 8 proteins interacting with TSEN54-WT (class A), we found TSEN34 and CLP1, which are also found to interact with the A307S mutant. On contrary, the Ins47 and Q339* lost their interaction with TSEN34 and CLP1, respectively (**Complementary Figure 1A and 1B**). Interestingly, we identified the KPNA1 protein (karyopherin subunit alpha 1 or importin alpha 5), which is involved in the transport of molecules between the nucleus and the cytoplasm, and which might be a potential transporter for TSEN54, since TSEN complex is localized in the nucleus to exert its function. Of note, KPNA1 is also interacting with the A307S and Q339* mutant proteins, but not with the Ins47 mutant. Strikingly, among the 79 proteins interacting with Ins47 mutant (class A proteins with FC>2), one third was linked to protein degradation, including proteasome subunits and ubiquitin related proteins, suggesting that the Ins47 mutant may undergo massive proteasomal degradation, consistent with the fact that we were not able to detect the Ins47 mutant protein by WB in LCL protein lysates. Analysis of the statistically enriched ontology terms using Metascape (https://metascape.org) confirmed this enrichment in proteasome components (**Complementary Figure 2A**). These proteasomal/ubiquitin proteins were not found in the interactome of the Q339* protein, nor in that of the WT and A307S mutant, suggesting that the Q339* mutant, if translated, is not a target for proteasomal degradation. The enrichment for ontology terms in the TSEN54-WT and Q339* conditions, presented in **Complementary Figure 2B**, showed that signaling by Rho GTPases is the most significantly enriched for Q339*, whereas it is the mesenchyme migration, linked to cytoskeleton proteins, for WT. However, the Nop56p-associated pre-rRNA complex cluster is significantly enriched in WT, Q339* and Ins47 conditions, suggesting a potential undescribed role of TSEN54 in pre-ribosomal RNA processing (**Complementary Figure 2B**).

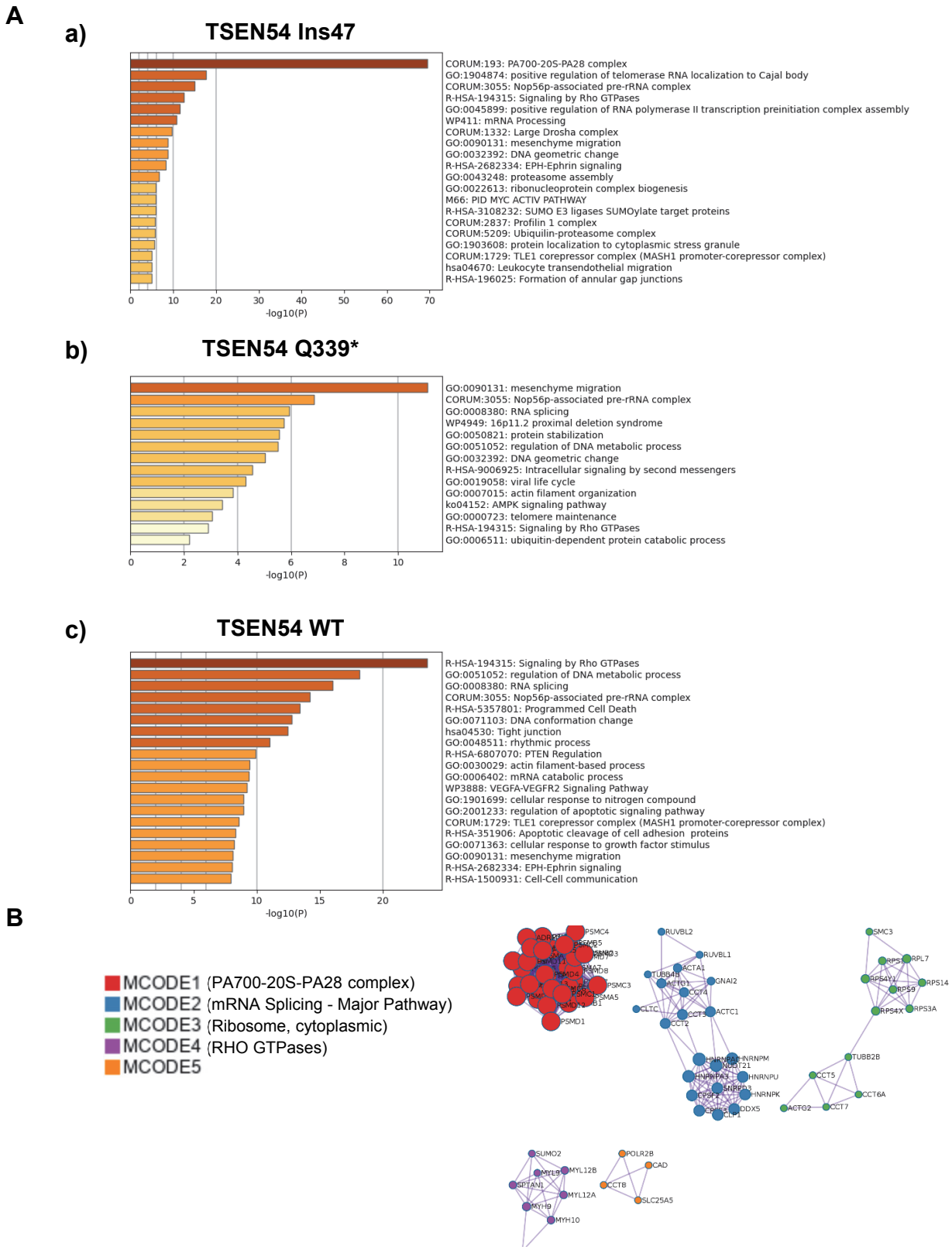

Complementary Figure 2: Gene Ontology cluster analysis of TSEN54 interacting proteins. (A) Enrichment analysis with statistically enriched clusters ordered according to their respective –Log10 (P) value (**a**) Enrichment analysis of the 115 proteins (class A significance) interacting with TSEN54 Ins47 mutant protein. (**b**) Enrichment analysis of the 172 proteins (class A significance) interacting with TSEN54 Q339* mutant protein, and (**c**) Enrichment analysis of the 30 proteins (class B significance) interacting with TSEN54 WT protein. (**B**) MCODE network corresponding to TSEN54 Ins47 – interacting proteins. A subset of the representative terms from the most significant cluster in (A) was converted into an MCODE enrichment network. GO enrichment analysis was applied to each MCODE network to assign « meanings » to the network components (shown on the right). Analyses were performed using the Metascape software.

In order to validate mass spectrometry analysis, we performed co-IP experiments using GFP-tagged TSEN54 WT or TSEN54 mutant GFP-tagged transiently overexpressed in HEK293 cells, since antibodies against the four TSEN subunits did not work for endogenous IP, preventing us to confirm the interaction between endogenous proteins. The GFP-TSEN54 WT immunoprecipitated endogenous TSEN34 and to a lesser extent TSEN2 and TSEN15, although both proteins seemed to be well expressed (**Complementary Figure 3A**). The TSEN54 A307S and Q339* mutant proteins behaved the same way as the WT, whereas the interaction seemed to be decreased or lost with TSEN54 Ins47 mutant protein. This might suggests that the Ins47 mutant protein, if translated, could alter TSEN complex assembly. We next assessed by co-IP the interaction between GFP-TSEN54 WT with either 2HA-tagged CLP1 or KPNA1 and demonstrated that TSEN54 WT interacts with both CLP1 and KPNA1 (**Complementary Figure 3B**).

A

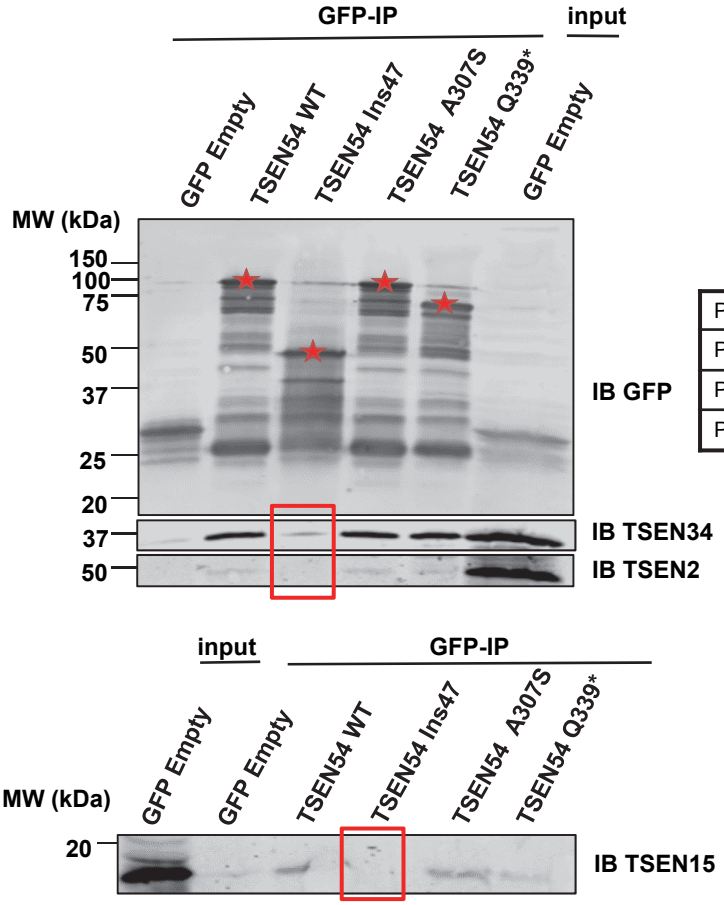

PLEX-GFP-TSEN54-WT	WT	81 kDa
PLEX-GFP-TSEN54-ins47	Ins47	47 kDa
PLEX-GFP-TSEN54-A307S	A307S	81 kDa
PLEX-GFP-TSEN54-Q339*	Q339*	64 kDa

B

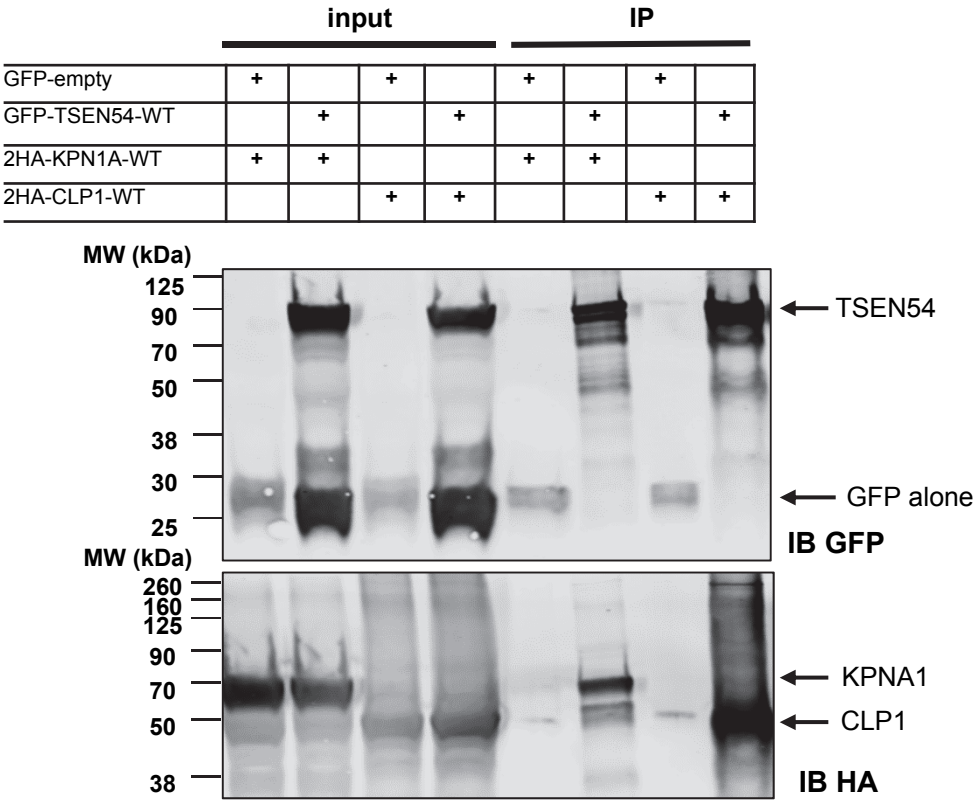

Complementary Figure 3. Validation of interaction by co-IP experiments in HEK293T cells. (**A**) GFP-IP from HEK293T cells transiently expressing either GFP or GFP-TSEN54 WT or Ins47, A307S or Q339* mutants. Antibodies against GFP are used to reveal expression of the TSEN54 proteins and antibodies against TSEN34, TSEN2 and TSEN15 are used to reveal the endogenous proteins. (**B**) GFP-IP from HEK293T cells transiently expressing either GFP or GFP-TSEN54 WT, with or without 2HA-CLP1 or 2HA-KPNA1. Antibodies against GFP are used to reveal expression of the TSEN54 WT protein and antibodies against HA are used to reveal expression of CLP1 and KPNA1.

Summary of the results obtained in this section and short-term perspectives

Even though TSEN54 mutated proteins are not detected by WB in LCLs, we have shown that Ins47 protein does not interact with TSEN34, which could lead to the destabilization of the TSEN complex and could have an impact on its function. On the other hand, Q339* does not seem to impact the assembly of the complex, but does not interact with CLP1. If the mutant proteins are expressed, they have a very different interactome compared to the TSEN54 WT protein, with predominantly proteasome components for Ins47, suggesting massive proteasomal degradation, which is in line with the fact that the mutant Ins47 protein is not detected by WB. Conversely, Q339* mutant protein has a different interactome, rather linked to cytoskeleton proteins involving RhoGTPase signaling. Interestingly, the TSEN54 A307S behaves like TSEN54 WT protein, interacting with TSEN34 and CLP1. Finally, TSEN54 WT and the two TSEN54 mutant proteins identified in this study have common interactor proteins mainly involved in RNA splicing and pre-rRNA processing. These results need to be confirmed in podocytes and neural progenitors/neurons, the two relevant cell types in these disorders. In addition, the identification of KPNA1 as a potential transporter of TSEN54 into the nucleus, needs further investigations such as the depletion of *KPNA1* using shRNA in order to confirm the involvement of KPNA1 in the subcellular localization of TSEN54.

B) Investigation of *TSEN54* variants impact on mRNA and protein levels using patient-derived and CRISPR/Cas9 gene-edited iPSCs

We decided to take advantage of iPSC technology to better model the renal and neural aspects of *TSEN54*-linked GAMOS or SRNS by differentiating our iPSC lines into disease relevant cell types, namely podocytes and neural progenitors/neurons. To do so, iPSCs were reprogrammed from PBMC obtained from a SRNS affected individual, from the parents of a GAMOS affected child and from healthy individuals. The reprograming was performed at the iPSC plateform de Nantes (PFiPSC Nantes) or at *Imagine* Institute iPSC platform (for the healthy individuals) using the non-integrating Sendai virus approach. We then used CRISPR/Cas9 gene-editing to introduce a nonsense *TSEN54* variant in the iPSC line obtained from the GAMOS child father, which harbors the Ins47 variant in the heterozygous state, to mimic the GAMOS child's genotype. After a quality control (karyotype, assessment of pluripotency and trilineage differentiation potential), iPSCs have been further differentiated towards renal and neural lineages, namely kidney organoids and neural stem cells (NSCs), to investigate alterations in molecular and cellular pathways that might be responsible for kidney and brain defects observed in SRNS and GAMOS affected individuals. iPSC lines generated and used in this study are listed in **Table C1** below.

Table C1 – iPSC and neural stem cell (NSC) lines used in the study

Clone number	Abbreviation in the text*	Abbreviation in figures*	Genotype at *TSEN54* locus	Disease
SN289-01 SN289-02	SRNS 1 SRNS 2	SN289c01 SN289c02	c.468+48A>G (Hom)	SRNS
CT297-03	Heterozygous 1	CT297c03	c.468+48 A>G (het)	healthy control
IMAGINi005c04	Control 1	CT05c4	WT	healthy control
IMAGINi013c19	Control 2	CT13c19	WT	healthy control
IMAGINi009c09	Control 3	CT09c9	WT	healthy control
CT297c03D CT297c03J	Heterozygous 2 Heterozygous 3	CT297-3D CT297-3J	c.468+48A>G (het)	control
CT297c03B CT297c03H	GAMOS 1 GAMOS 2	GAM-3B GAM-3H	c.468+48A>G (het) + c.410 del (het)	GAMOS

NSC, neural stem cells, SRNS, steroid-resistant nephrotic syndrome, GAMOS, Galloway-Mowat syndrome. Hom, homozygous; het, heterozygous. ***** when experiments are done on NSC, "NSC" is added before the abbreviation.

We first checked the impact of the *TSEN54* variants on mRNA and protein levels in iPSC lines. We confirmed the previous results obtained in LCLs by RT-PCR, showing that the clones harbouring the intronic Ins47 splice variant, either in homozygous (SRNS 1 and SRNS 2) or heterozygous state (Heterozygous 1, Heterozygous 2, Heterozygous 3, GAMOS 1 and GAMOS 2) have two different transcripts, one corresponding to the WT (446 bp) and one to mutant (493 bp). This result confirms that in iPSCs, both canonical and cryptic splicing sites are used (**Complementary Figure 4A)**. Then, we performed WBs using the same antibody directed against the N-terminal part of TSEN54 protein to detect both WT and mutant proteins. Also in this case, we observed that both mutant proteins are not detected in the concerned iPSC clones. Unexpectedly, we observed a high variability in the expression level of TSEN54 WT between SRNS 1 and SRNS 2 iPSC clones, homozygous for the Ins47 variant, with the SRNS 1 clone having a similar expression compared to the control line (Control 2). However, the TSEN54 WT expression level in SRNS 2 and GAMOS 1/GAMOS 2 are lower than the control 2, as expected (**Complementary Figure 4B and 4C**).

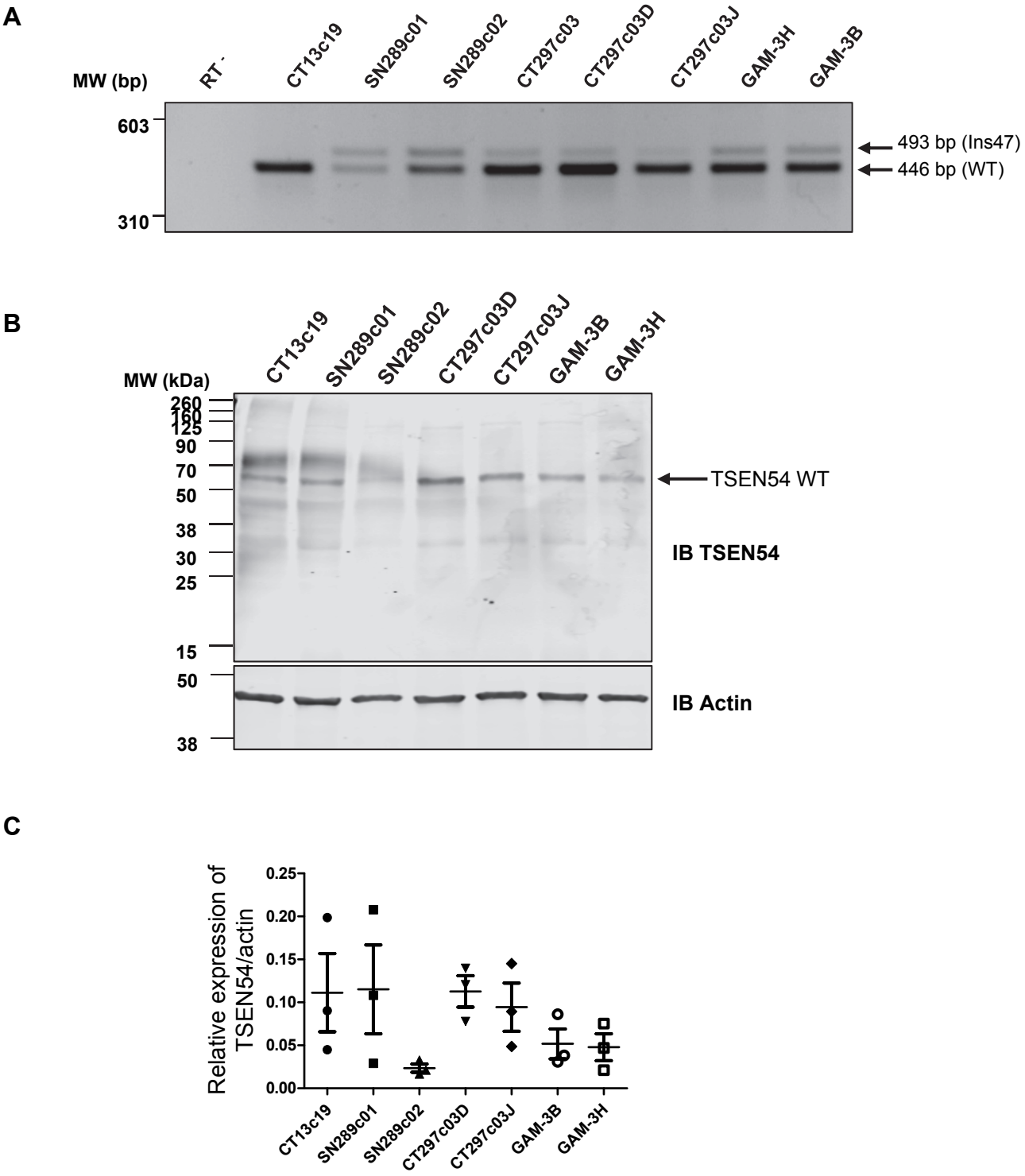

Complementary Figure 4. Characterization of *TSEN54* iPSC lines. (**A**) RT-PCR on iPSCs. RT-PCR have been performed with primers covering *TSEN54* exon 3 to exon 8. (**B**) Western blot analysis of protein lysates obtained from iPSC clones with Ins47 variant in homozygous (SN289-01 and SN289-02) or heterozygous (CT297c03D and CT297c03J) state, and clones bearing both Ins47 with I137Tfs*9 variants (GAM-3B and GAM-3H). Antibody against the N-terminal part of TSEN54 is used to detect the TSEN54 protein, and actin is used as loading control. (**C**) Quantification of the relative expression of TSEN54 normalized to Actin protein from three independent experiments in (B).

Summary of the results obtained in this section

Both cryptic and canonical splice sites are used in iPSCs. However, both mutant proteins were not detected in the concerned iPSC clones. These studies allowed us to confirm that our iPSC lines are suitable for further disease modeling studies.

C) Investigation of *TSEN54* variants impact on mRNA and protein levels and on cellular processes using iPSC-derived neural progenitor cells (NSCs)

We used the dual-SMAD inhibition protocol from Boissart et al. for neural induction of our iPSC lines (Boissart *et al.* 2013) and successfully obtain neural stem cells (NSCs). The expression of human natural killer-1 (HNK1) and the p75 neurotrophin receptor P75 at the surface of NSCs was verified by flow cytometry to assess their cortical neural fate, NSCs being HNK1-positive, but P75-negative. NSC high quality is defined as a population with at least 95% of $HNK1^{+}/P75^{-}$ cells, this percentage varying in our NSC lines from 87% to 97 % (**Complementary Figure 5)**. NSC cell lines used in this study are listed in **Table C1**.

We next checked the impact of the *TSEN54* variants on mRNA and protein levels on iPSC-derived NSCs. RT-PCR on NSC cDNA confirmed the previous results obtain in LCLs and iPSCs with the presence of two different transcripts in the NSC lines harbouring the Ins47 variant, either in an homozygous or heterozygous state (SRNS 1, SRNS 2, Heterozygous 2, Heterozygous 3, GAMOS 1 and GAMOS 2), thus confirming that both canonical and cryptic splicing sites are used in the NSCs (**Complementary Figure 6A**). We next performed qRT-PCR to assess the amount of total, WT and Ins47 *TSEN54* transcripts. Our results showed that GAMOS NCS lines (GAMOS 1 and GAMOS 2), carrying the nonsense I137Tfs*9 and Ins47 variants, seem to express less total *TSEN54* transcripts than the other lines, suggesting that the I137Tfs*9 mutant transcript might be subjected to nonsense-mediated RNA decay (NMD). Of note, the SRNS NSC lines (SRNS 1 and SRNS 2), homozygous for the Ins47 variant, also presents, to a lesser extent, a decreased total transcript level, however, the variability existing between the control NSC clones (Control 1, Control 2 and Control 3) makes the analysis more complex (**Complementary Figure 6B-a**). As expected, the SRNS NSC clones (SRNS 1 and SRNS 2) exhibited more Ins47 transcripts compared to the Ins47 heterozygous clones (Heterozygous 2, Heterozygous 3, GAMOS 1 and GAMOS 2), and both SRNS (SRNS 1 and SRNS 2) and GAMOS (GAMOS 1 and GAMOS 2) NSC clones exhibited a very low level of WT *TSEN54* transcripts compared to control and heterozygous for Ins47 variant NSC lines (Control 1, Control 2 and Control 3, Heterozygous 2 and Heterozygous 3) (**Complementary Figure 6B-b and -c**). Then, we performed WB using the same antibody directed against the N-terminal part of TSEN54 protein to detect both WT and mutant TSEN54 proteins. As previously shown in LCLs and iPSC protein lysates, both mutant proteins were undetectable in the NSC lines harbouring the corresponding variants. In addition, the SRNS (SRNS 1 and SRNS 2) and GAMOS (GAMOS 1 and GAMOS 2) NSC lines expressed a very low level of WT TSEN54

protein compared to the control and heterozygous NSC lines (Control 1, Control 2 and Control 3, Heterozygous 2 and Heterozygous 3), reflecting what was observed at the mRNA levels for the WT *TSEN54* transcript (**Complementary Figure 7A and B)**.

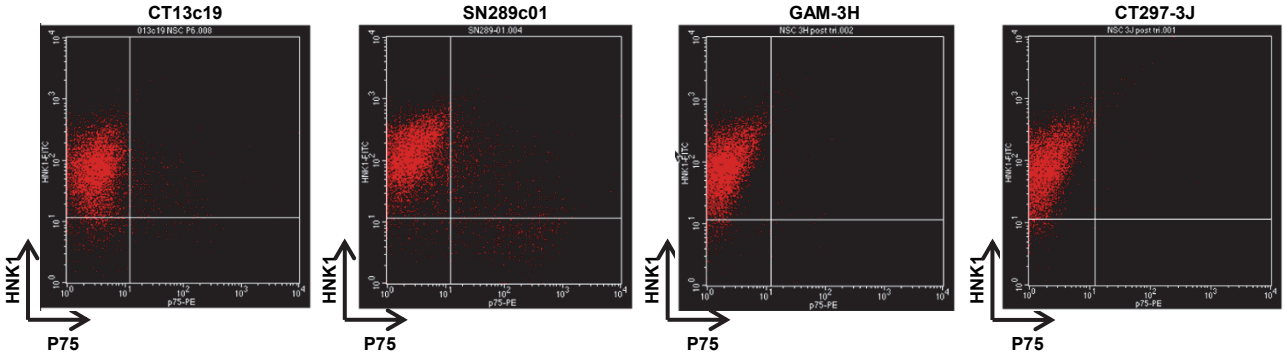

NSC line name	Passage number	HNK1^{+}	P75 $^{-}$
CT13c19	P6	92 %	4 %
SN289c01	P5	87 %	1 %
SN289c02	P6	93 %	3 %
CT297-3J and 3D	P8	97 %	2 %
GAM-3H and 3B	P8	97 %	2 %

Complementary Figure 5. FACS analysis of HNK1^{+} / P75^{-} cell population in NSCs.
Percentage of HNK1^{+} / P75^{-} cells are indicated in the table.

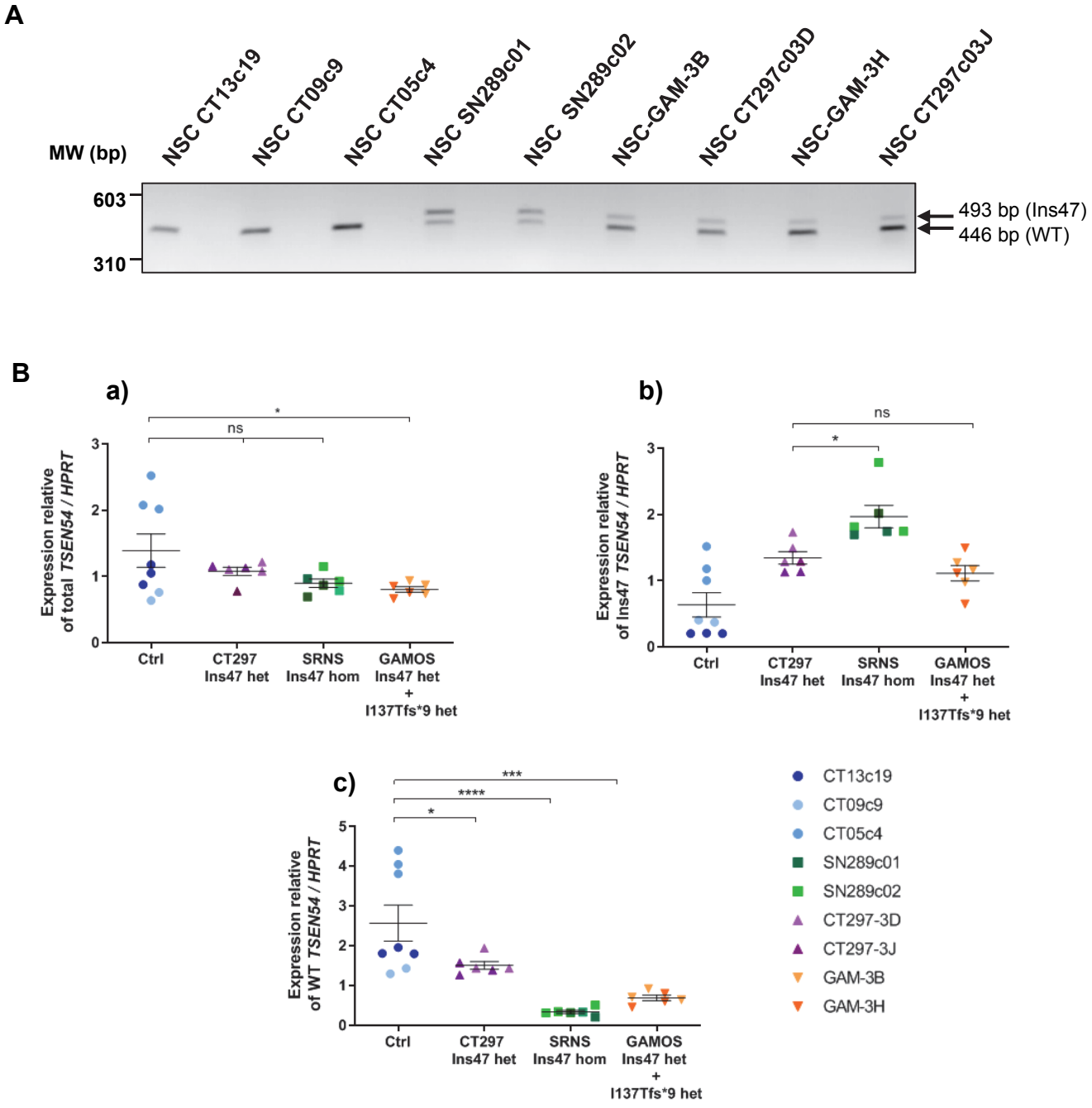

Complementary Figure 6. Characterization of *TSEN54* gene-edited NSCs lines. (**A**) RT-PCR on iPSCs. RT-PCR have been performed with primers covering *TSEN54* exon 3 to exon 8. (**B**) qRT-PCR analysis showing relative expression of total, WT and Ins47 *TSEN54* transcripts normalized to *HPRT* in iPSC-derived NSC lines. Data for control (Ctrl) NSCs correspond to the pooled data of 3 unrelated NSC lines (CT05c04, CT13c19 and CT09c09), data for CT297 correspond to the pooled data of CT297c03D et CT297c03J (heterozygous for Ins47 variant), data for SRNS corresponds to the pooled data of SN289c01 and SN289c02, and data for GAMOS corresponds to the pooled data of GAM-3B and GAM-3H. (**a**) Relative expression of Total *TSEN54* transcripts compared to Ctrl NSCs (mean ±s.e.m of *n*=3 experiments, with each experiment performed in triplicate; one-way ANOVA (F (3,22) =2.719, p=0.069), Dunnett's multiple comparisons test, ns=0,4013 for Ins47 het, ns=0.1031 for Ins47 hom,*p= 0.0437); (**b**) Relative expression of Ins47 *TSEN54* transcripts compared to CT297 NSCs (mean ±s.e.m of *n*=3 experiments, with each experiment performed in triplicate; one-way ANOVA (F (3,22) =13.30, p<0.0001), Dunnett's multiple comparisons test ,*p=0.0245, ns= 0.3223); (**c**) Relative expression of WT*TSEN54* transcripts compared to Ctrl NSCs (mean ±s.e.m of *n*=3 experiments, with each experiment performed in triplicate; one-way ANOVA (F (3,22) =12.71, p<0.0001), Dunnett's multiple comparisons test ,****p=<0.0001, ***p=0.0003*p= 0.0380). Ctrl, control; het, heterozygous; hom, homozygous.

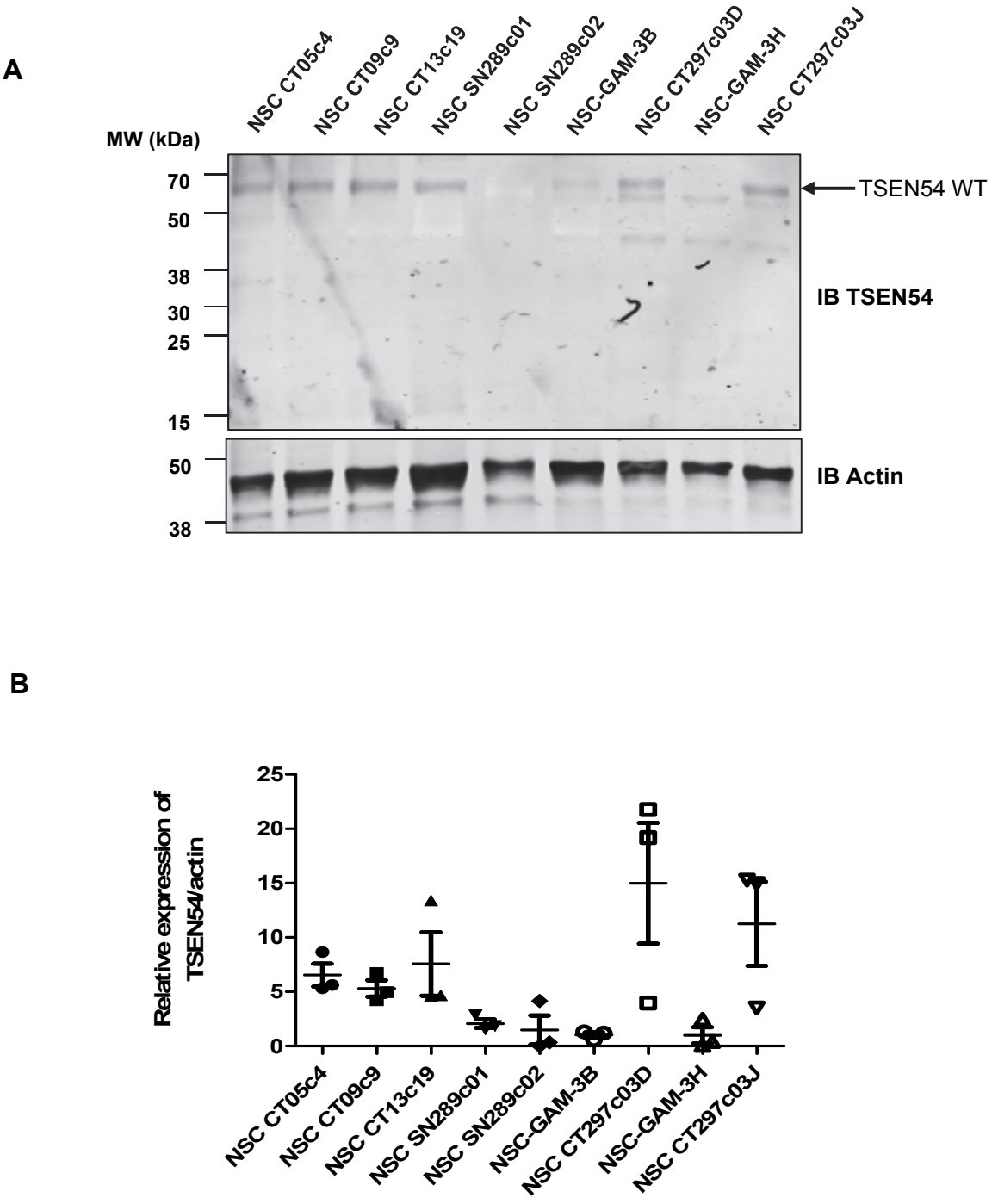

Complementary Figure 7. Characterization of *TSEN54* gene-edited NSCs lines. (**A**) Western blot analysis of protein lysates obtained from NSCs: 3 control NSC lines (CT05c4, CT09c9,CT13c19), 2 NSC lines homozygous for the Ins47 variant (SN289-01,SN289-02) (SRNS genotype), 2 NSC lines heterozygous forthe Ins47 variant (CT297c03D and CT297c03J), and 2 NSC lines bearing both Ins47 and the nonsense I137Tfs*9 variants (GAM-3H and GAM-3B) (GAMOS-like genotype). (**B**) Quantification of the relative expression of TSEN54 normalized to Actin protein from three independent experiments in (A).

Since we previously demonstrated a proliferation defect upon *TSEN54* depletion in podocyte cell lines, we wondered whether *TSEN54* variants could affect NSC proliferation, a potential mechanism known to affect cortical development and cause microcephaly. We thus assessed proliferation in the different NSC lines using a colorimetric MTT assay over 4 days (**Complementary Figure 8A)**. We first noticed a high variability in the cell proliferation rates between NSC lines of the same genotype, and or same genetic background, as shown in **Complementary Figure 8A-a to c**. We noticed that the NSC lines derived from the same Heterozygous 1 iPSC line seem to have a reduced proliferation rate, regardless of their genotype (**Complementary Figure 8A-c**). However, when we pooled the data according to the genotype of the NSC lines, we showed that the GAMOS (GAMOS 1 and GAMOS 2) NSC lines have a reduced proliferation rate compared to Ctrl (Control 1, Control 2 and Control 3), whereas the SRNS (SRNS 1 and SRNS 2) did not (**Complementary Figure 8A-d**), suggesting that the presence of the nonsense variant, associated to the Ins47 variant, has a deleterious effect on proliferation rate of NSC lines, which is not the case in the presence of the Ins47 variant in the homozygous state. This is also in accordance with the clinical phenotype associated with the genotype, with neurological defects in the individual bearing both variants (Ins47 and I137Tfs*9) compared to the SRNS affected individual bearing the Ins47 variant in the homozygous state. These results do not allow us to determine whether the observed variability is intrinsically due to the NSC lines or due to the MTT method, which is not suitable for that kind of cells. Indeed, this method evaluates the cell metabolic activity, which can varies with the physiological state of the cell (growth rate, differentiation efficiency, cell confluence). Therefore, these results should be confirmed by using alternative methods such as BrdU incorporation or Ki67 immunostaining, allowing us to simultaneously evaluate their cortical identity as revealed by PAX6 staining. Finally, by measuring Caspase-3/7 activity, we demonstrated absence of apoptosis in all NSC lines (**Complementary Figure 8B)**, as we previously shown upon *TSEN54* depletion in podocyte cell lines (data not shown).

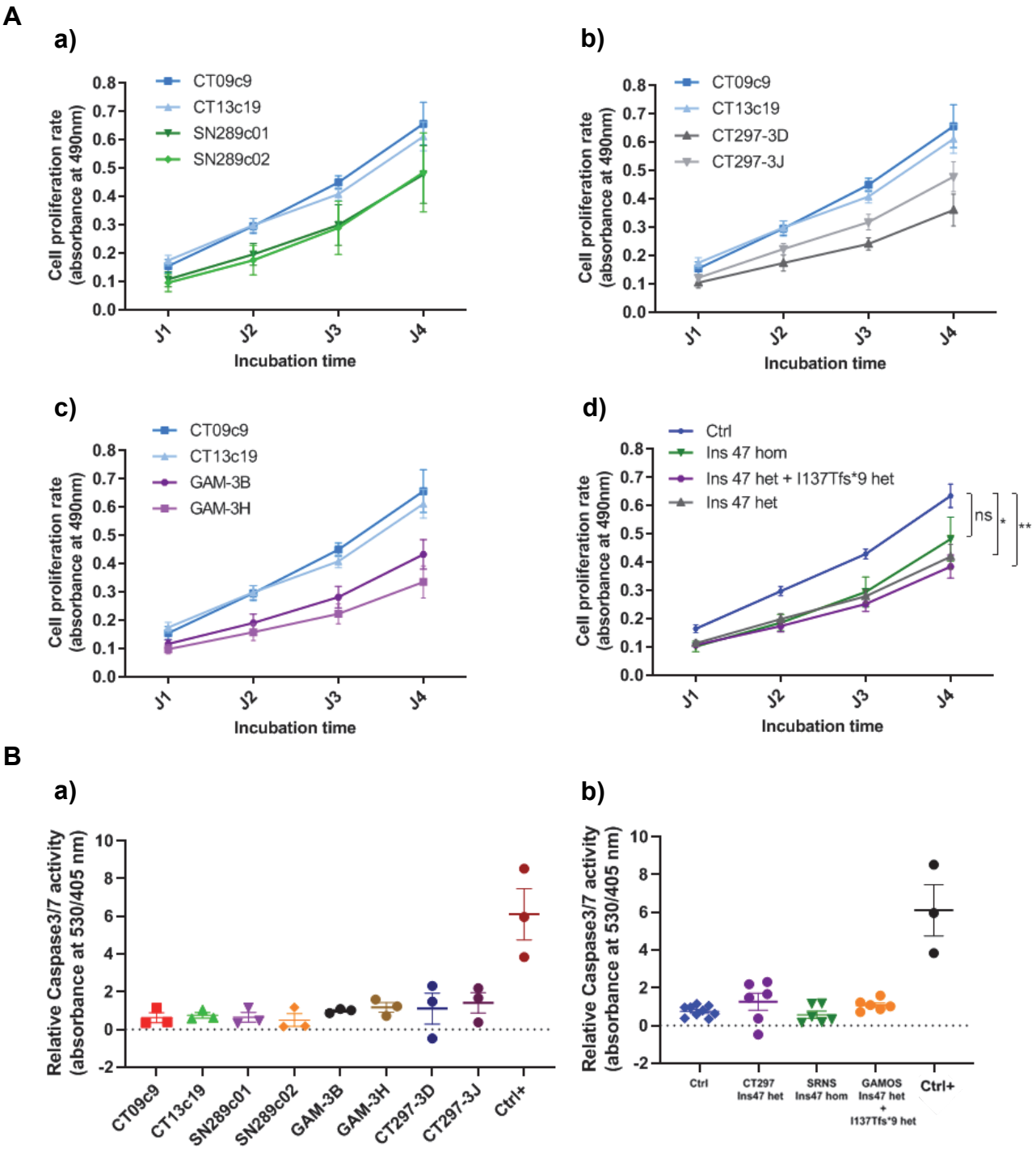

Complementary Figure 8. Assessment of proliferation and apoptosis in NSC lines. (**A**) Cell proliferation was assessed using a colorimetric MTT assay over 4 days, measuring absorbance at 490 nm at days 1, 2, 3, 4, (mean ± s.e.m. of n=4 experiments, with each experiment performed in triplicate (panel **d**; two-way ANOVA ($p < 0.0001$), Dunnett's multiple comparisons test n.s. = 0.2680, *p =0.0135, **$p < 0.0043$). In panel (**d**), data of graphs (**a**), (**b**) and (**c**) have been pooled according to the NSC line genotype. (**B**) Cell apoptosis was evaluated by quantification of caspase 3/7 activation on the basis of fluorescence intensity (530/405 nm). Absolute values were normalized to DAPI fluorescence intensity as an internal control. In panel (**a**)**,** values were compared to CT09c9 control cells (mean ± s.e.m. of n=3 experiments with each experiment performed in triplicate (one-way ANOVA ($F(9,20) = 8.899$, $p < 0.0001$), Dunnett's multiple comparisons test, n.s. = 0.09971) and in **(b),** data were pooled according to the NSC genotype and compared to the Ctrl group (one-way ANOVA ($F(4,25) = 24.46$, $p < 0.0001$), Dunnett's multiple comparisons test, n.s. = 0.6956). Ctrl+: CT13c19 NSC line treated with staurosporine at a final concentration of 25µM during 4h. Ctrl or CT, control; hom, homozygous; het, heterozygous.

Summary of the results obtained in this section and short-term perspectives

We successfully generated iPSC-derived NSCs, indicating that *TSEN54* variants do not impact the early stages of neuronal differentiation. Both canonical and cryptic splicing sites are used in NSCs. However, both mutant proteins were not detected in the concerned NSC clones. Furthermore, we observed a very low level of TSEN54 WT protein expressed in both SRNS and GAMOS NSCs, in line with qRT-PCR results. Although the high variability between NSC clones with the same genotype, we observed in MTT experiment that GAMOS NSCs seem to have a reduced proliferation rate compared to SRNS and control NSCs, which is a potential mechanism known to cause microcephaly. It would be interesting to further differentiate these NSCs toward cortical neurons to see whether or not the *TSEN54* variants have an impact on the later stages of neuronal differentiation as already evidenced in *MINPP1*$^{-/-}$ iPSCs (involved in PCH14, (Ucuncu *et al.* 2020), which exhibited a delayed neuronal differentiation associated with an increased rate of early onset-apoptosis. It would be also interesting to see whether the proteasome inhibition in NSCs could have an impact on INS47 mutant protein expression level, since proteomic studies identified proteasomal proteins as major interacting proteins.

D) Generation of iPSC-derived kidney organoids and isolation of kidney organoid-derived podocytes.

Kidney organoid differentiation has been performed using the Morizane protocol (Morizane *et al.* 2015). The workflow of the differentiation process is illustrated in **Complementary Figure 9A**. We used basic differentiation medium (BDM), which was supplemented with CHIR99021 and Noggin for 3-4 days to induce the late primitive streak. Then, Activin A was used for the following 3 days to direct the differentiation towards the posterior intermediate mesoderm. Finally, FGF9 was applied alone during 3 days, before its combination with a pulse of CHIR 99021 for 2-3 days to induce the metanephric mesenchyme (MM) containing the renal progenitors, then the pretubular aggregates (**Complementary Figure 9B)** and subsequently the renal vesicles (**Complementary Figure 9C)**. Starting from day 14th, kidney organoid development occurs spontaneously (**Complementary Figure 9D)**. However, despite using the same protocol, we observed a marked variability during the course of the protocol between the different clones. In particular, all iPSC clones derived from the Heterozygous 1 (CT297c03) iPSC line, bearing the Ins47 variant in the heterozygous state, were more sensible to CHIR99021 treatment, including Heterozygous 1 (CT297c03) iPSC clone, resulting in an unexpected detachment of cells associated with high apoptosis level. Overall, we obtained kidney organoids from all iPSC clones, including the gene-edited ones.

Once kidney organoids obtained, we then purified podocytes from them by fluorescence-activated cell sorting (FACS) using a combination of the podocyte-specific marker, nephrin, and a marker of proximal tubular cells, LTL (**Complementary Figure 9E)**. iPSC cell lines used in this study for kidney organoid differentiation and the number of NPHS1 positive cells are listed below in **Table C2**. The number of podocytes was extremely low in comparison with the number of kidney organoids (data not shown).

Table C2 – Number of FACS-sorted NPHS1$^+$ podocytes derived from kidney organoids

Kidney Organoid derived from iPSCs	Number of NPHS1$^+$ cells[1]	Number of NPHS1$^+$ cells[2]	Number of NPHS1$^+$ cells[3]	Number of NPHS1$^+$ cells[4])	Genotype at *TSEN54* locus
SN289-01	/	207 k	360 k	105 k	c.468+48A>G (Hom)
SN289-02	46 k	/	67 k	/	
CT05c04	93 k	/	/	41 k	WT
CT13c19	404 k	140 k	/	/	WT
CT297c03D	/	/	310 k	/	c.468+48A>G
CT297c03J	37 k	/	109 k	/	(het)
GAM-3B	/	83 k	380 k	130 k	c.468+48A>G (het)
GAM-3H	592 k	400 k	/	20 k	+ c.410 del (het)
CT297-03	/	/	69 k	63 k	c.468+48A>G (het)

Hom, homozygous; het, heterozygous. Superscript numbers indicate the number of the kidney organoid differentiation experiment.

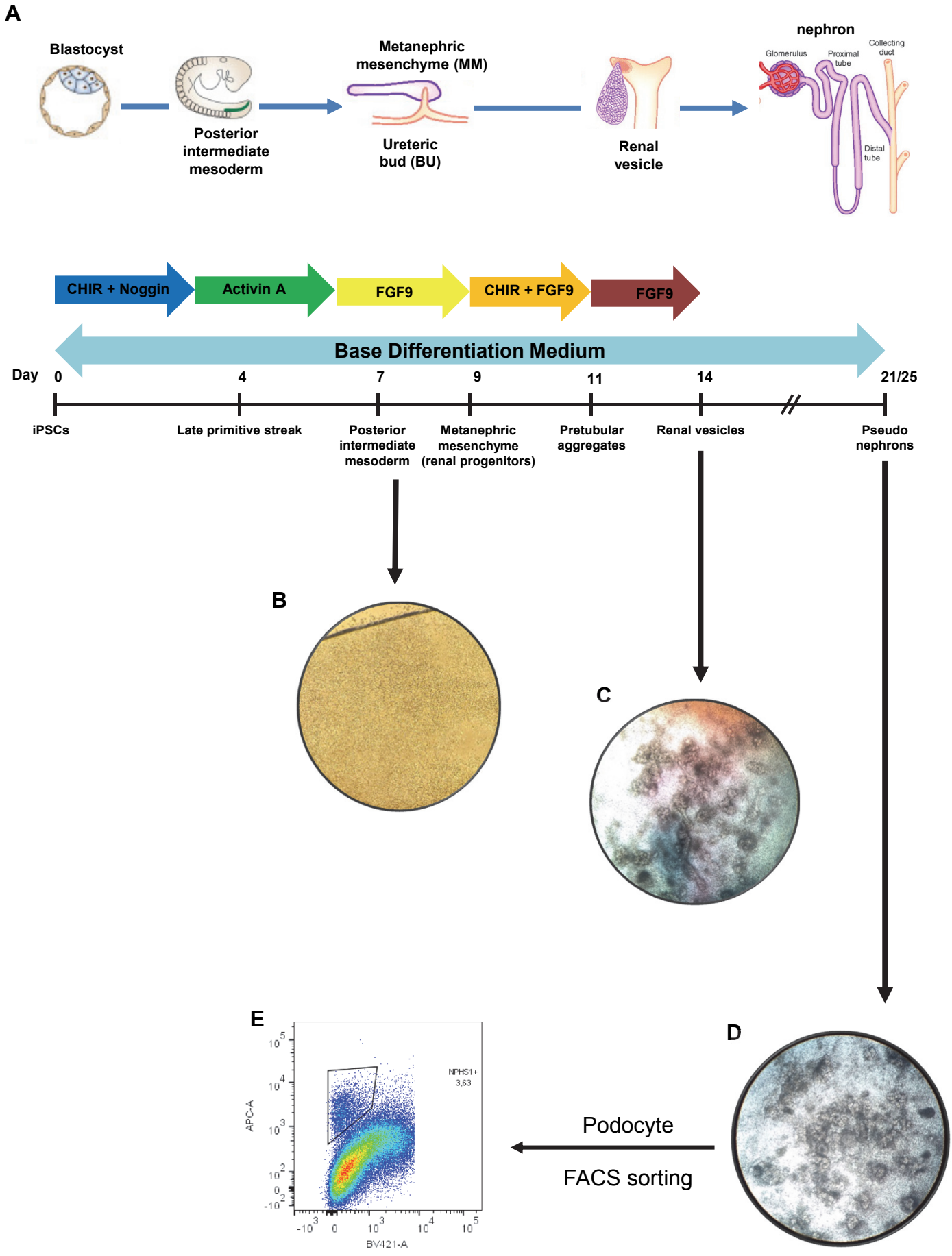

Complementary Figure 9. (**A**) Kidney organoid differentiation protocol using Morizane's protocol (From G. Mollet). Example of iPSCs SN289c01 differentiation into kidney organoids. (**B**) Pretubular aggregates at day 8, (**C**) Renal vesicle and kidney organoids, day 15, (**D**) Mature kidney organoids, day 21.(**E**) Cytofluorimetric profile of NPHS1-positive cells in kidney organoids.

E) Investigation of *TSEN54* variants impact on transcriptomic profiles of iPSC-derived NSCs and kidney organoid-derived podocytes, and on tRNA-intron splicing in NSCs

iPSCs, that have been differentiated towards kidney organoids to obtain podocytes, and towards neural stem cells (NSCs), will be instrumental to further investigate common and/or distinct deregulated molecular mechanisms at the origin of the renal and neurological manifestations in individuals harboring *TSEN54* variants.

Therefore, we first decided to perform RNA-sequencing on iPSC-derived NSCs and kidney organoid-derived podocytes. The experimental design is presented in **Complementary Figure 10A and B**. We will perform the RNA-sequencing using the following iPSC-derived NSCs clones: Control 1, Control 2, Control 3, SRNS 1, SRNS 2, Heterozygous 2, Heterozygous 3, GAMOS 1 and GAMOS 2 and kidney organoid-derived podocytes clones: Control 1, Control 2, SRNS 1, SRNS 2, Heterozygous 1, Heterozygous 2, Heterozygous 3, GAMOS 1 and GAMOS 2. RNAs have been extracted from NSCs and are now ready for RNA-sequencing, whereas we have to extract RNA from isolated podocytes before giving them to the Genomic Plateform at *Imagine* Institute.

To confirm the preliminary tRNA-sequencing data obtained on LCLs (see results in the main article), we decided to repeat the experiment on the same LCL lines (Ctrl-2 and B.II-4, Figure 2A from main article), but with the addition of a supplemental control (Ctrl-3) (**Complementary Figure 10C-1**). In addition, since we demonstrated that in shRNA *TSEN54*–depleted podocytes a very low level of TSEN54 protein leads to proliferation and protein synthesis defects (see results in the main article), we wondered whether these alterations were associated with a defect in tRNA intron splicing due to a low amount of active TSEN complex. We thus decided to perform tRNA-seq on *TSEN54*–depleted podocytes using a scrambled shRNA as a control and the shRNA Sh1 against *TSEN54* (**Complementary Figure 10C-2**). Finally, we performed tRNA-seq on NSC lines corresponding to the ones described above (**Complementary Figure 10C-3**).

Unfortunately, the data/analyses corresponding to all these experiments are still in progress and not available at the time of writing my thesis manuscript.

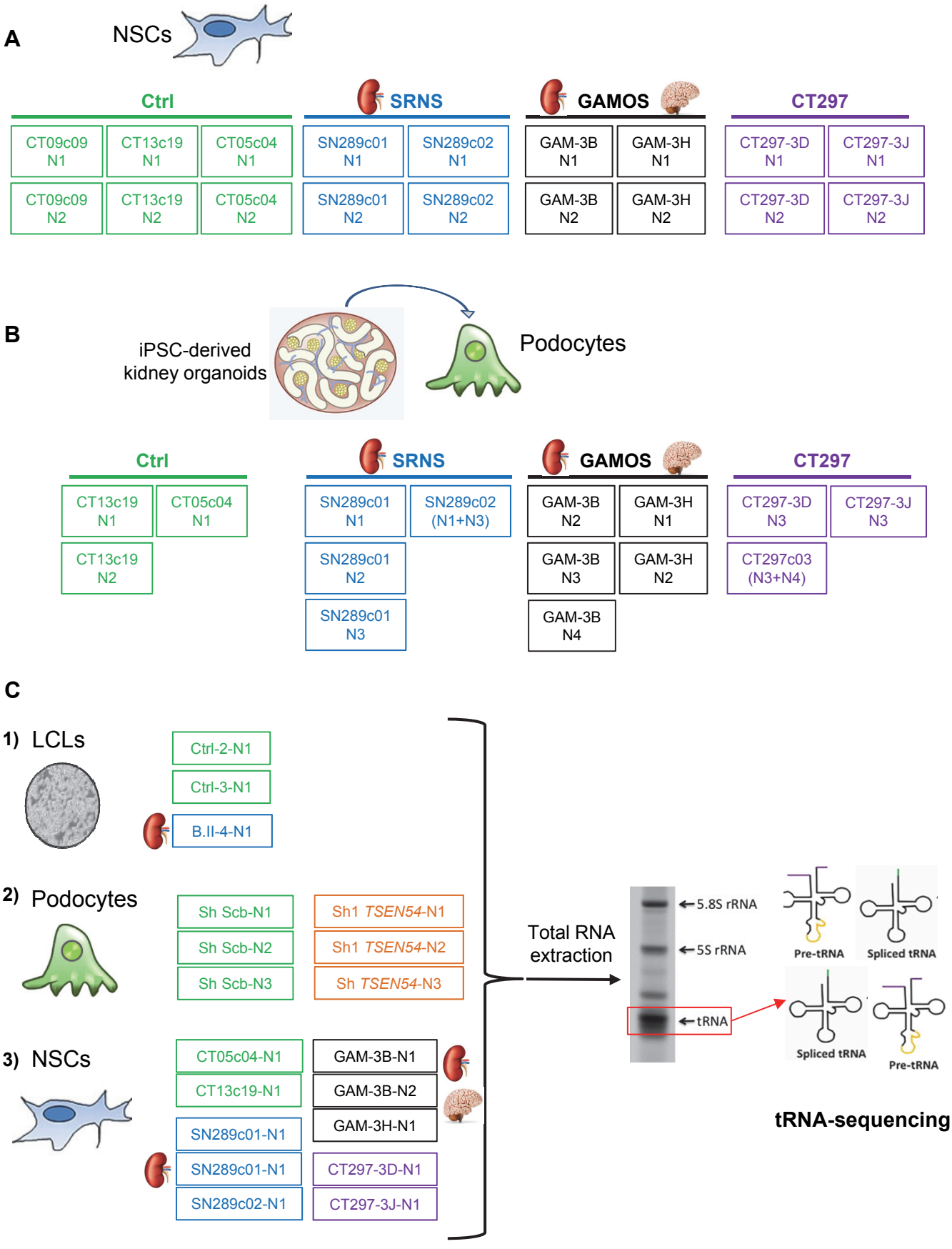

Complementary Figure 10. Experimental design for RNA-sequencing in iPSC-derived NSCs and kidney organoid-derived podocytes, and tRNA-sequencing in LCLs, TSEN54 Sh1-KD podocyte cell lines and NSCs. Nx correspond to the number of the experiment, either a collection of cell pellet for NSCs and LCLs, or the lentiviral transduction for the shRNA in podocytes, or the kidney differentiation experiment with FACS for the isolated podocytes.

MATERIAL AND METHODS

Patients and families

Written informed consent was obtained from participants or their legal guardians. All methods were performed in accordance with relevant guidelines and regulations. Methods of sample collection, storage and experimental protocols for induced human pluripotent stem cells (iPSCs) and their derivatives were declared to the French research ministry (identification DC 2015-2595) and have obtained approval from the ethical Committee "CPP Ile-de-France II" on September 5th, 2016. Genomic DNA samples were isolated from peripheral blood leukocytes using standard procedures.

Whole-exome sequencing and mutation calling

We performed whole-exome sequencing using Agilent SureSelect All Exon 51 Mb V5 capture-kit on a HiSeq2500 (Illumina) sequencer (paired-end reads: 2 × 100 bases). Sequences were aligned to the human Genome Reference Consortium Human Build 37 (GRCh37) genome assembly with the Lifescope suite from Life Technologies. Variant calling was made using the Genome Analysis Toolkit pipeline. Then, variants were annotated using a pipeline designed by the Paris Descartes University Bioinformatics platform. We assumed the causal variant: (i) segregates with the disease status, (ii) is novel or has a minor allele frequency <1/1000 in gnomAD, (iii) was not found in >10/2352 projects of our in-house database. Splice site variant pathogenicity was evaluated using in silico prediction tools (MaxEntScan and Human Splice Finder). Sanger sequencing was used to validate the variant identified by exome sequencing and to perform segregation analysis in the families. Sequences were analyzed with the Sequencher software (Gene Codes, Ann Arbor, MI) and positions of mutations were numbered from the A of the ATG-translation initiation codon.

Antibodies

Primary antibodies used in this work include: mouse anti-TSEN34 [Abnova, Cat. No. H00079042-A01, used at 1:1000 for western blot (WB)], mouse anti-GFP [Roche clones 7.1 and 13.1, Cat. No. 11 814 460 001, used at 1:2000 for western blot (WB) or immunoprecipitation (IP)], mouse anti-HA [Ozyme Cat. No. BLE901502, used at 1/1000 for western blot (WB) or immunoprecipitation

(IP)], mouse anti-actin [Sigma Cat. No. A2228, used at 1:2000 for western blot (WB)], mouse anti-nephrine [48E11 From Tryggvason's Laboratory, used at 1:200 for FACS sorting], mouse anti-OCT3/4 (C-10) [Santa Cruz Biotechnology Cat. No. sc-5279, used at 1:100 for immunofluorescence (IF)], Fluorescein-labeled lotus tetragonolobus Lectin [Vector laboratories Cat. No. FL-1321, used at 1:50 for FACS sorting], rabbit anti-TSEN54 [Abcam, Cat. No. EPR10062 (ab178696), used at 1:1000 for western blot (WB)], rabbit anti-TSEN2 [Proteintech, Cat. No. 13103-2-AP BC019582, used at 1:1000 for western blot (WB)], rabbit anti-TSEN15 [Thermofisher, Cat. No. PA5-68435, used at 1/1000 for western blot (WB)], rabbit anti-SOX2 [EMD Millipore Corp Cat. No. AB 5603-25 VG, used at 1:1000 for immunofluorescence (IF)]. Secondary antibodies used in this study include: IRDye 800CW Donkey anti-rabbit, [LI-COR Cat. No. 926-32213, used at 1:15000 for western-blot (WB)], IRDye 680RD Donkey anti-mouse [LI-COR Cat. No. 926-68072, used at 1:15000 for western-blot (WB)], Alexa Fluor 488 Donkey anti-rabbit IgG, [Life Technologies ThermoFischer Cat. No. A21206, used at 1:400 for immunofluorescence (IF)] and Alexa Fluor 555 Donkey anti-mouse IgG [Life Technologies ThermoFischer Cat. No. A31570, used at 1:400 for immunofluorescence (IF)].

Plasmids

We used the following expression vectors in this work: LentiORF pLEX-MCS (Open Biosystems) and pLKO.1-TRC Cloning Vector (Plasmid 10878, Addgene). Previous modifications made to the LentiORF pLEX-MCS plasmid are described in (Arrondel *et al.* 2019). They allow the expression of cDNA in frame with two copies of the Human influenza hemagglutinin (HA) tag (pLEX-2HA vector) or with the green fluorescent protein (GFP) tag (pLEX-GFP vector) allowing epitope-tagging at the N-terminal of the encoded protein. Human full-length *TSEN54*, *CLP1* and *KPNA1* cDNA (NM_207346.3, NM_006831.3 and NM_002264.4, respectively) were amplified by PCR from pCMVsport6 *TSEN54* (IMAGE CLONE 6500549), pcDNA3.1^{+}/C-(K)DYK *CLP1* (OHu26557) and pcDNA3.1^{+}/C-(K)DYK *KPNA1* (OHu12306C), respectively and then subcloned in-frame into the modified pLEX-MCS plasmid using NheI and NotI restriction sites (New England Biolabs). Site-directed mutagenesis (QuickChange kit, Agilent) was used to generate the mutations in *TSEN54* used in this study (Q339* and A307S). To insert the region corresponding to the intronic 47 base pairs, we amplified a PCR fragment from Exon 3 to 8 starting from individual B.II-7

cDNA, and subcloned this fragment into HindIII and BglII sites of pLEX GFP TSEN54 wild-type (WT). The following constructs were generated: pLEX GFP TSEN54 wild-type (WT), pLEX GFP TSEN54 A307S, pLEX GFP TSEN54 Q339*, pLEX GFP TSEN54 Ins47, pLEX CLP1 WT 2HA, pLEX KPNA1 WT 2HA. All primers used for subcloning and site-directed mutagenesis are listed in **Supplementary Table 1**. For gene silencing, the shRNA sequences described below (**Supplementary Table 2**) were cloned into the lentiviral pLKO.1-TRC Cloning Vector using the AgeI and EcoRI restriction sites. Lentiviral particles were produced by the lentivector production facility "Structure Fédérative de Recherche BioSciences Gerland-Lyon Sud (UMS3444/US8). To establish a line of immortalized podocytes stably expressing Sh1 or Sh2 *TSEN54*, cells were transduced at a multiplicity of infection (MOI) of 2; the minimum MOI at which cells also survived the subsequent puromycin selection (2µg/ml). All constructs were verified by Sanger sequencing.

Cell culture and establishment of podocyte cell lines

Embryonic Kidney 293T (HEK293T) cells were cultured at 37°C with 7% CO_2 and maintained in Dulbecco's Modified Eagle Medium (DMEM, Gibco®, Life Technologies) supplemented with 10% fetal bovine serum (FBS), glutamine and penicillin/streptomycin. Lymphoblastoid cells were cultured at 37°C with 7% CO_2 and maintained in RPMI 1640 (Gibco®, Life Technologies) supplemented with 10% fetal bovine serum (FBS), glutamine and penicillin/streptomycin. Conditionally immortalized human podocytes (Saleem *et al.* 2002) were routinely cultured at 33°C with 7% CO_2 and maintained in RPMI 1640 (Gibco®, Life Technologies), supplemented with 10% FBS, 1% insulin/transferrin/selenium, glutamine and penicillin/streptomycin (all from Life Technologies). Neural progenitor cells (NPCs) were cultured in neural induction media (50% Neurobasal media, 50% DMEM/F-12 GlutaMAX (both Gibco), supplemented with 2% NeuroCult SM1 without Vitamin A, 1% N2 Supplement-B (both STEMCELL Technologies), 1% penicillin/streptomycin (Gibco), 10ng/ml fibroblast growth factor 2, 10ng/ml epidermal growth factor and 20ng/ml bone-derived neurotrophic factor (all Peprotech). Cell culture plates, flasks for NPCs were coated first with Poly-L-Ornithine diluted 1/6 in cell culture grade PBS (Gibco) at 37°C for at least 6 hours. After this time, the cell culture plates were washed twice in 1X PBS, then coated in laminin (Invitrogen, cat. # 23017-015) diluted 1/500 in 1X PBS. After coating with the

laminin solution for at least 4 hours, the solution was removed and the cells plated were directly onto the coated surface.

RNA isolation, RT-PCR and real-time quantitative RT-PCR

Total RNA was extracted using RNeasy® columns and DNAse-treated using RNase-free DNase (Qiagen). For RT-PCR and quantitative PCR, first-strand cDNAs were synthetized from 1µg of RNA, using SuperScript™ II Reverse Transcriptase (Invitrogen), 10ng/µl random primers (Invitrogen), dNTP 1.25mM, dithiothreitol 10mM and RiboLock Rnase inhibitor (2U/µl). To quantitate transcripts, absolute quantitative PCR was performed using Power SYBR Green ROX Mix (ThermoFischer Scientific). For each sample, the expression was normalized to HGPRT. Experimental results are analyzed with the $2^{-\Delta\Delta Ct}$ method. All primers are listed in **Supplementary Table 2**.

Immunoblotting

Proteins were extracted in lysis buffer containing 150 mM NaCl, 50 mM Tris-HCl pH 7, 0.5% Triton-X100, 1mM EDTA, with CompleteTM protease inhibitors (Roche). Cells were incubated on ice for 10 minutes and centrifuged at 12,500 rpm at 4°C for 10 minutes. Protein concentration was determined using BCA assay (Thermo). Equal amounts of proteins, diluted in 4X sample buffer (Bio-Rad) supplemented with β-mercaptoethanol were loaded onto acrylamide gels and transferred onto nitrocellulose membranes (Bio-Rad). The membranes were blocked in Odyssey (LI-COR Bioscience) blocking buffer. Membranes were then incubated with the indicated primary antibodies overnight at 4°C, washed three times with PBS, and then incubated for 1 hour at room temperature (RT) with LI-COR IRDye secondary antibodies and then washed a further 3 times before revelation. Signals were acquired with Odyssey CLx LICOR near-infrared fluorescent imaging system (LI-COR Bioscience). Densitometry quantification was performed using Image studio lite software (version 5.2).

Overexpression/Expression Cloning and Immunoprecipitation

HEK293T cells were transiently transfected using FuGENE® HD Transfection Reagent (Promega) according to the manufacturer's instructions. The reagent and DNA were mixed at a ratio 1:3 in OptiMEM (Gibco) for 15 minutes at room temperature and then added in the Dulbecco's Modified Eagle Medium (DMEM, Gibco®, Life Technologies) supplemented with 10% fetal bovine serum (FBS), glutamine and penicillin/streptomycin. Cells were collected after 48 hours and lysed in the required volume of lysis buffer (as used for immunoblotting). Then cells were incubated 10 minutes on ice before centrifugation (12,500 rpm, 4°C, 10 minutes). 10% of the lysate volume was removed and diluted in an equal volume of 4x sample buffer supplemented with β-mercaptoethanol. For IP of tagged proteins, the GFP tag or the 2HA tag were immunoprecipitated using the µMACSTM Epitope Tag Protein Isolation Kit (Miltenyi Biotec). The remaining supernatants were then added to a separate tubes containing 30-50 µl of anti-GFP beads (Miltenyi) or anti-2HA beads (Miltenyi) and incubated for 2 hours at 4°C with rotation. After 2 hours, beads were loaded onto µMACs separation columns (Miltenyi), washed three times in lysis buffer and once in 20mM Tris-HCl pH7.4 before elution into 70µl hot 2x sample buffer supplemented with β-mercaptoethanol.

Protein identification using mass spectrometry (Proteomic studies*)*

Proteomic analysis was carried out by the Proteomic Platform of Hôpital Necker Enfants-Malades.

<u>NanoLC-MS/MS protein identification and quantification</u>

S-TrapTM micro spin column (Protifi, Hutington, USA) digestion was performed on IP eluates in laemmli buffer according to manufacturer's protocol, but using 4 washing steps for thorough SDS elimination. Samples were digested with 12.5 µg of trypsin (Promega) at 47°C overnight. After elution, peptides were finally vacuum dried down and resuspended in 35 µL of 10% ACN, 0.1% TFA in HPLC-grade water prior MS analysis. For each run, 5 µL were injected in a nanoRSLC-Q Exactive PLUS (RSLC Ultimate 3000) (Thermo Scientific,Waltham MA, USA). Peptides were loaded onto a µ-precolumn (Acclaim PepMap 100 C18, cartridge, 300 µm i.d.×5 mm, 5 µm) (Thermo Scientific), and were separated on a 50 cm reversed-phase liquid chromatographic column (0.075 mm ID, Acclaim PepMap 100, C18, 2 µm) (Thermo Scientific). Chromatography solvents were (A) 0.1% formic acid in water, and (B) 80% acetonitrile, 0.08% formic acid. Peptides were

eluted from the column with the following gradient 5% to 40% B (38 minutes), 40% to 80% (1 minutes). At 39 minutes, the gradient stayed at 80% for 4 minutes and, at 43 minutes, it returned to 5% to re-equilibrate the column for 16 minutes before the next injection. Two blanks were run between each series to prevent sample carryover. Peptides eluting from the column were analyzed by data dependent MS/MS, using top-10 acquisition method. Peptides were fragmented using higher-energy collisional dissociation (HCD). Briefly, the instrument settings were as follows: resolution was set to 70,000 for MS scans and 17,500 for the data dependent MS/MS scans in order to increase speed. The MS AGC target was set to 3.10^6 counts with maximum injection time set to 200 ms, while MS/MS AGC target was set to 1.10^5 with maximum injection time set to 120 ms. The MS scan range was from 400 to 2000 m/z.

Data Processing Following LC-MS/MS acquisition

The MS files were processed with the MaxQuant software version 1.5.3.30 and searched with Andromeda search engine against the database of *Homo sapiens* from swissprot 04/2019. To search parent mass and fragment ions, we set an initial mass deviation of 4.5 ppm and 20 ppm respectively. The minimum peptide length was set to 7 aminoacids and strict specificity for trypsin cleavage was required, allowing up to two missed cleavage sites. Carbamidomethylation (Cys) was set as fixed modification, whereas oxidation (Met) and N-term acetylation were set as variable modifications. Match between runs was not allowed. LFQ minimum ratio count was set to 2. The false discovery rates (FDRs) at the protein and peptide level were set to 1%. Scores were calculated in MaxQuant as described previously (Cox and Mann 2008). The reverse and common contaminants hits were removed from MaxQuant output. Proteins were quantified according to the MaxQuant label-free algorithm using LFQ intensities [Luber, 2010 #1907; Cox, 2008 #1906]. Six independent immunoprecipitations of GFP-TSEN54 WT, GFP-TSEN54 ins47, GFP-TSEN54 A307S, GFP-TSEN54 Q339* and the empty vector (EV) were analysed with Perseus software (version 1.6.7.0) freely available at www.perseus-framework.org (Tyanova *et al.* 2016). The LFQ (Label-free Quantification) data were transformed in log2, all the proteins identified in all 6 replicates in at least one group (GFP-TSEN54 WT, GFP-TSEN54 ins47, GFP-TSEN54 A307S, GFP-TSEN54 Q339*) were submitted to statistical test after imputation of the missing value by a Gaussian distribution of random numbers with default parameters (width:0.3, down shift:1.8). We plotted

Hawaii volcano plots using as common negative control the IP IP on EV cells, FDR=0.01-0.05 (inner and outer Volcano lines) and S0=0.1.

Immunofluorescence

IPSCs were grown on matrigel coverslips (10-20 000 cells/cm2). Cells were fixed in 4% paraformaldehyde (PFA) for 20 minutes at RT. After fixing, samples were washed once in 1X PBS and once in 1X PBS 30 mM glycine. The day after, cells were permeabilized with 0.5% Triton TX-100 (Sigma) in 1X PBS for 5 minutes and incubated in blocking buffer containing 1% bovine serum albumin (BSA, Sigma) for 1 hour at RT. Then, cells were incubated in the appropriate primary and secondary antibodies for 1 hour each at RT. Finally, cells were washed once in 1X PBS, nuclei were stained with DAPI (sc-3598, Santa Cruz Biotechnology) at RT for 5 minutes and mounted on slides using Mowiol 4-88 mounting medium (81381, Sigma-Aldrich).

Cell proliferation and protein synthesis assays

Cell proliferation rates and protein synthesis were assessed in shRNA scrambled- or *TSEN54*-treated podocytes and Neural stem cells (NSCs) using the CellTiter 96 Aqueous Non-Radioactive Cell Proliferation Assay (MTT) (G5421, Promega), and the Click-iT HPG Alexa Fluor 488 Protein Synthesis Assays (C10428 ThermoFisher Scientific), respectively, according to the manufacturer's instructions, described in (Arrondel *et al.* 2019). NSCs were plated with a density of 50 000 cells/cm^2. Absorbance measurement was performed on day 1, 2, 3, 4 for NSCs s and 7 for podocytes on a TriStar multimode reader (LB941, Berthold Technologies) using a 560 measurement filter and subtracting the blank background absorbance. The shRNA *TSEN54*-treated podocytes were seeded at density of 15 000 cells per well into 96 well-plates and HPG protein synthesis assay were performed 48 hours later, the fluorescence intensities were normalized to nuclear fluorescence intensity as internal control.

Generation and characterization of human induced pluripotent stem cell (iPSC) lines

The iPSC lines from patients and controls were generated from peripheral blood mononuclear cells (PBMCs) either at the iPSC core facility of Nantes University or at Imagine Institute iPSC platform. At the iPSC core facility of Nantes University PBMCs were reprogrammed by Sendai viruses expressing Oct4, Sox2, Klf4 and c-Myc (CytoTune^{TM}-IPS 2.0 Sendai Reprogramming kit, Life Technologies). The iPSC clones were picked and expanded on mouse embryonic fibroblasts (MEFs) feeder cells in KSR-FGF2 medium (DMEM/F12 supplemented with 0.1% β-mercaptoethanol, 20% knockout serum replacement, 10 ng/mL basic fibroblast growth factor, 2 mmol/L l-glutamine and 1% NEAA). Until P10, colonies were mechanically passaged with a needle. At P10, iPSC clones were adapted to feeder-free culture conditions: stem cell-qualified Matrigel-coated plates (0.1 mg/mL; BD Bioscience) with mTeSR (Stem Cell Technologies). Feeder-free iPSCs were passaged using the Passaging Solution XF (StemMACS^{TM}, Miltenyi Biotec). The control iPSC lines from the Imagine Institute iPSC plateform (IMAGINi005 and IMAGINi013) are described at https://hpscreg.eu/cell-line/IMAGINi013-A *and* https://hpscreg.eu/cell-line/IMAGINi005-A, and in Quelennec et al 2020 (PMID: **32866896**) for IMAGINi005). Mycoplasma detection is realized with the MycoAlert™ kit (LONZA, LT07-318). Quality controls included the expression assessment of pluripotency markers (OCT4 and SOX2) by immunofluorescence, the verification of absence of chromosomal anomalies using a SNP array (Infinium Core-24 v1.2 Kit (Illumina) 300,000 SNPs), and identity match (matching the iPSC genotype with that of parental PBMCs for 8 informative SNPs), and trilineage potential evaluation was performed using immunofluorescence staining with ectodermal TUJ1, mesodermal α-SMA and endodermal α-FP markers. Human iPSC culture and storage protocols were performed with approval from the French research Ministry (DC2015-2595, 09/05/2016). iPSCs were cultured in mTeSR Plus (05825, StemCell Technologies) medium on Matrigel LDEV-free hESC-qualified matrix, (354277, Corning) coated 35 or 60 mm dishes according to the Stemcell technologies protocols. iPSC colonies morphology was daily monitored under a Lynx Stereo Dynascopic Microscope (Vision Engineering) to manually remove differentiated cells and ensure maintenance of an undifferentiated state. iPSCs were passaged once a week by mechanical procedure or using RelesR reagent according to the provider protocol (05872, Stemcell technologies).

Generation of genome-edited iPSCs

RNA guide design

The CRISPR RNA guide was designed online with the tool proposed by http://crispor.tefor.net. Potential off-target sites for the guide RNA (gRNA) were determined using the CFD score (Cutting Frequently Determination). We choose our gRNA (3' AGACCTGCCACTGTCTATCC 5') focusing on the MIT score that is more reliable on sensitivity and specificity. This score uses the formula from the MIT Crispr Website (Hsu guide score).

Nucleofection, cell sorting (FACS) and iPSC clone selection

Nucleofection was performed with the "CA-137" program of the 4D Nucleofector *(AAF-1002B, AAF-1002X, Lonza)* with the "P3 Primary Cell X-unit Kit S" (Lonza, Reference: V4XP-3032). In order to reduce off-target probability we choose a High Fidelity Cas9 (mutated in p.R691A) "Alt-R® S.p. HiFi Cas9 Nuclease V3" (integrated DNA technologies (IDT), reference: 1081061) with "Alt-R® CRISPR-Cas9 crRNA XT" (IDT, reference: 1081061) and "Alt-R® CRISPR-Cas9 tracrRNA, ATTO550" (IDT, reference: 1075928) to be able to sort transfected cells based on ATTO550 signal. The first step consisted in assembling crRNA (800 pmol) and tracrRNA-ATTO550 (800 pmol) at an equal concentration of 400pmol/µL in a Nuclease-Free Duplex Buffer to reconstitute a functional gRNA at 200µM. To ensure a correct hybridation at room temperature the complex was heated to 95°C for 5 minutes followed by a slow cool-down of 20 minutes at room temperature. Then, 150 pmol of Cas9 was added to 300 pmol of gRNA and kept 20 minutes at room temperature (Cas9/gRNA ratio of 1:2). Due to the low clonal cell survival of hiPSCs we must treat cells 2 hours before dissociation with 10 µM Y-27632 (1683, AxonMed) cell culture medium. Before nucleofection, iPSCs were seeded at 10000cells/cm² on matrigel coated 60 mm dishs from 3 to 4 days and dissociated with TrypLE select (Life Technology Reference: 12563011). We used 800 000 cells for nucleofection including two non-nucleofected negative control (with and without ATTO550 RNP complex). Pellet of $0,8.10^6$ cells was resuspended in 30 µl of nucleofection solution and the first negative control was constituted by kept apart 25% of this cellular solution (represent non-transfected and non-fluorescent cells). The remaining 75% of the cellular solution were mixed with the RNP complex (4µL) and separate in two part of 1/3 and 2/3 of the total volume to constitute the ATTO550 non-transfected control (11µL) and the transfected cellular solution (22µL). The

ATTO550 non-transfected control is mandatory to identify ATTO550 signal due to extra-cellular aggregation of RNP complex before to sort the transfected cells. Cells ($0{,}4.10^6$ cells in 22µL) were nucleofected using the CA-137 program and kept 5 minutes in the nucleocuvette before culture on matrigel coated 4-well Nunc plate (Dutscher, ref055617) at $0{,}2.10^6$ cells/cm² in 10 µM Y-27632 supplemented mTeSR Plus medium. When cells reached confluency of at least 20% (24-48 hours of culture), nucleofected cells were sorted on SH800 Cell Sorter (130µm nozzle) using the ATTO550 highest signal intensity. The nucleofected cells were seeded at a clonal density of 25 cells/cm² on CellAdhere Laminin-521 (77003, StemCell Technologies) - coated culture dishes in mTeSR Plus medium supplemented with CloneR (05888, StemCell Technologies) to increase clonal cell survival. After two weeks of culture the clones of interests were identified by Sanger sequencing (**Supplementary Table 3**), amplified and frozen.

Off-target

Selected potential off-target sites of the gRNA determined using the CFD score were Sanger sequenced on the DNA of gene edited IPSC clones (**Supplementary Table 3**).

Kidney organoid differentiation

The procedure for kidney organoid differentiation from iPSCs was performed according to a published protocol adapted from Morizane *et al.* (Morizane *et al.* 2015). It was performed on iPSC colonies about one week after mechanical clumps passing. Alternatively, iPSCs were detached using TrypLE select (Gibco/Thermofischer) and seeded at a density of 1,6×104 cells/cm2 on matrigel coated supports. Cells were cultured in mTeSR Plus medium for about 3 or 4 days before differentiation induction until they reach an appropriate confluence between 30% and 50% to start differentiation. Differentiation was started by switching to Basic Differentiation Medium (BDM), consisting by Advanced RPMI 1640 (12633020, Thermo Fisher scientific) medium with 1X GlutaMAX supplement (35050061, Thermo Fisher scientific), which was supplemented with 4 µM CHIR99021 for the first day and from 6 to 8µM for the two next days (1386, Axon Medchem) and with 5 ng/ml Noggin (120-10C, PeproTech) for 3/4 days to induce the late primitive streak. 10 ng/ml Activin A (120-14E, PeproTech) was used for the following 3 days to lead differentiation

towards the posterior intermediate mesoderm. Medium was then supplemented with 10 ng/ml FGF9 (273-F9-025, R&D Systems) for seven days, combined with a 1 to 2 days pulse of 3 μM CHIR 99021 from day 7 or 9, depending on observation of cell morphology. From the induced metanephric mesenchyme, pretubular aggregates and subsequently renal vesicles raised. Kidney organoids development occurred spontaneously during the following week, without addition of any other factor. All along differentiation medium was changed every 2 or 3 days.

Generation of neural progenitor cells

NSCs were generated from induced pluripotent stem cells derived from peripheral blood mononuclear cells (PBMCs). PBMCs were reprogrammed using Oct4, Sox2, Klf4 and cMyc delivered using Sendaï virus (CytoTunee^{TM}_IPS 2.0 Sendaï Reprogramming kit, lot 21300018) in the reprogramming medium StemPro®-34 medium supplemented with IL-3, IL-6, SCF, Flt3-L, then StemPro®-34 without cytokines on a vitronectin reprogramming support. The protocol used to obtain NSCs from iPS cells had 2 steps. The first was the production of neuroepithelial cells (NEPs) from human iPS cells; the second was the production of NSCs from NEPs (Varela et al. 2012). NEPs differentiation was based on dual SMAD inhibition (Boissart *et al.* 2013). Human iPS cells were manually detached and collected in differentiation medium composed of neurobasal, DMEM/F12, N2 supplement, B27 supplement, 0.55 mM β-mercaptoethanol (all from Invitrogen) complemented with LDN-193189 (0.1 μM, Sigma) and SB431542 (20 μM; Tocris). They were transferred for 6 hours into a low-attachment plate and then seeded on polyornithine (300 ng/cm^2, Sigma) and laminin (100 μg/cm^2, Thermofischer) coated tissue culture plates. The first day, ROCK inhibitor Y27632 was used (10 μM) to optimize cell survival and seeding. The medium was changed daily until the appearance of neural rosettes containing NEPs after 10–14 days of differentiation. At this time, rosettes were manually collected, trypsinized using 0.05% trypsin (Invitrogen) and seeded at 100 000 cells per cm2 in polyornithine and laminin-coated tissue culture plates in N2B27 medium supplemented with hEGF (10 ng/ml), hFGF2 (10 ng/ml); and human brain-derived neurotrophic factor (hBDNF, 10 ng/ml) (from PeproTech). NSCs were maintained in the same medium and passaged every 3–4 days for no more than 15 passages. To ensure the correct identity of the NSCs used in this study, we performed a flow-cytometry based quality control check. Cells were first isolated using trypsin, filtered on a 40μm strainer and counted to

have an equal number of cells for each cell line tested and all controls. Trypsin was then inactivated by adding an equal volume of Opti-MEM (Gibco) 10% FCS and then centrifuged for 5min at 1,200rpm at 4°C before resuspension in Fc blocking solution (Fc blocking reagent diluted 1/5 in FACS buffer (PBS, 2.5% FCS, 2.5mM EDTA). Cells were incubated for 15 minutes on ice before washing in FACS buffer and a second centrifugation at 1,200rpm for 5 minutes at 4°C. The pellets were resuspended in fluorescently-conjugated primary antibodies CD57-FITC (HNK1) and CD271-PE (P75) diluted 1/10 in FACS buffer and incubated on ice for 30 minutes. The cells were then again washed in FACS buffer, centrifuged a final time at 1,200 rpm for 5 minutes at 4°C before resuspension in FACS buffer. Cells were then acquired on LSR Fortessa flow cytometer (BD). Cells passed the quality control check if the population of $HNK1^{+}/P75^{-}$ cells was greater than 80%.

RNA-sequencing and analysis

RNA was extracted from cells using the RNeasy Micro kit (74004, Qiagen), according to manufacturer's instructions. RNA quantity and quality was assessed by automated electrophoresis using the TapeStation system (Agilent Technologies). RNA-Seq libraries were prepared starting from 1μg of total RNA using the Ovation SoLoRNA-Seq System kit (0500-32, Nugen) according to manufacturer's instructions. Briefly, after DNase treatment and random primer annealing, the first cDNA strand was synthetized from total RNA. Second cDNA strand was produced and then ligated to Illumina compatible adaptors containing both sample index and a Unique Molecular Index (UMI). The cDNA produced was PCR amplified after an initial test to evaluate the suitable number of PCR cycles to apply to each sample. cDNAs corresponding to ribosomal RNA were selectively fragmented using the AnyDeplete technology. Few PCR cycles were performed to finalize the RNAseq library preparation. An equimolar pool of the final indexed RNA-Seq libraries was prepared and sequenced on a HiSeq2500 (paired-end reads of 130 bases + 130 bases; Illumina). A total of ~50 millions of passing filter paired-end reads was produced per library. FASTQ files were mapped to the ENSEMBL GRCh38/hg38 reference human genome using Hisat2 and counted by featureCounts from the Subread R package. Read count normalizations and groups comparisons were performed by three independent and complementary statistical methods: DESeq2, edgeR and LimmaVoom. Flags were computed from counts normalized to the mean coverage. All normalized

counts <20 were considered as background (flag 0) and ≥20 as signal (flag=1). Cluster analysis was performed on DESeq2 P50 lists, regrouping the genes showing flag=1 for at least half of the compared samples, by hierarchical clustering using the Spearman's correlation similarity measure and Ward's linkage algorithm. Samples were compared using the DESeq2 statistical method, applying the Bonferroni and Benjamin-Hochberg corrections for multiple hypothesis testing. Statistically significant upregulated and downregulated gene lists (BH-corrected p-value<0.05) were subjected to GO enrichment analysis for biological process on geneontology.org.

tRNA-sequencing and analysis

For tRNA-seq library preparation a protocol adapted from a method described by Gogakos et al., 2017, (Gogakos *et al.* 2017) was followed. First, 800 ng total RNA was used for size selection on 15% urea-polyacrylamide gels; a 60-100 nt size window was selected to enrich for tRNAs followed by elution in 0,3 M NaCl overnight at 4 °C. Eluted RNA was precipitated and resuspended in 10 µL water. Fragmentation was done using 4 µL RNA in a 15 µL reaction volume containing 10 mM Na_2CO_3 and 10 mM $NaHCO_3$ (pH 10.3) at 60 °C for 1 hour. Fragmented RNA was then purified on RNeasy columns (Qiagen) and eluted in 16 µL water, followed by a treatment to generate RNA fragments with 5' monophosphate and 3' OH ends. RNA fragments were first treated with antarctic phosphatase (New England Biolabs - NEB) in a 20 µL reaction volume containing 16 µL RNA, 2 µL 10x reaction buffer, 1 µL antarctic phosphatase, and 1 µL RNase inhibitor (NEB) for 30 minutes at 37 °C followed by 5 minutes 65 °C to inactivate the enzyme. Next, 5' monophosphate ends were generated by adding 17 µL water, 5 µL 10x antarctic phosphatase reaction buffer, 5 µL 10 mM ATP, 1 µL RNase inhibitor and 2 µL polynucleotide kinase (NEB) and further incubation at 37 °C for 1 hour. RNA was then again purified using RNeasy columns and eluted in 17 µL water followed by Speedvac concentration to 5 µL. The resulting fragmented and end-repaired RNA was used for small RNA library preparation using the NEBNext kit (NEB) following the manufacturer's instructions. FASTQ files were mapped to the ENSEMBL Human (GRCh38/hg38) reference using Hisat2 allowing no soft clip and intron length max at 25. Bams were then filtered at mapping quality >1. To detect the junctions we have filtered the CIGAR strings including «N» and computed the coordinates. To detect the absence of junctions we have selected the reads mapped inside or at least with 5 bases overlapping to the position of intron. We then

counted those reads with or without junction for each tRNA. All the counts have been normalized to the mean of total number of reads of the two samples.

Statistical analysis

Statistical analysis were performed using GraphPad PRISM 8.0 software. All values are shown as mean ±s.e.m. of a least 3 independent experiments. data sets comparing more than three conditions (to a control group) were analyzed with ANOVA followed by Dunnett's multiple comparisons test or by using Kruskal–Wallis test followed by a Dunn's multiple comparisons test. A standard confidence interval of 95% was applied in all analyses. Displayed in the figures are the mean values of all technical replicates for each of the independent experiments (displayed as single data points).

Supplementary Table 1: Primers used for subcloning and site-directed mutagenesis reactions

Primer name	**Sequence 5'-3'**
NHE1-HA-*TSEN54* Forward	CTAGCTAGCCCACCATGTACCCATACGATGTTCCAGATTACGCTG AGCCCGAGCCCCACCC
NHE1-*TSEN54*-Forward	CTAGCTAGCGAGCCCGAGCCCGAGCC
3' UTR Reverse	AGCCGAGATGGTCCCTGAGAAC
Muta HA1-HA2-*TSEN54* Forward	ACCAGACTACGCTGAGCCCGATCCCGAGCCC
Muta HA1-HA2-*TSEN54* Reverse	ACGTCGTATGGGTAAGCGTAATCTGGAACATCGTATGGG
Muta *TSEN54* Gln339* Forward	GTCCTGGTGCTAGAAGCTGAAC
Muta *TSEN54* Gln339* Reverse	TCAGCGTCTGTCTCCCGC
Muta HA *TSEN54* Forward	ATGTTCCAGATTACGCTGAGCCCGATCCCGAGCCC
Muta HA *TSEN54* Reverse	CGTATGGGTACATGGTGGGCTAGCCCCGGACGCGTG
Muta *TSEN54* A307S Forward	CCCCAACATGTCTTCAGACAG
Muta *TSEN5*4 A307S Reverse	AAGGAGATCTGCTCGAAG
Muta NHE1-*TSEN54* Forward	CGCGTCCGGGGCTAGCGAGCCCGATCCCGAG
Muta NHE1-*TSEN54* Reverse	TGGGTCGACGATATCCCG
Plex Forward	CACCAAAATCAACGGGACTT
Plex Reverse	ATATAGACAAACGCACACCGGCCT
KPNA1-59-Forward	CAAATCTCTGAATCCCGATGA
KPNA1-443-Forward	GTTTGAATCAGCTTGGGTACT
KPNA1-1577-Reverse	CACTGTTGGAAGATGTACTGC
KPNA1-895-Forward	CGGGAGTATGTAGGAG
KPNA1-491-Reverse	TGAATCACAATTCGGGTCTGA
CLP1-751-Forward	GTGGATGTCGTTGTTGTTCT
CLP1-11267-Reverse	GGTACCCTCGAGCCTTCAGATC
TSEN54 cDNA Exon 3 Forward	GCTTGGTGGCTGCCGAGTGGA
TSEN54 cDNA Exon 8 Reverse	CTTGGGTTGCAGGGAGTTGTC

Supplementary Table 2: Primers used for sh and primers used in RT-PCR and quantitative PCR experiments

Primer name	**Sequence 5'-3'**
sh1	GTACCCAGACTCTAACCTGTA
sh2	CCAGACTCTAACCTGTAGCTT
TSEN54 cDNA Exon 3 Forward	GCTTGGTGGCTGCCGAGTGGA
TSEN54 cDNA Exon 8 Reverse	CTTGGGTTGCAGGGAGTTGTC
qPCR *TSEN54* Exon 3 Forward	AGAGGGCTTCGTGGAGTTGA
qPCR *TSEN54* Exon 4 Reverse	TACAAGGCCTCTTCCGGGTGAA
qPCR *TSEN54* Exon 5-6 Forward	AGTACCAGGTCTTCAGCCA
qPCR *TSEN54* Exon 7 Reverse	TTGCCATCTCCATCCTCCAAGT
qPCR *TSEN54* INS47 Forward 2	GCTGCTGCTGACCGACCACACT
qPCR *TSEN54* INS47 Reverse 2	GGATGGGTGGCTCCCGGAGG
HPRT Forward	TCTTTGCTGACCTGCTGGATT
HPRT Reverse	GTTGAGAGATCATCTCCACCAATTACT

Supplementary Table 3: Genomic location of the 20 selected off target sites and primers used for Sanger sequencing

Name	Amplicon Location (hg19)	Forward Primer Sequence	Reverse Primer Sequence
TSEN54 Exon 5-Intron 5-6	chr17:73513523-73514018	TTCTTGATGCGCTGCTGAGA	CAACTCTACCCACCCCCAAC
pGEMT easy M13 primers	-	M13 forward GTTTTCCCAGTCACGACGTT	M13 Reverse GGAAACAGCTATGACCATGA
T01	chr3:124487489-124488372	CCGTTGATGGACATGTGGTT	ACTAGGACAATGTTGGGGCA
T02	chr21:46840558-46841090	TTTCCTGGGCCTGTATCCTG	CTGTCTGTCCGTCTGTCCTT
T03	chr7:29546652-29547108	CTCAGACCCTACCTCCCTCT	TGCCCTCACTTGACAAGACA
T04	chr10:12876606-12877068	TTGTCTCCGGGGAACTTCTC	GCCCCATCTTTCGAAGCAAA
T05	chr6:144980750-144981330	TGGCCTCTTGTCCTGTGTTT	CCGGCAAACTTCCTTCAGAC
T06	chr2:152536279-152536786	TCGCATCAGTTCTCAGGTCA	CCCAGAGGTTCCTACTGCAA
T07	chr22:39771889-39772417	TCCCCTCTCTCTTCCCCTAC	TCTCCAGTGACCATGCTACC
T08	chr17:72355298-72355885	CTAGCCCTGTGGTTCCAAAC	CCCCTCAGAGCTGTTTCCAA
T09	chr8:95734885-95735351	ACCTGTCTGTCTATGTGCCA	ACATCCACAAAAGTAACCTGCT
T10	chr20:30650801-30651387	CATTCTCCCCTTCCCCTTCA	CACTGAAGCCATGCCTTAAAAG
T11	chr7:7494570-7495141	ACTAGGACCTCTGCCAATGG	ATAAATGACACCTGGCCCCT
T12	chr4:97574338-97574999	CCCTGTGCCTGCTTTGATTT	GAGTGACAGACCAGCTCTCA
T13	chr7:39462846-39463397	CCATCTTGACTGTCCTGCCT	CTGTTTGGGCAAGGGAAGTG
T14	chr20:44587802-44588368	GCCTCACTCTGTCATCCTGA	TACAGAAAAGGAGCCAGGGG
T15	chr8:141959646-141960309	CTGAGCCTGAGTCTGTCACA	AGCTCTTTCAGTCCCTGCAT
T16	chr5:12717313-12717989	CAAGTATGTGCACTCAGGGC	GGCAATGTGGTGAGCAAGAA
T17	chrX:42225383-42226071	GGATTTTGGTATCTTTGCAGGGA	CTTAGGCCCCACTCTTGTCA
T18	chr7:157985910-157986587	AGGACAAGGCCAAGAACCAG	CTTGCTGGAATGTGGAGGTG
T19	chr4:171967327-171967873	GAGAGAGGTACCGTGTAGCC	CTAGGAGCTATGGGTGTGGG
T20	chr11:85675186-85675733	TCAGAAAGTGAGGCTAGTGGA	GACATAACAGAGCACGGCAG

DISCUSSION AND CONCLUSIONS

1. Major finding of the study: Identification of novel genetic causes of SRNS and GAMOS.

GAMOS is a rare autosomal disorder, associating SRNS with microcephaly and neurological impairment. Our study was interested in identifying novel genetic causes of SRNS or GAMOS. Here, we reported the identification of two novel variants in *TSEN54* gene, encoding a subunit of the TSEN complex involved in tRNA intron splicing, in a compound heterozygous patient affected with GAMOS. This study represents the first work that demonstrate the unexpected involvement of *TSEN54* and its role in the tRNA splicing processing as a cause of GAMOS and SRNS, providing novel insights into the genetic, molecular and phenotypic spectrum of these diseases. Therefore, it is essential to draw the attention to this gene due to its involvement in different phenotypes that the variants are likely to induce ranging from one single organ disease to multi organ involvement syndromes.

The GAMOS affected child presented a renal phenotype consisting of early-onset proteinuria at 6 months, which rapidly progressed towards nephrotic syndrome (NS) at 2 years, and with a neurological phenotype consisting of developmental delay and microcephaly detected at birth. Intriguingly, some of structural brain anomalies involving the pons and the cerebellum are reminiscent of type 2 pontocerebellar hypoplasia (PCH). On the other hand, in SRNS affected individuals from families B and C, the renal disease was discovered at an advanced stage with proteinuria, which progressively evolved to end-stage kidney disease in the adolescence or in early adulthood. Neither displayed extra-renal symptoms at the age of 28 to 46 years.

In the literature, *TSEN54* has been previously associated with the pontocerebellar hypoplasia (PCH), a group of rare autosomal recessive neurodegenerative disorders, principally with prenatal onset. Most of the patients affected with PCH present severe prenatal-onset hypoplasia/atrophy of cerebellum and ventral pons, with variable cerebral involvement and severe psychomotor retardation (Namavar, Barth, Kasher *et al.* 2011; Namavar, Barth, Poll-The *et al.* 2011; Namavar, Chitayat *et al.* 2011). PCHs have been classified into 14 types according to different clinical features, neuroimaging results and genetic causes (van Dijk *et al.* 2018; Ucuncu *et al.* 2020). Families carrying biallelic mutations in *TSEN54*, exhibit only neurological findings (Budde *et al.* 2008). PCH type 2, and in particular PCH2A, is the most prevalent and also well-known type of all the PCH subtypes, concerning 50% of the PCH affected patients. Patients

affected by PCH2A harbor the homozygous founder mutation p.A307S in the *TSEN54* gene (missense c.919G>T) and represent the majority of patients affected by PCH2 (Budde *et al.* 2008). A more severe clinical course can depend upon the type of mutations that occurs in *TSEN54*. Indeed, a compound heterozygous mutation (c.919G>T) associated to a splice site, or a nonsense mutations in *TSEN54* are both associated with the more severe PCH type, classified as PCH4 and PCH5, respectively (Patel *et al.* 2006; Namavar, Barth, Kasher *et al.* 2011; Namavar, Barth, Poll-The *et al.* 2011; Namavar, Chitayat, Barth *et al.* 2011). Strikingly, no renal involvement has been reported to date in PCH cases, particularly in those linked to *TSEN54* mutations. However, it could be possible that no renal abnormalities are detected in PCH affected individuals due to the severe early-onset phenotype from birth and the early death, mostly occurring before one year of age. Of note, it has been shown in mice that a missense mutation (p.Ala341Ser) or a knock-out of *Ampd2* gene, known to be responsible of PCH type 9 when mutated in humans, lead to a renal phenotype characterized by mild proteinuria or nephrotic syndrome, respectively, with foot process effacement (Juan *et al.* 2009; Toyama *et al.* 2012), suggesting that PCH genes could also be responsible for renal manifestations.

In addition, we described in this study, patients with different *TSEN54* mutations exhibiting either isolated SRNS or GAMOS, with a renal disease-onset ranging from congenital to early adulthood. This is in line with previous studies showing that mutations in the same gene lead in varying organ involvement such as mutations in *NUP133*/*107* or *PRDM15* genes that can cause either isolated SRNS or GAMOS (Rosti *et al.* 2017; Fujita *et al.* 2018b). Likewise, mutations in *WDR73* gene have been described in patients presenting a neurological involvement without any renal manifestation at the age of 31 years (Colin *et al.* 2014; Vodopiutz *et al.* 2015). However, from our functional data, we cannot clearly conclude whether this specific intronic variant, never described in *TSEN54*-linked PCH affected individuals, could be responsible on its own for the isolated renal phenotype in the SRNS and GAMOS affected individuals, and whether the nonsense Q339* variant could be responsible on its own for the brain phenotype in the GAMOS affected child, or would worsen a neuronal vulnerability due to the Ins47 mutation. We hope that our ongoing RNA-seq and tRNA-seq experiments will contribute to answer to these questions.

2. Pathogenicity of *TSEN54* mutations in GAMOS/SRNS or alternative explanations

Our data showed that in all the cells (LCLs, iPSCs and NSCs) carrying the intronic mutation in the homozygous or heterozygous state, we can detect two transcripts by RT-PCR, one corresponding to the WT and the other one to the Ins47 mutant transcript, containing the 47 intronic base pair retention, confirming that both, canonical and cryptic splicing sites are used in those cells. This is also evidenced by our qRT-PCR results showing the expression of a transcript corresponding to the Ins47 mutant allele. On contrary, our results seem to indicate that the mutant c.1015C>T transcript (Q339*) is subjected to nonsense mediated mRNA decay. This led us to hypothesize in the first place that the presence of the mutant Ins47 transcript could cause the kidney disease, by interacting with potential kidney-specific proteins, thereby disrupting the normal function of the TSEN complex. However, western blots analysis revealed that the two putative TSEN54 mutant proteins were absent in all cells derived from the patients, dismissing our first initial hypothesis that mutated proteins could led to different clinical phenotypes. This could be explained for the TSEN54 Q339* protein mutant by NDM of the corresponding transcript, whereas for TSEN54 Ins47 mutant protein, it is probably due to the proteolytic cleavage/proteasomal degradation, as suggested by our proteomic results.

Mutations in the genes encoding TSEN complex subunits have been shown to contribute to the disease by interfering with the assembly of the complex, with its stability or with its endonuclease activity. Indeed, pull-down and/or co-IP experiments with tagged HisFlag-TSEN15 WT and mutants, or TSEN54 WT and the A307S mutant showed that some mutations in *TSEN15* affect the stability of the mutant proteins themselves and/or alter the stoichiometry of the TSEN complex, whereas the *TSEN54* A307S mutation does not alter the stability of the mutant protein, neither the stoichiometry, but affects the thermal stability of TSEN complex thereby affecting complex assembly. However, whatever the origin of the alteration, it results in defects in pre-tRNA cleavage activity (Breuss *et al.* 2016; Sekulovski *et al.* 2020). In our proteomic and co-IP studies, we observed that the mutation Ins47 affects the intermolecular interactions between the TSEN subunits, contrary to the mutation Q339* which is still able to interact with the three subunits. In line with the published data, the mutation A307S does not affect the apparent intermolecular interactions between the TSEN subunits.

To summarize, both *TSEN54* variants lead to the decrease of *TSEN54* WT transcripts and TSEN54 WT protein expression levels, with none of the mutant proteins expressed, which could result in a residual amount of active TSEN complex in the cells. Given the genotype and phenotype of the SRNS and GAMOS affected individuals, we can hypothesize that there is a threshold below which the level of active TSEN complex could be more deleterious in neural progenitors/neurons than in podocytes. This hypothesis would be in agreement with our qRT-PCR results, the SRNS affected individual harbouring the Ins47 variant in the homozygous state would have more TSEN54 WT protein than the GAMOS affected child with the Ins47 variant associated with the nonsense variant. However, this hypothesis does not explain that individuals with PCH linked to mutations in *TSEN15* and *TSEN54* genes, in which a decrease in the activity of the TSEN complex has been demonstrated, do not show any renal manifestation.

3. Differential use of the suboptimal cryptic splicing site may led to the different phenotypes

Another hypothesis to explain the different phenotypes resulting from the same mutation would be the different use of the suboptimal cryptic splicing site created by the ins47 mutation. We cannot rule out that the cryptic splicing site may be regulated in a spatiotemporal manner, such as this cryptic splice site is only used in specific cell-types, such as in podocytes and/or neural stem cells, at specific developmental stages (mature podocytes, neural progenitor cells or neurons) (Boisson *et al.* 2018). Therefore, the use of the canonical or cryptic splicing site may not be unique and may vary in different tissues or cell types. For that reason, the use of appropriate cell types, such as neurons or podocytes, for mRNA analysis might be fundamental to highlight the different use of the cryptic splicing donor. The observation of cell type-dependent use of a cryptic splice site has been previously reported in patients with an intronic mutation in *IKBKG*, also known as *NEMO*, which encodes an essential modulator of NF-kβ required for its activation (Boisson *et al.* 2018). This intronic mutation creates a new splicing donor site leading to the insertion of 44-nucleotide generating a frameshift. In this study, they observed that the residual amount of the WT *IKBKG* ranged from 3% in leukocytes and 17% in iPSCs, to 35% in iPSC-derived neuronal progenitor cells, thus demonstrating that the suboptimal cryptic splicing site is more used in certain cell types explaining patient phenotype. In turn, they also observed that the decrease of protein WT level in

certain cells impacted the activation of NF-kβ, contributing to the outcome of the disease (Boisson *et al.* 2018).

To conclude, this previous observation confirms that intronic mutations, creating cryptic splice sites (donor or acceptor), may give rise to diversity of cellular and clinical phenotypes, permitting us to explain the different phenotypes observed with the same *TSEN54* mutation.

Therefore, the decrease in the expression of TSEN54 WT protein in a specific cell type, resulting from the differential use of the cryptic splice site, would lead to a reduction in the pool of TSEN complex and therefore to a partial loss of TSEN complex enzymatic activity, leading to defect in tRNA intron splicing.

4. Cellular mechanism of the disease in different organs: *TSEN54* knock-down in podocytes

The accumulation of unspliced tRNA would lead to protein translation defects, and thus proteostasis defects to which neurons and podocytes may be particularly sensitive (Kapur *et al.* 2017; Navarro-Betancourt *et al.* 2020). Indeed, experiments on *TSEN54* knock-down (KD) podocytes are in favor of this hypothesis since the *TSEN54*-depleted podocytes exhibited decreased newly protein synthesis. This result has also been observed in patients harboring mutations in genes encoding all the subunits of the KEOPS complex, involved in tRNA t^6A modification biosynthesis, which might suggest that alterations in tRNAs misprocessing, and consequently defect in protein synthesis and proteostasis, may represent a common pathological feature in GAMOS (Braun *et al.* 2017; Arrondel *et al.* 2019). However, evidence of such defect in iPSC-derived NCSs is needed to confirm this potential pathophysiological mechanism. In addition, it is interesting to note that PCH forms linked to *AMPD2* mutations lead to protein synthesis defects in iPSC-derived NSCs upon metabolic stress induction (Akizu *et al.* 2013).

The transient KD of *TSEN54* also leads to cell proliferation defect, as previously shown in KEOPS KD podocytes (Braun *et al.* 2017; Arrondel *et al.* 2019). Interestingly, a similar trend to a proliferation defect is also evidenced in our iPSC-derived NSCs harbouring the GAMOS-like genotype. In addition, we did not evidence apoptosis neither in *TSEN54* KD podocytes, nor in iPSC-derived NSCs, whatever their genotype, contrary to what has been observed in the study on KEOPS KD podocytes, in which it has been hypothesized that in patients harboring mutations in KEOPS complex, the microcephaly is cause by an increased apoptosis of neuronal progenitors cells

(Arrondel *et al.* 2019). Our results would favor the hypothesis that *TSEN54* depletion may block cells in a quiescent state or non-proliferative-state that might mostly explain the microcephaly phenotype in *TSEN54*-linked GAMOS.

Altogether, these results suggest that perturbations of the protein synthesis and cell proliferation are particularly critical for podocytes and NSC, and likely contribute to GAMOS and SNRS pathogenesis.

5. Molecular mechanism: accumulation of unspliced tRNAs

Previous observations demonstrated that mutations in genes encoding for proteins with functions related to RNA metabolism, in particular tRNA, UsnRNA, and in transcriptional regulation, such as WDR73, KEOPS complex subunits or PRDM15, are responsible of GAMOS (Braun *et al.* 2017; Arrondel *et al.* 2019; Mann *et al.* 2021; Tilley *et al.* 2021), thus suggesting that defects in RNAs mainly impact the brain, as in PCH, or is responsible of a multi-organ dysfunction syndrome as in GAMOS.

Furthermore, cells harboring mutations in *TSEN15* and *CLP1*, responsible of PCH type 2 and 10 respectively, lead to an accumulation of linear introns or intron-containing tRNAs, respectively (Karaca 2014; Schaffer *et al.* 2014; Breuss *et al.* 2016). In addition, mutations in *CLP1* lead to increased cell death of neuronal progenitors associated with decrease in cortical neurons number (Karaca 2014) and are responsible for the accumulation of tRNA fragments which induce an oxidative stress (Schaffer *et al.* 2014).

Our preliminary data are in favor of a defect in tRNAs processing, mainly at the intron splicing step, and reinforce the idea that RNAs misprocessing represent a common molecular dysfunction mechanism between GAMOS and PCH. Indeed, the impact of *TSEN54* mutations on tRNA intron splicing was observed in lymphoblastoid cells derived from a SRNS affected individual, in which we observed an increase in unspliced tRNAs. As observed in cells depleted for *CLP1*, we might also hypothesize that *TSEN54* loss of function is responsible for the accumulation of unspliced/unprocessed introns-containing tRNA under stress condition (Kumar *et al.* 2015; Li *et al.* 2018), which may remain immature into the nucleus or be degraded by some enzymes, including angiogenin, giving rise to tRNA-derived fragments (tRFs) (Karaca 2014;

Schaffer *et al.* 2014). Then, tRFs can act by deregulating the proliferation rate or the protein synthesis causing GAMOS or SRNS.

As a matter of fact 5' tRNA-derived small RNA fragments (tiRNAs) or tRFs are not random products, but they represent functional molecules, which might function as microRNAs, regulating transcription factors involved in proliferation, migration (Mo 2019), signaling between cells and in immune response (Chiou *et al.* 2018). This may directly lead to the alteration of the cellular homeostasis, but also to the alteration of the intracellular and extracellular signalling leading to defect in proliferation. Furthermore, tsRNAs have other regulatory functions. Among them, we can mentioned regulation of rRNA synthesis, regulation of RNA reverse transcription, stress granule formation, inhibition of mRNA translation initiation, canonical and non-canonical miRNA pathway and regulation of oncogenic mRNA stability (Kawaji *et al.* 2008; Fu *et al.* 2009; Emara *et al.* 2010; Ivanov *et al.* 2012; Maute *et al.* 2013; Huang *et al.* 2017) . The molecular mechanism with whom tsRNAs deregulate the protein synthesis do not only concern microRNA interference, but they also use alternative mechanisms including the binding of ribosomal subunits (Gebetsberger *et al.* 2012) or repressing of translation proteins (Yamasaki *et al.* 2009).

Over the last year, different works showed the involvement of tRFs or tiRNAs in the occurrence and development of various types of diseases, including cancers, neurological and metabolic diseases, and all these observations reinforce our hypothesis that tRFs or tiRNAs may be causative of GAMOS and SRNS. In addition, neurological diseases, and in particular neurodegenerative diseases, are the most correlated with the accumulation of tsRNAs. For example, accumulation of tiRNAs, responsible for protein synthesis defects, has been observed in mice deficient for *nsun2* (Abbasi-Moheb 2012; Blanco *et al.* 2014). These mice displayed microcephaly, whereas patients harbouring mutations in *NSUN2* are diagnosed with Dubowitz-like syndrome and an intellectual disability syndromic form.

Another example of the involvement of tRFs in disease, is the accumulation of 22 nucleotide tRF derived from tRNA glycine, called CU1276, which regulates cell proliferation and DNA damage, acting as a miRNA in lymphoma cell lines (Maute *et al.* 2013; Anderson and Ivanov 2014). Furthermore, recent studies showed also the involvement of tRFs in podocyte differentiation and injury, caused by changes in tRFs expression levels (Shi *et al.* 2020; Li *et al.* 2020). In the first publication, they found 147 differentially expressed tRFs, which may regulate podocyte differentiation, acting as miRNA (Shi *et al.* 2020). Whereas, in the second publication, they

detected 203 differently expressed tRFs, which play a key role by targeting the PI3K-Akt, Ras and Wnt signalling pathway, causing podocyte injury (Li *et al.* 2020).

6. The specific involvement of neuron and podocyte cell types

Although *TSEN54* is ubiquitously expressed, it remains still challenging for us to explain why different mutations in *TSEN54* specifically cause neuronal and/or renal phenotypes. We propose three hypotheses to explain the specific involvement of neurons and podocytes:

1) tRNAs are differentially expressed between tissues and cells, during the development or in stress conditions.

In the past years, tRNAs were considered as housekeeping RNAs, equally distributed and required for the translation process. Therefore, changes in abundance and expression should have an effect on the general translation. However, different studies showed that the availability of certain tRNAs is regulated at various levels. Among them, we can include amino acid loading or degradation, transcriptional and posttranscriptional processing (Gingold *et al.* 2014; Goodarzi *et al.* 2016). For that reason, these processes might contribute to the abundance of specific tRNAs pools in different cells and tissues, based on the coordination and the demand in translation, modulating protein expression and being responsible of certain diseases. For example in breast cancer cell lines, it has been shown that specific tRNAs, including tRNA-Arg-CCG, were upregulated in comparison with epithelial cells and even more upregulated in metastatic cell lines (Goodarzi *et al.* 2016). The authors conclude by saying that the metastic phenotype is directly linked with the upregulation of certain tRNAs, enhancing the translation efficiency of metastatic genes (Goodarzi *et al.* 2016). In particular, oncogenic transcription factors can directly induce or repress tRNAs gene expression. Others studies showed that the impact on translation depends on tRNA isoacceptor availability (Fredrick and Ibba, 2010). Thus, hypothesising that tRNA expression reflects the tissue-specific proteins codon usage, and showing the association between the presence of a tRNA pool and translation request. Elegantly, Gingold et al (Gingold *et al.* 2014), using microarrays and histone modifications maps, demonstrated that tRNA expression levels vary also between the proliferative and differentiated status of the cell types. Therefore, they confirmed

that tRNAs, in comparison with others RNAs, are regulated also by the proliferation or differentiation state.

Overall, these observations lead us to hypothesize that the different phenotypes could be caused by the different abundance of specific pre-tRNAs in neurons and podocytes, which can also rapidly change during organ development or cell differentiation, causing defects in translation and/or regulation of proliferation (Wilusz 2015).

2) We also hypothesized that neural progenitors and/or neurons might be more sensible or susceptible to translation defects than podocytes.

Neurons may be more susceptible to the lack of TSEN54 WT, since TSEN54 is highly expressed in neurons of the pons, cerebellar dentate, and olivary nuclei (Namavar, Barth, Poll-The *et al.* 2011; Kasher *et al.* 2011; Namavar, Chitayat, Barth *et al.* 2011), suggesting that TSEN complex is more essential for the development of these regions than others such as the nephron. This is in line with the neurodevelopmental aspect of GAMOS and PCH, and the fact that the renal manifestation is not due to developmental defects, but more to defects in maintaining podocyte homeostasis.

Neural progenitors undergo rapid proliferation, generating a high demand of $tRNA^{aa}$ that will take part to mRNA translation. Therefore, it can be hypothesized that the major sensitivity to the availability of certain mature spliced tRNAs could be explained by the fact that neurons, more than podocytes, need a huge amount of $tRNA^{aa}$, including those that are spliced, namely Arginine-TCT, Isoleucine-TAT, Leucine-CAA and Tyrosine-GTA, impacting the translation and proliferation processes and giving rise to a more severe phenotype. Furthermore, neurons are more vulnerable to the deregulation of translation, due to their extraordinary complex morphology, composed of axons and dendrites, which depend on local translation of pre-existing mRNA in order to respond to different stimulus, mostly for synaptic plasticity (Tahmasebi *et al.* 2018). However, the complex morphology of podocytes, with their primary and secondary processes, might also require local protein translation to respond rapidly to mechanical stress emphasizing the great plasticity of mature podocytes. It is also important to underline the fact that the brain consume up to 20% of glucose-derived energy, so translation deregulation of mRNAs involved in glucose metabolism may potentially give rise to neurological disorders (Tahmasebi *et al.* 2018). Finally, neural progenitors or neurons, could be more sensitive to the accumulation of tRNA-derived

fragments, by being less effective in degrading them, these latter acting as cell proliferation or protein synthesis inhibitors (Zong *et al.* 2021).

In line with these arguments, we can propose as putative molecular mechanisms leading to microcephaly in GAMOS phenotype, the depletion of the neural progenitor cells pool, which may not proliferate, resulting in a depletion of mature differentiated neurons, due to translation arrest (Lancaster *et al.* 2013).

3) Finally we propose that the balance between translation and degradation, and thereby the proteostasis, is altered in podocytes harbouring the homozygous Ins47 mutation.

Alteration of the balance between translation and degradation is commonly found in neurodegenerative diseases, including Alzheimer's disease or Parkinson's disease, which are marked by the accumulation and aggregation of specific neurotoxic proteins (Vilchez *et al.* 2014). Although the molecular mechanisms have not been fully elucidated, it has been observed that in Parkinson's disease the accumulation and aggregation of neurotoxic proteins will later lead to motor neurons loss and locomotor dysfunction (Vilchez *et al.* 2014).

Starting from these observations we might hypothesize that accumulation of toxic proteins is not exclusively responsible of neurodegenerative diseases, but might occurs also in other differentiated post-mitotic cells, such as podocytes. In particular, we can hypothesize that the Ins47 protein could be produced and not be degraded rapidly, contributing to the SRNS disease. The proteasome might not be extremely efficient in these cells, causing the accumulation of the Ins47 protein which could be toxic. Further experiments might be performed in patient kidney organoids-derived podocytes in order to validate this hypothesis and completely incriminate a proteasome dysfunction.

7. Loss-of-function of TSEN54 using neural progenitors and podocytes derived from kidney organoids

To go deeper into our understanding of the pathophysiological mechanisms leading to SRNS and GAMOS in *TSEN54* mutated individuals, we took advantage of iPSC lines to model both renal and neural aspects of GAMOS, by differentiating them into disease-relevant derivatives, namely podocytes and late cortical progenitor cells. This study set out to develop cellular models

to gain initial insights into the disease mechanisms of *TSEN54*-GAMOS/SRNS. In our project, we succeeded in generating iPSCs from patient PBMCs that were reprogrammed in iPSCs, which made it possible to personalize the disease model, using cells with the patient's genetic background. Furthermore, gene editing using CRISPR/Cas9 technology has been used to introduce causative mutation into a control iPSC line. This was the case in our study, due to the premature death of the GAMOS affected child. We used iPSCs derived from the patient's father (heterozygous for one of the mutation) to introduce the nonsense mutation to mimic the GAMOS child genotype. Using iPSCs, we found that the two *TSEN54* mutations do not affect the potential of iPSCs to proliferate or differentiate. However, we noticed a variability associated with iPSCs. Furthermore, kidney organoids differentiated from patient iPSCs harbouring *TSEN54* mutations did not denote any major developmental defects in nephron morphogenesis or structural anomalies in the general organoid architecture and cellular organization. As well, iPSCs have been differentiated in neural progenitor cells, suggesting that these mutations do not affect the neuronal differentiation process. The use of iPSC-derived kidney organoids and neural stem cells (NSCs)/neurons, from control or patients harbouring *TSEN54* mutations, will be instrumental to further investigate the common molecular and cellular mechanisms of both podocytes and NSCs/neurons. Indeed, these latter cells will be used for transcriptomic analyses, and/or for tRNA-sequencing to assess the impact of both variants on the intron splicing activity of the TSEN complex.

8. Conclusions and Perspectives

In line with our results, we proposed several arguments that let us strongly incriminate *TSEN54* mutations and consider them as pathogenic. We tried to recapitulate all results and hypothesis in the following figure (**Figure 30**).

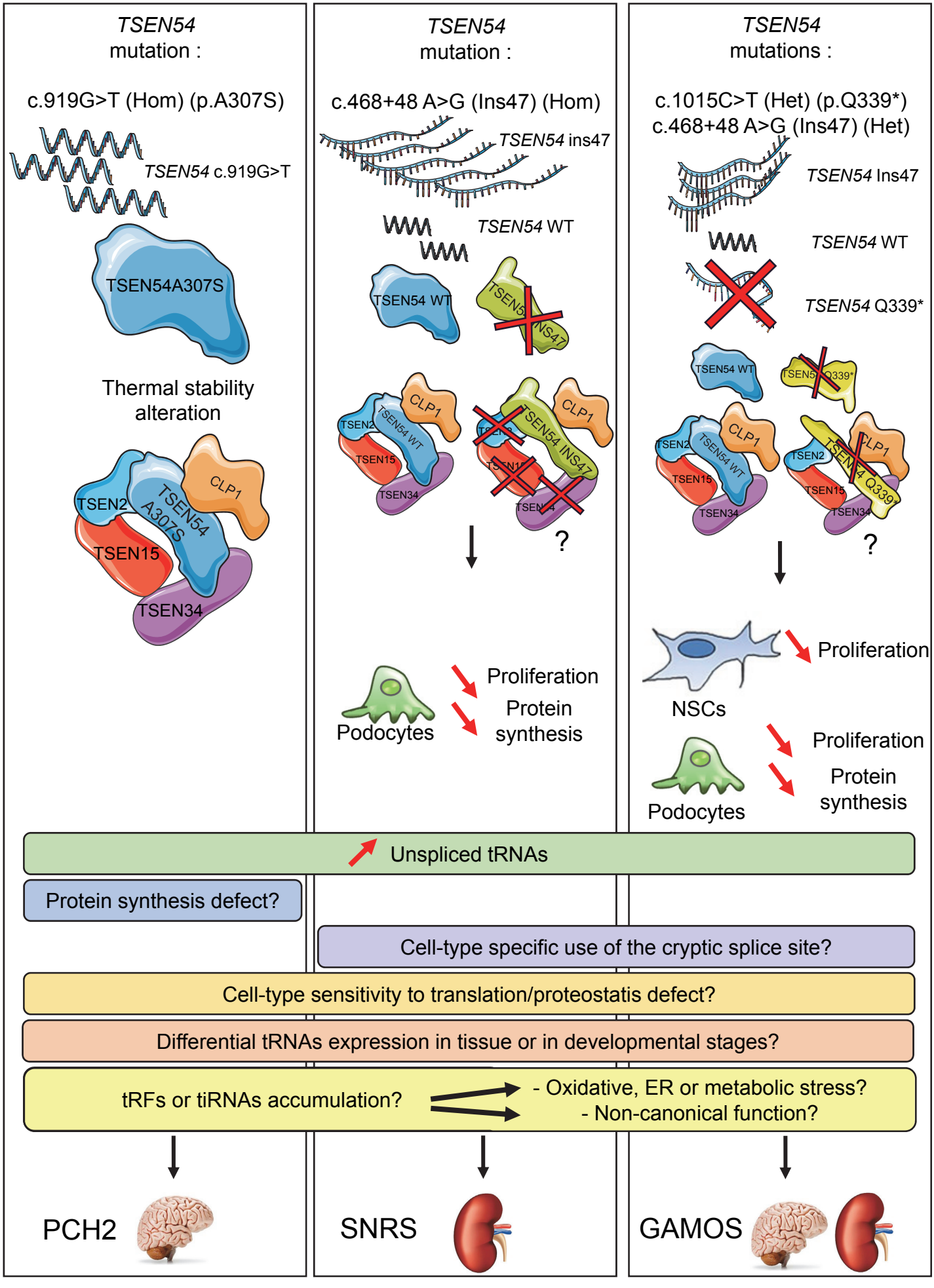
TSEN54 mutation :
c.919G>T (Hom) (p.A307S)
TSEN54 c.919G>T
TSEN54A307S
Thermal stability alteration
TSEN2
TSEN54 A307S
CLP1
TSEN15
TSEN34
PCH2
TSEN54 mutation :
c.468+48 A>G (Ins47) (Hom)
TSEN54 ins47
TSEN54 WT
TSEN54 WT
TSEN54 INS47
TSEN2
TSEN54 WT
CLP1
TSEN15
TSEN34
?
Podocytes
Proliferation
Protein synthesis
SNRS
TSEN54 mutations :
c.1015C>T (Het) (p.Q339*)
c.468+48 A>G (Ins47) (Het)
TSEN54 Ins47
TSEN54 WT
TSEN54 Q339*
TSEN54 WT
TSEN54 Q339*
TSEN2
TSEN54 WT
CLP1
TSEN15
TSEN34
?
NSCs
Proliferation
Podocytes
Proliferation
Protein synthesis
GAMOS
Unspliced tRNAs
Protein synthesis defect?
Cell-type specific use of the cryptic splice site?
Cell-type sensitivity to translation/proteostatis defect?
Differential tRNAs expression in tissue or in developmental stages?
tRFs or tiRNAs accumulation?
- Oxidative, ER or metabolic stress?
- Non-canonical function?

Figure 30: Schematic representation of all results and hypothesis (From F. Miscia).
We described in this study, patients with different *TSEN54* mutations exhibiting either isolated SRNS or GAMOS, with a renal disease-onset ranging from congenital to early adulthood. Our data showed that in all the cells (LCLs, iPSCs and NSCs) carrying the intronic mutation in the homozygous or heterozygous state, we can detect two transcripts by RT-PCR, one corresponding to the WT and the other one to the Ins47 mutant transcript, containing the 47 intronic base pair retention, confirming that both, canonical and cryptic splicing sites are used in those cells. On contrary, our results seem to indicate that the mutant c.1015C>T transcript (Q339*) is subjected to nonsense mediated mRNA decay. Both *TSEN54* variants lead to the decrease of *TSEN54* WT transcripts and TSEN54 WT protein expression levels, with none of the mutant proteins expressed in all cells derived from the patients. Proteomic and co-IP studies, showed that the mutation Ins47 affects the intermolecular interactions between the TSEN subunits, contrary to the mutation Q339* which is still able to interact with the three subunits. In line with the published data, the mutation A307S does not affect the apparent intermolecular interactions between the TSEN subunits. *TSEN54*-depleted podocytes exhibited decreased newly protein synthesis and cell proliferation defect. A similar trend to a proliferation defect is also evidenced in our iPSC-derived NSCs harbouring the GAMOS-like genotype. The impact of *TSEN54* mutations on tRNA intron splicing was observed in lymphoblastoid cells derived from a SRNS affected individual, in which we observed an increase in unspliced tRNAs. For that reason we hypothesized that *TSEN54* loss of function may be responsible for the accumulation of unspliced/unprocessed introns-containing tRNA, which may remain immature into the nucleus or be degraded by some enzymes, including angiogenin, giving rise to tRNA-derived fragments (tRFs). The accumulation of unspliced tRNA and/or the generation of tRFs/tiRNAs could lead to protein translation defects, and ultimately to proteostasis defects to which neurons and podocytes are particularly sensitive. We also hypothesized that the use of the cryptic splicing site may be tissue- or cell-type specific resulting in a different impact of the TSEN54 Ins47 mutant protein in podocytes and NSCs and/or neurons. Similarly, tRNAs can be expressed in a tissue- and/or cell-type dependent manner, but also differentially expressed during development or in stress conditions impacting podocytes and NSC/neurons differently.

However, this study has also raised several questions requiring further investigation. For example, one of them concerns the subcellular localization of TSEN54. The TSEN complex is reported to be a nuclear complex. However, due to concerns regarding antibody specificity, we were unable to investigate the localization of endogenous TSEN54 protein by immunofluorescence, and concomitantly whether TSEN54 co-localizes with endogenous TSEN34, TSEN2, TSEN15 and CLP1. Furthermore, we did not performed immunofluorescence experiments on HEK 293 cell line transiently overexpressing GFP-tagged TSEN54 wild-type or mutants, because the high molecular weight of the GFP might have influenced the TSEN54 bi-directional flow between the nucleus and cytoplasm. For that reason, further studies have to be undertaken in order to well understand how TSEN54 is shuttling between the nucleus and the cytosol. More investigations on the role of KPNA1 in TSEN54 import into the nucleus are needed.

This study raised also the problem of tRNAs technique limitations. For example, intron-containing tRNA have been predicted through the use of predictive tools. For that reason, advances in tRNA-sequencing technology and analysis could reveal other subsets of intron-containing tRNA. Furthermore, the similarity among tRNAs that belong to the same family, makes the bioinformatics analysis of the tRNA splicing defect even more complicated. Finally, due to the short length of tRNA and tsRNAs, tRNA sequencing techniques may lose tRNAs and tsRNAs pools during the experiment or the analysis may impede the recognition of these fragments that will be considered as background. All these limitations prevent us to fully incriminate tRNA splicing defects as causative of GAMOS/SRNS diseases, but as soon as new technologies will be settle down, the involvement of tRNA in disease will be easily to demonstrate.

For all these reasons, we thought that it is extremely important to share these results, because only the discoveries of new patients harbouring the same mutations in *TSEN54* will permit us to better elucidate and confirm the involvement of this gene in the occurrence of GAMOS /SRNS or other diseases.

REFERENCES

Abbasi-Moheb L. (2012). Mutations in NSUN2 Cause Autosomal- Recessive Intellectual Disability. *Am J Hum Genet.* **90**, 847–55. doi:10.1016/j.ajhg.2012.03.021

Abelson J., Trotta C. R., and Li H. (1998). tRNA Splicing. *J. Biol. Chem.* **273**, 12685–12688. doi:10.1074/jbc.273.21.12685

Akizu N., Cantagrel V., Schroth J., Cai N., Vaux K., McCloskey D., Naviaux R. K., Van Vleet J., Fenstermaker A. G., Silhavy J. L., Scheliga J. S., Toyama K., Morisaki H., Sonmez F. M., Celep F., Oraby A., Zaki M. S., Al-Baradie R., Faqeih E. A., Saleh M. A. M., Spencer E., Rosti R. O., Scott E., Nickerson E., Gabriel S., Morisaki T., Holmes E. W., and Gleeson J. G. (2013). AMPD2 Regulates GTP Synthesis and Is Mutated in a Potentially Treatable Neurodegenerative Brainstem Disorder. *Cell* **154**, 505–517. doi:10.1016/j.cell.2013.07.005

Alazami A. M., Patel N., Shamseldin H. E., Anazi S., Al-Dosari M. S., Alzahrani F., Hijazi H., Alshammari M., Aldahmesh M. A., Salih M. A., Faqeih E., Alhashem A., Bashiri F. A., Al-Owain M., Kentab A. Y., Sogaty S., Al Tala S., Temsah M.-H., Tulbah M., Aljelaify R. F., Alshahwan S. A., Seidahmed M. Z., Alhadid A. A., Aldhalaan H., AlQallaf F., Kurdi W., Alfadhel M., Babay Z., Alsogheer M., Kaya N., Al-Hassnan Z. N., Abdel-Salam G. M. H., Al-Sannaa N., Al Mutairi F., El Khashab H. Y., Bohlega S., Jia X., Nguyen H. C., Hammami R., Adly N., Mohamed J. Y., Abdulwahab F., Ibrahim N., Naim E. A., Al-Younes B., Meyer B. F., Hashem M., Shaheen R., Xiong Y., Abouelhoda M., Aldeeri A. A., Monies D. M., and Alkuraya F. S. (2015). Accelerating Novel Candidate Gene Discovery in Neurogenetic Disorders via Whole-Exome Sequencing of Prescreened Multiplex Consanguineous Families. *Cell Reports* **10**, 148–161. doi:10.1016/j.celrep.2014.12.015

Alexandrov A., Chernyakov I., Gu W., Hiley S. L., Hughes T. R., Grayhack E. J., and Phizicky E. M. (2006). Rapid tRNA Decay Can Result from Lack of Nonessential Modifications. *Molecular Cell* **21**, 87–96. doi:10.1016/j.molcel.2005.10.036

Alexandrov A., Martzen M. R., and Phizicky E. M. (2002). Two proteins that form a complex are required for 7-methylguanosine modification of yeast tRNA. *RNA* **8**, 1253–1266. doi:10.1017/S1355838202024019

Al-Rakan M. A., Abothnain M. D., Alrifai M. T., and Alfadhel M. (2018). Extending the ophthalmological phenotype of Galloway-Mowat syndrome with distinct retinal dysfunction: a report and review of ocular findings. *BMC Ophthalmol* **18**, 147. doi:10.1186/s12886-018-0820-4

Anderson P., and Ivanov P. (2014). tRNA fragments in human health and disease. *FEBS Letters* **588**, 4297–4304. doi:10.1016/j.febslet.2014.09.001

Andrews P. M. (1981). Investigations of cytoplasmic contractile and cytoskeletal elements in the kidney glomerulus. *Kidney Int.* **20**, 549–62. doi:10.1038/ki.1981.176

Antignac C. (2002). Genetic models: clues for understanding the pathogenesis of idiopathic nephrotic syndrome. *J. Clin. Invest.* **109**, 447–449. doi:10.1172/JCI0215094

Arrondel C., Missoury S., Snoek R., Patat J., Menara G., Collinet B., Liger D., Durand D., Gribouval O., Boyer O., Buscara L., Martin G., Machuca E., Nevo F., Lescop E., Braun D. A., Boschat A.-C., Sanquer S., Guerrera I. C., Revy P., Parisot M., Masson C., Boddaert N., Charbit M., Decramer S., Novo R., Macher M.-A., Ranchin B., Bacchetta J., Laurent A., Collardeau-Frachon S., van Eerde A. M., Hildebrandt F., Magen D., Antignac C., van Tilbeurgh H., and Mollet G. (2019). Defects in t6A tRNA modification due to GON7 and YRDC mutations lead to Galloway-Mowat syndrome. *Nat Commun* **10**, 3967. doi:10.1038/s41467-019-11951-x

Arts G.-J. (1998). The role of exportin-t in selective nuclear export of mature tRNAs. *The EMBO Journal* **17**, 7430–7441. doi:10.1093/emboj/17.24.7430

Ashraf S., Gee H. Y., Woerner S., Xie L. X., Vega-Warner V., Lovric S., Fang H., Song X., Cattran D. C., Avila-Casado C., Paterson A. D., Nitschké P., Bole-Feysot C., Cochat P., Esteve-Rudd J., Haberberger B., Allen S. J., Zhou W., Airik R., Otto E. A., Barua M., Al-Hamed M. H., Kari J. A., Evans J., Bierzynska A., Saleem M. A., Böckenhauer D., Kleta R., Desoky S. E., Hacihamdioglu D. O., Gok F., Washburn J., Wiggins R. C., Choi M., Lifton R. P., Levy S., Han Z., Salviati L., Prokisch H., Williams D. S., Pollak M., Clarke C. F., Pei Y., Antignac C., and Hildebrandt F. (2013). ADCK4 mutations promote steroid-resistant nephrotic syndrome through CoQ10 biosynthesis disruption. *J Clin Invest.* **123**, 5179–89. doi:10.1172/JCI69000

Baldi M. I., MATrOCCIA E., Bufardeci E., Fabbri S., and TOCCHani-VALENTINI G. P. (1992). Participation of the Intron in te Reaction Catalyzed by the Xenopus tRNA. *Science* **255**, 1404–8. doi:10.1126/science.1542788

Barbaux S., Niaudet P., Gubler M.-C., Grtinfeld J.-P., Jaubert F., Kuttenn F., Fekete C. N., Souleyreau-Therville N., Thibaud E., Fellous M., and McElreavey K. (1997). Donor splice-site mutations in WT1 are responsible for Frasier syndrome. *Nat Genet.* **17**, 467–70. doi:10.1038/ng1297-467

Barhoom S., Kaur J., Cooperman B. S., Smorodinsky N. I., Smilansky Z., Ehrlich M., and Elroy-Stein O. (2011). Quantitative single cell monitoring of protein synthesis at subcellular resolution using fluorescently labeled tRNA. *Nucleic Acids Research* **39**, e129–e129. doi:10.1093/nar/gkr601

Barth P. G., Aronica E., de Vries L., Nikkels P. G. J., Scheper W., Hoozemans J. J., Poll-The B.-T., and Troost D. (2007). Pontocerebellar hypoplasia type 2: a neuropathological update. *Acta Neuropathol* **114**, 373–386. doi:10.1007/s00401-007-0263-0

Beck M., and Hurt E. (2017). The nuclear pore complex: understanding its function through structural insight. *Nat Rev Mol Cell Biol* **18**, 73–89. doi:10.1038/nrm.2016.147

Ben-Omran T., Fahiminiya S., Sorfazlian N., Almuriekhi M., Nawaz Z., Nadaf J., Abu Khadija K., Zaineddin S., Kamel H., Majewski J., and Tropepe V. (2015). Nonsense mutation in the *WDR73* gene is associated with Galloway-Mowat syndrome. *J Med Genet* **52**, 381–390. doi:10.1136/jmedgenet-2014-102707

Bierhals T. (2013). Pontocerebellar hypoplasia type 2 and TSEN2: Review of the literature and two novel mutations. *European Journal of Medical Genetics* **56**, 325–30. doi:10.1016/j.ejmg.2013.03.009

Bierzynska A., McCarthy H. J., Soderquest K., Sen E. S., Colby E., Ding W. Y., Nabhan M. M., Kerecuk L., Hegde S., Hughes D., Marks S., Feather S., Jones C., Webb N. J. A., Ognjanovic M., Christian M., Gilbert R. D., Sinha M. D., Lord G. M., Simpson M., Koziell A. B., Welsh G. I., and Saleem M. A. (2017). Genomic and clinical profiling of a national nephrotic syndrome cohort advocates a precision medicine approach to disease management. *Kidney International* **91**, 937–947. doi:10.1016/j.kint.2016.10.013

Blanco S., Dietmann S., Flores J. V., Hussain S., Kutter C., Humphreys P., Lukk M., Lombard P., Treps L., Popis M., Kellner S., Hölter S. M., Garrett L., Wurst W., Becker L., Klopstock T., Fuchs H., Gailus-Durner V., Hrab M., Helm M., Ule J., Gleeson J. G., Odom D. T., and Frye M. (2014). Aberrant methylation of tRNAs links cellular stress to neurodevelopmental disorders. *The EMBO Journal* **33**, 2020–39. doi:10.15252/embj.201489282

Blomen V. A., Majek P., Jae L. T., Bigenzahn J. W., Nieuwenhuis J., Staring J., Sacco R., van Diemen F. R., Olk N., Stukalov A., Marceau C., Janssen H., Carette J. E., Bennett K. L., Colinge J., Superti-Furga G., and Brummelkamp T. R. (2015). Gene essentiality and synthetic lethality in haploid human cells. *Science* **350**, 1092–1096. doi:10.1126/science.aac7557

Boccaletto P., Machnicka M. A., Purta E., Piątkowski P., Bagiński B., Wirecki T. K., de Crécy-Lagard V., Ross R., Limbach P. A., Kotter A., Helm M., and Bujnicki J. M. (2018). MODOMICS: a database of RNA modification pathways. 2017 update. *Nucleic Acids Research* **46**, D303–D307. doi:10.1093/nar/gkx1030

Bohnsack M. T. (2004). Exportin 5 is a RanGTP-dependent dsRNA-binding protein that mediates nuclear export of pre-miRNAs. *RNA* **10**, 185–191. doi:10.1261/rna.5167604

Boissart C., Poulet A., Georges P., Darville H., Julita E., Delorme R., Bourgeron T., Peschanski M., and Benchoua A. (2013). Differentiation from human pluripotent stem cells of cortical neurons of the superficial layers amenable to psychiatric disease modeling and high-throughput drug screening. *Transl Psychiatry* **3**, e294–e294. doi:10.1038/tp.2013.71

Boisson B., Honda Y., Ajiro M., Bustamante J., Bendavid M., Gennery A. R., Kawasaki Y., Ichishima J., Osawa M., Nihira H., Shiba T., Tanaka T., Chrabieh M., Bigio B., Hur H., Itan Y., Liang Y., Okada S., Izawa K., Nishikomori R., Ohara O., Heike T., Abel L., Puel A., Saito M. K., Casanova J.-L., Hagiwara M., and Yasumi T. (2018). Rescue of recurrent deep intronic mutation underlying cell type–dependent quantitative NEMO deficiency. *Journal of Clinical Investigation* **129**, 583–597. doi:10.1172/JCI124011

Bouchireb K., Boyer O., Gribouval O., Nevo F., Huynh-Cong E., Morinière V., Campait R., Ars E., Brackman D., Dantal J., Eckart P., Gigante M., Lipska B. S., Liutkus A., Megarbane A., Mohsin N., Ozaltin F., Saleem M. A., Schaefer F., Soulami K., Torra R., Garcelon N., Mollet G., Dahan K., and Antignac C. (2014). *NPHS2* Mutations in Steroid-Resistant

Nephrotic Syndrome: A Mutation Update and the Associated Phenotypic Spectrum. *Human Mutation* **35**, 178–186. doi:10.1002/humu.22485

Boute N., Gribouval O., Roselli S., Benessy F., Lee H., Fuchshuber A., Dahan K., Gubler M.-C., Niaudet P., and Antignac C. (2000). NPHS2, encoding the glomerular protein podocin, is mutated in autosomal recessive steroid-resistant nephrotic syndrome. *Nat Genet* **24**, 349–354. doi:10.1038/74166

Boyer O., Emmanuelle P., Benoit F., Olivier G., Geneviève B., Huynh C. E., Christelle A., Marie-Josèphe T., Rodrick M., Laurence R., Alexandre K., Claire P.-N., Leila B., Alain B., Guillaume C., Christophe C., Jacques D., Georges D., Patrice D., Odile D., Philippe P., Dominique P., Eric L., Anne G.-M., Isabelle B., Marie-Claire G., Sophie S., Pierre R., Jean-Michel V., Angel A. M., Corinne A., Géraldine M., and Fabien N. (2011). INF2 Mutations in Charcot–Marie–Tooth Disease with Glomerulopathy. *The New England Journal of Medicine* **365**, 2377–88. doi:10.1056/NEJMoa1109122

Boyer O., Woerner S., Yang F., Oakeley E. J., Linghu B., Gribouval O., Tête M.-J., Duca J. S., Klickstein L., Damask A. J., Szustakowski J. D., Heibel F., Matignon M., Baudouin V., Chantrel F., Champigneulle J., Martin L., Nitschké P., Gubler M.-C., Johnson K. J., Chibout S.-D., and Antignac C. (2013). LMX1B Mutations Cause Hereditary FSGS without Extrarenal Involvement. *J Am Soc Nephrol* **24**, 1216–22. doi:10.1681/ASN.2013020171

Braun D. A., Lovric S., Schapiro D., Schneider R., Marquez J., Asif M., Hussain M. S., Daga A., Widmeier E., Rao J., Ashraf S., Tan W., Lusk C. P., Kolb A., Jobst-Schwan T., Schmidt J. M., Hoogstraten C. A., Eddy K., Kitzler T. M., Shril S., Moawia A., Schrage K., Khayyat A. I. A., Lawson J. A., Gee H. Y., Warejko J. K., Hermle T., Majmundar A. J., Hugo H., Budde B., Motameny S., Altmüller J., Noegel A. A., Fathy H. M., Gale D. P., Waseem S. S., Khan A., Kerecuk L., Hashmi S., Mohebbi N., Ettenger R., Serdaroğlu E., Alhasan K. A., Hashem M., Goncalves S., Ariceta G., Ubetagoyena M., Antonin W., Baig S. M., Alkuraya F. S., Shen Q., Xu H., Antignac C., Lifton R. P., Mane S., Nürnberg P., Khokha M. K., and Hildebrandt F. (2018). Mutations in multiple components of the nuclear pore complex cause nephrotic syndrome. *Journal of Clinical Investigation* **128**, 4313–4328. doi:10.1172/JCI98688

Braun D. A., Rao J., Mollet G., Schapiro D., Daugeron M.-C., Tan W., Gribouval O., Boyer O., Revy P., Jobst-Schwan T., Schmidt J. M., Lawson J. A., Schanze D., Ashraf S., Ullmann J. F. P., Hoogstraten C. A., Boddaert N., Collinet B., Martin G., Liger D., Lovric S., Furlano M., Guerrera I. C., Sanchez-Ferras O., Hu J. F., Boschat A.-C., Sanquer S., Menten B., Vergult S., De Rocker N., Airik M., Hermle T., Shril S., Widmeier E., Gee H. Y., Choi W.-I., Sadowski C. E., Pabst W. L., Warejko J. K., Daga A., Basta T., Matejas V., Scharmann K., Kienast S. D., Behnam B., Beeson B., Begtrup A., Bruce M., Ch'ng G.-S., Lin S.-P., Chang J.-H., Chen C.-H., Cho M. T., Gaffney P. M., Gipson P. E., Hsu C.-H., Kari J. A., Ke Y.-Y., Kiraly-Borri C., Lai W., Lemyre E., Littlejohn R. O., Masri A., Moghtaderi M., Nakamura K., Ozaltin F., Praet M., Prasad C., Prytula A., Roeder E. R., Rump P., Schnur R. E., Shiihara T., Sinha M. D., Soliman N. A., Soulami K., Sweetser D. A., Tsai W.-H., Tsai J.-D., Topaloglu R., Vester U., Viskochil D. H., Vatanavicharn N., Waxler J. L., Wierenga K. J., Wolf M. T. F., Wong S.-N., Leidel S. A., Truglio G., Dedon P. C., Poduri

A., Mane S., Lifton R. P., Bouchard M., Kannu P., Chitayat D., Magen D., Callewaert B., van Tilbeurgh H., Zenker M., Antignac C., and Hildebrandt F. (2017). Mutations in KEOPS-complex genes cause nephrotic syndrome with primary microcephaly. *Nat Genet* **49**, 1529–1538. doi:10.1038/ng.3933

Braun D. A., Shril S., Sinha A., Schneider R., Tan W., Ashraf S., Hermle T., Jobst-Schwan T., Widmeier E., Majmundar A. J., Daga A., Warejko J. K., Nakayama M., Schapiro D., Chen J., Airik M., Rao J., Schmidt J. M., Hoogstraten C. A., Hugo H., Meena J., Lek M., Laricchia K. M., Bagga A., and Hildebrandt F. (2018). Mutations in *WDR4* as a new cause of Galloway-Mowat syndrome: Mutations in *WDR4* as a new cause of Galloway-Mowat syndrome. *Am J Med Genet* **176**, 2460–2465. doi:10.1002/ajmg.a.40489

Breuss M. W., Sultan T., James K. N., Rosti R. O., Scott E., Musaev D., Furia B., Reis A., Sticht H., Al-Owain M., Alkuraya F. S., Reuter M. S., Abou Jamra R., Trotta C. R., and Gleeson J. G. (2016). Autosomal-Recessive Mutations in the tRNA Splicing Endonuclease Subunit TSEN15 Cause Pontocerebellar Hypoplasia and Progressive Microcephaly. *The American Journal of Human Genetics* **99**, 785. doi:10.1016/j.ajhg.2016.08.009

Brown E. J., Pollak M. R., and Barua M. (2014). Genetic testing for nephrotic syndrome and FSGS in the era of next-generation sequencing. *Kidney Int.* **85**, 1030–8. doi:10.1038/ki.2014.48

Brown E. J., Schlöndorff J. S., Becker D. J., Uscinski A. L., Higgs H. N., and Henderson J. M. (2010). Mutations in the formin protein INF2 cause focal segmental glomerulosclerosis. *Nat Genet.* **42**, 76–6. doi:10.1038/ng.505

Budde B. S., Namavar Y., Barth P. G., Poll-The B. T., Nürnberg G., Becker C., van Ruissen F., Weterman M. A. J., Fluiter K., T te Beek E., Aronica E., van der Knaap M. S., Höhne W., Toliat M. R., Crow Y. J., Steinlin M., Voit T., Roelens F., Brussel W., Brockmann K., Kyllerman M., Boltshauser E., Hammersen G., Willemsen M., Basel-Vanagaite L., Krägeloh-Mann I., de Vries L. S., Sztriha L., Muntoni F., Ferrie C. D., Battini R., Hennekam R. C. M., Grillo E., Beemer F. A., Stoets L. M. E., Wollnik B., Nürnberg P., and Baas F. (2008). tRNA splicing endonuclease mutations cause pontocerebellar hypoplasia. *Nature Genetics* **40**, 1113–1118. doi:10.1038/ng.204

Burghardt T., Hochapfel F., Salecker B., Meese C., Gröne H.-J., Rachel R., Wanner G., Krahn M. P., and Witzgall R. (2015). Advanced electron microscopic techniques provide a deeper insight into the peculiar features of podocytes. *American Journal of Physiology-Renal Physiology* **309**, F1082–F1089. doi:10.1152/ajprenal.00338.2015

Byrne S. M., Mali P., and Church G. M. (2014). Genome Editing in Human Stem Cells. 'Methods in Enzymology'. pp. 119–138. (Elsevier) doi:10.1016/B978-0-12-801185-0.00006-4

Calado A., Treichel N., Müller E.-C., Otto A., and Kutay U. (2002). Exportin-5-mediated nuclear export of eukaryotic elongation factor 1A and tRNA. *EMBO J* **21**, 6216–6224. doi:10.1093/emboj/cdf620

Calvin K., and Li H. (2008). RNA-splicing endonuclease structure and function. *Cell. Mol. Life Sci.* **65**, 1176–1185. doi:10.1007/s00018-008-7393-y

Canaud G., Bienaimé F., Viau A., Treins C., Baron W., Nguyen C., Burtin M., Berissi S., Giannakakis K., Muda A. O., Zschiedrich S., Huber T. B., Friedlander G., Legendre C., Pontoglio M., Pende M., and Terzi F. (2013). AKT2 is essential to maintain podocyte viability and function during chronic kidney disease. *Nat Med* **19**, 1288–1296. doi:10.1038/nm.3313

Chambers S. M., Fasano C. A., Papapetrou E. P., Tomishima M., Sadelain M., and Studer L. (2009). Highly efficient neural conversion of human ES and iPS cells by dual inhibition of SMAD signaling. *Nat Biotechnol* **27**, 275–280. doi:10.1038/nbt.1529

Chan P. P., and Lowe T. M. (2016). GtRNAdb 2.0: an expanded database of transfer RNA genes identified in complete and draft genomes. *Nucleic Acids Res* **44**, D184–D189. doi:10.1093/nar/gkv1309

Chatterjee K., Majumder S., Wan Y., Shah V., Wu J., Huang H.-Y., and Hopper A. K. (2017). Sharing the load: Mex67–Mtr2 cofunctions with Los1 in primary tRNA nuclear export. *Genes Dev.* **31**, 2186–2198. doi:10.1101/gad.305904.117

Chatterjee K., Nostramo R. T., Wan Y., and Hopper A. K. (2018). tRNA dynamics between the nucleus, cytoplasm and mitochondrial surface: Location, location, location. *Biochimica et Biophysica Acta (BBA) - Gene Regulatory Mechanisms* **1861**, 373–386. doi:10.1016/j.bbagrm.2017.11.007

Chen D.-F. (2016). An La-related protein controls cell cycle arrest by nuclear retrograde transport of tRNAs during diapause formation in Artemia. *BMC Biol.* doi:10.1186/s12915-016-0239-4

Chen J., Boyle S., Zhao M., Su W., Takahashi K., Davis L., DeCaestecker M., Takahashi T., Breyer M. D., and Hao C.-M. (2006). Differential Expression of the Intermediate Filament Protein Nestin during Renal Development and Its Localization in Adult Podocytes. *JASN* **17**, 1283–1291. doi:10.1681/ASN.2005101032

Chen Y., Cao J., Xiong M., Petersen A. J., Dong Y., Tao Y., Huang C. T.-L., Du Z., and Zhang S.-C. (2015). Engineering Human Stem Cell Lines with Inducible Gene Knockout using CRISPR/Cas9. *Cell Stem Cell* **17**, 233–244. doi:10.1016/j.stem.2015.06.001

Chen C.-P., Lin S.-P., Liu Y.-P., Tsai J.-D., Chen C.-Y., Shih S.-L., Tsai F.-J., Wu P.-C., and Wang W. (2011). Galloway-Mowat syndrome: Prenatal ultrasound and perinatal magnetic resonance imaging findings. *Taiwanese Journal of Obstetrics and Gynecology* **50**, 212–216. doi:10.1016/j.tjog.2011.04.005

Chen F., Pruett-Miller S. M., Huang Y., Gjoka M., Duda K., Taunton J., Collingwood T. N., Frodin M., and Davis G. D. (2011). High-frequency genome editing using ssDNA oligonucleotides with zinc-finger nucleases. *Nat Methods* **8**, 753–755. doi:10.1038/nmeth.1653

Cherkasova V., Lopez Maury L., Bacikova D., Pridham K., Bähler J., and Maraia R. J. (2012). Altered nuclear tRNA metabolism in La-deleted *Schizosaccharomyces pombe* is

accompanied by a nutritional stress response involving Atf1p and Pcr1p that is suppressible by Xpo-t/Los1p (AG Matera, Ed.). *MBoC* **23**, 480–491. doi:10.1091/mbc.e11-08-0732

Chernyakov I., Whipple J. M., Kotelawala L., Grayhack E. J., and Phizicky E. M. (2008). Degradation of several hypomodified mature tRNA species in Saccharomyces cerevisiae is mediated by Met22 and the 5'-3' exonucleases Rat1 and Xrn1. *Genes & Development* **22**, 1369–1380. doi:10.1101/gad.1654308

Cherry P. D., White L. K., York K., and Hesselberth J. R. (2018). Genetic bypass of essential RNA repair enzymes in budding yeast. *RNA* **24**, 313–323. doi:10.1261/rna.061788.117

Chiou N.-T., Kageyama R., and Ansel K. M. (2018). Selective Export into Extracellular Vesicles and Function of tRNA Fragments during T Cell Activation. *Cell Reports* **25**, 3356-3370.e4. doi:10.1016/j.celrep.2018.11.073

Choulika A., Perrin A., Dujon B., and Nicolas J.-F. O. (1995). Induction of Homologous Recombination in Mammalian Chromosomes by Using the I-SceI System of Saccharomyces cerevisiae. *MOL. CELL. BIOL.* **15**, 1968–73. doi:10.1128/mcb.15.4.1968

Chu H.-Y., and Hopper A. K. (2013). Genome-Wide Investigation of the Role of the tRNA Nuclear-Cytoplasmic Trafficking Pathway in Regulation of the Yeast Saccharomyces cerevisiae Transcriptome and Proteome. *Molecular and Cellular Biology* **33**, 4241–4254. doi:10.1128/MCB.00785-13

Colin E., Huynh Cong E., Mollet G., Guichet A., Gribouval O., Arrondel C., Boyer O., Daniel L., Gubler M.-C., Ekinci Z., Tsimaratos M., Chabrol B., Boddaert N., Verloes A., Chevrollier A., Gueguen N., Desquiret-Dumas V., Ferré M., Procaccio V., Richard L., Funalot B., Moncla A., Bonneau D., and Antignac C. (2014). Loss-of-Function Mutations in WDR73 Are Responsible for Microcephaly and Steroid-Resistant Nephrotic Syndrome: Galloway-Mowat Syndrome. *The American Journal of Human Genetics* **95**, 637–648. doi:10.1016/j.ajhg.2014.10.011

Cook A. G. (2009). Structures of the tRNA export factor in the nuclear and cytosolic states. *Nature* **461**, 60–5. doi:10.1038/nature08394

Copela L. A., Fernandez C. F., Sherrer R. L., and Wolin S. L. (2008). Competition between the Rex1 exonuclease and the La protein affects both Trf4p-mediated RNA quality control and pre-tRNA maturation. *RNA* **14**, 1214–1227. doi:10.1261/rna.1050408

Costessi A., Mahrour N., Sharma V., Stunnenberg R., Stoel M. A., Tijchon E., Conaway J. W., Conaway R. C., and Stunnenberg H. G. (2012). The Human EKC/KEOPS Complex Is Recruited to Cullin2 Ubiquitin Ligases by the Human Tumour Antigen PRAME (L Tora, Ed.). *PLoS ONE* **7**, e42822. doi:10.1371/journal.pone.0042822

Cox J., and Mann M. (2008). MaxQuant enables high peptide identification rates, individualized p.p.b.-range mass accuracies and proteome-wide protein quantification. *Nat Biotechnol* **26**, 1367–1372. doi:10.1038/nbt.1511

Crothers D. M., Seno T., and Soll D. G. (1972). Is There a Discriminator Site in Transfer RNA? *Proceedings of the National Academy of Sciences* **69**, 3063–3067. doi:10.1073/pnas.69.10.3063

Culver G. M., McCraith S. M., Consaul S. A., Stanford D. R., and Phizicky E. M. (1997). A 2′-Phosphotransferase Implicated in tRNA Splicing Is Essential in *Saccharomyces cerevisiae*. *J. Biol. Chem.* **272**, 13203–13210. doi:10.1074/jbc.272.20.13203

D'Agati V. D. (2008). Podocyte injury in focal segmental glomerulosclerosis: Lessons from animal models (a play in five acts). *Kidney International* **73**, 399–406. doi:10.1038/sj.ki.5002655

Daugeron M.-C., Lenstra T. L., Frizzarin M., El Yacoubi B., Liu X., Baudin-Baillieu A., Lijnzaad P., Decourty L., Saveanu C., Jacquier A., Holstege F. C. P., de Crécy-Lagard V., van Tilbeurgh H., and Libri D. (2011). Gcn4 misregulation reveals a direct role for the evolutionary conserved EKC/KEOPS in the t6A modification of tRNAs. *Nucleic Acids Research* **39**, 6148–6160. doi:10.1093/nar/gkr178

van Dijk T., Baas F., Barth P. G., and Poll-The B. T. (2018). What's new in pontocerebellar hypoplasia? An update on genes and subtypes. *Orphanet J Rare Dis* **13**, 92. doi:10.1186/s13023-018-0826-2

Ding W. Y., Koziell A., McCarthy H. J., Bierzynska A., Bhagavatula M. K., Dudley J. A., Inward C. D., Coward R. J., Tizard J., Reid C., Antignac C., Boyer O., and Saleem M. A. (2014). Initial Steroid Sensitivity in Children with Steroid-Resistant Nephrotic Syndrome Predicts Post-Transplant Recurrence. *JASN* **25**, 1342–1348. doi:10.1681/ASN.2013080852

Dixit S., Henderson J. C., and Alfonzo J. D. (2019). Multi-Substrate Specificity and the Evolutionary Basis for Interdependence in tRNA Editing and Methylation Enzymes. *Front. Genet.* **10**, 104. doi:10.3389/fgene.2019.00104

Downey M., Houlsworth R., Maringele L., Rollie A., Brehme M., Galicia S., Guillard S., Partington M., Zubko M. K., Krogan N. J., Emili A., Greenblatt J. F., Harrington L., Lydall D., and Durocher D. (2006). A Genome-Wide Screen Identifies the Evolutionarily Conserved KEOPS Complex as a Telomere Regulator. *Cell* **124**, 1155–68. doi:10.1016/j.cell.2005.12.044

Doyonnas R., Kershaw D. B., Duhme C., Merkens H., Chelliah S., Graf T., and McNagny K. M. (2001). Anuria, Omphalocele, and Perinatal Lethality in Mice Lacking the Cd34-Related Protein Podocalyxin. *Journal of Experimental Medicine* **194**, 13–28. doi:10.1084/jem.194.1.13

Dreyer S. D., Zhou G., Baldini A., Winterpacht A., Zabel B., Cole W., Johnson R. L., and Lee B. (1998). Mutations in LMX18 cause abnormal skeletal patterning and renal dysplasia in nail patella syndrome. *Nat Genet* **19**, 47–50. doi:10.1038/ng0598-47

Edvardson S., Prunetti L., Arraf A., Haas D., Bacusmo J. M., Hu J. F., Ta-Shma A., Dedon P. C., de Crécy-Lagard V., and Elpeleg O. (2017). tRNA N6-adenosine threonylcarbamoyltransferase defect due to KAE1/TCS3 (OSGEP) mutation manifest by

neurodegeneration and renal tubulopathy. *European Journal of Human Genetics* **25**, 545–551. doi:10.1038/ejhg.2017.30

Ekstrand J. J. (2012). Galloway-Mowat Syndrome: Neurologic Features in Two Sibling Pairs. *Pediatric Neurology* 4.

El Yacoubi B., Hatin I., Deutsch C., Kahveci T., Rousset J.-P., Iwata-Reuyl D., G Murzin A., and de Crécy-Lagard V. (2011). A role for the universal Kae1/Qri7/YgjD (COG0533) family in tRNA modification: t ^{6} A biosynthesis. *The EMBO Journal* **30**, 882–893. doi:10.1038/emboj.2010.363

Emara M. M., Ivanov P., Hickman T., Dawra N., Tisdale S., Kedersha N., Hu G.-F., and Anderson P. (2010). Angiogenin-induced tRNA-derived Stress-induced RNAs Promote Stress-induced Stress Granule Assembly*. *Journal of Biological Chemistry* **285**, 10959–10968. doi:10.1074/jbc.M109.077560

Englert M. (2005). Plant tRNA ligases are multifunctional enzymes that have diverged in sequence and substrate specificity from RNA ligases of other phylogenetic origins. *Nucleic Acids Research* **33**, 388–399. doi:10.1093/nar/gki174

Espiritu E. B., Jiang H., Moreau-Marquis S., Sullivan M., Yan K., Beer Stolz D., Sampson M. G., Hukriede N. A., and Swiatecka-Urban A. (2019). The human nephrin Y1139RSL motif is essential for podocyte foot process organization and slit diaphragm formation during glomerular development. *Journal of Biological Chemistry* **294**, 10773–10788. doi:10.1074/jbc.RA119.008235

Espuny-Camacho I., Michelsen K. A., Gall D., Linaro D., Hasche A., Bonnefont J., Bali C., Orduz D., Bilheu A., Herpoel A., Lambert N., Gaspard N., Péron S., Schiffmann S. N., Giugliano M., Gaillard A., and Vanderhaeghen P. (2013). Pyramidal Neurons Derived from Human Pluripotent Stem Cells Integrate Efficiently into Mouse Brain Circuits In Vivo. *Neuron* **77**, 440–456. doi:10.1016/j.neuron.2012.12.011

Farquhar M. G. (2006). The glomerular basement membrane: not gone, just forgotten. *Journal of Clinical Investigation* **116**, 2090–2093. doi:10.1172/JCI29488

Ferraris P., Cochet M., Hamel R., Gladwyn-Ng I., Alfano C., Diop F., Garcia D., Talignani L., Montero-Menei C. N., Nougairède A., Yssel H., Nguyen L., Coulpier M., and Missé D. (2019). Zika virus differentially infects human neural progenitor cells according to their state of differentiation and dysregulates neurogenesis through the Notch pathway. *Emerging Microbes & Infections* **8**, 1003–1016. doi:10.1080/22221751.2019.1637283

Flores A., Briand J.-F., Gadal O., Andrau J.-C., Rubbi L., Van Mullem V., Boschiero C., Goussot M., Marck C., Carles C., Thuriaux P., Sentenac A., and Werner M. (1999). A protein-protein interaction map of yeast RNA polymerase III. *Proceedings of the National Academy of Sciences* **96**, 7815–7820. doi:10.1073/pnas.96.14.7815

Forbes T. A., Howden S. E., Lawlor K., Phipson B., Maksimovic J., Hale L., Wilson S., Quinlan C., Ho G., Holman K., Bennetts B., Crawford J., Trnka P., Oshlack A., Patel C., Mallett A.,

Simons C., and Little M. H. (2018). Patient-iPSC-Derived Kidney Organoids Show Functional Validation of a Ciliopathic Renal Phenotype and Reveal Underlying Pathogenetic Mechanisms. *The American Journal of Human Genetics* **102**, 816–831. doi:10.1016/j.ajhg.2018.03.014

Freedman B. S., Brooks C. R., Lam A. Q., Fu H., Morizane R., Agrawal V., Saad A. F., Li M. K., Hughes M. R., Werff R. V., Peters D. T., Lu J., Baccei A., Siedlecki A. M., Valerius M. T., Musunuru K., McNagny K. M., Steinman T. I., Zhou J., Lerou P. H., and Bonventre J. V. (2015). Modelling kidney disease with CRISPR-mutant kidney organoids derived from human pluripotent epiblast spheroids. *Nat Commun* **6**, 8715. doi:10.1038/ncomms9715

Fu H., Feng J., Liu Q., Sun F., Tie Y., Zhu J., Xing R., Sun Z., and Zheng X. (2009). Stress induces tRNA cleavage by angiogenin in mammalian cells. *FEBS Letters* **583**, 437–42. doi:10.1016/j.febslet.2008.12.043

Fujishima K., and Kanai A. (2014). tRNA gene diversity in the three domains of life. *Front. Genet.* **5**,. doi:10.3389/fgene.2014.00142

Fujita A., Tsukaguchi H., Koshimizu E., Nakazato H., Itoh K., Kuraoka S., Komohara Y., Shiina M., Nakamura S., Kitajima M., Tsurusaki Y., Miyatake S., Ogata K., Iijima K., Matsumoto N., and Miyake N. (2018a). Homozygous splicing mutation in NUP133 causes Galloway-Mowat syndrome. *ANNALS of Neurology* **84**, 15.

Fujita A., Tsukaguchi H., Koshimizu E., Nakazato H., Itoh K., Kuraoka S., Komohara Y., Shiina M., Nakamura S., Kitajima M., Tsurusaki Y., Miyatake S., Ogata K., Iijima K., Matsumoto N., and Miyake N. (2018b). Homozygous splicing mutation in *NUP13* 3 causes Galloway-Mowat syndrome: Galloway-Mowat Syndrome. *Ann Neurol.* **84**, 814–828. doi:10.1002/ana.25370

Fukasawa H., Bornheimer S., Kudlicka K., and Farquhar M. G. (2009). Slit Diaphragms Contain Tight Junction Proteins. *JASN* **20**, 1491–1503. doi:10.1681/ASN.2008101117

Fusaki N., Ban H., Nishiyama A., Saeki K., and Hasegawa M. (2009). Efficient induction of transgene-free human pluripotent stem cells using a vector based on Sendai virus, an RNA virus that does not integrate into the host genome. *Proc. Jpn. Acad., Ser. B* **85**, 348–362. doi:10.2183/pjab.85.348

Gabriel E., Ramani A., Karow U., Gottardo M., Natarajan K., Gooi L. M., Goranci-Buzhala G., Krut O., Peters F., Nikolic M., Kuivanen S., Korhonen E., Smura T., Vapalahti O., Papantonis A., Schmidt-Chanasit J., Riparbelli M., Callaini G., Krönke M., Utermöhlen O., and Gopalakrishnan J. (2017). Recent Zika Virus Isolates Induce Premature Differentiation of Neural Progenitors in Human Brain Organoids. *Cell Stem Cell* **20**, 397-406.e5. doi:10.1016/j.stem.2016.12.005

Gagliardini E., Conti S., Benigni A., Remuzzi G., and Remuzzi A. (2010). Imaging of the Porous Ultrastructure of the Glomerular Epithelial Filtration Slit. *JASN* **21**, 2081–2089. doi:10.1681/ASN.2010020199

Galloway W. H., and Mowat A. P. (1968). Congenital Microcephaly with Hiatus Hernia and Nephrotic Syndrome in Two Sibs. *J Med Genet.* **5**, 319–21. doi:10.1136/jmg.5.4.319

Garreta E., Prado P., Tarantino C., Oria R., Fanlo L., Martí E., Zalvidea D., Trepat X., Roca-Cusachs P., Gavaldà-Navarro A., Cozzuto L., Campistol J. M., Izpisúa Belmonte J. C., Hurtado del Pozo C., and Montserrat N. (2019). Fine tuning the extracellular environment accelerates the derivation of kidney organoids from human pluripotent stem cells. *Nat. Mater.* **18**, 397–405. doi:10.1038/s41563-019-0287-6

Gebetsberger J., Zywicki M., Künzi A., and Polacek N. (2012). tRNA-Derived Fragments Target the Ribosome and Function as Regulatory Non-Coding RNA in *Haloferax volcanii*. *Archaea* **2012**, 1–11. doi:10.1155/2012/260909

Gilbert (2010). 'Developmental Biology.'

Gingold H., Tehler D., Christoffersen N. R., Nielsen M. M., Asmar F., Kooistra S. M., Christophersen N. S., Christensen L. L., Borre M., Sørensen K. D., Andersen L. D., Andersen C. L., Hulleman E., Wurdinger T., Ralfkiær E., Helin K., Grønbæk K., Ørntoft T., Waszak S. M., Dahan O., Pedersen J. S., Lund A. H., and Pilpel Y. (2014). A Dual Program for Translation Regulation in Cellular Proliferation and Differentiation. *Cell* **158**, 1281–1292. doi:10.1016/j.cell.2014.08.011

Gogakos T., Brown M., Garzia A., Meyer C., Hafner M., and Tuschl T. (2017). Characterizing Expression and Processing of Precursor and Mature Human tRNAs by Hydro-tRNAseq and PAR-CLIP. *Cell Reports* **20**, 1463–1475. doi:10.1016/j.celrep.2017.07.029

González-Aguilera C., and Askjaer P. (2012). Dissecting the NUP107 complex: Multiple components and even more functions. *Nucleus* **3**, 340–348. doi:10.4161/nucl.21135

Goodarzi H., Liu X., Nguyen H. C. B., Zhang S., Fish L., and Tavazoie F. (2015). Endogenous tRNA-derived fragments suppress breast cancer progression via YBX1 displacement. *Displacement. Cell* **161**, 790–802. doi:10.1016/j.cell.2015.02.053

Goodarzi H., Nguyen H. C. B., Zhang S., Dill B. D., Molina H., and Tavazoie S. F. (2016). Modulated Expression of Specific tRNAs Drives Gene Expression and Cancer Progression. *Cell* **165**, 1416–1427. doi:10.1016/j.cell.2016.05.046

Grahammer F., Schell C., and Huber T. B. (2013). The podocyte slit diaphragm—from a thin grey line to a complex signalling hub. *Nat Rev Nephrol* **9**, 587–598. doi:10.1038/nrneph.2013.169

Grahammer F., Wigge C., Schell C., Kretz O., Patrakka J., Schneider S., Klose M., Kind J., Arnold S. J., Habermann A., Rinschen M. M., Völker L., Bregenzer A., Rubbenstroth D., Boerries M., Kerjaschki D., Miner J. H., Walz G., Benzing T., Fornoni A., Frangakis A. S., and Huber T. B. (2016). A flexible, multilayered protein scaffold maintains the slit in between glomerular podocytes. *JCI Insight* **1**, e86177. doi:10.1172/jci.insight.86177

Gray M. C. Michael W. (2000). Pseudouridine in RNA: What, Where, How, and Why. *IUBMB Life (International Union of Biochemistry and Molecular Biology: Life)* **49**, 341–351. doi:10.1080/152165400410182

Grosjean H., Söll D. G., and Crothers D. M. (1976). Studies of the complex between transfer RNAs with complementary anticodons. *Journal of Molecular Biology* **103**, 499–519. doi:10.1016/0022-2836(76)90214-X

Haddad R., Maurice F., Viphakone N., Voisinet-Hakil F., Fribourg S., and Minvielle-Sébastia L. (2012). An essential role for Clp1 in assembly of polyadenylation complex CF IA and Pol II transcription termination. *Nucleic Acids Research* **40**, 1226–1239. doi:10.1093/nar/gkr800

Hale L. J., Howden S. E., Phipson B., Lonsdale A., Er P. X., Ghobrial I., Hosawi S., Wilson S., Lawlor K. T., Khan S., Oshlack A., Quinlan C., Lennon R., and Little M. H. (2018). 3D organoid-derived human glomeruli for personalised podocyte disease modelling and drug screening. *Nat Commun* **9**, 5167. doi:10.1038/s41467-018-07594-z

Hanada T., Weitzer S., Mair B., Bernreuther C., Wainger B. J., Ichida J., Hanada R., Orthofer M., Cronin S. J., Komnenovic V., Minis A., Sato F., Mimata H., Yoshimura A., Tamir I., Rainer J., Kofler R., Yaron A., Eggan K. C., Woolf C. J., Glatzel M., Herbst R., Martinez J., and Penninger J. M. (2013). CLP1 links tRNA metabolism to progressive motor-neuron loss. *Nature* **495**, 474–480. doi:10.1038/nature11923

Haussecker D., Huang Y., Lau A., Parameswaran P., Fire A. Z., and Kay M. A. (2010). Human tRNA-derived small RNAs in the global regulation of RNA silencing. *RNA* **16**, 673–95. doi:10.1261/rna.2000810

Hecker A., Graille M., Madec E., and Forterre P. (2009). The universal Kae1 protein and the associated Bud32 kinase (PRPK), a mysterious protein couple probably essential for genome maintenance in Archaea and Eukarya. *Biochemical Society Transactions* **37**, 7.

Hellmuth K., Lau D. M., Bischoff F. R., Künzler M., Hurt E., and Simos G. (1998). Yeast Los1p Has Properties of an Exportin-Like Nucleocytoplasmic Transport Factor for tRNA. *Mol. Cell. Biol.* **18**, 6374–6386. doi:10.1128/MCB.18.11.6374

Helm M., Brule H., Degoul F., Cepanec C., Leroux J.-P., Giege R., and Florentz C. (1998). The presence of modified nucleotides is required for cloverleaf folding of a human mitochondrial tRNA. *Nucleic Acids Research* **26**, 1636–1643. doi:10.1093/nar/26.7.1636

Hinkes B. G., Mucha B., Vlangos C. N., Gbadegesin R., Liu J., Hasselbacher K., Hangan D., Ozaltin F., Zenker M., and Hildebrandt F. (2007). Nephrotic Syndrome in the First Year of Life: Two Thirds of Cases Are Caused by Mutations in 4 Genes (NPHS1, NPHS2, WT1, and LAMB2). *Pediatrics* **119**, e907. doi:10.1542/peds.2006-2164

Hirata A. (2019). Recent Insights Into the Structure, Function, and Evolution of the RNA-Splicing Endonucleases. *Front. Genet.* **10**, 103. doi:10.3389/fgene.2019.00103

Hockemeyer D., and Jaenisch R. (2017). Induced pluripotent stem cells meet genome editing. *Cell Stem Cell* **18**, 573–86. doi:10.1016/j.stem.2016.04.013

Hopper A. K., and Nostramo R. T. (2019). tRNA Processing and Subcellular Trafficking Proteins Multitask in Pathways for Other RNAs. *Front. Genet.* **10**, 96. doi:10.3389/fgene.2019.00096

Hopper A., Schultz L., and Shapiro R. (1980). Processing of intervening sequences: a new yeast mutant which fails to excise intervening sequences from precursor tRNAs. *Cell* **19**, 741–751. doi:10.1016/S0092-8674(80)80050-X

Hou P., Li Y., Zhang X., Liu C., Guan J., Li H., Zhao T., Ye J., Yang W., Liu K., Ge J., Xu J., Zhang Q., Zhao Y., and Deng H. (2013). Pluripotent Stem Cells Induced from Mouse Somatic Cells by Small-Molecule Compounds. *Science* **341**, 651–4. doi:10.1126/science.1239278

Hou J.-W., and Wang T.-R. (1995). Galloway-Mowat syndrome in Taiwan. *Am. J. Med. Genet.* **58**, 245–248. doi:10.1002/ajmg.1320580310

Huang H.-Y., and Hopper A. K. (2015). In vivo biochemical analyses reveal distinct roles of β-importins and eEF1A in tRNA subcellular traffic. *Genes Dev.* **29**, 772–783. doi:10.1101/gad.258293.115

Huang B., Yang H., Cheng X., Wang D., Fu S., Shen W., Zhang Q., Zhang L., Xue Z., Li Y., Da Y., Yang Q., Li Z., Liu L., Qiao L., Kong Y., Yao Z., Zhao P., Li M., and Zhang R. (2017). tRF/miR-1280 Suppresses Stem Cell–like Cells and Metastasis in Colorectal Cancer. *Cancer Res* **77**, 3194–3206. doi:10.1158/0008-5472.CAN-16-3146

Huber T. B., Hartleben B., Kim J., Schmidts M., Schermer B., Keil A., Egger L., Lecha R. L., Borner C., Pavenstädt H., Shaw A. S., Walz G., and Benzing T. (2003). Nephrin and CD2AP Associate with Phosphoinositide 3-OH Kinase and Stimulate AKT-Dependent Signaling. *MCB* **23**, 4917–4928. doi:10.1128/MCB.23.14.4917-4928.2003

Huber T. B., Hartleben B., Winkelmann K., Schneider L., Becker J. U., Leitges M., Walz G., Haller H., and Schiffer M. (2009). Loss of Podocyte aPKCλ/ι Causes Polarity Defects and Nephrotic Syndrome. *JASN* **20**, 798–806. doi:10.1681/ASN.2008080871

Huber T. B., Schermer B., and Benzing T. (2007). Podocin Organizes Ion Channel-Lipid Supercomplexes: Implications for Mechanosensation at the Slit Diaphragm. *Nephron Exp Nephrol* **106**, e27–e31. doi:10.1159/000101789

Huet J., and Sentenac A. (1992). The TATA-binding protein participates in TFIIIB assembly on tRNA genes. *Nucl Acids Res* **20**, 6451–6454. doi:10.1093/nar/20.24.6451

Hunter C. A., Aukerman M. J., Sun H., Fokina M., and Poethig R. S. (2003). *PAUSED* Encodes the Arabidopsis Exportin-t Ortholog. *Plant Physiol.* **132**, 2135–2143. doi:10.1104/pp.103.023309

Hurt D. J., Wang S. S., Lin Y. H., and Hopper A. K. (1987). Cloning and characterization of LOS1, a Saccharomyces cerevisiae gene that affects tRNA splicing. *Mol. Cell. Biol.* **7**, 1208–1216. doi:10.1128/MCB.7.3.1208

Hutten S., and Kehlenbach R. H. (2007). CRM1-mediated nuclear export: to the pore and beyond. *Trends in Cell Biology* **17**, 193–201. doi:10.1016/j.tcb.2007.02.003

Huynh L.-N., Thangavel M., Chen T., Cottrell R., Mitchell J. M., and Prætorius-Ibba M. (2010). Linking tRNA localization with activation of nutritional stress responses. *Cell Cycle* **9**, 3184–3190. doi:10.4161/cc.9.15.12525

Hyun H. S., Kim S. H., Park E., Cho M. H., Kang H. G., Lee H. S., Miyake N., Matsumoto N., Tsukaguchi H., and Cheong H. I. (2018). A familial case of Galloway-Mowat syndrome due to a novel TP53RK mutation: a case report. *BMC Med Genet* **19**, 131. doi:10.1186/s12881-018-0649-y

Ichimura K., Kurihara H., and Sakai T. (2003). Actin Filament Organization of Foot Processes in Rat Podocytes. *J Histochem Cytochem.* **51**, 1589–1600. doi:10.1177/002215540305101203

Intine R. V. A., Sakulich A. L., Koduru S. B., Huang Y., Pierstorff E., Goodier J. L., Phan L., and Maraia R. J. (2000). Control of Transfer RNA Maturation by Phosphorylation of the Human La Antigen on Serine 366. *Molecular Cell* **6**, 339–348. doi:10.1016/S1097-2765(00)00034-4

Ivanov P., Emara M. M., Villen J., and Gygi S. P. (2012). Angiogenin-induced tRNA fragments inhibit translation initiation. *Mol Cell.* **43**, 613–23. doi:10.1016/j.molcel.2011.06.022

Jackman J. E., and Alfonzo J. D. (2013). Transfer RNA modifications: nature's combinatorial chemistry playground: Transfer RNA modifications. *WIREs RNA* **4**, 35–48. doi:10.1002/wrna.1144

Jia F., Wilson K. D., Sun N., Gupta D. M., Huang M., Li Z., Panetta N. J., Chen Z. Y., Robbins R. C., Kay M. A., Longaker M. T., and Wu J. C. (2010). A nonviral minicircle vector for deriving human iPS cells. *Nat Methods* **7**, 197–199. doi:10.1038/nmeth.1426

Jinek M., Chylinski K., Fonfara I., Hauer M., Doudna J. A., and Charpentier E. (2012). A Programmable Dual-RNA-Guided DNA Endonuclease in Adaptive Bacterial Immunity. *Science* **337**, 816–821. doi:10.1126/science.1225829

Jinks R. N., Puffenberger E. G., Baple E., Harding B., Crino P., Fogo A. B., Wenger O., Xin B., Koehler A. E., McGlincy M. H., Provencher M. M., Smith J. D., Tran L., Al Turki S., Chioza B. A., Cross H., Harlalka G. V., Hurles M. E., Maroofian R., Heaps A. D., Morton M. C., Stempak L., Hildebrandt F., Sadowski C. E., Zaritsky J., Campellone K., Morton D. H., Wang H., Crosby A., and Strauss K. A. (2015). Recessive nephrocerebellar syndrome on the Galloway-Mowat syndrome spectrum is caused by homozygous protein-truncating mutations of *WDR73*. *Brain* **138**, 2173–2190. doi:10.1093/brain/awv153

Jones N., Blasutig I. M., Eremina V., Ruston J. M., Bladt F., Li H., Huang H., Larose L., Li S. S.-C., Takano T., Quaggin S. E., and Pawson T. (2006). Nck adaptor proteins link nephrin to the actin cytoskeleton of kidney podocytes. *Nature* **440**, 818–823. doi:10.1038/nature04662

Juan T., Véniant M. M., Helmering J., Babij P., Baker D. M., Damore M. A., Bass M. B., Gyuris T., Chhoa M., Li C.-M., Ebeling C., Amato J., Carlson G. A., and Lloyd D. J. (2009). Identification of three loci affecting HDL-cholesterol levels in a screen for chemically induced recessive mutations in mice. *Journal of Lipid Research* **50**, 534–545. doi:10.1194/jlr.M800471-JLR200

Kadaba S. (2004). Nuclear surveillance and degradation of hypomodified initiator tRNAMet in S. cerevisiae. *Genes & Development* **18**, 1227–1240. doi:10.1101/gad.1183804

Kalluri R. (2006). Proteinuria with and without Renal Glomerular Podocyte Effacement. *JASN* **17**, 2383–2389. doi:10.1681/ASN.2006060628

Kaplan J. M., Kim S. H., North K. N., Rennke H., Correia L. A., Tong H.-Q., Mathis B. J., Rodríguez-Pérez J.-C., Allen P. G., Beggs A. H., and Pollak M. R. (2000). Mutations in ACTN4, encoding α-actinin-4, cause familial focal segmental glomerulosclerosis. *nature genetics* **24**, 6.

Kapur M., Monaghan C. E., and Ackerman S. L. (2017). Regulation of mRNA Translation in Neurons—A Matter of Life and Death. *Neuron* **96**, 616–637. doi:10.1016/j.neuron.2017.09.057

Karaca E. (2014). Human CLP1 Mutations Alter tRNA Biogenesis, Affecting Both Peripheral and Central Nervous System Function. *Cell* **157**, 636–50. doi:10.1016/j.cell.2014.02.058

Karnovsky M., and Ryan G. (1975). Substructure of the glomerular slit diaphragm in freeze-fractured normal rat kidney. *Journal of Cell Biology* **65**, 233–236. doi:10.1083/jcb.65.1.233

Kasher P. R., Namavar Y., van Tijn P., Fluiter K., Sizarov A., Kamermans M., Grierson A. J., Zivkovic D., and Baas F. (2011). Impairment of the tRNA-splicing endonuclease subunit 54 (tsen54) gene causes neurological abnormalities and larval death in zebrafish models of pontocerebellar hypoplasia. *Human Molecular Genetics* **20**, 1574–1584. doi:10.1093/hmg/ddr034

Kawachi H. (2000). Cloning of rat nephrin: Expression in developing glomeruli and in proteinuric states. *Kidney Int.* **57**, 1949–61. doi:10.1046/j.1523-1755.2000.00044.x

Kawaji H., Nakamura M., Takahashi Y., Sandelin A., Katayama S., Fukuda S., Daub C. O., Kai C., Kawai J., Yasuda J., Carninci P., and Hayashizaki Y. (2008). Hidden layers of human small RNAs. *BMC Genomics* **9**,. doi:10.1186/1471-2164-9-157

Kerjaschki D., Sharkey D. J., and Farquhar M. G. (1984). Identification and characterization of podocalyxin--the major sialoprotein of the renal glomerular epithelial cell. *Journal of Cell Biology* **98**, 1591–1596. doi:10.1083/jcb.98.4.1591

Kessler A. C., Silveira d'Almeida G., and Alfonzo J. D. (2018). The role of intracellular compartmentalization on tRNA processing and modification. *RNA Biology* **15**, 554–566. doi:10.1080/15476286.2017.1371402

Kestila M., and Lenkkeri U. (1998). Positionally Cloned Gene for a Novel Glomerular Protein—Nephrin—Is Mutated in Congenital Nephrotic Syndrome. *Molecular Cell* **1**, 575–82. doi:10.1016/s1097-2765(00)80057-x

Kim J. S., Bellew C. A., Silverstein D. M., Aviles D. H., Boineau F. G., and Vehaskari V. M. (2005). High incidence of initial and late steroid resistance in childhood nephrotic syndrome. *Kidney International* **68**, 1275–1281. doi:10.1111/j.1523-1755.2005.00524.x

Kim Y. K., Refaeli I., Brooks C. R., Jing P., Gulieva R. E., Hughes M. R., Cruz N. M., Liu Y., Churchill A. J., Wang Y., Fu H., Pippin J. W., Lin L. Y., Shankland S. J., Vogl A. W., McNagny K. M., and Freedman B. S. (2017). Gene-Edited Human Kidney Organoids Reveal Mechanisms of Disease in Podocyte Development: Podocyte Development and Disease in Organoids. *Stem Cells* **35**, 2366–2378. doi:10.1002/stem.2707

Konevega A. L., Soboleva N. G., Makhno V. I., Semenkov Y. P., Wintermeyer W., Rodnina M. V., and Katunin V. I. (2004). Purine bases at position 37 of tRNA stabilize codon–anticodon interaction in the ribosomal A site by stacking and Mg2+-dependent interactions. *RNA* **10**, 90–101. doi:10.1261/rna.5142404

Kraemer N., Ravindran E., Zaqout S., Neubert G., Schindler D., Ninnemann O., Gräf R., Seiler A. E., and Kaindl A. M. (2015). Loss of CDK5RAP2 affects neural but not non-neural mESC differentiation into cardiomyocytes. *Cell Cycle* **14**, 2044–2057. doi:10.1080/15384101.2015.1044169

Kretzler M. (2002). Regulation of adhesive interaction between podocytes and glomerular basement membrane. *Microsc. Res. Tech.* **57**, 247–253. doi:10.1002/jemt.10083

Kriz W., Hackenthal E., Nobiling R., Sakai T., Elger M., and Hähnel B. (1994). A role for podocytes to counteract capillary wall distension. *Kidney International* **45**, 369–376. doi:10.1038/ki.1994.47

Kriz W., Shirato I., Nagata M., LeHir M., and Lemley K. V. (2013). The podocyte's response to stress: the enigma of foot process effacement. *American Journal of Physiology-Renal Physiology* **304**, F333–F347. doi:10.1152/ajprenal.00478.2012

Kuersten S., Arts G.-J., Walther T. C., Englmeier L., and Mattaj I. W. (2002). Steady-State Nuclear Localization of Exportin-t Involves RanGTP Binding and Two Distinct Nuclear Pore Complex Interaction Domains. *MCB* **22**, 5708–5720. doi:10.1128/MCB.22.16.5708-5720.2002

Kumar P., Mudunuri S. B., Anaya J., and Dutta A. (2015). tRFdb: a database for transfer RNA fragments. *Nucleic Acids Research* **43**, D141–D145. doi:10.1093/nar/gku1138

Kutay U., Lipowsky G., Izaurralde E., Bischoff F. R., Schwarzmaier P., and Hartmann E. (1998). Identification of a tRNA-Specific Nuclear Export Receptor. *Molecular Cell* **1**, 359–69. doi:10.1016/s1097-2765(00)80036-2

Lahdenperä J., Kilpeläinen P., Liu X. L., Pikkarainen T., Reponen P., Ruotsalainen V., and Tryggvason K. (2003). Clustering-induced tyrosine phosphorylation of nephrin by Src family kinases11See Editorial by Mathieson, p. 756. *Kidney International* **64**, 404–413. doi:10.1046/j.1523-1755.2003.00097.x

Lancaster M. A., Renner M., Martin C.-A., Wenzel D., Bicknell L. S., Hurles M. E., Homfray T., Penninger J. M., Jackson A. P., and Knoblich J. A. (2013). Cerebral organoids model human brain development and microcephaly. *Nature* **501**, 373–379. doi:10.1038/nature12517

Lauhon C. T. (2012). Mechanism of N6-Threonylcarbamoyladenonsine (t ^{6} A) Biosynthesis: Isolation and Characterization of the Intermediate Threonylcarbamoyl-AMP. *Biochemistry* **51**, 8950–8963. doi:10.1021/bi301233d

Lawrence M. G., Altenburg M. K., Sanford R., Willett J. D., Bleasdale B., Ballou B., Wilder J., Li F., Miner J. H., Berg U. B., and Smithies O. (2017). Permeation of macromolecules into the renal glomerular basement membrane and capture by the tubules. *Proc Natl Acad Sci USA* **114**, 2958–2963. doi:10.1073/pnas.1616457114

Lee Y. S., Shibata Y., Malhotra A., and Dutta A. (2009). A novel class of small RNAs: tRNA-derived RNA fragments (tRFs). *Genes Dev.* **23**, 2639–2649. doi:10.1101/gad.1837609

Lehtonen S., Lehtonen E., Kudlicka K., Holthöfer H., and Farquhar M. G. (2004). Nephrin Forms a Complex with Adherens Junction Proteins and CASK in Podocytes and in Madin-Darby Canine Kidney Cells Expressing Nephrin. *The American Journal of Pathology* **165**, 923–936. doi:10.1016/S0002-9440(10)63354-8

Lennon R., Randles M. J., and Humphries M. J. (2014). The Importance of Podocyte Adhesion for a Healthy Glomerulus. *Front. Endocrinol.* **5**,. doi:10.3389/fendo.2014.00160

Li H. (2004). Src-Family Kinase Fyn Phosphorylates the Cytoplasmic Domain of Nephrin and Modulates Its Interaction with Podocin. *Journal of the American Society of Nephrology* **15**, 3006–3015. doi:10.1097/01.ASN.0000146689.88078.80

Li J., and Chen X. (2003). *PAUSED* , a Putative Exportin-t, Acts Pleiotropically in Arabidopsis Development But Is Dispensable for Viability. *Plant Physiol.* **132**, 1913–1924. doi:10.1104/pp.103.023291

Li S., Liu Y., He X., Luo X., Shi H., Qu G., Wen X., Gan W., Wang J., and Zhang A. (2020). tRNA-Derived Fragments in Podocytes with Adriamycin-Induced Injury Reveal the Potential Mechanism of Idiopathic Nephrotic Syndrome. *BioMed Research International* **2020**, 1–12. doi:10.1155/2020/7826763

Li C., Ruotsalainen V., Tryggvason K., Shaw A. S., and Miner J. H. (2000). CD2AP is expressed with nephrin in developing podocytes and is found widely in mature kidney and elsewhere. *Am J Physiol Renal Physiol.* **279**, F785-92. doi:10.1152/ajprenal.2000.279.4.F785

Li S., and Sprinzl M. (2006). Interaction of Immobilized Human Exportin-t with Calf Liver tRNA. *RNA Biology* **3**, 145–149. doi:10.4161/rna.3.4.3679

Li S., Xu Z., and Sheng J. (2018). tRNA-Derived Small RNA: A Novel Regulatory Small Non-Coding RNA. 15.

Lipowsky G., Bischoff F. R., Izaurralde E., Kutay U., Schäfer S., Gross H. J., Beier H., and Görlich D. (1999). Coordination of tRNA nuclear export with processing of tRNA. *RNA* **5**, 539–549. doi:10.1017/S1355838299982134

Lopes R. R. S., Kessler A. C., Polycarpo C., and Alfonzo J. D. (2015). Cutting, dicing, healing and sealing: the molecular surgery of tRNA: Molecular surgery of tRNA. *WIREs RNA* **6**, 337–349. doi:10.1002/wrna.1279

Lund E. (1998). Proofreading and Aminoacylation of tRNAs Before Export from the Nucleus. *Science* **282**, 2082–2085. doi:10.1126/science.282.5396.2082

Mann N., Mzoughi S., Schneider R., Kühl S. J., Schanze D., Klämbt V., Lovric S., Mao Y., Shi S., Tan W., Kühl M., Onuchic-Whitford A. C., Treimer E., Kitzler T. M., Kause F., Schumann S., Nakayama M., Buerger F., and Shril S. (2021). Mutations in PRDM15 Are a Novel Cause of Galloway-Mowat Syndrome. *J Am Soc Nephrol.* **32**, 580–596. doi:10.1681/ASN.2020040490

Maraş-Genç H., Uyur-Yalçın E., Rosti R. Ö., Gleeson J. G., and Kara B. (2015). TSEN54 gene-related pontocerebellar hypoplasia type 2 presenting with exaggerated startle response: report of two cases in a family. *Turk J Pediatr* **57**, 286–9.

Marraffini L. A. (2013). CRISPR-Cas Immunity against Phages: Its Effects on the Evolution and Survival of Bacterial Pathogens (J Heitman, Ed.). *PLoS Pathog* **9**, e1003765. doi:10.1371/journal.ppat.1003765

Mathew S., Chen X., Pozzi A., and Zent R. (2012). Integrins in renal development. *Pediatr Nephrol* 10.

Maute R. L., Schneider C., Sumazin P., Holmes A., Califano A., Basso K., and Dalla-Favera R. (2013). tRNA-derived microRNA modulates proliferation and the DNA damage response and is down-regulated in B cell lymphoma. *Proc Natl Acad Sci USA* **110**, 1404–1409. doi:10.1073/pnas.1206761110

Meng X. (2012). Efficient Reprogramming of Human Cord Blood CD34+ Cells Into Induced Pluripotent Stem Cells With OCT4 and SOX2 Alone. *Cell Therapy* **20**, 408–16. doi:10.1038/mt.2011.258

Meyers K. E. C., Kaplan P., and Kaplan B. S. (1999). Nephrotic syndrome, microcephaly, and developmental delay: Three separate syndromes. *Am J Med Genet.* **82**, 257–60.

Miyagawa R., Mizuno R., Watanabe K., and Ijiri K. (2012). Formation of tRNA granules in the nucleus of heat-induced human cells. *Biochemical and Biophysical Research Communications* **418**, 149–155. doi:10.1016/j.bbrc.2011.12.150

Miyake N., Tsukaguchi H., Koshimizu E., Shono A., Matsunaga S., Shiina M., Mimura Y., Imamura S., Hirose T., Okudela K., Nozu K., Akioka Y., Hattori M., Yoshikawa N., Kitamura A., Cheong H. I., Kagami S., Yamashita M., Fujita A., Miyatake S., Tsurusaki Y., Nakashima M., Saitsu H., Ohashi K., Imamoto N., Ryo A., Ogata K., Iijima K., and Matsumoto N. (2015). Biallelic Mutations in Nuclear Pore Complex Subunit NUP107 Cause Early-Childhood-Onset Steroid-Resistant Nephrotic Syndrome. *The American Journal of Human Genetics* **97**, 555–566. doi:10.1016/j.ajhg.2015.08.013

Mo D. (2019). A tRNA fragment, 5′-tiRNAVal, suppresses the Wnt/β-catenin signaling pathway by targeting FZD3 in breast cancer. *Cancer Letters* **457**, 60–73. doi:10.1016/j.canlet.2019.05.007

Moqtaderi Z., Wang J., Raha D., White R. J., Snyder M., Weng Z., and Struhl K. (2010). Genomic binding profiles of functionally distinct RNA polymerase III transcription complexes in human cells. *Nat Struct Mol Biol* **17**, 635–640. doi:10.1038/nsmb.1794

Morchoisne-Bolhy S., Geoffroy M.-C., Bouhlel I. B., Alves A., Audugé N., Baudin X., Van Bortle K., Powers M. A., and Doye V. (2015). Intranuclear dynamics of the Nup107-160 complex (K Weis, Ed.). *MBoC* **26**, 2343–2356. doi:10.1091/mbc.E15-02-0060

Morizane R., Lam A. Q., Freedman B. S., Kishi S., Valerius M. T., and Bonventre J. V. (2015). Nephron organoids derived from human pluripotent stem cells model kidney development and injury. *Nat Biotechnol* **33**, 1193–1200. doi:10.1038/nbt.3392

Nagaike T., Suzuki T., Tomari Y., Takemoto-Hori C., Negayama F., Watanabe K., and Ueda T. (2001). Identification and Characterization of Mammalian Mitochondrial tRNA nucleotidyltransferases. *J. Biol. Chem.* **276**, 40041–40049. doi:10.1074/jbc.M106202200

Namavar Y., Barth P. G., Kasher P. R., van Ruissen F., and Brockmann K. (2011). Clinical, neuroradiological and genetic findings in pontocerebellar hypoplasia. *Brain* **134**, 143–56. doi:10.1093/brain/awq287

Namavar Y., Barth P. G., Poll-The B., and Baas F. (2011). Classification, diagnosis and potential mechanisms in Pontocerebellar Hypoplasia. *Orphanet J Rare Dis* **6**, 50. doi:10.1186/1750-1172-6-50

Namavar Y., Chitayat D., Barth P. G., van Ruissen F., de Wissel M. B., Poll-The B. T., Silver R., and Baas F. (2011). TSEN54 mutations cause pontocerebellar hypoplasia type 5. *Eur J Hum Genet* **19**, 724–726. doi:10.1038/ejhg.2011.8

Navarro-Betancourt J. R., Papillon J., Guillemette J., Iwawaki T., Chung C.-F., and Cybulsky A. V. (2020). Role of IRE1α in podocyte proteostasis and mitochondrial health. *Cell Death Discov.* **6**, 128. doi:10.1038/s41420-020-00361-4

Nishi S., Ubara Y., Utsunomiya Y., Okada K., Obata Y., Kai H., Kiyomoto H., Goto S., Konta T., Sasatomi Y., Sato Y., Nishino T., Tsuruya K., Furuichi K., Hoshino J., Watanabe Y., Kimura K., and Matsuo S. (2016). Evidence-based clinical practice guidelines for nephrotic syndrome 2014. *Clin Exp Nephrol* **20**, 342–370. doi:10.1007/s10157-015-1216-x

Oberto J., Breuil N., Hecker A., Farina F., Brochier-Armanet C., Culetto E., and Forterre P. (2009). Qri7/OSGEPL, the mitochondrial version of the universal Kae1/YgjD protein, is essential for mitochondrial genome maintenance. *Nucleic Acids Research* **37**, 5343–5352. doi:10.1093/nar/gkp557

Ohira T., and Suzuki T. (2011). Retrograde nuclear import of tRNA precursors is required for modified base biogenesis in yeast. *Proceedings of the National Academy of Sciences* **108**, 10502–10507. doi:10.1073/pnas.1105645108

Ohmori T., De S., Tanigawa S., Miike K., Islam M., Soga M., Era T., Shiona S., Nakanishi K., Nakazato H., and Nishinakamura R. (2021). Impaired NEPHRIN localization in kidney organoids derived from nephrotic patient iPS cells. *Sci Rep* **11**, 3982. doi:10.1038/s41598-021-83501-9

Okita K., Nakagawa M., Hyenjong H., Ichisaka T., and Yamanaka S. (2008). Generation of Mouse Induced Pluripotent Stem Cells Without Viral Vectors. *Science* **322**, 949–953. doi:10.1126/science.1164270

Ozanick S. G., Wang X., Costanzo M., Brost R. L., Boone C., and Anderson J. T. (2009). Rex1p deficiency leads to accumulation of precursor initiator tRNAMet and polyadenylation of substrate RNAs in Saccharomyces cerevisiae. *Nucleic Acids Research* **37**, 298–308. doi:10.1093/nar/gkn925

Pankratz M. T., Li X.-J., LaVaute T. M., Lyons E. A., Chen X., and Zhang S.-C. (2007). Directed Neural Differentiation of Human Embryonic Stem Cells via an Obligated Primitive Anterior Stage. *Stem Cells* **25**, 1511–1520. doi:10.1634/stemcells.2006-0707

Park M. Y., Wu G., Gonzalez-Sulser A., Vaucheret H., and Poethig R. S. (2005). Nuclear processing and export of microRNAs in Arabidopsis. *Proceedings of the National Academy of Sciences* **102**, 3691–3696. doi:10.1073/pnas.0405570102

Patel M. S., Becker L. E., Toi A., Armstrong D. L., and Chitayat D. (2006). Severe, fetal-onset form of olivopontocerebellar hypoplasia in three sibs: PCH type 5? *Am. J. Med. Genet.* **140A**, 594–603. doi:10.1002/ajmg.a.31095

Paushkin S. V., Patel M., Furia B. S., Peltz S. W., and Trotta C. R. (2004). Identification of a Human Endonuclease Complex Reveals a Link between tRNA Splicing and Pre-mRNA 3′ End Formation. *Cell* **117**, 311–321. doi:10.1016/S0092-8674(04)00342-3

Pavenstädt H. (1998). The Charge for Going by Foot: Modifying the Surface of Podocytes. *Nephron Exp Nephrol* **6**, 98–103. doi:10.1159/000020511

Pavenstädt H., Kriz W., and Kretzler M. (2003). Cell Biology of the Glomerular Podocyte. *Physiological Reviews* **83**, 253–307. doi:10.1152/physrev.00020.2002

Peebles C. L., Gegenheimer P., and Abelson J. (1983). Precise excision of intervening sequences from precursor tRNAs by a membrane-associated yeast endonuclease. *Cell* **32**, 525–536. doi:10.1016/0092-8674(83)90472-5

Pelletier J., Haber D. A., and Glaser T. (1991). WT1 mutations contribute to abnormal genital system development and hereditary Wilms' tumour. *Nature.* **353**, 431–4. doi:10.1038/353431a0

Perez E. E., Wang J., Miller J. C., Jouvenot Y., Kim K. A., Liu O., Wang N., Lee G., Bartsevich V. V., Lee Y.-L., Guschin D. Y., Rupniewski I., Waite A. J., Carpenito C., Carroll R. G., S Orange J., Urnov F. D., Rebar E. J., Ando D., Gregory P. D., Riley J. L., Holmes M. C., and June C. H. (2008). Establishment of HIV-1 resistance in CD4+ T cells by genome editing using zinc-finger nucleases. *Nat Biotechnol* **26**, 808–816. doi:10.1038/nbt1410

Perico L. (2016). Podocyte–actin dynamics in health and disease. *Nat Rev Nephrol.* **12**, 692–710. doi:10.1038/nrneph.2016.127

Peterson D., Lee J., Lei X. C., Forrest W. F., Davis D. P., Jackson P. K., and Belmont L. D. (2010). A Chemosensitization Screen Identifies TP53RK, a Kinase that Restrains Apoptosis after Mitotic Stress. *Cancer Research* **70**, 6325–35. doi:10.1158/0008-5472.CAN-10-0015

Pezzella M., Yeghiazaryan N. S., Veggiotti P., Bettinelli A., Giudizioso G., Zara F., Striano P., and Minetti C. (2010). Galloway–Mowat syndrome: An early-onset progressive encephalopathy with intractable epilepsy associated to renal impairment. Two novel cases and review of literature. *Seizure* **19**, 132–135. doi:10.1016/j.seizure.2009.12.002

Popow J., Englert M., Weitzer S., Schleiffer A., Mierzwa B., Mechtler K., Trowitzsch S., Will C. L., Luhrmann R., Soll D., and Martinez J. (2011). HSPC117 Is the Essential Subunit of a Human tRNA Splicing Ligase Complex. *Science* **331**, 760–764. doi:10.1126/science.1197847

Ramirez A., Shuman S., and Schwer B. (2008). Human RNA 5'-kinase (hClp1) can function as a tRNA splicing enzyme in vivo. *RNA* **14**, 1737–1745. doi:10.1261/rna.1142908

Ran F. A., Hsu P. D., Wright J., Agarwala V., and Zhang F. (2013). Genome engineering using the CRISPR-Cas9 system. *Nat Protoc.* **8**, 2281–2308. doi:10.1038/nprot.2013.143

Rauhut R., Green P. R., and Abelson J. (1990). Yeast tRNA-splicing endonuclease is a heterotrimeric enzyme. *Journal of Biological Chemistry* **265**, 18180–18184. doi:10.1016/S0021-9258(17)44735-1

Reiser J., Kriz W., Kretzler M., and Mundel P. (2000). The Glomerular Slit Diaphragm Is a Modified Adherens Junction. *J Am Soc Nephrol* 8.

Robertson H. D., Altman S., and Smith J. D. (1972). Purification and Properties of a Specific Escherichia coli Ribonuclease which Cleaves a Tyrosine Transfer Ribonucleic Acid Precursor. *Journal of Biological Chemistry* **247**, 5243–5251. doi:10.1016/S0021-9258(19)44963-6

Robertus J. D., Ladner J. E., Finch J. T., Rhodes D., Brown R. S., Clark B. F. C., and Klug A. (1974). Structure of yeast phenylalanine tRNA at 3 Å resolution. *Nature* **250**, 546–551. doi:10.1038/250546a0

Rodewald R., and Karnovsky M. J. (1974). Porous substructure of the glomerular slit diaphragm in the rat and mouse. *J Cell Biol.* **60**, 423–33. doi:10.1083/jcb.60.2.423

Rosti R. O., Dikoglu E., Zaki M. S., Abdel-Salam G., Makhseed N., Sese J. C., Musaev D., Rosti B., Harbert M. J., Jones M. C., Vaux K. K., and Gleeson J. G. (2016). Extending the mutation spectrum for Galloway-Mowat syndrome to include homozygous missense mutations in the WDR73 gene. *Am. J. Med. Genet.* **170**, 992–998. doi:10.1002/ajmg.a.37533

Rosti R. O., Sotak B. N., Bielas S. L., Bhat G., Silhavy J. L., Aslanger A. D., Altunoglu U., Bilge I., Tasdemir M., Yzaguirrem A. D., Musaev D., Infante S., Thuong W., Marin-Valencia I., Nelson S. F., Kayserili H., and Gleeson J. G. (2017). Homozygous mutation in *NUP107* leads to microcephaly with steroid-resistant nephrotic condition similar to Galloway-Mowat syndrome. *J Med Genet* **54**, 399–403. doi:10.1136/jmedgenet-2016-104237

Rudaks L. I., Moore L., Shand K. L., Wilkinson C., and Barnett C. P. (2011). Novel TSEN54 Mutation Causing Pontocerebellar Hypoplasia Type 4. *Pediatric Neurology* **45**, 185–188. doi:10.1016/j.pediatrneurol.2011.05.009

Ruf R. G., Schultheiss M., Lichtenberger A., Karle S. M., Zalewski I., Mucha B., Everding A. S., Neuhaus T., Patzer L., Plank C., Haas J. P., Ozaltin F., Imm A., Fuchshuber A., Bakkaloglu A., and Hildebrandt F. (2004). Prevalence of WT1 mutations in a large cohort of patients with steroid-resistant and steroid-sensitive nephrotic syndrome. *Kidney International* **66**, 564–570. doi:10.1111/j.1523-1755.2004.00775.x

Ruotsalainen V., Ljungberg P., Wartiovaara J., Lenkkeri U., Kestila M., Jalanko H., Holmberg C., and Tryggvason K. (1999). Nephrin is specifically located at the slit diaphragm of glomerular podocytes. *Proceedings of the National Academy of Sciences* **96**, 7962–7967. doi:10.1073/pnas.96.14.7962

Sadowski C. E., Lovric S., Ashraf S., Pabst W. L., Gee H. Y., Kohl S., Engelmann S., Vega-Warner V., Fang H., Halbritter J., Somers M. J., Tan W., Shril S., Fessi I., Lifton R. P., Bockenhauer D., El-Desoky S., Kari J. A., Zenker M., Kemper M. J., Mueller D., Fathy H. M., Soliman N. A., the SRNS Study Group, and Hildebrandt F. (2015). A Single-Gene Cause in 29.5% of Cases of Steroid-Resistant Nephrotic Syndrome. *JASN* **26**, 1279–1289. doi:10.1681/ASN.2014050489

Sahali D., Audard V., Rémy P., and Lang P. (2012). Syndromes néphrotiques idiopathiques : physiopathologie et prise en charge thérapeutique spécifique chez l'adulte. *Néphrologie & Thérapeutique* **8**, 180–192. doi:10.1016/j.nephro.2011.11.010

Saikia M., Krokowski D., Guan B.-J., Ivanov P., Parisien M., Hu G., Anderson P., Pan T., and Hatzoglou M. (2012). Genome-wide Identification and Quantitative Analysis of Cleaved tRNA Fragments Induced by Cellular Stress. *J Biol Chem.* **287**, 42708–25. doi:10.1074/jbc.M112.371799

Saleem M. A., O'Hare M. J., Reiser J., Coward R. J., Inward C. D., Farren T., Xing C. Y., Ni L., Mathieson P. W., and Mundel P. (2002). A Conditionally Immortalized Human Podocyte Cell Line Demonstrating Nephrin and Podocin Expression. *JASN* **13**, 630–638. doi:10.1681/ASN.V133630

Sánchez-Albisua I., Frölich S., Barth P. G., Steinlin M., and Krägeloh-Mann I. (2014). Natural course of pontocerebellar hypoplasia type 2A. *Orphanet J Rare Dis* **9**, 70. doi:10.1186/1750-1172-9-70

Sanna-Cherchi S., Reese A., Hensle T., Caridi G., Izzi C., Kim Y. Y., Konka A., Murer L., Scolari F., Ravazzolo R., Ghiggeri G. M., and Gharavi A. G. (2005). Familial Vesicoureteral Reflux: Testing Replication of Linkage in Seven New Multigenerational Kindreds. *JASN* **16**, 1781–1787. doi:10.1681/ASN.2004121034

Sarkar S., and Hopper A. K. (1998). tRNA Nuclear Export in *Saccharomyces cerevisiae* : In Situ Hybridization Analysis (PA Silver, Ed.). *MBoC* **9**, 3041–3055. doi:10.1091/mbc.9.11.3041

Sartelet H., Pietrement C., Birembaut P., Oligny L. L., Roussel B., and Doco-Fenzy M. (2008). Collapsing glomerulopathy in Galloway–Mowat syndrome: A case report and review of the literature. *Pathol Res Pract.* **204**, 401–6. doi:10.1016/j.prp.2007.12.007

Satchell S. C., and Braet F. (2009). Glomerular endothelial cell fenestrations: an integral component of the glomerular filtration barrier. *American Journal of Physiology-Renal Physiology* **296**, F947–F956. doi:10.1152/ajprenal.90601.2008

Sawaya R., Schwer B., and Shuman S. (2003). Genetic and Biochemical Analysis of the Functional Domains of Yeast tRNA Ligase. *J. Biol. Chem.* **278**, 43928–43938. doi:10.1074/jbc.M307839200

Schaffer A. E., Eggens V. R. C., Caglayan A. O., Reuter M. S., Scott E., Coufal N. G., Silhavy J. L., Xue Y., Kayserili H., Yasuno K., Rosti R. O., Abdellateef M., Caglar C., Kasher P. R., Cazemier J. L., Weterman M. A., Cantagrel V., Cai N., Zweier C., Altunoglu U., Satkin N. B., Aktar F., Tuysuz B., Yalcinkaya C., Caksen H., Bilguvar K., Fu X.-D., Trotta C. R., Gabriel S., Reis A., Gunel M., Baas F., and Gleeson J. G. (2014). CLP1 Founder Mutation Links tRNA Splicing and Maturation to Cerebellar Development and Neurodegeneration. *Cell* **157**, 651–663. doi:10.1016/j.cell.2014.03.049

Schiffer S. (2002). Assigning a function to a conserved group of proteins: the tRNA 3'-processing enzymes. *The EMBO Journal* **21**, 2769–2777. doi:10.1093/emboj/21.11.2769

Schmidt C. A., Giusto J. D., Bao A., Hopper A. K., and Matera A. G. (2019). Molecular determinants of metazoan tricRNA biogenesis. *Nucleic Acids Research* **47**, 6452–6465. doi:10.1093/nar/gkz311

Schnabel E., Anderson J. M., and Farquhar M. G. (1990). The tight junction protein ZO-1 is concentrated along slit diaphragms of the glomerular epithelium. *Journal of Cell Biology* **111**, 1255–1263. doi:10.1083/jcb.111.3.1255

Schramm L. (2002). Recruitment of RNA polymerase III to its target promoters. *Genes & Development* **16**, 2593–2620. doi:10.1101/gad.1018902

Sekulovski S., Devant P., Panizza S., Gogakos T., Pitiriciu A., Heitmeier K., Ramsay E. P., Barth M., Schmidt C., Weitzer S., Tuschl T., Baas F., Martinez J., and Trowitzsch S. (2020). Assembly defects of the human tRNA splicing endonuclease contribute to impaired pre-tRNA processing in pontocerebellar hypoplasia. Biochemistry, preprint doi:10.1101/2020.08.03.234229

Shaheen R., Abdel-Salam G. M. H., Guy M. P., Alomar R., Abdel-Hamid M. S., Afifi H. H., Ismail S. I., Emam B. A., Phizicky E. M., and Alkuraya F. S. (2015). Mutation in WDR4 impairs tRNA m7G46 methylation and causes a distinct form of microcephalic primordial dwarfism. *Genome Biol* **16**, 210. doi:10.1186/s13059-015-0779-x

Shaheen H. H., and Hopper A. K. (2005). Retrograde movement of tRNAs from the cytoplasm to the nucleus in Saccharomyces cerevisiae. *Proceedings of the National Academy of Sciences* **102**, 11290–11295. doi:10.1073/pnas.0503836102

Shi H., Yu M., Wu Y., Cao Y., Li S., Qu G., Gong J., Gan W., and Zhang A. (2020). tRNA-derived fragments (tRFs) contribute to podocyte differentiation. *Biochemical and Biophysical Research Communications* **521**, 1–8. doi:10.1016/j.bbrc.2019.09.009

Shibata S., Sasaki M., Miki T., Shimamoto A., Furuichi Y., Katahira J., and Yoneda Y. (2006). Exportin-5 orthologues are functionally divergent among species. *Nucleic Acids Research* **34**, 4711–4721. doi:10.1093/nar/gkl663

Soldner F., Hockemeyer D., Beard C., Gao Q., Bell G. W., Cook E. G., Hargus G., Blak A., Cooper O., Mitalipova M., Isacson O., and Jaenisch R. (2009). Parkinson's Disease Patient-Derived Induced Pluripotent Stem Cells Free of Viral Reprogramming Factors. *Cell* **136**, 964–977. doi:10.1016/j.cell.2009.02.013

Sprinzl M., and Cramer F. (1979). The -C-C-A End of tRNA and Its Role in Protein Biosynthesis. 'Progress in Nucleic Acid Research and Molecular Biology'. (Ed WE Cohn) pp. 1–69. (Academic Press) doi:10.1016/S0079-6603(08)60798-9

Srinivasan M., Mehta P., Yu Y., Prugar E., Koonin E. V., Karzai A. W., and Sternglanz R. (2011). The highly conserved KEOPS/EKC complex is essential for a universal tRNA modification, t6A: Proteins essential for a tRNA modification, t6A. *The EMBO Journal* **30**, 873–881. doi:10.1038/emboj.2010.343

Stadtfeld M., Nagaya M., Utikal J., Weir G., and Hochedlinger K. (2008). Induced Pluripotent Stem Cells Generated Without Viral Integration. *Science* **322**, 945–949. doi:10.1126/science.1162494

Stirnimann C. U., Petsalaki E., Russell R. B., and Müller C. W. (2010). WD40 proteins propel cellular networks. *Trends in Biochemical Sciences* **35**, 565–574. doi:10.1016/j.tibs.2010.04.003

Strobel M. C., and Abelson J. (1986). Effect of intron mutations on processing and function of Saccharomyces cerevisiae SUP53 tRNA in vitro and in vivo. *Mol. Cell. Biol.* **6**, 2663–2673. doi:10.1128/MCB.6.7.2663

Suh J. H., and Miner J. H. (2013). The Glomerular Basement Membrane as a Barrier to Albumin. *Nat Rev Nephrol.* **9**, 470–7. doi:10.1038/nrneph.2013.109

Swinehart W. E., and Jackman J. E. (2015). Diversity in mechanism and function of tRNA methyltransferases. *RNA Biology* **12**, 398–411. doi:10.1080/15476286.2015.1008358

Taguchi A., Kaku Y., Ohmori T., Sharmin S., Ogawa M., Sasaki H., and Nishinakamura R. (2014). Redefining the In Vivo Origin of Metanephric Nephron Progenitors Enables Generation of Complex Kidney Structures from Pluripotent Stem Cells. *Cell Stem Cell* **14**, 53–67. doi:10.1016/j.stem.2013.11.010

Tahmasebi S., Khoutorsky A., Mathews M. B., and Sonenberg N. (2018). Translation deregulation in human disease. *Nat Rev Mol Cell Biol* **19**, 791–807. doi:10.1038/s41580-018-0034-x

Takahashi K., Tanabe K., Ohnuki M., Narita M., Ichisaka T., Tomoda K., and Yamanaka S. (2007). Induction of Pluripotent Stem Cells from Adult Human Fibroblasts by Defined Factors. *Cell* **131**, 861–872. doi:10.1016/j.cell.2007.11.019

Takahashi K., and Yamanaka S. (2006). Induction of Pluripotent Stem Cells from Mouse Embryonic and Adult Fibroblast Cultures by Defined Factors. *Cell.* **126**, 663–76. doi:10.1016/j.cell.2006.07.024

Takaku H. (2003). A candidate prostate cancer susceptibility gene encodes tRNA 3' processing endoribonuclease. *Nucleic Acids Research* **31**, 2272–2278. doi:10.1093/nar/gkg337

Takano A., Kajita T., Mochizuki M., Endo T., and Yoshihisa T. (2015). Cytosolic Hsp70 and co-chaperones constitute a novel system for tRNA import into the nucleus. *eLife* **4**, e04659. doi:10.7554/eLife.04659

Takano K., Kawasaki Y., Imaizumi T., Matsuura H., Nozawa R., Tannji M., Suyama K., Isome M., Suzuki H., and Hosoya M. (2007). Development of Glomerular Endothelial Cells, Podocytes and Mesangial Cells in the Human Fetus and Infant. *Tohoku J. Exp. Med.* **212**, 81–90. doi:10.1620/tjem.212.81

Takasato M., Er P. X., Chiu H. S., Maier B., Baillie G. J., Ferguson C., Parton R. G., Wolvetang E. J., and Roost M. S. (2015). Kidney organoids from human iPS cells contain multiple lineages and model human nephrogenesis. *Nature* **526**, 564–8. doi:10.1038/nature15695

Tanaka N., Chakravarty A. K., Maughan B., and Shuman S. (2011). Novel Mechanism of RNA Repair by RtcB via Sequential 2′,3′-Cyclic Phosphodiesterase and 3′-Phosphate/5′-Hydroxyl Ligation Reactions. *J. Biol. Chem.* **286**, 43134–43143. doi:10.1074/jbc.M111.302133

Tanigawa S., Islam M., Sharmin S., Naganuma H., Yoshimura Y., Haque F., Era T., Nakazato H., Nakanishi K., Sakuma T., Yamamoto T., Kurihara H., Taguchi A., and Nishinakamura R. (2018). Organoids from Nephrotic Disease-Derived iPSCs Identify Impaired NEPHRIN Localization and Slit Diaphragm Formation in Kidney Podocytes. *Stem Cell Reports* **11**, 727–740. doi:10.1016/j.stemcr.2018.08.003

Terry L. J., Shows E. B., and Wente S. R. (2007). Crossing the Nuclear Envelope: Hierarchical Regulation of Nucleocytoplasmic Transport. *Science* **318**, 1412–1416. doi:10.1126/science.1142204

Thiaville P. C., Iwata-Reuyl D., and de Crécy-Lagard V. (2014). Diversity of the biosynthesis pathway for threonylcarbamoyladenosine (t^6A), a universal modification of tRNA. *RNA Biology* **11**, 1529–1539. doi:10.4161/15476286.2014.992277

Tilley F. C. (2021). Disruption of pathways regulated by Integrator complex in Galloway–Mowat syndrome due to WDR73 mutations. *Scientific Reports* 13.

Tilley F. C., Arrondel C., Chhuon C., Boisson M., Cagnard N., Parisot M., Menara G., Lefort N., Guerrera I. C., Bole-Feysot C., Benmerah A., Antignac C., and Mollet G. (2021). Disruption of pathways regulated by Integrator complex in Galloway–Mowat syndrome due to WDR73 mutations. *Sci Rep* **11**, 5388. doi:10.1038/s41598-021-84472-7

van Tol H., and Beier H. (1988). All human $tRNA^{Tyr}$ genes contain introns as a prerequisite for pseudouridine biosynthesis in the anticodon. *Nucl Acids Res* **16**, 1951–1966. doi:10.1093/nar/16.5.1951

Toyama K., Morisaki H., Cheng J., Kawachi H., Shimizu F., Ikawa M., Okabe M., and Morisaki T. (2012). Proteinuria in AMPD2-deficient mice: Proteinuria in AMPD2 KO Mice. *Genes to Cells* **17**, 28–38. doi:10.1111/j.1365-2443.2011.01568.x

Trimouille A., Lasseaux E., Barat P., Deiller C., Drunat S., Rooryck C., Arveiler B., and Lacombe D. (2018). Further delineation of the phenotype caused by biallelic variants in the *WDR4* gene: TRIMOUILLE et al. *Clin Genet* **93**, 374–377. doi:10.1111/cge.13074

Trotta C. R., Miao F., Arn E. A., Stevens S. W., Ho C. K., Rauhut R., and Abelson J. N. (1997). The Yeast tRNA Splicing Endonuclease: A Tetrameric Enzyme with Two Active Site Subunits Homologous to the Archaeal tRNA Endonucleases. *Cell* **89**, 849–858. doi:10.1016/S0092-8674(00)80270-6

Trotta C. R., Paushkin S. V., Patel M., Li H., and Peltz S. W. (2006). Cleavage of pre-tRNAs by the splicing endonuclease requires a composite active site. *Nature* **441**, 375–377. doi:10.1038/nature04741

Tyanova S., Temu T., Sinitcyn P., Carlson A., Hein M. Y., Geiger T., Mann M., and Cox J. (2016). The Perseus computational platform for comprehensive analysis of (prote)omics data. *Nat Methods* **13**, 731–740. doi:10.1038/nmeth.3901

Ucuncu E., Rajamani K., Wilson M. S. C., Medina-Cano D., Altin N., David P., Barcia G., Lefort N., Banal C., Vasilache-Dangles M.-T., Pitelet G., Lorino E., Rabasse N., Bieth E., Zaki M. S., Topcu M., Sonmez F. M., Musaev D., Stanley V., Bole-Feysot C., Nitschké P., Munnich A., Bahi-Buisson N., Fossoud C., Giuliano F., Colleaux L., Burglen L., Gleeson J. G., Boddaert N., Saiardi A., and Cantagrel V. (2020). MINPP1 prevents intracellular accumulation of the chelator inositol hexakisphosphate and is mutated in Pontocerebellar Hypoplasia. *Nat Commun* **11**, 6087. doi:10.1038/s41467-020-19919-y

Vainio S., and Lin Y. (2002). Coordinating early kidney development: lessons from gene targeting. *Nat Rev Genet* **3**, 533–543. doi:10.1038/nrg842

Verma R. (2006). Nephrin ectodomain engagement results in Src kinase activation, nephrin phosphorylation, Nck recruitment, and actin polymerization. *Journal of Clinical Investigation* **116**, 1346–1359. doi:10.1172/JCI27414

Verma R., Wharram B., Kovari I., Kunkel R., Nihalani D., Wary K. K., Wiggins R. C., Killen P., and Holzman L. B. (2003). Fyn Binds to and Phosphorylates the Kidney Slit Diaphragm Component Nephrin. *Journal of Biological Chemistry* **278**, 20716–20723. doi:10.1074/jbc.M301689200

Vilchez D., Saez I., and Dillin A. (2014). The role of protein clearance mechanisms in organismal ageing and age-related diseases. *Nat Commun* **5**, 5659. doi:10.1038/ncomms6659

Vodopiutz J., Seidl R., Prayer D., Khan M. I., Mayr J. A., Streubel B., Steiß J.-O., Hahn A., Csaicsich D., Castro C., Assoum M., Müller T., Wieczorek D., Mancini G. M. S., Sadowski C. E., Lévy N., Mégarbané A., Godbole K., Schanze D., Hildebrandt F., Delague V., Janecke A. R., and Zenker M. (2015). *WDR73* Mutations Cause Infantile Neurodegeneration and Variable Glomerular Kidney Disease. *Human Mutation* **36**, 1021–1028. doi:10.1002/humu.22828

Voigts-Hoffmann F., Hengesbach M., Kobitski A. Y., van Aerschot A., Herdewijn P., Nienhaus G. U., and Helm M. (2007). A Methyl Group Controls Conformational Equilibrium in Human Mitochondrial tRNALys. *J Am Chem Soc.* **129**, 13382–3. doi:10.1021/ja075520+

Wan Y., and Hopper A. K. (2018). From powerhouse to processing plant: conserved roles of mitochondrial outer membrane proteins in tRNA splicing. *Genes Dev.* **32**, 1309–1314. doi:10.1101/gad.316257.118

Wan L. C. K., Maisonneuve P., Szilard R. K., Lambert J.-P., Ng T. F., Manczyk N., Huang H., Laister R., Caudy A. A., Gingras A.-C., Durocher D., and Sicheri F. (2017). Proteomic

analysis of the human KEOPS complex identifies C14ORF142 as a core subunit homologous to yeast Gon7. *Nucleic Acids Res* **45**, 805–817. doi:10.1093/nar/gkw1181

Wang P. Z. T., Prasad C., Rodriguez Cuellar C. I., and Filler G. (2018). Nephrological and urological complications of homozygous c.974G>A (p.Arg325Gln) OSGEP mutations. *Pediatr Nephrol* **33**, 2201–2204. doi:10.1007/s00467-018-4060-x

Warren L., Manos P. D., Ahfeldt T., Loh Y.-H., Li H., Lau F., Ebina W., Mandal P. K., Smith Z. D., Meissner A., Daley G. Q., Brack A. S., Collins J. J., Cowan C., Schlaeger T. M., and Rossi D. J. (2010). Highly Efficient Reprogramming to Pluripotency and Directed Differentiation of Human Cells with Synthetic Modified mRNA. *Cell Stem Cell* **7**, 618–630. doi:10.1016/j.stem.2010.08.012

Wartiovaara J., Öfverstedt L.-G., Khoshnoodi J., Zhang J., Mäkelä E., Sandin S., Ruotsalainen V., Cheng R. H., Jalanko H., Skoglund U., and Tryggvason K. (2004). Nephrin strands contribute to a porous slit diaphragm scaffold as revealed by electron tomography. *J. Clin. Invest.* **114**, 1475–1483. doi:10.1172/JCI22562

Watanabe K., Miyagawa R., Tomikawa C., Mizuno R., Takahashi A., Hori H., and Ijiri K. (2013). Degradation of initiator tRNA Met by Xrn1/2 via its accumulation in the nucleus of heat-treated HeLa cells. *Nucleic Acids Research* **41**, 4671–4685. doi:10.1093/nar/gkt153

Weitzer S., Hanada T., Penninger J. M., and Martinez J. (2015). CLP1 as a novel player in linking tRNA splicing to neurodegenerative disorders: CLP1 in linking tRNA splicing to neurodegenerative disorders. *WIREs RNA* **6**, 47–63. doi:10.1002/wrna.1255

Weitzer S., and Martinez J. (2007). The human RNA kinase hClp1 is active on 3′ transfer RNA exons and short interfering RNAs. *Nature* **447**, 222–226. doi:10.1038/nature05777

Wente S. R., and Rout M. P. (2010). The Nuclear Pore Complex and Nuclear Transport. *Cold Spring Harbor Perspectives in Biology* **2**, a000562–a000562. doi:10.1101/cshperspect.a000562

Whitney M. L., Hurto R. L., Shaheen H. H., and Hopper A. K. (2007). Rapid and Reversible Nuclear Accumulation of Cytoplasmic tRNA in Response to Nutrient Availability□D. *Molecular Biology of the Cell* **18**, 9.

Wiggins R.-C. (2007). The spectrum of podocytopathies: A unifying view of glomerular diseases. *Kidney International* **71**, 1205–1214. doi:10.1038/sj.ki.5002222

Wilusz J. E. (2015). Controlling translation via modulation of tRNA levels: Controlling translation via modulation of tRNA levels. *WIREs RNA* **6**, 453–470. doi:10.1002/wrna.1287

Winn M. P., Conlon P. J., Lynn K. L., Farrington M. K., Creazzo T., Hawkins A. F., Daskalakis N., Kwan S. Y., Ebersviller S., Burchette J. L., Pericak-Vance M. A., Howell D. N., Vance J. M., and Rosenberg P. B. (2005). A Mutation in the TRPC6 Cation Channel Causes Familial Focal Segmental Glomerulosclerosis. *Science.* **308**, 1801–4. doi:10.1126/science.1106215

Wolin S. L., and Matera A. G. (1999). The trials and travels of tRNA. *Genes & Development* **13**, 1–10. doi:10.1101/gad.13.1.1

Woltjen K., Michael I. P., Mohseni P., Desai R., Mileikovsky M., Hämäläinen R., Cowling R., Wang W., Liu P., Gertsenstein M., Kaji K., Sung H.-K., and Nagy A. (2009). piggyBac transposition reprograms fibroblasts to induced pluripotent stem cells. *Nature* **458**, 766–770. doi:10.1038/nature07863

Wu J., Chatterjee K., Wan Y., and Hopper A. K. (2015). Genome-wide screen uncovers novel pathways for tRNA processing and nuclear–cytoplasmic dynamics. *Genes Dev.* **29**, 2633–44. doi:10.1101/gad.269803.115

Xiao S., Scott F., Fierke C. A., and Engelke D. R. (2002). Eukaryotic Ribonuclease P: A Plurality of Ribonucleoprotein Enzymes. *Annu. Rev. Biochem.* **71**, 165–189. doi:10.1146/annurev.biochem.71.110601.135352

Xu R.-H., Sampsell-Barron T. L., Gu F., Root S., Peck R. M., Pan G., Yu J., Antosiewicz-Bourget J., Tian S., Stewart R., and Thomson J. A. (2008). NANOG Is a Direct Target of TGFβ/Activin-Mediated SMAD Signaling in Human ESCs. *Cell Stem Cell* **3**, 196–206. doi:10.1016/j.stem.2008.07.001

Yacoubi B. E., and Bailly M. (2012). Biosynthesis and Function of Posttranscriptional Modifications of Transfer RNAs. *Annu Rev Genet.* **46**, 69–95. doi:10.1146/annurev-genet-110711-155641

Yamasaki S., Ivanov P., Hu G., and Anderson P. (2009). Angiogenin cleaves tRNA and promotes stress-induced translational repression. *J Cell Biol.* **185**, 35–42. doi:10.1083/jcb.200811106

Yarian C., Townsend H., Czestkowski W., Sochacka E., Malkiewicz A. J., Guenther R., Miskiewicz A., and Agris P. F. (2002). Accurate Translation of the Genetic Code Depends on tRNA Modified Nucleosides*. *J Biol Chem.* **277**, 16391–5. doi:10.1074/jbc.M200253200

Yoshihisa T. (2014). Handling tRNA introns, archaeal way and eukaryotic way. *Front. Genet.* **5**,. doi:10.3389/fgene.2014.00213

Yoshihisa T., Ohshima C., Yunoki-Esaki K., and Endo T. (2007). Cytoplasmic splicing of tRNA in Saccharomyces cerevisiae. *Genes Cells* **12**, 285–297. doi:10.1111/j.1365-2443.2007.01056.x

Yoshihisa T., Yunoki-Esaki K., Ohshima C., Tanaka N., and Endo T. (2003). Possibility of Cytoplasmic pre-tRNA Splicing: the Yeast tRNA Splicing Endonuclease Mainly Localizes on the Mitochondria. *MBoC* **14**, 3266–3279. doi:10.1091/mbc.e02-11-0757

Yoshimura Y., Taguchi A., Tanigawa S., Yatsuda J., Kamba T., Takahashi S., Kurihara H., Mukoyama M., and Nishinakamura R. (2019). Manipulation of Nephron-Patterning Signals Enables Selective Induction of Podocytes from Human Pluripotent Stem Cells. *JASN* **30**, 304–321. doi:10.1681/ASN.2018070747

Yu J., Hu K., Smuga-Otto K., Tian S., Stewart R., Slukvin I. I., and Thomson J. A. (2009). Human Induced Pluripotent Stem Cells Free of Vector and Transgene Sequences. *Science* **324**, 797–801. doi:10.1126/science.1172482

Yu J., Vodyanik M. A., Smuga-Otto K., Antosiewicz-Bourget J., Frane J. L., Tian S., Nie J., Jonsdottir G. A., Ruotti V., Stewart R., Slukvin I. I., and Thomson J. A. (2007). Induced Pluripotent Stem Cell Lines Derived from Human Somatic Cells. *Science* **318**, 1917–20. doi:10.1126/science.1151526

Zaitseva L., Myers R., and Fassati A. (2006). tRNAs Promote Nuclear Import of HIV-1 Intracellular Reverse Transcription Complexes (M Emerman, Ed.). *PLoS Biol* **4**, e332. doi:10.1371/journal.pbio.0040332

Zasloff M. (1983). tRNA transport from the nucleus in a eukaryotic cell: carrier-mediated translocation process. *Proceedings of the National Academy of Sciences* **80**, 6436–6440. doi:10.1073/pnas.80.21.6436

Zeybek C., Basbozkurt G., Hamcan S., Ozcan A., Gul D., and Gok F. (2016). Collapsing Glomerulopathy in a Child with Galloway-Mowat Syndrome. *Case Reports in Nephrology* **2016**, 1–5. doi:10.1155/2016/4386291

Zhang X.-B. (2013). Cellular Reprogramming of Human Peripheral Blood Cells. *Genomics, Proteomics & Bioinformatics* **11**, 264–274. doi:10.1016/j.gpb.2013.09.001

Zhang S.-C., Wernig M., Duncan I. D., Brüstle O., and Thomson J. A. (2001). In vitro differentiation of transplantable neural precursors from human embryonic stem cells. *Nat Biotechnol* **19**, 1129–1133. doi:10.1038/nbt1201-1129

Zhou H., Wu S., Joo J. Y., Zhu S., Han D. W., Lin T., Trauger S., Bien G., Yao S., Zhu Y., Siuzdak G., SchOler H. R., Duan L., and Ding S. (2009). Generation of Induced Pluripotent Stem Cells Using Recombinant Proteins. *Cell Stem Cell* **4**, 381–4. doi:10.1016/j.stem.2009.04.005

Zhu J., Attias O., Aoudjit L., Jiang R., Kawachi H., and Takano T. (2010). p21-Activated kinases regulate actin remodeling in glomerular podocytes. *American Journal of Physiology-Renal Physiology* **298**, F951–F961. doi:10.1152/ajprenal.00536.2009

Zhu L., Ge J., Li T., Shen Y., and Guo J. (2019). tRNA-derived fragments and tRNA halves: The new players in cancers. *Cancer Letters* **452**, 31–37. doi:10.1016/j.canlet.2019.03.012

Zong T., Yang Y., Zhao H., Li L., Liu M., Fu X., Tang G., Zhou H., Aung L. H. H., Li P., Wang J., Wang Z., and Yu T. (2021). tsRNAs: Novel small molecules from cell function and regulatory mechanism to therapeutic targets. *Cell Prolif.* **54**, e12977. doi:10.1111/cpr.12977